frontiers | Research Topics

Sustainable catalytic production of bio-based heteroatom-containing compounds, volume III

Edited by
Hu Li, Yaqiong Su and Song Yang

Published in
Frontiers in Chemistry
Frontiers in Environmental Science

ISSN 1664-8714
ISBN 978-2-8325-2426-8
DOI 10.3389/978-2-8325-2426-8

About Frontiers

Frontiers is more than just an open access publisher of scholarly articles: it is a pioneering approach to the world of academia, radically improving the way scholarly research is managed. The grand vision of Frontiers is a world where all people have an equal opportunity to seek, share and generate knowledge. Frontiers provides immediate and permanent online open access to all its publications, but this alone is not enough to realize our grand goals.

Frontiers journal series

The Frontiers journal series is a multi-tier and interdisciplinary set of open-access, online journals, promising a paradigm shift from the current review, selection and dissemination processes in academic publishing. All Frontiers journals are driven by researchers for researchers; therefore, they constitute a service to the scholarly community. At the same time, the *Frontiers journal series* operates on a revolutionary invention, the tiered publishing system, initially addressing specific communities of scholars, and gradually climbing up to broader public understanding, thus serving the interests of the lay society, too.

Dedication to quality

Each Frontiers article is a landmark of the highest quality, thanks to genuinely collaborative interactions between authors and review editors, who include some of the world's best academicians. Research must be certified by peers before entering a stream of knowledge that may eventually reach the public - and shape society; therefore, Frontiers only applies the most rigorous and unbiased reviews. Frontiers revolutionizes research publishing by freely delivering the most outstanding research, evaluated with no bias from both the academic and social point of view. By applying the most advanced information technologies, Frontiers is catapulting scholarly publishing into a new generation.

What are Frontiers Research Topics?

Frontiers Research Topics are very popular trademarks of the *Frontiers journals series*: they are collections of at least ten articles, all centered on a particular subject. With their unique mix of varied contributions from Original Research to Review Articles, Frontiers Research Topics unify the most influential researchers, the latest key findings and historical advances in a hot research area.

Find out more on how to host your own Frontiers Research Topic or contribute to one as an author by contacting the Frontiers editorial office: frontiersin.org/about/contact

Sustainable catalytic production of bio-based heteroatom-containing compounds, volume III

Topic editors

Hu Li — Guizhou University, China

Yaqiong Su — Xi'an Jiaotong University, China

Song Yang — Guizhou University, China

Citation

Li, H., Su, Y., Yang, S., eds. (2023). *Sustainable catalytic production of bio-based heteroatom-containing compounds, volume III*. Lausanne: Frontiers Media SA. doi: 10.3389/978-2-8325-2426-8

Table of contents

frontiers | Frontiers in Chemistry

TYPE Editorial
PUBLISHED 02 May 2023
DOI 10.3389/fchem.2023.1210932

OPEN ACCESS

EDITED AND REVIEWED BY
James Clark,
University of York, United Kingdom

*CORRESPONDENCE
Hu Li,
hli13@gzu.edu.cn
Song Yang,
jhzx.msm@gmail.com

RECEIVED 23 April 2023
ACCEPTED 24 April 2023
PUBLISHED 02 May 2023

CITATION
Wu H, Li H, Su Y and Yang S (2023), Editorial: Sustainable catalytic production of bio-based heteroatom-containing compounds Volume III.
Front. Chem. 11:1210932.
doi: 10.3389/fchem.2023.1210932

Editorial: Sustainable catalytic production of bio-based heteroatom-containing compounds Volume III

Hongguo Wu[1], Hu Li[1]*, Yaqiong Su[2] and Song Yang[1]*

[1]National Key Laboratory of Green Pesticide, Key Laboratory of Green Pesticide and Agricultural Bioengineering, Ministry of Education, State-Local Joint Laboratory for Comprehensive Utilization of Biomass, Center for R&D of Fine Chemicals, College of Pharmacy, Guizhou University, Guiyang, Guizhou, China, [2]School of Chemistry, Xi'an Key Laboratory of Sustainable Energy Materials Chemistry, State Key Laboratory of Electrical Insulation and Power Equipment, Xi'an Jiaotong University, Xi'an, China

KEYWORDS

green chemistry, biomass and biofuels, heterogeneous catalysis, waste valorization, biological activity

Editorial on the Research Topic
Sustainable catalytic production of bio-based heteroatom-containing compounds Volume III

Heteroatom-containing compounds are core scaffolds in a variety of medicines, and important building blocks for the synthesis of fine chemicals (Li et al., 2016; Meng et al., 2022; Wang et al., 2023a). As a promising alternative to fossil fuels, biomass sources rich in oxygen species can be used as versatile feedstocks for producing both biofuels and task-specific molecules (Li et al., 2018; Wang et al., 2023b; Huang et al., 2023; Meng et al., 2023). For the sustainable conversion processes developed for biomass upgrading, the used catalytic pathways and strategies are key to regulating product distribution. Also, increasing attention has been paid to investigating the reaction mechanisms using advanced or *in situ* characterization techniques and theoretical calculations. Moreover, environmental and energy issues (e.g., the greenhouse effect and energy depletion) encountered in the conventional use of fossil resources have arisen more concerns in the exploration of renewable biomass and waste CO_2 for the manufacture of carbon-based functional materials/substances employing well-tailored catalysts or catalytic systems.

This Research Topic is Volume III of a series, and here we present a Research Topic of original research and review articles (12 papers in total) with topics on green and sustainable chemistry, including catalytic production of biodiesel (Zhang et al., and Pan et al.), catalytic upgrading of biomass derivatives (Wang et al., Li et al., Zheng et al., and Huang et al.), selective hydrogenation of CO_2 to CH_4 (Xiang et al.), bioactive assessment of natural products (Qu et al.), and environmental issues involved in the biomass utilization processes (Liu et al., Yang et al., Yang et al., and Yang et al.).

A research paper by Wang et al. reports the preparation of Pt-WO_x catalysts supported on TiO_2 with different crystal forms and WO_x loadings for catalytic performance in the hydrogenolysis of glycerol to 1,3-propanediol. The anatase-type TiO_2-supported catalyst (Pt/W/A-Ti) with higher stability shows superior catalytic performance to the rutile-type TiO_2 catalyst (Pt/W/R-Ti). Also, the catalytic mechanisms are investigated by *in situ*

characterization techniques, manifesting that glycerol is first transformed into 3-hydroxypropanal over Pt/W/A-Ti, followed by succeeding conversion steps to give 1,3-propanediol. Xiang et al. detailedly study the formation process of methane (up to 100% selectivity) from catalytic hydrogenation of CO_2 at 280°C over a Ni-based ETS-10 zeolite catalyst, which is prepared by *in situ* doping and impregnation. Intensive characterizations and measurements are conducted to get insights into the catalyst promotional mechanisms, with attention to the impact of different Ni incorporation methods on the catalyst stability. In addition, the antifungal activities of the *Allium mongolicum* Regel leaf (Qu et al.), and the health risks of heavy metals in soils and food crops (Liu et al.) are assessed, as well.

This Research Topic also features several Mini reviews with varying scopes (Zhang et al., Pan et al., Li et al., Zheng et al., Huang et al., Yang et al., Yang et al., and Yang et al.). Zhang et al. summarize recent advances in the development of magnetic catalytic materials for producing biodiesel, with a focus on the catalyst physicochemical properties, performance, and recyclability. The involved catalytic mechanisms and reaction conditions in biodiesel production are discussed, and attention is also paid to the limitations and challenges for future research. Viewing that ionic liquid-functionalized materials have the unique characteristics of both homogeneous and heterogeneous catalysts, they are recently considered as one of the promising alternatives to conventional homogeneous acid/base catalysts for biodiesel production. Accordingly, a review on the topic of developing supported acid/base ionic liquids as heterogeneous catalysts for producing biodiesel is presented (Pan et al.). The merits and demerits of various supports (e.g., mesoporous silica, porous polymers, carbonaceous materials, metal-organic frameworks, and ferromagnetic materials) in biodiesel production are collected, and their performance in immobilization of ionic liquids is compared, with emphasis on the developed methods effective for immobilizing ionic liquids onto solid supports to prepare the functional ionic liquids. The ionic liquid-based solid catalysts are also reported to be efficient for the pretreatment of lignocellulosic biomass, and the obtained cellulose and hemicellulose components can be further converted to 5-hydroxymethylfurfural in the presence of the tailored acidic ionic liquids (Li et al.).

Instead of chemocatalysis, Zheng et al. make a brief introduction to the classification, source and application of alginate lyases in the biocatalytic degradation of carbohydrates, which primarily concentrates on screening of strains, mining of genes, and analysis of degradation substrate and product structure. In addition to the comprehensive utilization of saccharides, Huang et al. introduce the development of a variety of anodes (e.g., Pt, Pb, Ir, Ni, and Co) for electro-oxidative degradation of lignin, with emphasis on the product distribution caused by different electrodes, as well as the involved reaction pathways and catalytic mechanisms. For the construction of ecological civilization and the goal of carbon peak and carbon neutralization, several reviews regarding carbon effect calculation and upgrading strategy (Yang et al.), improvement of rural soil properties and states by biomass carbon (Yang et al.), and rural resilience research from the perspective of the ecosystem (Yang et al.) are also showcased.

We wish this Research Topic enlightens more sustainable and eco-friendly conversion pathways, sheds light on reaction mechanisms, and develops novel catalytic strategies for producing biofuels and high-value chemicals. Enjoy its reading!

Author contributions

All authors listed have made a substantial, direct, and intellectual contribution to the work and approved it for publication.

Acknowledgments

HL thanks financial support of the Guizhou Provincial S&T Project [ZK(2022)011].

Conflict of interest

The authors declare that the research was conducted in the absence of any commercial or financial relationships that could be construed as a potential conflict of interest.

Publisher's note

References

Huang, J., Wang, J., Huang, Z., Liu, T., and Li, H. (2023). Photothermal technique-enabled ambient production of microalgae biodiesel: Mechanism and life cycle assessment. *Bioresour. Technol.* 369, 128390. doi:10.1016/j.biortech.2022.128390

Li, H., Fang, Z., Smith, R. L., Jr, and Yang, S. (2016). Efficient valorization of biomass to biofuels with bifunctional solid catalytic materials. *Prog. Energy Combust. Sci.* 55, 98–194. doi:10.1016/j.pecs.2016.04.004

Li, H., Riisager, A., Saravanamurugan, S., Pandey, A., Sangwan, R. S., Yang, S., et al. (2018). Carbon-increasing catalytic strategies for upgrading biomass into energy-intensive fuels and chemicals. *ACS Catal.* 8, 148–187. doi:10.1021/acscatal.7b02577

Meng, Y., Jian, Y., Li, J., Wu, H., Zhang, H., Saravanamurugan, S., et al. (2023). Surface-active site engineering: Synergy of photo- and supermolecular catalysis in hydrogen transfer enables biomass upgrading and H_2 evolution. *Chem. Eng. J.* 452, 139477. doi:10.1016/j.cej.2022.139477

Meng, Y., Yang, S., and Li, H. (2022). Electro- and photocatalytic oxidative upgrading of biobased 5-hydroxymethylfurfural. *ChemSusChem* 15, e202102581. doi:10.1002/cssc.202102581

Wang, B., Li, M., Zhang, S., Wu, H., Liao, Y., and Li, H. (2023a). Synergistic effect between Co single atoms and nanoparticles enables selective synthesis of bio-based benzimidazoles. *Appl. Catal. B Environ.* 327, 122454. doi:10.1016/j.apcatb.2023.122454

Wang, B., Zhou, P., Yan, X., Li, H., Wu, H., and Zhang, Z. (2023b). Cooperative catalysis of Co single atoms and nanoparticles enables selective C_{Ar}-OCH_3 cleavage for sustainable production of lignin-based cyclohexanols. *J. Energy Chem.* 79, 535–549. doi:10.1016/j.jechem.2022.12.020

frontiers | Frontiers in Chemistry

TYPE Original Research
PUBLISHED 24 August 2022
DOI 10.3389/fchem.2022.993893

OPEN ACCESS

EDITED BY
Yaqiong Su,
Xi'an Jiaotong University, China

REVIEWED BY
Baobing Zhao,
Shandong University, China
Jian Zhang,
Gansu University of Chinese Medicine, China
Xiaobo Xu,
Huanghuai University, China

*CORRESPONDENCE
Huan Qu,
rosalie42@163.com
Yang Chen,
ychen1@gzu.edu.cn

SPECIALTY SECTION
This article was submitted to Organic Chemistry, a section of the journal Frontiers in Chemistry

RECEIVED 14 July 2022
ACCEPTED 21 July 2022
PUBLISHED 24 August 2022

CITATION
Qu H, Guo Z, Ma L, Zhang X, Ma H and Chen Y (2022), Antifungal effects and active compounds of the leaf of Allium mongolicum Regel.
Front. Chem. 10:993893.
doi: 10.3389/fchem.2022.993893

Antifungal effects and active compounds of the leaf of *Allium mongolicum* Regel

Huan Qu[1,2]*, Zhen Guo[1], Li Ma[1], Xiu Zhang[2], Haijun Ma[3] and Yang Chen[4]*

[1]College of Biological Science and Engineering, North Minzu University, Yinchuan, Ningxia, China, [2]Ningxia Key Laboratory of Microbial Resources Development and Applications in Special Environment, Yinchuan, Ningxia, China, [3]Ningxia Grape and Wine Innovation Center, Yinchuan, Ningxia, China, [4]State Key Laboratory Breeding Base of Green Pesticide and Agricultural Bioengineering, Key Laboratory of Green Pesticide and Agricultural Bioengineering, Ministry of Education, Research and Development Center for Fine Chemicals, Guizhou University, Guiyang, China

Taking plant metabolites as material to develop new biological fungicides is still an important mission for pesticide development, and the preliminary study confirmed that *Allium mongolicum* showed a certain inhibitory effect on plant pathogens. In this study, the antifungal activity of extracts of *A. mongolicum* was studied and the compounds were isolated, purified, and identified by HPLC, NMR, and ESI-MS. The methanol extract of *A. mongolicum* exhibited certain inhibitory activity against almost all nine tested pathogens at concentration of 0.5 mg/ml. Sixteen compounds were isolated and purified from the extract, which were identified as nine flavonoids, six phenolic acids, and an amino acid. Among them, cinnamic acid derivatives **1**, **2**, and **3** and flavonoids **7**, **8**, **9**, and **13** were separated in *A. mongolicum* for the first time.

KEYWORDS

***Allium mongolicum*, antifungal activity, flavonoids, phenolic acids, tryptophan**

1 Introduction

Food and Agriculture Organization of the United Nations (FAO) estimates that about 25% of the world's crops are affected by plant diseases every year (Xing, 2018), which lead to the yield losses as well as reduced quality of crop production (Gao et al., 2016; Liu and Wang, 2016) and secrete a variety of toxins and harmful metabolites (Guo et al., 2021). As is reported, 70%–80% of the plant diseases are caused by plant phytopathogenic fungi, such as *Magnaporthe oryzae*, *Fusarium graminearum*, *Valsa mali*, and *Botrytis cinerea*, which are hard to control (Qin et al., 2013). For a long time, chemical antimicrobial agents play an important role in inhibiting plant-pathogenic fungi and promoting agricultural production. However, the long-term use of chemical agents has gradually been limited by the problems of food safety, environmental pollution, and the tendency of pathogenic microorganisms to develop resistance to them (Kim and Hwang, 2007; Akhter et al., 2015; Zhang et al., 2018). Therefore, development of new compounds with effectively inhibiting activity is still an important mission (Kang, 2010). *Alliaceae* has become an important source for finding useful compounds due to its significant and extensive antifungal activity, some of which

have been used for agricultural diseases (Ma et al., 2014). As representative plants of *Alliaceae*, *Allium sativum* and *Allium cepa* gained more attention and significantly inhibited many kinds of microorganisms (Nicastro et al., 2015; Martins et al., 2016; Chen et al., 2017). Especially, the fungicides with garlic oil and ethylicin as the main effective components were successfully used for control of agricultural fungal and bacterial diseases.

As a kind of characteristic xerophytic plant of *Allium*, *A. mongolicum* is widely distributed in the desert regions of northwest China and its leaves are used as a high-quality forage plant as well as a natural green uncontaminated food (Zhang et al., 2017). However, for a long time, studies of *A. mongolicum* have focused only on its morphology and geographic distribution, artificial cultivation and nutritional value, seed germination characteristics, and genetic diversity (Yang et al., 2008; Zhang, et al., 2014; Hu et al., 2017). Recent studies have found that *A. mongolicum* has broad-spectrum antimicrobial activity. The aqueous and ethanol extracts of *A. mongolicum* exhibited certain inhibitory effects on *Staphylococcus aureus* and *Escherichia coli* and showed greater tolerance to ultraviolet light and temperature. In the course of studying the effect of *A. mongolicum* on mutton quality, it found that volatile oil, polysaccharide, and flavonoids showed an inhibitory effect on animal-related foodborne pathogens (Sa et al., 2014; Muqier et al., 2017). As an important material for finding antimicrobial compounds, some monomeric compounds of flavonoid and ethyl cinnamate, dibutyl oxalate, and 2-hexenal from the essential oil of *A. mongolicum* were gained in recent years (Wang et al., 2012; Dong et al., 2015; Dong et al., 2020). However, the antimicrobial activity compounds of *A. mongolicum* have not been systematically explored at present. Therefore, comparatively systematic research about the inhibitory effect of extracts of *A. mongolicum* on common plant-pathogenic fungi was made based on the above in this article, and monomeric compound of extracts of *A. mongolicum* were isolated, purified, and identified, which would lay a foundation for the research and development of new botanical pesticides.

2 Materials and methods

2.1 Materials

A. mongolicum were collected from Luanjingtan in Alxa Zuoqi, Inner Mongolia in July (E 105°23′46.12″, N 37°51′36.42″, altitude 1,430 m). Healthy plants were selected, and aboveground parts were collected to be taken back to the laboratory. Tested plant pathogenic fungi: *Fusarium oxysporum*, *Exserohilum turcicum*, *Valsa mali*, *Fusarium graminearum*, *Botrytis cinerea*, *Alternaria solani,* and *Fusarium sulphureum* were provided by Northwest A&F University; *Fusarium solani* and *Corynespora cassiicola* were preserved and provided by Ningxia Key Laboratory of Microbial Resources Development and Applications in Special Environment.

2.2 Preparation of extracts of *A. mongolicum*

Plant extracts were prepared by solvent extraction with some modification (Prashith et al., 2015). The leaves of *A. mongolicum* were cut into small pieces and dried under shade for 7 days at 32–35°C, then powdered in a blender and stored in a sealed fresh-storage bottle away from light. Dry powder was separately extracted by soaking in 10times the volume of petroleum ether, dichloromethane, ethyl acetate, and methanol for 48 h. The extract was filtered out, and the same process is repeated three times. The filtrates were combined and concentrated to paste at 45–50°C by a rotary evaporator and stored in a refrigerator at 4°C for later used.

2.3 Antifungal activity assays of extracts of *A. mongolicum*

Antifungal activity of petroleum ether, dichloromethane, ethyl acetate, and methanol extracts was evaluated by the poisoned food technique (Liu et al., 2017). The extracts were prepared using acetone as the initial solvent carrier followed by dilution with PDA (at about 60°C) to produce the desired concentrations of 0.5 mg/ml, then poured into a sterile petri dish (9 cm in diameter) to make a medium-filled plate. After the medium was solidified, a mycelial disk (with a diameter of 4 mm) containing tested pathogenic fungi was placed in each medium plane. The PDA plates were incubated in the light-dark cycle at 28 ± 1°C for 5 days. PDA plates treated with an equal quantity of acetone were used as control. Each treatment was treated using three biological replicates. The mycelial growth inhibition was calculated by the formula.

$$\text{Inhibition rate}\,(\%) = (C - T)/(C - 4) \times 100$$

where C is the mycelial diameter (mm) of the control and T is the mycelial diameter (mm) under extract solution treatment.

2.4 Isolation, purification, and structure identification of compounds from *A. mongolicum*

A. mongolicum powder (6.4 kg) was extracted with methanol-water (4:1, v/v) for 1 h three times by using ultrasonic treatment. The extracts were combined and centrifuged, then discard precipitation; the filtrate was concentrated to paste at 45°C, dispersed in appropriate amount of water. The aqueous phase was extracted with petroleum ether and ethyl acetate in turn three times. The petroleum ether phase was discarded, and the ethyl acetate and water phase were retained.

The ethyl acetate phase was concentrated under reduced pressure at 45°C to obtain crude extract. The extract was isolated

TABLE 1 Toxicity test results of extracts of *A. mongolicum* against nine plant-pathogenic fungi at a concentration of 0.5 mg/ml (96 h of incubation).

Plant-pathogenic fungi	Inhibition rate (%; mean ± SD; $N = 3$)[a]			
	Petroleum ether extract	Dichloromethane extract	Ethyl acetate extract	Methanol extract
Fusarium solani	36.61 ± 0.23	36.96 ± 0.11	34.46 ± 0.04	30.36 ± 0.20
Valsa mali	42.63 ± 0.20	20.59 ± 0.12	30.88 ± 0.13	32.35 ± 0.18
Fusarium oxysporum	44.77 ± 0.18	15.95 ± 0.12	12.95 ± 0.13	43.55 ± 0.25
Fusarium sulphureum	47.94 ± 0.19	5.39 ± 0.12	17.41 ± 0.12	19.21 ± 0.21
Botrytis cinerea	47.33 ± 0.23	22.81 ± 0.25	11.25 ± 0.15	38.73 ± 0.35
Alternaria solani	26.67 ± 0.13	10.00 ± 0.42	6.67 ± 0.12	33.33 ± 0.20
Fusarium graminearum	27.16 ± 0.16	45.31 ± 0.16	37.04 ± 0.12	33.70 ± 0.18
Exserohilum turcicum	3.45 ± 0.43	13.79 ± 0.24	25.29 ± 0.08	11.49 ± 0.16
Corynespora cassiicola	48.70 ± 0.17	5.44 ± 0.20	42.55 ± 0.15	13.24 ± 0.09
CK	0.00 ± 0.00	0.00 ± 0.00	0.00 ± 0.00	0.00 ± 0.00

[a]Values are the mean ± SE of three replicates.

by normal-phase silica gel chromatography and then eluted with petroleum ether-ethyl acetate-methanol, ethyl acetate, and methanol-ethyl acetate fractions were collected. Ethyl acetate fraction was concentrated and dissolved in methanol, and separated based on high-performance liquid chromatography to gain the compounds of **1** (100 mg), **2** (90 mg), and **3** (125 mg). Methanol-ethyl acetate (5:1, v/v) fraction was concentrated and dissolved in methanol, separated using high-performance liquid chromatography (HPLC) to gain the compounds of **4** (240 mg) and **5** (40 mg). Methanol-ethyl acetate (1:1, v/v) fraction was concentrated and dissolved in methanol and separated using HPLC to gain the compounds of **6** (210 mg).

The aqueous phase was separated by AB-8 macroporous resin column chromatography with methanol-water as a mobile phase for gradient elution. Methanol-water (7:3, v/v) phase was collected, evaporated by rotary evaporator and dissolved in methanol for HPLC separation to gain 1, 2, 3, 4, and 5 fractions, fractions (1, 2, 3, 4, and 5) were further isolated through HPLC. Fraction 1 was eluted with methanol-water and acetonitrile-water to obtain compounds numbered **7** (60 mg), **8** (40 mg), **9** (30 mg), **10** (200 mg). Fraction 2 was eluted with methanol-water and acetonitrile-water to obtain compounds numbered **11** (10 mg), **12** (20 mg), **13** (40 mg). Fraction 3 was concentrated to remove some solvents and the compound **14** (1,500 mg) separated out with standing for 24 h. Fraction 5 was eluted with methanol-water and acetonitrile-water to obtain compounds numbered **15** (60 mg), **6** (905 mg), and **16**(70 mg).

2.5 Compound structure identification

The mass spectrum, ^{1}H-NMR (400 MHz), and ^{13}C-NMR (100 MHz) spectra of the compounds were determined. The chemical structure of the compounds was identified according to spectroscopic data.

3 Results and discussion

3.1 Results

3.1.1 Toxicity determination of extracts of *A. mongolicum*

The extract of *A. mongolicum* showed different degrees of inhibition on the mycelial growth of nine different plant-pathogenic fungi (Table 1). Among them, the inhibitory effects of all tested extracts on *Fusarium solani* and *Fusarium graminearum* were better, and the inhibition rate was about over 30%. Generally, the inhibitory effects of petroleum ether extract and methanol extract were higher than that of dichloromethane extract and ethyl acetate extract, and petroleum ether extract and methanol extract almost showed inhibitory activity on all tested pathogens. Based on the former results, the methanol extract with the yield of 23.31% was much higher than that of petroleum ether extract (4.27%), as well as, petroleum ether extract contained more pigment. Considering the polarity of the solvent, the methanol extract is richer in types of compounds compared with petroleum ether extract. Therefore, methanol was selected as the solvent in the subsequent extract experiment.

3.1.2 Chemical structure identification of compounds from *A. mongolicum*

Data for compound **1**: gray powder, m. p. 212–213°C; ESI-MS: Calcd for $C_{17}H_{17}NO_3$ ([M + H]$^+$), 284.16; ^{1}H NMR (400 MHz, Methanol-d_4) δ: 7.44 (d, J = 15.7 Hz, 1H, H-7), 7.39 (d, J = 8.6 Hz, 2H, H-2, 6), 7.09–7.02 (m, 2H, H-2′, 6′), 6.82–6.76 (m, 2H, H-3, 5), 6.75–6.66 (m, 2H, H-3′, 5′), 6.38

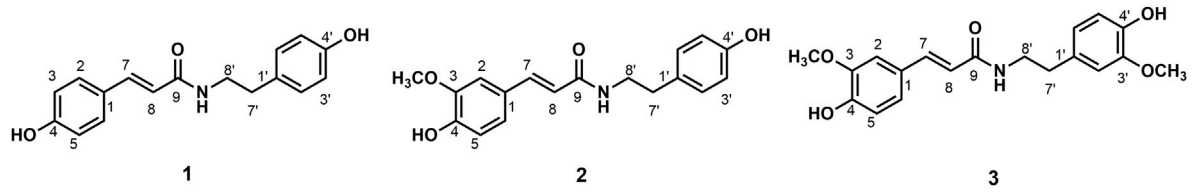

FIGURE 1
Chemical structure of compounds **1**, **2**, and **3**

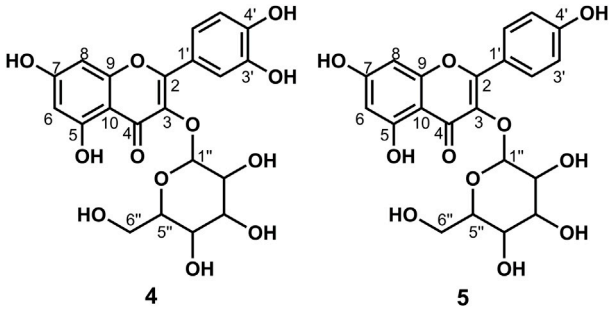

FIGURE 2
Chemical structure of compounds **4** and **5**

(d, J = 15.7 Hz, 1H,H-8), 3.46 (t, J = 7.4 Hz, 2H, H-8′), 2.75 (t, J = 7.4 Hz, 2H, H-7′); ^{13}C NMR (100 MHz, Methanol-d_4) δ: 169.25 (C-9), 160.49 (C-4), 156.91 (C-4′), 141.77 (C-7), 131.33 (C-1′), 130.72 (C-2′, 6′), 130.54 (C-2, 6), 127.75 (C-1), 118.47 (C-8), 116.72 (C-3′, 5′), 116.27 (C-3, 5), 42.53 (C-8′), and 35.80 (C-7′). According to the abovementioned data and literature (Kim and Lee, 2003), compound **1** was identified as *trans-N-p*-coumaroyl tyramine and its molecular formula is shown in Figure 1. MS diagrams and ^{1}H-NMR and ^{13}C-NMR spectra were shown in Supplementary Figures S1–S3, respectively.

Data for compound **2**: white powder, m. p. 123–125°C; ESI-MS: Calcd for $C_{18}H_{19}NO_4$([M + H]$^+$), 314.16; ^{1}H NMR (400 MHz, Methanol-d_4) δ: 7.47–7.40 (m, 1H, H-7), 7.11 (d, J = 1.9 Hz, 1H, H-2), 7.07–7.04 (m, 2H, H-2′, 6′), 7.02 (dd, J = 8.2, 2.0 Hz, 1H, H-6), 6.81 (s, 1H, H-5), 6.74–6.70 (m, 2H, H-3′, 5′), 6.40 (d, J = 15.7 Hz, 1H, H-8), 3.88 (s, 3H, H-3), 3.47 (dd, J = 8.0, 6.7 Hz, 2H, H-8′), 2.75 (t, J = 7.3 Hz, 2H, H-7′); ^{13}C NMR (100 MHz, Methanol-d_4) δ: 169.18 (C-9), 156.92 (C-4′), 149.82 (C-3), 149.29 (C-4), 142.01 (C-7), 131.32 (C-1′), 130.72 (C-2′, 6′), 128.31 (C-1), 123.22 (C-6), 118.80 (C-8), 116.47 (C-3′, 5′), 116.28 (C-5), 111.59 (C-2), 56.41 (OCH_3-3), 42.52 (C-8′), and 35.79 (C-7′). According to the abovementioned data and literature (Jiang and Ying, 2017), compound **2** was identified as *N-trans*-feruloyl tyramine and its molecular formula is shown in Figure 1. MS diagrams and ^{1}H-NMR and ^{13}C-NMR spectra were shown in Supplementary Figures S4–S6, respectively.

Data for compound **3**: steel gray solid, m. p. 132–134°C; ESI-MS: Calcd for $C_{19}H_{21}NO_5$([M + H]$^+$), 344.19; ^{1}H NMR (400 MHz, Methanol-d_4) δ: 7.44 (d, J = 15.7 Hz, 1H, H-7), 7.11 (d, J = 1.9 Hz, 1H, H-6), 7.02 (dd, J = 8.2, 2.0 Hz, 1H, H-2), 6.84–6.74 (m, 2H,H-2′, 6′), 6.72 (d, J = 8.0 Hz, 1H, H-3), 6.66 (dd, J = 8.0, 1.9 Hz, 1H), 6.41 (d, J = 15.7 Hz, 1H, H-8), 3.87 (s, 3H, H-5), 3.82 (s, 3H, H-3′), 3.49 (dd, J = 8.0, 6.7 Hz, 2H, H-8′), 2.77 (t, J = 7.3 Hz, 2H, H-7′); ^{13}C NMR (100 MHz, Methanol-d_4) δ: 169.19 (C-9), 149.84 (C-4), 149.29 (C-3), 148.95 (C-3′), 146.05 (C-4′), 142.02 (C-7), 132.05 (C-1′), 128.29 (C-1), 123.19 (C-6), 122.26 (C-6′), 118.80 (C-8), 116.48 (C-5), 116.21 (C-5′), 113.49 (C-2′), 111.59 (C-2), 56.40 (OCH_3-3), 56.37 (OCH_3-3′), 42.46 (C-8′), and 36.20 (C-7′). According to the abovementioned data and literature (Jiang and Ying, 2017), compound **3** was identified as *N-trans*-feruloyl-3-methoxy tyramine and its molecular formula is shown in Figure 1. MS diagrams and ^{1}H-NMR and ^{13}C-NMR spectra were shown in Supplementary Figures S7–S9, respectively.

Data for compound **4**: pale yellow powder, m. p. 179–182°C; ESI-MS: Calcd for $C_{21}H_{20}O_{12}$ ([M + H]$^+$), 465.12; ^{1}H NMR (400 MHz, DMSO-d_6) δ: 12.63 (s, 1H, H-5), 10.91 (s, 1H,H-4′),

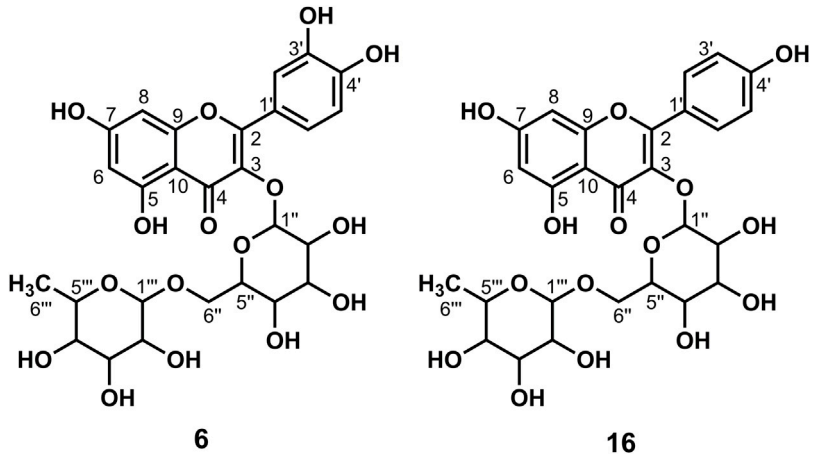

FIGURE 3
Chemical structure of compounds **6** and **16**.

9.72 (s, 1H, H-7), 9.21 (s, 1H, H-3′), 7.62–7.52 (m, 2H, H-2′, 6′), 6.89–6.76 (m, 1H, H-5′), 6.42 (d, J = 2.1 Hz, 1H, H-8), 6.21 (d, J = 2.0 Hz, 1H, H-6), 5.46 (d, J = 7.4 Hz, 1H, H-1″), 5.27 (d, J = 3.8 Hz, 1H), 5.07–5.02 (m, 1H), 4.94 (d, J = 3.6 Hz, 1H), 4.24 (t, J = 5.7 Hz, 1H), 3.59 (dd, J = 11.5, 4.4 Hz, 1H), 3.30–3.20 (m, 3H), 3.20–3.05 (m, 2H, H-6″); ^{13}C NMR (100 MHz, DMSO-d_6) δ: 177.45 (C-4), 164.15 (C-7), 161.24 (C-5), 156.32 (C-9), 156.20 (C-2), 148.47 (C-4′), 144.82 (C-3′), 133.35 (C-3), 121.60 (C-6′), 121.16 (C-1′), 116.21 (C-2′), 115.22 (C-5′), 103.98 (C-10), 100.91 (C-1″), 98.67 (C-6), 93.51 (C-8), 77.55 (C-3″), 76.52 (C-5″), 74.10 (C-2″), 69.95 (C-4″), and 60.98 (C-6″). According to the abovementioned data and literature (Dong et al., 2016), compound **4** was identified as Isoquercitrin and its molecular formula is shown in Figure 2. MS diagrams and ^{1}H-NMR and ^{13}C-NMR spectra were shown in Supplementary Figures S10–S12, respectively.

Data for compound **5**: pale yellow powder, m. p. 196–198°C; ESI-MS: Calcd for $C_{21}H_{20}O_{11}$([M + H]$^+$), 449.14; ^{1}H NMR (400 MHz, DMSO-d_6) δ: 12.61 (s, 1H, H-5), 10.89 (s, 1H, H-4′), 10.18 (s, 1H, H-7), 8.08–8.00 (m, 2H, H-2′, 6′), 6.97–6.85 (m, 2H, H-3′, 5′), 6.44 (d, J = 2.1 Hz, 1H, H-8), 6.22 (d, J = 2.1 Hz, 1H, H-6), 5.45 (d, J = 7.3 Hz, 1H, H-1″), 5.31 (d, J = 4.3 Hz, 1H), 5.02 (d, J = 4.4 Hz, 1H), 4.92 (d, J = 3.7 Hz, 1H), 4.23 (t, J = 5.6 Hz, 1H), 3.57 (dd, J = 11.6, 5.0 Hz, 1H), 3.28–3.15 (m, 3H), 3.14–3.04 (m, 2H, H-6″); ^{13}C NMR (100 MHz, DMSO-d_6) δ: 177.47 (C-4), 164.15 (C-7), 161.21 (C-5), 159.96 (C-4′), 156.38 (C-2), 156.26 (C-9), 133.21 (C-3), 130.86 (C-2′, C-6′), 120.88 (C-1′), 115.10 (C-3′, 5′), 104.00 (C-10), 100.91 (C-1″), 98.69 (C-6), 93.64 (C-8), 77.47 (C-3″), 76.44 (C-5″), 74.21 (C-2″), 69.91 (C-4″), and 60.85 (C-6″). According to the abovementioned data and combined with the literature (Dong et al., 2015), compound **5** was identified as Kaempferol-3-*O*-glucoside and its molecular formula is shown in Figure 2. MS diagrams and ^{1}H-NMR and ^{13}C-NMR spectra were shown in Supplementary Figures S13–S15, respectively.

Data for compound **6**: pale yellow powder, m. p. 175–177°C; ESI-MS: Calcd for $C_{27}H_{30}O_{16}$ ([M + H]$^+$), 611.19; ^{1}H NMR (400 MHz, DMSO-d_6) δ: 12.59 (s, 1H, H-5), 10.81 (s, 1H,H-4′), 9.61 (s, 1H, H-7), 9.16 (s, 1H, H-3′), 7.54 (d, J = 7.5 Hz, 2H, H-2′, 6′), 6.85–6.84 (m, 1H, H-5′), 6.39 (d, J = 2.1 Hz, 1H, H-8), 6.20 (d, J = 2.1 Hz, 1H,H-6), 5.39–5.30 (m, 1H, 1″), 5.2 (s, 1H), 5.05 (s, 1H), 4.39 (d, J = 1.6 Hz, 2H), 4.34 (s, 1H), 3.71 (d, J = 10.6 Hz, 1H), 3.40 (dd, J = 3.5, 1.6 Hz, 1H), 3.31–3.20 (m, 7H), 3.08 (t, J = 9.2 Hz, 3H), 1.00 (d, J = 6.2 Hz, 3H, H-6‴); ^{13}C NMR (100 MHz, DMSO-d_6) δ: 177.35 (C-4), 164.07 (C-7), 161.20 (C-5), 156.57 (C-9), 156.40 (C-2), 148.39 (C-4′), 144.73 (C-3′), 133.30 (C-3), 121.56 (C-6′), 121.16 (C-1′), 116.25 (C-2′), 115.21 (C-5′), 103.94 (C-10), 101.18 (C-1″), 100.72 (C-1‴), 98.65 (C-6), 93.55 (C-8), 76.45 (C-3″), 75.90 (C-5″), 74.06 (C-2″), 71.84 (C-4‴), 70.55 (C-3‴), 70.35 (C-2‴), 69.99 (C-4″), 68.21 (C-5‴), 66.97 (C-6″), and 17.70 (C-6‴). According to the abovementioned data and literature (Dong et al., 2016), compound **6** was identified as Rutin and its molecular formula is shown in Figure 3. MS diagrams and ^{1}H-NMR and ^{13}C-NMR spectra were shown in Supplementary Figures S16–S18, respectively.

Data for compound **7**: pale yellow powder, m. p. 187–189°C; ESI-MS: Calcd for $C_{33}H_{38}O_{23}$([M + H]$^+$), 803.05; ^{1}H NMR (400 MHz, DMSO-d_6) δ: 12.56 (s, 1H, H-5), 8.93 (s, 1H, H-3′), 7.68 (d, J = 2.2 Hz, 1H, H-2′), 7.64 (dd, J = 8.6, 2.3 Hz, 1H, H-6′), 7.23 (d, J = 8.7 Hz, 1H, H-5′), 6.85 (d, J = 2.1 Hz, 1H, H-8), 6.46 (d, J = 2.1 Hz, 1H, H-6), 5.56–5.44 (m, 4H), 5.30 (t, J = 2.4 Hz, 1H), 5.23 (d, J = 7.3 Hz, 2H), 5.09 (s, 3H), 4.97 (s, 1H), 4.87 (d, J = 7.1 Hz, 1H, H-1‴), 4.63 (t, J = 5.7 Hz, 1H), 4.31 (t, J = 5.8 Hz, 1H), 3.92 (d, J = 7.9 Hz, 1H), 3.77–3.70 (m, 2H), 3.59 (dd, J = 11.3, 5.0 Hz, 2H), 3.49 (d, J = 6.1 Hz, 2H), 3.26–3.15 (m, 7H), 3.10 (d, J = 4.1 Hz, 3H); ^{13}C NMR (100 MHz, DMSO-d_6) δ:

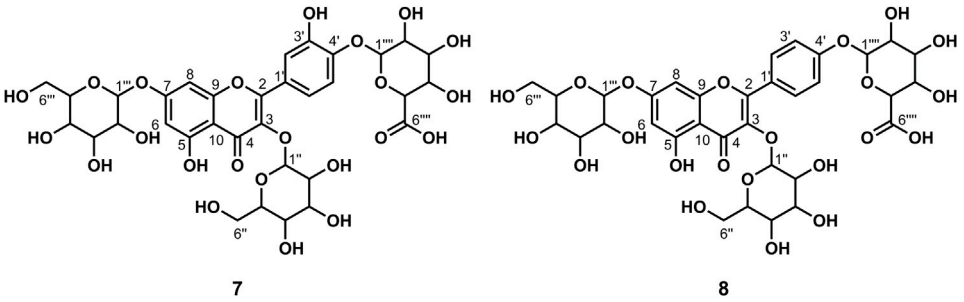

7 8

FIGURE 4
Chemical structure of compounds **7** and **8**

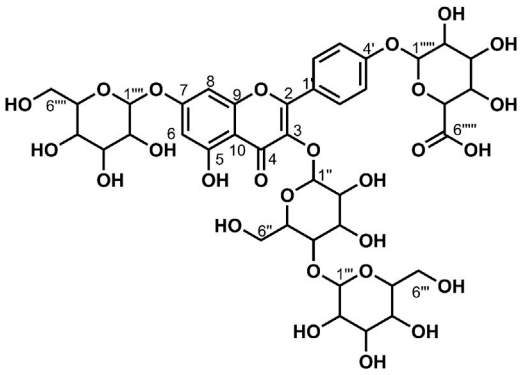

FIGURE 5
Chemical structure of compound **9**.

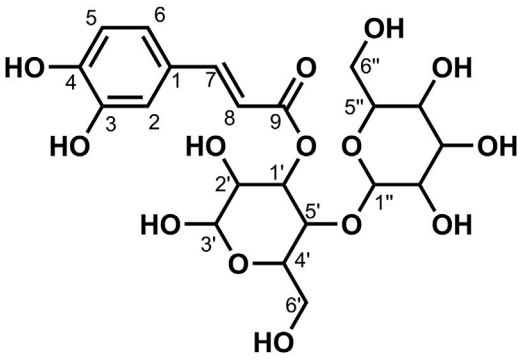

FIGURE 6
Chemical structure of compound **10**.

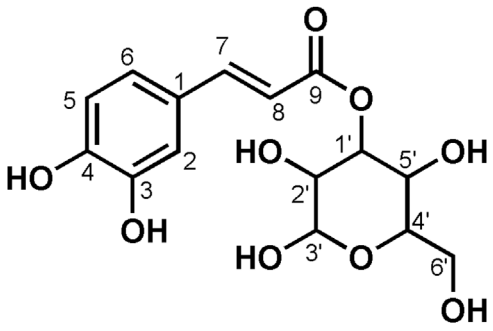

FIGURE 7
Chemical structure of compound **11**.

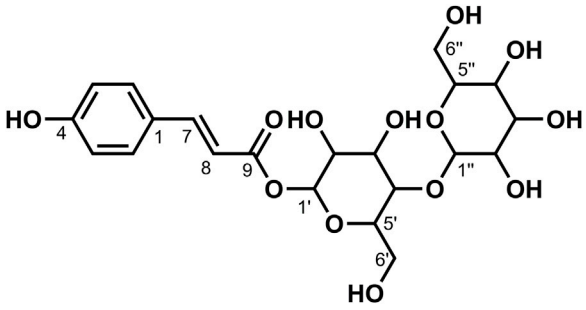

FIGURE 8
Chemical structure of compound **12**.

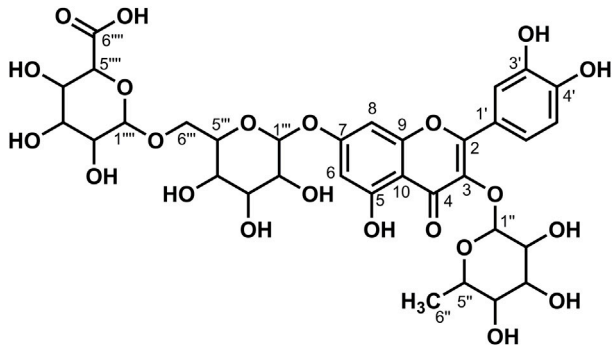

FIGURE 9
Chemical structure of compound **13**.

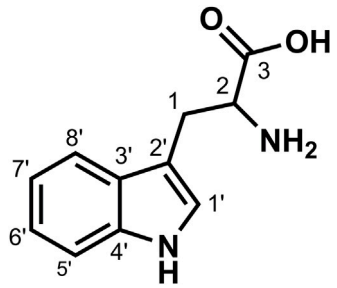

FIGURE 10
Chemical structure of compound **14**.

177.75 (C-4), 172.00 (C-6‴'), 162.68 (C-7), 160.85 (C-5), 156.07 (C-2), 156.07 (C-9), 147.67 (C-4′), 146.19 (C-3′), 134.16 (C-3), 124.33 (C-1′), 121.06 (C-6′), 116.64 (C-2′), 115.45 (C-5′), 105.81 (C-10), 101.48 (C-1‴), 100.65 (C-1″), 99.35 (C-1‴'), 99.20 (C-6), 94.33 (C-8),77.69 (C-5″), 77.26 (C-5‴), 76.50 (C-3″), 75.94 (C-3‴'), 75.83 (C-3‴), 74.85 (C-5‴'), 74.12 (C-2″), 73.26 (C-2‴), 72.80 (C-2‴'), 71.49 (C-4‴'), 70.00 (C-4″), 69.78 (C-4‴), 60.97 (C-6″), and 60.72 (C-6‴). According to the abovementioned data and literature (Fossen et al., 2006; Dong et al., 2020), compound **7** was identified as Quercetin-3,7-*O*-diglucoside-4′-*O*-glucuronide and its molecular formula is shown in Figure 4. MS diagrams and ^{1}H-NMR and ^{13}C-NMR spectra were shown in Supplementary Figures S19–S21, respectively.

Data for compound **8**: pale yellow powder, m. p. 185–187°C; ESI-MS: Calcd for $C_{33}H_{38}O_{22}$ ([M + H]$^+$), 787.29; ^{1}H NMR (400 MHz, DMSO-d_6) δ:12.56 (s, 1H, H-5), 8.15 (d, J = 8.9 Hz, 2H, H-2′, 6′), 7.18 (d, J = 8.9 Hz, 2H, H-3′, 5′), 6.87 (d, J = 2.2 Hz, 1H, H-8), 6.47 (d, J = 2.2 Hz, 1H, H-6), 5.52 (d, J = 4.7 Hz, 1H), 5.48 (d, J = 7.3 Hz, 1H, H-1″), 5.35 (dd, J = 11.6, 4.5 Hz, 2H), 5.28 (d, J = 6.7 Hz, 2H), 5.12 (s, 1H), 5.09–5.01 (m, 3H), 4.97 (d, J = 4.2 Hz, 1H), 4.65–4.52 (m, 1H), 4.31 (t, J = 5.8 Hz, 1H), 4.02 (d, J = 9.3 Hz, 1H), 3.71 (dd, J = 11.5, 4.7 Hz, 1H), 3.57 (dd, J = 11.7, 5.7 Hz, 2H), 3.52–3.47 (m, 3H), 3.30–3.05 (m, 11H);^{13}C NMR (100 MHz, DMSO-d_6) δ: 177.77 (C-4), 170.23 (C-6‴'), 162.54 (C-7), 160.91 (C-5), 159.38 (C-4′), 156.24 (C-9), 156.13 (C-2), 134.07 (C-3), 130.66 (C-2′, 6′), 123.58 (C-1′), 115.85 (C-3′, 5′), 105.91 (C-10), 100.76 (C-1″), 99.97 (C-1‴), 99.33 (C-6), 99.11 (C-1‴'), 94.39 (C-8), 77.62 (C-5″), 77.11 (C-5‴), 76.55 (C-3‴), 76.45 (C-3″), 75.73 (C-3‴'), 75.27 (C-5‴'), 74.20 (C-2″), 73.23 (C-2‴), 72.77 (C-2‴'), 71.28 (C-4‴'), 69.94 (C-4″), 69.66 (C-4‴), 60.88 (C-6″), and 60.66 (C-6‴). According to the abovementioned data and literature (Dong et al., 2020), compound **8** was identified as Kaempferol-3,7-*O*-diglucoside-4′-*O*-glucuronide and its molecular formula is shown in Figure 4. MS diagrams and ^{1}H-NMR and ^{13}C-NMR spectra were shown in Supplementary Figures S22–S24, respectively.

Data for compound **9**: pale yellow powder, m. p. 181–182°C; ESI-MS: Calcd for $C_{39}H_{48}O_{27}$([M + H]$^+$), 949.52; ^{1}H NMR (400 MHz, DMSO-d_6) δ: 12.54 (s, 1H, H-5), 8.18–8.06 (m, 2H, H-2′, 6′), 7.22–7.12 (m, 2H, H-3′, 5′), 6.86 (d, J = 2.1 Hz, 1H, H-8), 6.47 (d, J = 2.1 Hz, 1H, H-6), 5.57–5.42 (m, 4H), 5.36 (d, J = 4.6 Hz, 1H), 5.22 (dd, J = 12.1, 6.0 Hz, 4H), 5.12 (s, 1H, H-1‴'), 5.08–4.96 (m, 5H), 4.76 (d,

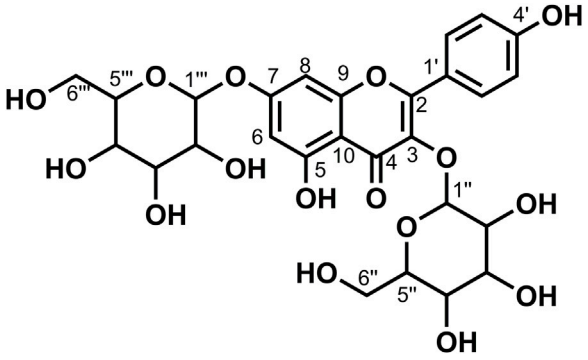

FIGURE 11
Chemical structure of compound **15**.

J = 1.9 Hz, 1H), 4.64–4.55 (m, 2H), 4.40 (t, *J* = 5.8 Hz, 1H), 4.27 (d, *J* = 7.8 Hz, 1H, H-1‴), 3.93 (d, *J* = 8.6 Hz, 1H), 3.76–3.68 (m, 3H), 3.67–3.59 (m, 2H), 3.58–3.43 (m, 5H), 3.26–3.11 (m, 7H), 3.07 (d, *J* = 9.5 Hz, 1H), 3.06–2.99 (m, 2H); ^{13}C NMR (100 MHz, DMSO-d_6) *δ*: 177.67 (C-4), 170.87 (C-6‴'), 162.69 (C-7), 160.86 (C-5), 159.39 (C-4′), 156.29 (C-2), 156.11 (C-9), 134.00 (C-3), 130.64 (C-2′, 6′), 123.50 (C-1′), 115.87 (C-3′, 5′), 105.84 (C-10), 103.09 (C-1‴), 100.51 (C-1″), 99.95 (C-1‴'), 99.40 (6), 99.21 (C-1‴'), 94.45 (C-8), 80.05 (C-4″), 77.09 (C-5‴'), 76.78 (C-5‴), 76.53 (C-3‴'), 76.44 (C-3‴),75.89 (C-3‴'), 75.50 (C-5″),74.74 (C-3″), 73.93 (C-5‴'), 73.26 (C-2‴, C-2‴'), 73.22 (C-2″), 72.80 (C-2‴'), 71.43 (C-4‴'), 70.03 (C-4‴), 69.64 (C-4‴'), 61.01 (C-6‴), 60.66 (C-6‴'), and 60.16 (C-6″). According to the abovementioned data and literature (Dong et al., 2020), compound **9** was identified as Kaempferol-3-*O*-gentiobiose-7-*O*-glucose-4′-*O*-glucuronide and its molecular formula is shown in Figure 5. MS diagrams and ^{1}H-NMR and ^{13}C-NMR spectra were shown in Supplementary Figures S25–S27, respectively.

Data for compound **10**: pale yellow crystal solid, m. p. 140–145°C; ESI-MS: Calcd for$C_{21}H_{28}O_{14}$ ([M-H]$^-$), 503.20; ^{1}H NMR (400 MHz, DMSO-d_6) *δ*: 7.55 (d, *J* = 15.9 Hz, 1H, H-7), 7.40 (d, *J* = 15.9 Hz, 1H, H-7), 7.06 (d, *J* = 2.1 Hz, 1H, H-2), 7.07–7.00 (m, 1H, H-2), 7.04–6.98 (m, 1H, H-6), 6.95 (dd, *J* = 8.2, 2.1 Hz, 1H, H-6), 6.76 (dd, *J* = 8.2, 6.0 Hz, 2H, H-5), 6.27 (d, *J* = 15.9 Hz, 1H, H-8), 6.16 (d, *J* = 15.9 Hz, 1H, H-8), 5.60–5.52 (m, 1H, H-3′), 5.15 (d, *J* = 3.4 Hz, 1H), 5.16–4.35 (m, 16H), 3.70–3.32 (m, 15H), 3.25–2.85 (m, 13H), 2.06 (s, 1H); ^{13}C NMR (100 MHz, DMSO-d_6) *δ*: 167.83 (C-9), 164.95 (C-9), 148.58 (C-4), 148.11 (C-4), 146.17 (C-7), 145.54 (C-3), 144.54 (C-3), 125.68 (C-1), 125.56 (C-1), 121.58 (C-6), 121.09 (C-6), 115.73 (C-5), 115.09 (C-5), 114.88 (C-2), 114.61 (C-2), 113.53 (C-8), 105.09 (C-1″), 104.56 (C-1″), 92.46 (C-1′), 91.44 (C-1′), 82.22 (C-2′), 81.66 (C-2′), 77.63 (C-5″), 76.83 (C-3″), 76.72 (C-3″), 76.38 (C-5′), 76.18 (C-5′), 75.75 (C-4′), 74.56 (C-3′), 73.87 (C-3′), 71.83 (C-2″), 71.68 (C-2″), 70.18 (C-2′), 70.08 (C-2′), 69.46 (C-4″), 69.17 (C-4″), 61.20 (C-6′), 61.11 (C-6″), 60.46 (C-6′), and 60.41 (C-6″). According to the abovementioned data and literature (Duan, et al., 2012; Dong et al., 2020), compound **10** was identified as 1-Caffeoyl gentiobioside (two kinds of sugar configurations: *α* and *β*) and its molecular formula is shown in Figure 6. MS diagrams and ^{1}H-NMR and ^{13}C-NMR spectra were shown in Supplementary Figures S27–S30, respectively.

Data for compound **11**: white powder, m. p. 142–144°C; ESI-MS: Calcd for $C_{15}H_{18}O_9$([M-H]$^-$), 341.17; ^{1}H NMR (400 MHz, DMSO-d_6) *δ*: 7.55 (d, *J* = 15.8 Hz, 1H, H-7), 7.08 (d, *J* = 2.1 Hz, 1H, H-2), 7.01 (dd, *J* = 8.2, 2.0 Hz, 1H, H-6), 6.78 (d, *J* = 8.2 Hz, 1H, H-5), 6.26 (d, *J* = 15.9 Hz, 1H,H-8), 5.45 (d, *J* = 7.9 Hz, 1H), 5.28 (s, 1H), 5.06 (s, 2H,H-6′), 4.58 (s, 1H), 3.69–3.62 (m, 2H), 3.31–3.10 (m, 6H); ^{13}C NMR (100 MHz, DMSO-d_6) *δ*: 165.39 (C-9), 148.81 (C-4), 146.47 (C-7), 145.70 (C-3), 125.42 (C-1), 121.74 (C-6), 115.86 (C-5), 114.91 (C-8), 113.41 (C-2), 94.31 (C-1′), 77.86 (C-5′), 76.52 (C-3′), 72.56 (C-2′), 69.60 (C-4′), and 60.67 (C-6′). According to the abovementioned data and literature (Dong et al., 2020), compound **11** was identified as 1-Caffeoyl glucoside and its molecular formula is shown in Figure 7. MS diagrams and ^{1}H-NMR and ^{13}C-NMR spectra were shown in Supplementary Figures S31–S33, respectively.

Data for compound **12**: pale yellow crystal solid, m. p. 118–119°C; ESI-MS: Calcd for $C_{21}H_{28}O_{13}$ ([M-H]$^-$), 487.21; ^{1}H NMR (400 MHz, DMSO-d_6) *δ*: 10.06 (s, 1H, H-4), 7.63 (d, *J* = 15.9 Hz, 1H, H-7), 7.59–7.54 (m, 2H,H-2, 6), 6.84–6.74 (m, 2H, H-3, 5), 6.40 (d, *J* = 16.0 Hz, 1H, H-8), 5.61–5.51 (m, 1H), 5.42 (s, 1H), 5.14 (s, 2H), 4.84 (s, 2H), 4.59 (s, 1H), 4.43 (d, *J* = 7.8 Hz, 1H), 3.67 (dd, *J* = 12.1, 2.0 Hz, 1H), 3.59–3.43 (m, 5H), 3.25–3.13 (m, 3H), 3.13–3.06 (m, 3H), 2.95 (dd, *J* = 8.9, 7.8 Hz, 1H); ^{13}C NMR (100 MHz, DMSO-d_6) *δ*: 165.01 (C-9), 160.00 (C-4), 145.74 (C-7), 130.40 (C-2), 130.04 (C-6), 125.13 (C-1), 115.78 (C-3), 11 5.31 (C-5), 113.76 (C-8), 104.57 (C-1″), 92.46 (C-1′), 81.67 (C-2′), 77.65 (C-5′), 76.76 (C-5″), 76.19 (C-3″), 75.77 (C-3′), 74.55 (C-2″), 69.52 (C-4″), 69.18 (C-4′), 60.50 (C-6″), and 60.41 (C-6′). According to the abovementioned data and literature (Dong et al., 2020), compound **12** was identified as 1-*p*-Coumaroyl gentiobioside and its molecular formula is shown in Figure 8. MS diagrams and ^{1}H-NMR and ^{13}C-NMR spectra were shown in Supplementary Figures S34–S36, respectively.

Data for compound **13**: pale yellow powder, m. p. 207–210°C; ESI-MS: Calcd for $C_{33}H_{38}O_{22}$ ([M + H]$^+$), 787.26; ^{1}H NMR (400 MHz, DMSO-d_6) *δ*: 12.62 (s, 1H, H-5), 9.74 (s, 1H, H-4′), 9.19 (s, 1H, H-3′),7.60–7.52 (m, 2H, H-2′, 6′), 6.86 (d, *J* = 8.2 Hz, 1H, H-5′), 6.74 (d, *J* = 2.1 Hz, 1H, H-8), 6.45 (d, *J* = 2.1 Hz, 1H, H-6), 5.48 (s, 1H, H-1′), 5.35 (d, *J* = 7.1 Hz, 1H), 5.25 (dd, *J* = 10.5, 5.6 Hz, 2H), 5.12–5.03 (m, 2H), 4.39 (d, *J* = 1.6 Hz, 1H), 3.94 (d, *J* = 8.8 Hz, 1H), 3.71 (d, *J* = 10.1 Hz, 1H), 3.36–3.21 (m, 15H), 3.17 (s, 1H), 3.12–3.03 (m, 2H, H-6‴), 0.98 (d, *J* = 6.2 Hz, 3H, H-6″); ^{13}C NMR (100 MHz, DMSO-d_6) *δ*: 177.51 (C-4), 170.68 (C-6‴'), 162.45 (C-7), 160.84 (C-5), 157.31 (C-2), 156.06 (C-9), 148.61 (C-4′), 144.77 (C-3′), 133.55 (C-3), 121.65 (C-1′), 121.03 (C-6′), 116.47 (C-2′), 115.21 (C-5′), 105.71 (C-10), 101.05 (C-1‴'), 100.83 (C-1″), 99.23 (C-6, 1‴), 94.45 (C-8), 76.44 (C-3‴), 75.94 (C-5‴), 75.81 (C-5‴'), 74.93 (C-3‴'), 74.02 (C-2‴), 72.85 (C-2‴'), 71.82 (C-4‴'), 71.41 (C-4″), 70.66 (C-2″), 70.35 (C-3″), 70.14 (C-4‴), 68.19 (C-5″), 67.23 (C-6‴), and 17.70 (C-6″). According to the abovementioned data and literature (Dong et al., 2020), compound **13** was identified as Quercetin-3-*O*-glucose-7-*O*-glucose (1→6)-*O*-glucuronide and its molecular formula is shown in Figure 9. MS diagrams and ^{1}H-NMR and ^{13}C-NMR spectra were shown in Supplementary Figures S37–S39, respectively.

Data for compound **14**: white powder, m. p. 211–213°C; ESI-MS: Calcd for $C_{11}H_{12}N_2O_2$ ([M + H]$^+$), 205.15; ^{1}H NMR (400 MHz, DMSO-d_6) *δ*: 11.04 (d, *J* = 2.5 Hz, 1H, H-3), 7.57

(d, J = 7.9 Hz, 1H, H-8′), 7.35 (d, J = 8.1 Hz, 1H, H-5′), 7.25 (d, J = 2.5 Hz, 1H, H-6′), 7.10–7.01 (m, 1H, H-1′), 7.01–6.92 (m, 1H, H-7′), 3.51–3.47 (m, 1H), 3.32 (dd, J = 15.1, 4.2 Hz, 1H), 3.02 (dd, J = 15.1, 8.6 Hz, 1H); ^{13}C NMR (100 MHz, DMSO-d_6) δ: 170.48 (C-3), 136.34 (C-4′), 127.30 (C-3′), 124.12 (C-1′), 120.79 (C-7′), 118.34 (C-6′), 118.20 (C-8′), 111.32 (C-5′), 109.56 (C-2′), 54.74 (C-2), and 27.11 (C-1). According to the abovementioned data, compound **14** was identified as tryptophan and its molecular formula is shown in Figure 10. MS diagrams and ^{1}H-NMR and ^{13}C-NMR spectra were shown in Supplementary Figures S40–S42, respectively.

Data for compound **15**: pale yellow powder, m. p. 179–181°C; ESI-MS: Calcd for $C_{27}H_{30}O_{16}$ ([M + H]$^+$), 611.19; ^{1}H NMR (400 MHz, DMSO-d_6) δ: 12.56 (s, 1H, H-5), 10.93 (s, 1H,H-4′), 8.16–8.08 (m, 2H, H-2′, 6′), 7.20–7.12 (m, 2H, H-3′, 5′), 6.47 (d, J = 2.1 Hz, 1H, H-8), 6.23 (d, J = 2.1 Hz, 1H, H-6), 5.47 (d, J = 7.4 Hz, 1H, 1″), 5.33 (dd, J = 14.0, 4.7 Hz, 2H), 5.12–5.00 (m, 4H), 4.93 (d, J = 4.2 Hz, 1H), 4.57 (t, J = 5.7 Hz, 1H), 4.29 (t, J = 5.6 Hz, 1H), 3.71–3.62 (m, 1H), 3.58 (dd, J = 11.3, 5.4 Hz, 1H), 3.49–3.39 (m, 1H), 3.40–3.37 (m, 1H), 3.32–3.15 (m, 6H), 3.09–3.01 (m, 2H, H-6″); ^{13}C NMR (100 MHz, DMSO-d_6) δ: 177.54 (C-4), 164.27 (C-7), 161.22 (C-5), 159.23 (C-4′), 156.45 (C-9), 155.60 (C-2), 133.73 (C-3), 130.57 (C-2′, 6′), 123.70 (C-1′), 115.81 (C-3′, 5′), 104.11 (C-10), 100.85 (C-1″), 100.00 (C-1‴), 98.76 (C-6), 93.73 (C-8), 77.56 (C-5″), 77.08 (C-5‴), 76.52 (C-3″), 76.43 (C-3‴), 74.18 (C-2″), 73.21 (C-2‴), 69.92 (C-4″), 69.61 (C-4‴), 60.87 (C-6″), and 60.63 (C-6‴). According to the abovementioned data and literature (Shan et al., 2020), compound **15** was identified as Kaempferol-3,7-*O*-diglucoside and its molecular formula is shown in Figure 11. MS diagrams and ^{1}H-NMR and ^{13}C-NMR spectra were shown in Supplementary Figures S43–S45, respectively.

Data for compound **16**: pale yellow powder, m. p. 166–168°C; ESI-MS: Calcd for $C_{27}H_{30}O_{15}$([M + H]$^+$), 595.15; ^{1}H NMR (400 MHz, DMSO-d_6) δ:12.56 (s, 1H, H-5), 10.86 (s, 1H, H-4′), 10.12 (s, 1H, H-7), 8.03–7.93 (m, 2H, H-2′, 6′), 6.92–6.84 (m, 2H, H-3′, 5′), 6.42 (d, J = 2.1 Hz, 1H, H-8), 6.21 (d, J = 2.1 Hz, 1H, H-6), 5.32 (d, J = 7.4 Hz, 1H, 1″), 4.38 (d, J = 1.6 Hz, 1H, H-1‴), 4.03 (s, 2H), 3.75–3.64 (m, 1H), 3.42 (dd, J = 3.4, 1.6 Hz, 1H), 3.32–3.25 (m, 4H), 3.69 (d, J = 9.8 Hz, 1H), 3.16–3.01 (m, 2H, H-6″), 0.99 (d, J = 6.2 Hz, 3H, H-6‴); ^{13}C NMR (100 MHz, DMSO-d_6) δ: 177.38 (C-4), 164.11 (C-7), 161.18 (C-5), 159.88 (C-4′), 156.82 (C-2), 156.48 (C-9), 133.22 (C-3), 130.84 (C-2′, 6′), 120.87 (C-1′), 115.08 (C-3′, 5′), 103.98 (C-10), 101.33 (C-1″), 100.74 (C-1‴), 98.70 (C-6), 93.72 (C-8), 76.37 (C-3″),75.75 (C-5″), 74.16 (C-2″), 71.82 (C-4‴), 70.60 (C-3‴), 70.33 (C-2‴), 69.93 (C-4″), 68.22 (C-5‴), 66.88 (C-6″), and 17.69 (C-6‴). According to the abovementioned data and literature (Dong et al., 2015), compound **16** was identified as Kaempferol-3-*O*-rutinoside and its molecular formula is shown in Figure 3. MS diagrams and ^{1}H-NMR and ^{13}C-NMR spectra were shown in Supplementary Figures S46–S48, respectively.

3.2 Disscusion

As a plant found in the desert of the Inner Mongolia, Ningxia, Gansu Region, *A. mongolicum* belongs to the genus *Allium* of the Liliaceae family (Wang et al., 2013; Wang et al., 2019). *A. mongolicum* was taken as a vegetable with local characteristics for cuisine and seasoning due to its unique flavor and high nutritional value, which can improve the cooking quality of mutton (Dong et al., 2020). There are a few reports about the extract of *A. mongolicum* to control some foodborne microorganism pathogens. The ethanol extract and aqueous extract of *A. mongolicum* showed antimicrobial activity against *Staphylococcus aureus*, *Escherichia coli*, *Saccharomyces cerevisiae*, and so on (Li and Luo, 2008; Liang et al., 2014). There have been some reports that essential oil, polysaccharides, and flavonoids of *A. mongolicum* exhibited good inhibitory activity against foodborne microorganism pathogens such as *Staphylococcus aureus*, *Escherichia coli*, and *Salmonella enteritidi* (Wu, et al., 2011; Sa, et al., 2014; Muqier et al., 2017). In this study, the effects of different extracts of *A. mongolicum* on agricultural pathogenic fungi were studied. It was found that methanol extract and petroleum ether extract of *A. mongolicum* showed a certain inhibitory effect on tested pathogenic fungi such as *Fusarium oxysporum* and *Botrytis cinerea*. Therefore, the extract of *A. mongolicum* has potential value as a botanical fungicide for the further study.

The chemical composition of *A. mongolicum* is diverse. So far, different chemical compositions of extracts of *A. mongolicum* have been discovered based on the reference and the related reports. Thirty-one flavonoids and phenolic acids were obtained and identified in the study of the effect of *A. mongolicum* to improve gastrointestinal function (Dong et al., 2020). The essential oils of *A. mongolicum* were analyzed and identified by gas chromatography-mass spectrometry and NIST Ms Search 2.0 database to identify 37 compounds, most of which were sulfur compounds such as three dimethyl sulfide, diallyl disulphide, and so on (Wu, et al., 2011). In this study, the chemical composition of methanol extract of *A. mongolicum* were separated and identified by the mass spectrum, HPLC, ^{1}H NMR, and ^{13}C NMR spectra to gain sixteen compounds, which include nine flavonoids and six phenolic acids (cinnamic acid derivatives **1**, **2**, **3**, and **12**; caffeic acid derivatives **10** and **11**) and tryptophan. Some of the flavonoids here have been reported in *A. mongolicum* (compounds **4**, **5**, **6**, **15**, and **16**), and those compounds are secondary metabolites, which are found in most *Allium* plants such as *Allium cepa* L., *Allium fistulosum* L., and *Allium sativum* L. and exert multiple biological activities such as antioxidant and gastrointestinal motility effect improvement. Three phenolic acids (cinnamic acid derivatives **1**, **2**, and **3**) were separated in *A. mongolicum* for the first time. Cinnamic acid is organic acid occurring naturally in plants (Sova, 2012; Merlani et al., 2019). They have been reported to have antibacterial and antifungal activities and are considered promising lead compounds for

structural modification to discover bioactive compounds with significant activity (Guzman, 2014; Khan et al., 2021). Based on the existing reports about the antimicrobial activity of cinnamic acid and its derivatives, therefor it is presumed that the antifungal activity of crude extract of *A. mongolicum* may be partly due to the three phenolic acids (**1**, **2**, and **3**), which antimicrobial activity is worth further studying. In subsequent experiments, we can take cinnamic acid as a lead compound to synthesize a series of cinnamic acid derivatives with similar structures reported in this article and make a systematic study on their antimicrobial activity. Among the nine isolated flavonoids, there are four new compounds (flavonoids **7**, **8**, **9**, and **13**) found in *A. mongolicum*. As is known, natural flavonoids exist in the form of its glycosides. Compared with flavonoids that have been reported, the four new compounds here are different mainly on the position and number of glucosyl of flavanone glycosides. This study laid a foundation for the further development and utilization of extracts of *A. mongolicum* as botanical fungicides.

4 Conclusion

In this article, based on the certain inhibitory activity against nine tested pathogens of extracts of *A. mongolicum*, 16compounds were isolated and identified by HPLC, NMR, and ESI-MS, and seven compounds including cinnamic acid derivatives and flavonoids were gained from *A. mongolicum* for the first time. According to our knowledge, the antimicrobial research of *A. mongolicum* almost focused on controlling some foodborne microorganism pathogens. Therefore, this study laid a foundation for the systematic research on the inhibitory effect of compounds of *A. mongolicum* on common plant-pathogenic fungi also provides good guidance for further study to discover potential antifungal agents. The follow-up study is in process, and more interesting results deserve attention.

Data availability statement

The original contributions presented in the study are included in the article/Supplementary Material, and further inquiries can be directed to the corresponding authors.

Author contributions

HQ: experimental design and the draft writing; ZG: experimental implementation and structural identification; LM, XZ, and HM: participating in part experimental processes; YC: improving manuscript quality and language polishing.

Funding

This work was supported by the National Natural Science Foundation of China (No. 31960551), The Fourth Batch of Ningxia Youth Talents Supporting Program, China (No. TJGC2019070), Postgraduate Innovation Project of North Minzu University, China (No. YCX22174), and the Science and Technology Foundation of Guizhou Province (2020) (1Y108).

Conflict of interest

The authors declare that the research was conducted in the absence of any commercial or financial relationships that could be construed as a potential conflict of interest.

Publisher's note

All claims expressed in this article are solely those of the authors and do not necessarily represent those of their affiliated organizations, or those of the publisher, the editors, and the reviewers. Any product that may be evaluated in this article, or claim that may be made by its manufacturer, is not guaranteed or endorsed by the publisher.

Supplementary material

The Supplementary Material for this article can be found online at: https://www.frontiersin.org/articles/10.3389/fchem.2022.993893/full#supplementary-material

References

Akhter, W., Bhuiyan, M. K. A., Sultana, F., and Hossain, M. M. (2015). Integrated effect of microbial antagonist, organic amendment and fungicide in controlling seedling mortality (*rhizoctonia solani*) and improving yield in pea (*pisum sativum* L.). *Comptes Rendus Biol.* 338, 21–28. doi:10.1016/j.crvi.2014.10.003

Chen, C., Liu, C. H., Cai, J., Zhang, W., Qi, W.-L., Wang, Z., et al. (2018). Broad-spectrum antimicrobial activity, chemical composition and mechanism of action of garlic (*Allium sativum*) extracts. *Food control.* 86, 117–125. doi:10.1016/j.foodcont.2017.11.015

Dong, Y. J., Qu, L., Li, X. X., Han, L. F., Wang, T., and Zhang, W. (2015). Isolation and structure identification of chemical constituents from *Allium mongolicum* Regel I. *Chin. J. Med. Chem.* 25 (4), 298–302. doi:10.14142/j.cnki.cn21-1313/r.2015.04.011

Dong, Y., Ruan, J., Ding, Z., Zhao, W., Hao, T., Zhang, Y., et al. (2020). Phytochemistry and comprehensive chemical profiling study of flavonoids and phenolic acids in the aerial parts of *Allium mongolicum* Regel and their intestinal motility evaluation. *Molecules* 25 (3), 577. doi:10.3390/molecules25030577

Dong, Y. Z., Shi, W. Z., Yang, S. C., Li, X. X., Zhang, W., and Wang, T. (2016). Isolation and structure identification of chemical constituents from *Allium mongolicum* Regel Ⅱ. *J. Tianjin Univ. Tradit. Chin. Med.* 35 (6), 404–408. doi:10.11656/j.issn.1673-9043.2016.06.11

Duan, Y., Dai, Y., He, R., Kurihara, H., Li, Y., and Yao, X. (2012). A new phenylpropanoid glucoside from the aerial parts ofLygodium japonicum. *J. Asian Nat. Prod. Res.* 14 (3), 286–292. doi:10.10.80/10286020.2011.65069010.1080/10286020.2011.650690

Fossen, T., Andersen, Ø. M., and Markham, K. R. (2005). *Flavonoids: Chemistry, biochemistry and Applications chapter: Spectroscopic techniques applied to flavonoids*. Boca Raton: Taylor and Francis CRC Press, 37–142. doi:10.1201/9781420039443.ch2 S3pectroscopic techniques applied to flavonoids

Gao, T., Zhou, H., Zhou, W., Hu, L., Chen, J., and Shi, Z. Q. (2016). The fungicidal activity of *thymol* against *Fusarium graminearum* via inducing lipid peroxidation and disrupting ergosterol biosynthesis. *Molecules* 21 (6), 770. doi:10.3390/molecules21060770

Guo, Y. Y., Chen, J. B., Ren, D., Du, B., Wu, L., Zhang, Y. Y., et al. (2021). Synthesis of osthol-based botanical fungicides and their antifungal application in crop protection. *Bioorg. Med. Chem.* 40, 116184. doi:10.1016/j.bmc.2021.116184

Guzman, D. J. (2014). Natural cinnamic acids, synthetic derivatives and hybrids with antimicrobial activity. *Molecules* 19 (12), 19292–19349. doi:10.3390/molecules191219292

Hu, J., Hu, X., Zhang, Q., Zhang, J., Fan, B., and Yu, Q. (2017). Development of SSR molecular markers for *Allium mongolicum*. *Genes. Genom.* 39, 1387–1394. doi:10.1007/s13258-017-0601-0

Jiang, M., and Ying, X. (2017). Isolation and identification of two tyramine alkaloids from *portulaca oleracea* L. *J. Liaoning Univ. Tcm.* 19 (9), 48–51. doi:10.13194/j.issn.1673-842x.2017.09.013

Kang, Z. S. (2010). Current status and development strategy for research on plant fungal diseases in China. *Plant Prot. Sci.* 36 (3), 9–12. doi:10.3969/j.issn.0529-1542.2010.03.003

Khan, F., Bamunuarachchi, N. I., Tabassum, N., and Kim, Y. M. (2021). Caffeic acid and its derivatives: antimicrobial drugs toward microbial pathogens. *J. Agr. Food Chem.* 69 10, 2979–3004. doi:10.1021/acs.jafc.0c07579

Kim, B. S., and Hwang, B. K. (2007). Microbial fungicides in the control of plant diseases. *J. Phytopathol.* 155, 641–653. doi:10.1111/j.1439-0434.2007.01314.x

Kim, D. K., and Lee, K. (2003). Inhibitory effect of *Trans*-N-p-coumaroyl tryamine from the twigs of *Celtis chinensis* on the acetylcholinesterase. *Arch. Pharm. Res.* 26 (9), 735–738. doi:10.1007/BF02976684

Li, Y. L., and Luo, M. R. (2008). Study on antibacterial effect of extracts from *Allium mongolicum* Regel. *J. Anhui Agri. Sci.* 36 (33), 14596–14597. 14618. doi:10.13989/j.cnki.0517-6611.2008.33.151

Liang, F., Li, Y. L., Zhao, J., Chai, C. F., and Wu, T. Y. (2014). Study on the extraction Technology of *Alium mongolicum* Regel bacteriostatic components and optimization. *Food Res. Dev.* 35 (20), 32–35. doi:10.3969/j.issn1005-6521.2014.20.008

Liu, W. D., and Wang, G. L. (2016). Plant innate immunity in rice: A defense against pathogen infection. *Natl. Sci. Rev.* 3 (3), 295–308. doi:10.1093/nsr/nww015

Liu, X., Yan, D., Ouyang, Y. C., Yang, D., Wang, Q., Li, L., et al. (2017). Oils extracted from *eupatorium adenophorum* leaves show potential to control *phythium myriotylum* in commercially-grown ginger. *Plos One* 12 (5), e0176126. doi:10.1371/journal.pone.0176126

Ma, C. J., Zhao, L. H., Yang, F., Li, J. Y., and Bao, B. (2014). A contrast research of bacteriostatic effect by three common liliaceous plants. *Sci. Technol. Food. Ind.* 35 (11), 52–56. doi:10.13386/j.issn1002-0306.2014.11.002

Martins, N., Petropoulos, S., and Ferreira, I. C. (2016). Chemical composition and bioactive compounds of garlic (*Allium sativum* L.) as affected by pre- and post-harvest conditions: A review. *Food Chem.* 211, 41–50. doi:10.1016/j.foodchem.2016.05.029

Merlani, M., Barbakadze, V., Amiranashvili, L., Gogilashvili, L., Poroikov, V., Petrou, A., et al. (2019). New caffeic acid derivatives as antimicrobial agents: design, synthesis, evaluation and docking. *Curr. Top. Med. Chem.* 19 4, 292–304. doi:10.2174/1568026619666190122152957

Muqier, Q. S., Qi, T., Wang, R. W., Chen, C. F., Wang, C. J., and Ao, C. (2017). Effects of flavonoids from *Allium mongolicum* Regel on growth performance and growth-related hormones in meat sheep. *Anim. Nutr.* 3 (1), 33–38. doi:10.1016/j.aninu.2017.01.003

Nicastro, H. L., Ross, S. A., and Milner, J. A. (2015). Garlic and onions: Their cancer prevention properties. *Cancer Prev. Res.* 8 (3), 181–189. doi:10.1158/1940-6207.CAPR-14-0172

Prashith Kekuda, K., Akarsh, S., Darshini, S. M., Prafulla, D., and Raghavendra, H. L. (2015). Antiradical and antimicrobial activity of atylosia lineata wt. and arn. *Sci. Technol. Arts Res. J.* 4 (3), 180–183. doi:10.4314/star.v4i3.27

Qin, J. H., He, H. Z., Luo, S. M., and Li, H. S. (2013). Effects of rice-water chestnut intercropping on rice sheath blight and rice blast diseases. *Crop Prot.* 43, 89–93. doi:10.1016/j.cropro.2012.09.009

Sa, R. L., Mu, Q. E., Wang, C. F., Bao, L. L., Ao, C. J., and Wang, S. Z. (2014). Total F1avonoids from *Alium mongolicum* Regel: Optimization of extnacton process and antioxidant and antibacterial effects in viro. *Food Sci.* 35 (24), 1–8. doi:10.7506/spkx1002-6630-201424001

Shan, X. M., Li, Z. X., Gao, Y., and Yu, X. P. (2020). Recent advances in chemical compositions and biological activity of *Allium mongolicum* Regel. *Spec. Wild Econ. Anim. Plant Res.* 42 (04), 89–94. doi:10.16720/j.cnki.tcyj.2020.04.015

Sova, M. (2012). Antioxidant and antimicrobial activities of cinnamic acid derivatives. *Mrmc* 12 (8), 749–767. doi:10.2174/138955712801264792

Wang, G. Z., Gao, S., Li, H. Q., and Wang, X. J. (2013). Physiological characteristics, functional components, development and utilization of *Allium mongolicum* Regel. *Hubei Agric. Sci.* 52 (15), 3. doi:10.3969/j.issn.0439-8114.2013.15.003

Wang, J. K., Yang, F., and Bao, B. (2012). Identification of volatile compounds in *Allium mongolicum* Regel by head space solid phase micro-extraction coupled to gas chromatography-mass spectrometry (HS-SPME-GC-MS). *Food Sci. Technol.* 33 (24), 171–173. doi:10.13386/j.issn1002-0306.2012.24.002

Wang, W., Li, L., Zhang, H., Wang, X., Fan, X., and Zhang, X. (2019). Phenolic compounds and bioactivity evaluation of aqueous and methanol extracts of *Allium mongolicum* Regel. *Food Sci. Nutr.* 7, 779–787. doi:10.1002/fsn3.926

Wu, R. Z. G., Zhang, X. F., and Ao, C. J. (2011). Studies on extracting technics of essential oils from *Allium mngolicum* Regel. *Feed Ind.* 32 (7), 37–40. doi:10.3969/j.issn.1001-991X.2011.07.011

Xing, X. K. (2018). Endophytic fungal resource of medicinal plants-A treasure need to Be developed urgently. *Mycosystema* 37 (1), 14–21. doi:10.13346/j.mycosystema.170250

Zhang, S. W., Xu, B. L., Zhang, J. H., and Gan, Y. T. (2018). Identification of the antifungal activity of *trichoderma longibrachiatum* T6 and assessment of bioactive substances in controlling phytopathgens. *Pesticide Biochem. Physiology* 147, 59–66. doi:10.1016/j.pestbp.2018.02.006

Zhang, T. Y., Chen, H. K., and Zhang, C. R. (2014). Polymorphic microsatellite markers for *Allium mongolicum* Regel (amaryllidaceae). *Genes. Genet. Syst.* 89 (3), 133–136. doi:10.1266/ggs.89.133

Zhang, Y., Yu, Q., Zhang, Q., Hu, X., Hu, J., and Fan, B. L. (2017). Regional-scale differentiation and phylogeography of a desert plant *Allium mongolicum* (Liliaceae) inferred from chloroplast DNA sequence variation. *Plant Syst. Evol.* 303 (4), 451–466. doi:10.1007/s00606-016-1383-6

Zhongren Yang, Z. R., Lizhen Hao, L. Z., Ping Wang, P., Fenglan Zhang, F. L., Qingyan Zhao, Q. Y., Xiaoing Li, fnm, et al. (2008). Nutrient composition of *Allium mongolicum* Regel seeds collected from inner Mongolia, China. *Acta Hortic.* 769, 91–95. doi:10.17660/actahortic.2008.769.10

frontiers | Frontiers in Chemistry

TYPE Original Research
PUBLISHED 01 September 2022
DOI 10.3389/fchem.2022.988587

OPEN ACCESS

EDITED BY
Hu Li,
Guizhou University, China

REVIEWED BY
Wei Wang,
Hunan Institute of Science and Technology, China
Dongmei Qi,
Zhejiang University, China
Yun Yang,
Hanjiang Normal University, China

*CORRESPONDENCE
Lei He,
helei0304@gmail.com

SPECIALTY SECTION
This article was submitted to Green and Sustainable Chemistry, a section of the journal Frontiers in Chemistry

RECEIVED 07 July 2022
ACCEPTED 26 July 2022
PUBLISHED 01 September 2022

CITATION
Liu Q, Li X and He L (2022), Health risk assessment of heavy metals in soils and food crops from a coexist area of heavily industrialized and intensively cropping in the Chengdu Plain, Sichuan, China. *Front. Chem.* 10:988587. doi: 10.3389/fchem.2022.988587

Health risk assessment of heavy metals in soils and food crops from a coexist area of heavily industrialized and intensively cropping in the Chengdu Plain, Sichuan, China

Qing Liu[1], Xiaohui Li[2] and Lei He[2]*

[1]School of Chemistry and Chemical Engineering, Anshun University, Anshun, China, [2]College of Life Science, Sichuan Normal University, Chengdu, China

Environmental pollution caused by rapid industrial activities are becoming increasingly drastic, particularly its impact on soil and plant health. The present study was conducted to investigate the heavy metal (loid) (As, Cd, Cu, Hg, Pb, and Zn) concentrations in soils and food biomass crops and estimate the potential health risks of metals to humans *via* consumption of contaminated food biomass crops from Shifang, a periurban agricultural areas in the Chengdu Plain, Sichuan, China. Results revealed that the soils have been experiencing a substantial accumulation of heavy metals, especially for Cd, with a mean of 0.84 mg kg^{-1}, about six times higher than the background values, of which 98% exceeded the pollution warning threshold of the China Soil Environmental Quality Standards. A total of 78% of all the grain part failed the national food standard for Cd. No significantly positive relationships between metal levels in food biomass crops and in the corresponding soils, indicated metals enrichment in soils were not entirely reflected to crops contaminant burdens. Estimated daily intake (EDI) of all the metals except for Pb, exceeded the oral reference dose (RfD) or the minimal risk levels recommended by USEPA and ATSDR. Target hazard quotients (THQs) of all the metals except for Cd was less than one indicated that potential health risk to the local inhabitant originated mainly from Cd exposure *via* cereals consumption. Mitigation strategies to curtail Cd-contaminated soils and crops Cd burdens need careful tailoring to meet the needs of health and safety in this region.

KEYWORDS

heavy metals, food crops, health risk, daily intake, Chengdu Plain

1 Introduction

Nowadays, environmental pollution and the greenhouse effect are becoming increasingly drastic. Among them, potential environmental and human risks of exposure to heavy metals through diet become an important issue of public health concern, but such information remains still fragmentary and scattered in an area of intensively cropping and heavily industrialized coexist (Masindi and Muedi, 2018; Briffa et al., 2020). Heavy metals are ubiquitous in the environment, with either natural or anthropogenic origin (Wu et al., 2016). Anthropogenic activities, such as mining, solid waste disposal, sludge applications, and industrial processing are the main sources of heavy metals soil contamination (Sodango et al., 2018; Timothy and Tagui Williams, 2019; Sharma et al., 2021). In addition, excessive use of pesticides and fertilizers, and wastewater irrigation also play an important role in the contamination of foodstuffs by heavy metals (Loutfy et al., 2012; Zwolak et al., 2019; Qin et al., 2021). Toxic heavy metals released by anthropogenic activities into ecosystems may lead to geo-accumulation, bio-accumulation, and biomagnification. In agricultural ecosystems, excessive accumulation of heavy metals in agricultural soils leads to elevated heavy metals uptake by food biomass crops, which is of great concern because of potential health risk to humans (Ali et al., 2019; Afonne and Ifediba, 2020; Hasan et al., 2020). Consumption of food biomass crops contaminated with heavy metals is a major food chain route for human exposure. Recently, there have been increasing interests in human health risk caused by consuming heavy metal contaminated food (Sall et al., 2020; Zheng et al., 2020; Ahmad et al., 2021; Alengebawy et al., 2021). The Food and Agricultural Organization of the United Nations (FAO), World Health Organization (WHO), United States Environmental Protection Agency (USEPA), the Agency for Toxic Substances and Disease Registry (ATSDR), and other regulatory bodies of various countries have established maximum permissible limits (MPL) of heavy metals in foodstuffs and offered some methods for health risk assessment. Based on these methods, numerous studies have been conducted on potential health risk assessment of heavy metals contaminated in soils and crops in different regions (Saha et al., 2016; Ishtiaq et al., 2018; Bello et al., 2019; Lien et al., 2021; Setia et al., 2021; Udom et al., 2022). But such information from an intensively cultivated areas remains still fragmentary (Bhatti et al., 2018; Zheng et al., 2020).

The Chengdu Plain, the"Land of Abundance" in China, is an important agricultural region and has also experiencing rapid change of socio-economic structur e changes. Urbanization, industrialization, and agricultural intensification have caused an increase of large amounts of metal-contained agrochemicals, wastes, and sewages in the agricultural environment. Previous studies in the Chengdu Plain reveal an obvious increase of heavy metals, especially cadmium (Cd) and mercury (Hg) in soils in the past decades (Qin et al., 2013; Wang et al., 2017; Deng et al., 2019; Wang et al., 2019). Increased heavy metals in soil results not only in soil quality deteriorating but may also affect agricultural product safety. There is a probable accumulation of heavy metals in crops grown in this region. However, studies have suggested that the knowledge of total concentration of metals alone is not sufficient to evaluate phytotoxic risk and human health risk (Yuswir et al., 2015; Tapia-Gatica et al., 2020); Huang et al. (2018) suggest that exposure to heavy metals through rice intake was the most important single health risk contributor. Dietary intake through contaminated foods has become the main route of heavy metal intake by humans (Chen et al., 2018). Therefore, the risk assessment of exposure to heavy metals through diet becomes an important health issue.

The coexist area of heavily industrialized and intensively cropping occupied a considerable proportion in the Chengdu Plain. Many previous studies only considered the levels of heavy metals in the soils and/or vegetables (Liu et al., 2004; Jin et al., 2008; Qin et al., 2013) and no studies have investigated the bio-accumulation of heavy metals in food crops from the soils in the coexist area. On the one hand, there are a large number of industrial pollution sources from such as the chemical industry, metal smelting, and cement production in the coexist areas, pollutants enter into farmland are inevitable through atmospheric deposition, wastewater, and solid waste discharge. On the other hand, highly intensive farming systems also bring a certain amount of heavy metals to the agricultural environment through the application of chemical fertilizers and pesticides. Health consequences of these pollution to local residents need to understand assessment, which has certain implications for changes in local planting structures and risk mitigation strategies or the safe usage of farmlands.

In order to enable the development of appropriate environmental and/or health guidelines, it is essential to have an understanding of the universal range of heavy metals concentrations in crops on the intensively cultivated area. Such data are also important to assist in assessing any potential risk to the environment or human health. The purpose of this study is to 1) identify the concentration of heavy metals in soils, rice, and maize; 2) evaluate the potential health risk associated with heavy metals through consumption of rice and maize using estimated daily intake (EDI) and target hazard quotient (THQ).

2 Materials and methods

2.1 Study area

The research area is composed of the whole flat area of Shifang city and parts of Guanghan city and Mianzhu city, situating at the northwest of the Chengdu Plain, Sichuan

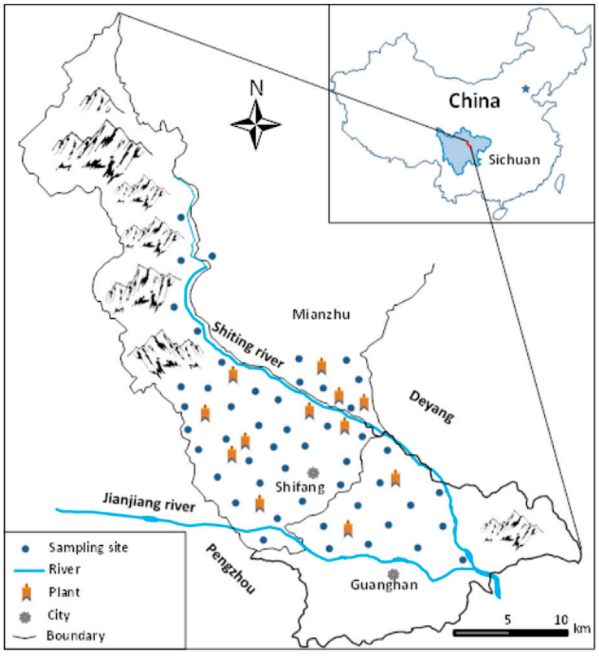

FIGURE 1
Schematic map of sampling sites in the study area, Sichuan province (southwest China).

province, southwestern China (103°58′–104°22′E, 30°58′–31°23′N) (Figure 1). Climate is subtropical humid climate, with mean annual temperature of −16°C and mean annual rainfall of 940 mm. Parent materials of soils are mainly alluvial of the Min River. Major soil types are Hapli-Stagnic Anthrosols and Gleyi-Stagnic Anthrosols in the Chinese Soil Taxonomy (Gong and Li, 2001).As a heavily industrial activities and intensively farming coexist area, the study area has diverse industrial clusters, including food, metallurgical, construction materials, pharmaceutical, chemical, and leather industry in the flat part, whereas the mountainous/hill part being phosphorus ore, coal, and limestone mining.

Rice is cultivated on 90% of the total arable lands, rest be used for maize, wheat, vegetable, and mushroom cultivating (Wang M. et al., 2016). Agriculture depends on agrochemicals. It is a typical area that intensive crop farming mingled with heavily industrial operations in the Chengdu Plain.

2.2 Sample collection

The systematic random sampling method was used to collect samples. A sampling grid overlay on the study region (Figure 1), then the samples were collected at the node areas of a regular grid of about 3 km × 3 km. At each sampling site, a clean plastic shovel was used to collect 5–7 randomly subsamples at the 0–20 cm depth to form one representative composite sample of at least 500 g by the quartering method and put in a cleaned zip-lock plastic bag for the laboratory analysis. At each soil sampling sites, 3–5 subsamples of the edible part of maize mature seeds and/or the ear of rice were collected at random, and a composite sample at least 300 g was made for each crop. In total, the samples of 40 paddy soils, 10 dryland soils, 40 rice, and 10 maize were collected.

2.3 Analyses of samples

Soil samples were screened of debris and stones, air-dried, and crushed to pass through a 2-mm sieve. Each sample was homogeneized and quartered, representative subsamples of ≤2 mm size fraction were grounded in an agate mortar to pass a 0.149-mm sieve and prepared for chemical analysis. Samples of rice and maize were washed with deionized water to remove all visible soil particles or dusts, oven-dried at 60°C. After rice husks were removed, rice grains were grounded in a stainless steel mill to a fine powder and stored in plastic bags for further chemical analysis. Corn kernels were also prepared in the same way as analytical samples.

Soil pH was measured by a pH meter with soil/H_2O ratio of 1:2.5 (soil:solution, dry w/v). The organic matter content was determined by the Walkley-Black procedure. Cation exchange capacity (CEC) was determined using NH_4OAc at pH 7.0, the leaching method of the Soil Survey Staff (1996). Soil samples were digested by concentrated acid mixture (HNO_3, $HClO_4$, and HF), and food crop samples were digested with HNO_3 and $HClO_4$ in a 5:1 ratio. The acid digested soil and crop samples were filtered and diluted with distilled water to 50 and 10 ml, respectively. Concentration of total Pb, Cd, Cu, and Zn in the digests was measured using an atomic absorption spectrophotometer (Analyst 800 P.E.) equipped with a heated graphite furnace system (THGA-800 P.E.), while As and Hg were determined by atomic fluorescence spectrometer (AFS-830a).

2.4 Quality control and assurance

To ensure the quality of metals analysis, certified reference material (CRM) (from the National Research Center for Standards in China, Beijing) including Sichuan basin soil (GBW07428) and Sichuan rice flour (GBW10044) was used to validate the analysis. The average rice flour CRM recoveries ranged from 91 to 101%, 94 to 100%, 96 to 101%, 98 to 101%, 96 to 103%, and 90 to 105% for Cd, As, Pb, Cu, Zn, and Hg, respectively. The mean recoveries for soil CRM's ranged from 89 to 100%, 97 to 104%, 98 to 102%, 97 to 100%, 98 to 101%, and 95 to 103% for Cd, As, Pb, Cu, Zn, and Hg.

2.5 Data analysis

2.5.1 Bio-accumulation factor

Metal concentrations of soils and grains were calculated on the basis of dry weight. The bio-accumulation factor (BAF), a ratio of the contaminant in food crops to the concentration in the soil substrate, was calculated using the following equation:

$$\mathrm{BAF} = \frac{C_{plant}}{C_{soil}},$$

where C_{plant} and C_{soil} represent the heavy metal (loid) concentration in the edible part of food crops and soils on dry weight basis, respectively.

2.5.2 Estimated daily intake of metals

The estimated daily intake (EDI) of the specific metal depended on both the metal concentration in the edible part of food crops and the amount of consumption of the respective food. The EDI was determined by the following equation:

$$\mathrm{EDI} = \frac{C_{metal} \times CF \times W_{food}}{BW},$$

where C_{metal} (mg kg^{-1}, on dry weight basis) is the concentration of metals in contaminated crops; CF denotes the conversion factor, the C_{metal} of both rice and maize were converted with a factor of 0.86 because home-stored rice and maize commonly contain water under 14% (w/w); W_{food} represents the daily average consumption of food crops in the study area; and BW is the average body weight. According to the dietary intake surveyed by Zhu et al. (2000), the local inhabitants had an average consumption per person (average 65 kg in body weight) of 363 and 45 g/day for rice and maize, respectively, for children (average 30 kg in body weight), estimated intake account for about 60% of consumption for adults.

2.5.3 Target hazard quotient

Health risks for locals through the consumption of contaminated rice and maize was assessed based on the target hazard quotient (THQ). The THQ is a ratio of determined dose of a pollutant to a reference dose level. If the ratio is less than one, the exposed population is assumed to be safe (USEPA, 2012); THQ is described by the following equation:

$$\mathrm{THQ} = \frac{EF \times ED \times FIR \times C}{RfD \times BW \times TA} \times 10^{-3},$$

where EF is the exposure frequency (365 days/year); ED is the exposure duration (70 years), equivalent to the average lifetime; FIR is the food ingestion rate (for adults, rice: 363 g/person/day, maize: 45 g/person/day; for children, rice: 218 g/person/day and maize: 27 g/person/day) (Zhu et al., 2000); C is the metal (loid) concentration in food (μg g^{-1}); RfD is the oral reference dose (As = 0.3 μg kg^{-1} d^{-1}, Hg = 0.16 μg kg^{-1} d^{-1}, Cd = 1 μg kg^{-1} d^{-1}, Pb = 4 μg kg^{-1} d^{-1}, Cu = 10 μg kg^{-1} d^{-1}, Zn = 300 μg kg^{-1} d^{-1}) (USEPA, 2008; USEPA, 2013; ATSDR, 2013); BW is the average body weight (65 kg), and TA is the averaging exposure time for non-carcinogens (365 days/year ×ED).

2.5.4 Statistical analysis

Data were statistically analyzed using a statistical package SPSS 20. Shapiro–Wilk test is used to determine whether sample data have been drawn from a normally distributed population. When the assumption of normality was met, the mean was selected to test the statistical significance of the data, including comparison the mean of two and multiple groups and analysis of variance (ANOVA), with a significance level of $p < 0.05$, and the figures also presented with the mean values and standard errors. When the assumption of normality was violated, the median was selected to do Mann–Whitney test for two groups and Kruskal–Wallis test for multiple groups, and Spearman's correlation analysis was used to test the correlation assumption.

3 Results

3.1 Heavy metals in soils

Basic soil characteristics and the concentrations of As, Cd, Hg, Pb, Cu, and Zn in soils are presented in Table 1. Soil is generally slightly acidic (mean pH 6.48), with a range of acidic (pH 4.54) to slightly alkaline (pH 7.99), in which pH value of 36 soil samples was less than seven, accounting for 72%. Soil organic matter (SOM) ranged between 54 and 112 g kg^{-1}, with a mean of 101 g kg^{-1}. Cation exchange capacity (CEC) varied considerably from 2.35 to 21.16 cmol kg^{-1}, a difference of approximately nine times. The pH value in the rainfed lands that maize cultivated soils were not markedly different, comparing with the paddy fields that rice cultivated soils ($p = 0.919$). There was also no obvious difference in SOM between rainfed lands and paddy fields ($p = 0.422$). CEC in the paddy land was significantly lower than that in rainfed lands ($p = 0.049$).

Mean concentrations of As, Cd, Hg, Pb, Cu, and Zn in soils were 8.01, 0.84, 0.19, 24.49, 25.72, and 80.12 mg kg^{-1}, respectively (Table 1). Except for Cd, all other metals were below the risk control standard for soil contamination of agricultural land (Ministry of Ecology and Environment of the PRC, 2018) (Table 1). A considerable buildup for all the metals in the soils were observed when comparison with the background values, indicating that soils in the study area had a considerably contaminated by heavy metals, especially Cd and As. Concentration of metals was higher in rainfed soil than in paddy soil (Figure 2), with As ($p = 0.001$), Cd ($p = 0.027$), and Cu ($p = 0.028$) significantly higher in rainfed soil than paddy soil, and the rest [Pb ($p = 0.156$), Hg ($p = 0.174$), Zn ($p = 0.47$)] insignificantly different.

TABLE 1 Characteristics and metal levels of the soils collected from the study area (matters content on dry weight basis).

Property	Range	Mean (n =50)	SE[a]	Background value[b]	SEPA RSV[c] (pH = 6.5–7.5)
pH (H_2O)	4.54–7.99	6.48	0.85	—	—
SOM(g kg^{-1})	54.04–112.23	101.04	20.31	—	—
CEC (cmol kg^{-1})	2.35–21.16	7.04	0.45	-	-
As (mg kg^{-1})	3.81–33.18	8.01	0.75	3.77	30
Cd (mg kg^{-1})	0.51–1.90	0.84	0.04	0.14	0.30
Hg (mg kg^{-1})	0.12–0.33	0.18	0.03	0.14	0.30
Pb (mg kg^{-1})	8.05–80.33	24.49	1.69	20.70	250
Cu (mg kg^{-1})	16.66–70.57	25.72	1.42	23.01	50
Zn (mg kg^{-1})	53.58–159.59	80.21	3.19	65.12	200

[a]SE denote standard error.
[b]Background value from Yao (1987).
[c]Risk-based screening values (RSV) of soil environmental quality risk control standard for soil contamination of agricultural land (GB 15618-2018) (Ministry of Ecology and Environment of the PRC, 2018).

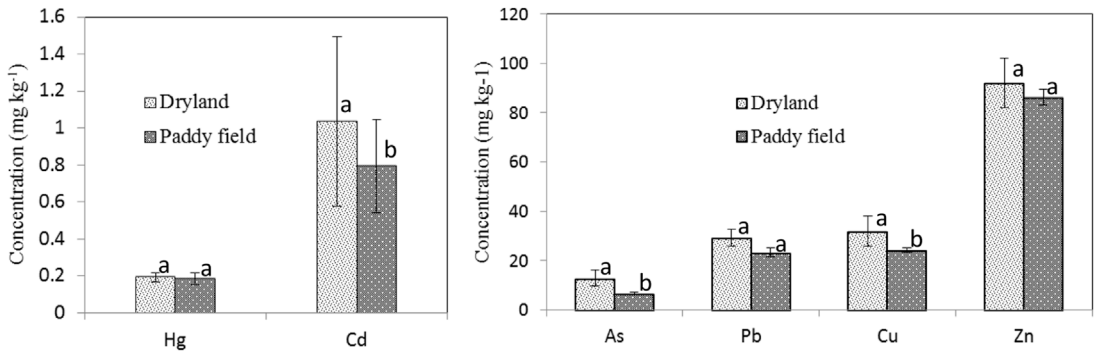

FIGURE 2
Metal concentrations (dry weight basis) in the soils from different types of farming in the study area. Data are mean ± 1SE, n = 40 for paddy soils and n = 10 for dryland soils. For each element, means with the same letter are not significantly (p > 0.05) different.

TABLE 2 Metals concentrations (on dry weight basis) in the edible parts of food crops collected from the study area.

Metal	Rice (n =40)		Maize (n =10)		
	Range	Mean ± SE	Range	Mean ± SE	MLs[a]
As (mg kg^{-1})	0.04–0.17	0.07 ± 0.01	0.04–0.13	0.06 ± 0.01	0.15 (0.2)[b]
Cd (mg kg^{-1})	0.09–1.78	0.46 ± 0.06	0.05–0.77	0.26 ± 0.08	0.2 (0.1)
Hg (mg kg^{-1})	0.002–0.21	0.01 ± 0.01	0.002–0.02	0.01 ± 0.01	0.02
Pb (mg kg^{-1})	0.06–0.58	0.30 ± 0.02	0.02–0.50	0.29 ± 0.05	0.2
Cu (mg kg^{-1})	1.48–6.33	4.14 ± 0.17	1.21–5.30	2.73 ± 0.48	10
Zn (mg kg^{-1})	27.49–53.54	39.55 ± 0.83	35.58–49.13	41.72 ± 1.48	50

[a]Maximum levels of contaminants in foods (GB 2762-2017) (Ministry of Health of the PRC, 2017).
[b]Number in parenthesis indicate maximum levels of metals in food grains other than rice.

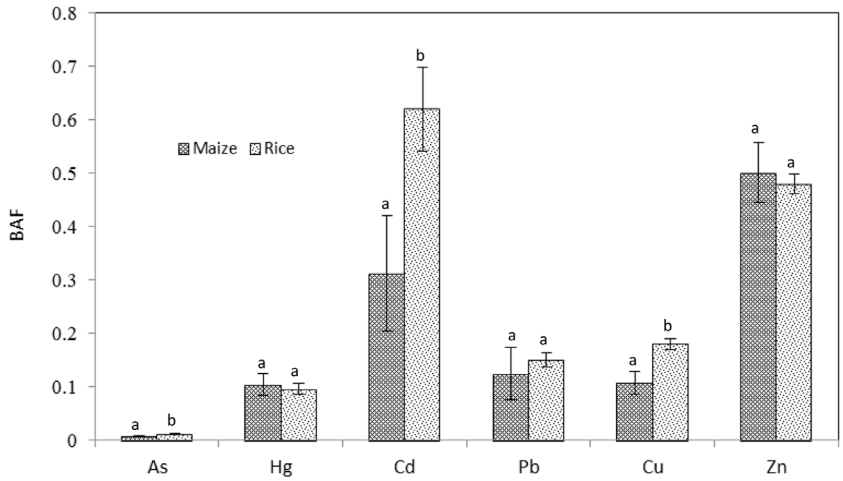

FIGURE 3
Bio-accumulation factors (BAF) for different metals, a ratio of heavy metals concentration in the edible part of maize and rice to that in the corresponding soil at the study area. Data are mean ± 1SE. For each element, means with the same letter are not significantly ($p > 0.05$) different.

3.2 Heavy metals in food crops

The average concentrations and ranges of heavy metals (on dry weight basis) in the edible portions of food crops grown in the investigated soils are given in Table 2. The average concentrations of Cd in rice and maize were 0.46 and 0.26 mg kg^{-1}, respectively (Table 2), 78% of crop samples exceeded the MPL for Cd of Chinese standard (Ministry of Health of the PRC, 2017). Mean content of Pb in rice and maize was 0.30 and 0.29 mg kg^{-1}, respectively, also overtaking the MPL. The results indicated that both rice and maize in the study area exhibited a conspicuous Cd and Pb pollution. But As, Hg, Cu, and Zn concentrations were substantially lower than the MPL in rice and maize grown in the soils of the research area (Table 2). All the metal contents except for Cu ($p = 0.001$) and Cd ($p = 0.05$) are insignificantly different between rice and maize, but the trends of heavy metal accumulations, in general, was in the order of rice > maize (Table 2).

3.3 Heavy metal transfer from soil to food crop

The bio-accumulation factor (BAF) for heavy metal transferring from soils to food crops tended to be in the order of Cd > Zn > Cu > Pb > Hg > As, and there was significantly difference in BAF values among metals ($p < 0.001$) (Figure 3). As, Cd, and Cu in the edible parts of rice were markedly higher than that of maize (Figure 3, all $p < 0.05$), whereas Hg, Pb, and Zn buildup in the corresponding parts of crops had no obvious difference. Correlation analysis reveals no significant correlation between metal concentrations in soils and in the edible parts of the plants except for Cu ($p = 0.026$), indicating that the metals content in plant does not fully reflect the total metal level in soils.

3.4 Daily intake of metals through food consumption and human health risks

Daily intake of heavy metal was estimated based on the average food consumption in the study area. The estimated daily intake (EDI) *via* consumption of rice and maize for adults and children is given in Table 3. EDI of Hg, As, Pb, Cd, Cu, and Zn for adults was 0.11, 0.44, 1.62, 2.43, 21.52, and 214.83, respectively, whereas for children it was 0.31, 0.55, 2.11, 3.12, 38.02, and 379.52, respectively. According to the oral reference dose (RfD) recommended by USEPA, ASTDR and Cal EPA, EDI of As, Cd, and Cu for adults had exceeded the reference dose (Table 3), while EDI, except for that of Pb, for children, surpassed the recommended limit. Moreover, EDIs through the consumption of rice were significantly higher than through the consumption of maize because the dietary habits of local inhabitant are centered on rice. In particular, EDI values to the local children tended to be higher over adults, indicating that the children had a relatively significant health risks *via* the consumption of metals contaminated foods.

Target hazard quotient (THQ) of metals through the ingestion of rice and maize for adults and children is shown in Figure 4. While THQ of As, Hg, Pb, Zn, and Cu for adults was below one, indicating health risk was low, THQ of Cd was close to one, suggesting a potential health threat. Analogously, THQ of As, Hg, Pb, and Zn for children from consumption of rice and maize was below one, which suggested that health risk was insignificant. Conversely, THQ of Cd and Cu was bigger than

TABLE 3 Estimated daily intake (EDI) of metals by consumption of rice and maize at the investigation area (the EDI values based on the body weight of 65 and 30kg for the adults and children, respectively).

Groups	Type of food	DI[a] (g d^{-1})	As	Hg	Cd	Pb	Cu	Zn
			μg kg^{-1} d^{-1}					
Adults	Rice	363	0.43	0.11	2.21	1.43	19.91	190.02
	Maize	45	0.04	0.01	0.22	0.21	1.62	24.81
	Total		**0.47**[e]	0.11	**2.43**	1.62	**21.52**	214.83
Children	Rice	218	0.51	0.33	2.92	1.91	25.92	247.22
	Maize	27	0.05	0.01	0.21	0.23	2.13	32.33
	Total		**0.55**	**0.31**	**3.12**	2.11	**38.02**	**379.52**
RfD[b]			0.3	0.16[c]	1	4	10[d]	300

[a]DI represents dietary intake (Zhu et al., 2000).
[b]Oral reference dose base on USEPA (2013).
[c]Oral reference exposure level (REL) recommended by OEHHA at CalEPA (2013).
[d]Minimal risk levels (MRLs) recommended by Agency for Toxic Substances and Disease Registry ATSDR (2013).
[e]Data in bold represents exceeding the RfD recommended by USEPA, indicating a potential health risk.

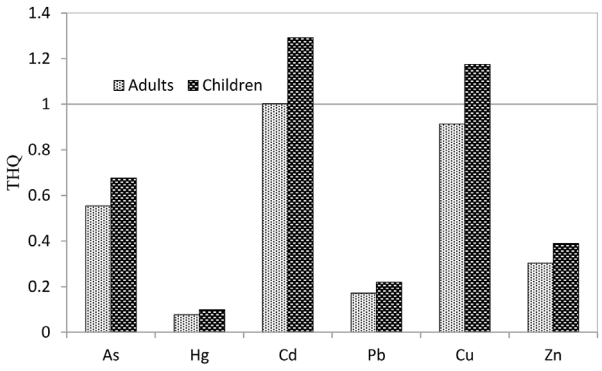

FIGURE 4
THQ values of metals through consumption of rice and maize grown at the sampling sites of the study area (a histogram above the reference line may be subjected to potentially higher health risk).

one, indicating that health risk these two metals was of a concern.

4 Discussion

4.1 Heavy metals in soils and crops

Increasing evidence (Ren et al., 2006; Tang et al., 2007; Jin et al., 2008; Qin et al., 2013) indicate that high Cd concentration in paddy soil and rice in the Chengdu Plain is a problem. All the metal concentrations except for Cd, although were still below the Grade II of the EQSS (SEPA, 2018), a substantial accumulation of metals in the soils was found when compared with the background values (Yao, 1987), on average concentrations of As, Hg, Pb, Cu, and Zn increasing up to 112, 30, 18, 12, and 23%, respectively (Table 1). These results agreed with the findings of previous studies in the Chengdu Plain (Qin et al., 2013; Wang et al., 2017; Deng et al., 2019). Cd concentrations in 49 soils were above the pollution warning threshold of the EQSS, accounting for about 98%, indicating that soils suffered generally from Cd contamination. This may have been due to the fact that diversity industries embedded in an intensively cultivated area, such as phosphorus chemicals, leather chemicals, old or currently active mining or ore processing facilities, with mine waste runoff or overspill tainted irrigation water, atmospheric deposition resulting from ore smelting, and application of agrochemicals, all may contribute to Cd contamination and others metals buildup in soils (Qin et al., 2013). Many previous studies suggested that long-term wastewater irrigation led to elevated levels of heavy metals in soils (Elbana et al., 2013; Christou et al., 2014; Meng et al., 2016; Abuzaid and Fadl, 2018) and revealed that the heavy metals content in soils were markedly influenced by stationary sources such as non-ferrous metal smelter, coal-fired power plant (Reza et al., 2015; Yang et al., 2017; Semenov et al., 2019; Wang et al., 2020), and non-point sources as use of fertilizers, pesticides, and bactericides (Ouyang et al., 2016; Zhang et al., 2021). These activities are inevitable in an intensively farming and heavily industrial activities coexist area.

Concentrations of Cd, As, and Cu in rainfed soils are significantly different from that in paddy soils (Figure 2), suggesting that different farming styles may potentially impact on metal concentrations in soil. It is a fact that rainfed lands are commonly used to cultivate vegetables, with a high ratio of rotation and increasing the input of agrochemicals, and more potential metals of anthropic sources being added to rainfed soils in compare to paddy soils. Metal elements may have different behaviors such as bioavailability, leachability, and mobility in various environments. An extractable form by DTPA is

commonly applied to evaluate availability in previous many studies (Kim et al., 2015; Zahedifar et al., 2017; Kaninga et al., 2020). It was reported that Cd and Cu were readily extracted by DTPA compared to Pb and Zn (Singh et al., 1998), suggesting that Cd and Cu have more bioavailability in the same field condition, and therefore it should be possible to incur more leachability and/or mobility in a wet–dry cropping rotation due to the function of water. The mobile behavior of As in soils was affected by many factors such as pH and amorphous Al and Fe contents (Violante et al., 2010; Álvarez-Ayuso et al., 2016), especially, reduction condition possibly facilitates As releasing from soil because of reducing As (V) to As (III) (Pigna et al., 2015; Guénet et al., 2017). These behaviors would show why that As levels was different between rainfed soils and paddy soils.

Heavy metal accumulation in crops is a serious concern due to potential public health implications. The data from present study indicated that the average concentration of Cd in rice and maize was 2.3 and 2.6-fold higher than the MPL (Table 2), respectively. Similarly, Pb contents in rice and maize also surpassed the MPL by about1.5 times (Table 2). The concentration of Cd in rice from the Chengdu Plain was in balance with the findings of previous studies in a mining-affected area of Hunan province (Du et al., 2013; Chen et al., 2016; Wang X. et al., 2016) but lower than those in the Dabaoshan mine area in Guangdong province (Zhuang et al., 2009). While the Cd level in corn grains was beyond that of the corn grown at Qingchengzi Pb/Zn mine soil in Liaoning province (Li et al., 2014). On average buildup of Pb in the edible part of both rice and maize reached up to about 0.30 mg kg^{-1}, ranging from 0.06 to 0.58 mg kg^{-1} for rice and 0.02–0.50 mg kg^{-1} for maize (Table 2), which was less than those in mining-affected areas (Zhuang et al., 2009). Analysis showed that no strong positive relationship between metals in the soils and in the crops. Conversely, a negative relationship between soil metal contents and crops for Cu, in addition to Cd were observed. Such inverse relationships were also reported by Khan et al. (2008) for vegetables. This may suggest that knowing total metal levels in soils use to assess health risk is inappropriate.

Soil-to-plant transfer is one of key pathways of human exposure to metals through food chain (Loutfy et al., 2006). Our results showed that BAF differ significantly among metals ($p < 0.001$) or between crops (Figure 3). Seemingly, Cd, As, and Cu transfer from soil to rice were easier than to maize (all $p < 0.05$), but the rest of the metals did not like such trend. However, the Cd, As, and Cu levels in rainfed soils where maize was cultivated, on the whole, are higher than those in paddy soils where rice was cultivated (Figure 2), suggesting that the accumulation effect depends not only on the crop's physiological properties but also on mobility and availability of metals in soils, it does not appear to be entirely associated with the total element concentrations in the soils. Some studies found that leafy vegetables can generally accumulate Pb and Cd to a higher extent than non-leafy vegetables (Zhuang et al., 2009; Nabulo et al., 2010; Chang et al., 2014; Gebeyehu and Bayissa, 2020). Cd is usually considered a highly mobile heavy metal in regard to moving from soil-to-plant and is of primary concern in soil and food contamination, particularly in rice cropping systems (Kim et al., 2015; Zhao et al., 2015). A high average BAF for Cd in rice correspond to a lower mean content of total Cd in paddy soils (Figures 2, 3). Gu et al. (2018) investigated the BAF of rice for Cd, Cu, Pb, and Zn, the results indicated that Cd and Zn showed stronger bio-accumulation and mobility capability. These findings demonstrate that Cd accumulation in rice is mainly influenced by its availability, rather than total amount in soils, which support the conclusions of many previous studies (Du et al., 2013; Jing et al., 2020).

4.2 Health risk assessment

An important aspect in assessing risk to human health from potentially harmful chemicals in food is the knowledge of the dietary intake of such substances. Based on average concentration of metals in the edible part of each food crops and the respective consumption rate (Zhu et al., 2000), EDIs of As, Cd, and Cu by consumption of rice and corn grains for the local adults were 0.44, 0.24, and 21.52 μg kg^{-1} d^{-1}, and for the local children were 0.55, 0.31, and 38.02 μg kg^{-1} d^{-1}, respectively (Table 3). These EDIs are far below those in the mining-affected areas (Zhuang et al., 2009; Du et al., 2013), but exceed the oral reference dose (RfD) recommended by USEPA (2013) and ATSDR (2013). Analogously, EDIs of Hg and Pb for the local children exceed also the RfD limits, but not for adults (Table 3). The EDIs through consumption of rice were significantly higher than that of maize due to rice as staple crop of local inhabitant. Thus, adverse health effects induced by ingesting contaminated food crops arise largely from rice consumption. Moreover, the local children intakes of metals by consumption of contaminated food crops was about 1.25–2.8 times higher than those of the local adults due to children consumption 1.3 times more food than adults relative to their body weight (Table 3). A similar phenomenon was also reported by Kim et al. (2013), they found that the mean intakes of Cd at ages 1–2 were the highest in different age groups of Korea through the intake of various agricultural products grown in greenhouse. Ding et al. (2018) investigated trace elements in soils and selected agricultural plants in the Tongling mining area of China, their findings revealed that EDI of the trace elements, except Cd, were generally below the maximum tolerable daily intake. These estimates were also consistent with the long-term dietary intake assessment on other contaminants performed by the FAO/WHO (FAO/WHO, 2005). Therefore, children as a susceptible group have a

higher health risk through consuming the same contaminated foodstuff than adults.

The estimation of target hazard quotient (THQ) offers an indication of the risk level due to pollutant exposure (USEPA, 2017; Shaheen et al., 2016; Miranzadeh Mahabadi et al., 2020). Estimated THQs of As, Hg, Pb, Zn, and Cu through consumption of rice and maize were below one for adults, while this value for Cd approached one. Concerning children, THQs of As, Hg, Pb, and Zn were also less than one, but for Cd and Cu were beyond one, suggesting that Cd and Cu exposure through daily intakes of rice and corn grains locally produced have posed a severe health risk to the local residents (Figure 4), in agreement with the conclusion of Jin et al. (2009). Although the ingested dose of heavy metals from cereals is not equal to the absorbed pollutant dose in reality due to a fraction of intake heavy metals being excreted (Balkhair and Ashraf, 2016; Yaradua et al., 2020), if considering dietary intakes from the locally produced non-cereal foods consumption such as vegetables, meat, eggs, and milk, THQ of metals, especially Cd, is certainly higher and the health risk even more severe. Consequently, effective mitigation measures are necessary to cure Cd-contaminated soils and to reduce the metal transferring from soil to crops in this region.

5 Conclusion

The soils from a heavily industrialized and intensively cultivated area in the Chengdu Plain have been experiencing a considerable accumulation of heavy metals comparison with the background values. These enrichments are not entirely reflected to crops metals burdens due to difference in bioavailability and/or mobility among metals and/or in physiological properties between crops. Health risk identified by the estimated daily intake (EDI) and target hazard quotients (THQ) suggest that potential health risk to the local inhabitant is mainly from Cd exposure, resulting from rice consumption. Mitigation strategies to curtail Cd-contaminated soils and crops Cd burdens need careful tailoring to meet the needs of health and safety in this region in the future.

Data availability statement

The original contributions presented in the study are included in the article/Supplementary Material; further inquiries can be directed to the corresponding author.

Author contributions

QL: Investigation, Visualization, Writing-original draft. XL: Methodology, Investigation, Formal analysis, LH: Conceptualization, Supervision, Writing-review and editing.

Funding

This work was financially supported by the Creative Research Groups Support Program of Guizhou Education Department [KY (2017) 049], the Guizhou Province Key Laboratory of Ecological Protection and Restoration of Typical Plateau Wetlands [(2020) 2002], and the Youth Growth S&T Personnel Foundation of the Guizhou Education Department [KY (2017) 278].

Conflict of interest

The authors declare that the research was conducted in the absence of any commercial or financial relationships that could be construed as a potential conflict of interest.

Publisher's note

All claims expressed in this article are solely those of the authors and do not necessarily represent those of their affiliated organizations, or those of the publisher, the editors, and the reviewers. Any product that may be evaluated in this article, or claim that may be made by its manufacturer, is not guaranteed or endorsed by the publisher.

References

Abuzaid, A. S., and Fadl, M. E. (2018). Mapping potential risks of long-term wastewater irrigation in alluvial soils, Egypt[J]. *Arabian J. Geosciences* 11 (15), 1–12. doi:10.1007/s12517-018-3780-3

Afonne, O. J., and Ifediba, E. C. (2020). Heavy metals risks in plant foods – need to step up precautionary measures. *Curr. Opin. Toxicol.* 22, 1–6. doi:10.1016/j.cotox.2019.12.006

Ahmad, W., Alharthy, R. D., Zubair, M., Ahmed, M., Hameed, A., and Rafique, S. (2021). Toxic and heavy metals contamination assessment in soil and water to evaluate human health risk. *Sci. Rep.* 11 (1), 17006–17012. doi:10.1038/s41598-021-94616-4

Alengebawy, A., Abdelkhalek, S. T., Qureshi, S. R., and Wang, M. Q. (2021). Heavy metals and pesticides toxicity in agricultural soil and plants: Ecological risks and human health implications. *Toxics* 9 (3), 42. doi:10.3390/toxics9030042

Ali, H., Khan, E., and Ilahi, I. (2019). Environmental Chemistry and ecotoxicology of hazardous heavy metals: Environmental persistence, toxicity, and bioaccumulation. *J. Chem.* 2019, 1–14. doi:10.1155/2019/6730305

Álvarez-Ayuso, E., Abad-Valle, P., Murciego, A., and Villar-Alonso, P. (2016). Arsenic distribution in soils and rye plants of a cropland located in an abandoned mining area[J]. *Sci. Total Environ.* 542, 238–246. doi:10.1016/j.scitotenv.2015.10.054

ATSDR (2013). "Toxicological profile for uranium," in *Agency for toxic Substances and Disease Registry (A TSDR) toxicological profiles* (Atlanta (GA): Agency for Toxic Substances and Disease Registry US).

Balkhair, K. S., and Ashraf, M. A. (2016). Field accumulation risks of heavy metals in soil and vegetable crop irrigated with sewage water in Western region of Saudi Arabia. *Saudi J. Biol. Sci.* 23 (1), S32–S44. doi:10.1016/j.sjbs.2015.09.023

Bello, S., Nasiru, R., Garba, N. N., and Adeyemo, D. (2019). Carcinogenic and non-carcinogenic health risk assessment of heavy metals exposure from Shanono and Bagwai artisanal gold mines, Kano state, Nigeria. *Sci. Afr.* 6, e00197. doi:10.1016/j.sciaf.2019.e00197

Bhatti, S. S., Kumar, V., Sambyal, V., Singh, J., and Nagpal, A. K. (2018). Comparative analysis of tissue compartmentalized heavy metal uptake by common forage crop: A field experiment. *Catena* 160, 185–193. doi:10.1016/j.catena.2017.09.015

Briffa, J., Sinagra, E., and Blundell, R. (2020). Heavy metal pollution in the environment and their toxicological effects on humans. *Heliyon* 6 (9), e04691. doi:10.1016/j.heliyon.2020.e04691

CalEPA (California Environmental Protection Agency) (2013). *Technical support document for noncancer RELs, Appendix D.1*. Sacramento, CA: Office of Environmental Health Hazard Assessment.

Chang, C. Y., Yu, H. Y., Chen, J. J., Li, F. B., Zhang, H. H., and Liu, C. P. (2014). Accumulation of heavy metals in leaf vegetables from agricultural soils and associated potential health risks in the Pearl River Delta, South China. *Environ. Monit. Assess.* 186 (3), 1547–1560. doi:10.1007/s10661-013-3472-0

Chen, D., Guo, H., Li, R., Li, L., Pan, G., Chang, A., et al. (2016). Low uptake affinity cultivars with biochar to tackle Cd-tainted rice — a field study over four rice seasons in hunan, China. *Sci. total Environ.* 541, 1489–1498. doi:10.1016/j.scitotenv.2015.10.052

Chen, L., Zhou, S., Shi, Y., Wang, C., Li, B., Li, Y., et al. (2018). Heavy metals in food crops, soil, and water in the Lihe River Watershed of the Taihu Region and their potential health risks when ingested. *Sci. total Environ.* 615, 141–149. doi:10.1016/j.scitotenv.2017.09.230

Christou, A., Eliadou, E., Michael, C., Hapeshi, E., and Fatta-Kassinos, D. (2014). Assessment of long-term wastewater irrigation impacts on the soil geochemical properties and the bioaccumulation of heavy metals to the agricultural products. *Environ. Monit. Assess.* 186 (8), 4857–4870. doi:10.1007/s10661-014-3743-4

Deng, S., Yu, J., Wang, Y., Xie, S., Ran, Z., and Wei, W. (2019). Distribution, transfer, and time-dependent variation of Cd in soil-rice system: A case study in the Chengdu Plain, southwest China. *Soil Tillage Res.* 195, 104367. doi:10.1016/j.still.2019.104367

Ding, Z., Li, Y., Sun, Q., and Zhang, H. (2018). Trace elements in soils and selected agricultural plants in the Tongling mining area of China. *Int. J. Environ. Res. Public Health*. 15 (2), 202. doi:10.3390/ijerph15020202

Du, Y., Hu, X. F., Wu, X. H., Shu, Y., Jiang, Y., and Yan, X. J. (2013). Affects of mining activities on Cd pollution to the paddy soils and rice grain in Hunan province, Central South China. *Environ. Monit. Assess.* 185 (12), 9843–9856. doi:10.1007/s10661-013-3296-y

Elbana, T. A., Ramadan, M. A., Gaber, H. M., Bahnassy, M. H., Kishk, F. M., and Selim, H. (2013). Heavy metals accumulation and spatial distribution in long term wastewater irrigated soils. *J. Environ. Chem. Eng.* 1 (4), 925–933. doi:10.1016/j.jece.2013.08.005

FAO/WHO (2005). *Food safety risk analysis. Part I. An overview and framework manual.* Rome: Food and Agriculture Organization of the United Nations and World Health Organization, 448. http://www.fao.org/3/a0822e/a0822e.

Gebeyehu, H. R., and Bayissa, L. D. (2020). Levels of heavy metals in soil and vegetables and associated health risks in Mojo area, Ethiopia. *PloS one* 15 (1), e0227883. doi:10.1371/journal.pone.0227883

Gong, Z., and Li, F. (2001). *Chinese soil taxonomy[M]*. Beijing: Science press.

Gu, Q., Yang, Z., Yu, T., Yang, Q., Hou, Q., and Zhang, Q. (2018). From soil to rice—a typical study of transfer and bioaccumulation of heavy metals in China. *Acta Agric. Scand. B Soil Plant Sci.* 68 (7), 631–642. doi:10.1080/09064710.2018.1455218

Guénet, H., Davranche, M., Vantelon, D., Bouhnik-Le Coz, M., Jardé, E., Dorcet, V., et al. (2017). Highlighting the wide variability in arsenic speciation in wetlands: A new insight into the control of the behavior of arsenic[J]. *Geochimica Cosmochimica Acta* 203, 284–302. doi:10.1016/j.gca.2017.01.013

Hasan, A. B., Reza, A. H. M., Kabir, S., Siddique, M. A. B., Ahsan, M. A., and Akbor, M. A. (2020). Accumulation and distribution of heavy metals in soil and food crops around the ship breaking area in southern Bangladesh and associated health risk assessment. *SN Appl. Sci.* 2 (2), 1–18. doi:10.1007/s42452-019-1933-y

Huang, Y., Chen, Q., Deng, M., Japenga, J., Li, T., Yang, X., et al. (2018). Heavy metal pollution and health risk assessment of agricultural soils in a typical peri-urban area in southeast China. *J. Environ. Manag.* 207, 159–168. doi:10.1016/j.jenvman.2017.10.072

Ishtiaq, M., Jehan, N., Khan, S. A., Muhammad, S., Saddique, U., Iftikhar, B., et al. (2018). Potential harmful elements in coal dust and human health risk assessment near the mining areas in Cherat, Pakistan. *Environ. Sci. Pollut. Res.* 25 (15), 14666–14673. doi:10.1007/s11356-018-1655-5

Jin, L. X., Hou, Q. Y., Bao, Y. H., Xu, Z., Li, Z. H., Yang, Z. F., et al. (2009). Assessment of ecological security and human health risk in cadmium-contaminated farmland areas in Deyang (in Chinese with English abstract)[J]. *Mod. Geol.* 22 (6), 984–989. doi:10.3969/j.issn.1000-8527.2008.06.014

Jin, L. X., Hou, Q. Y., Yang, Z. F., Bao, Y. H., Li, Z. H., Xu, Z., et al. (2008). Health risk assessment of heavy metals in farmland ecosystems in Deyang, Sichuan (in Chinese with English abstract) [J]. *Front. Geosciences* 15 (5), 47–56.

Jing, F., Chen, C., Chen, X., Liu, W., Wen, X., Hu, S., et al. (2020). Effects of wheat straw derived biochar on cadmium availability in a paddy soil and its accumulation in rice. *Environ. Pollut.* 257, 113592. doi:10.1016/j.envpol.2019.113592

Kaninga, B., Chishala, B. H., Maseka, K. K., Sakala, G. M., Young, S. D., Lark, R. M., et al. (2020). Do soil amendments used to improve agricultural productivity have consequences for soils contaminated with heavy metals? *Heliyon* 6 (11), e05502. doi:10.1016/j.heliyon.2020.e05502

Khan, S., Cao, Q., Zheng, Y. M., Huang, Y., and Zhu, Y. (2008). Health risks of heavy metals in contaminated soils and food crops irrigated with wastewater in Beijing, China. *Environ. Pollut.* 152 (3), 686–692. doi:10.1016/j.envpol.2007.06.056

Kim, R. Y., Yoon, J. K., Kim, T. S., Yang, J. E., and Owens, G. (2015). Bioavailability of heavy metals in soils: Definitions and practical implementation—a critical review. *Environ. Geochem. Health* 37 (6), 1041–1061. doi:10.1007/s10653-015-9695-y

Kim, W. I., Ji-Ho, L., Anitha, K., and Doo-Ho, K. (2013). Dietary exposure estimates of trace elements in selected agricultural products grown in greenhouse and associated health risks in Korean population. *J. Agric. Chem. Environ.* 2 (3), 35–41. doi:10.4236/jacen.2013.23006

Li, Z., Ma, Z., van der Kuijp, T. J., Yuan, Z., and Huang, L. (2014). A review of soil heavy metal pollution from mines in China: Pollution and health risk assessment. *Sci. total Environ.* 468, 843–853. doi:10.1016/j.scitotenv.2013.08.090

Lien, K. W., Pan, M. H., and Ling, M. P. (2021). Levels of heavy metal cadmium in rice (Oryza sativa L.) produced in Taiwan and probabilistic risk assessment for the Taiwanese population. *Environ. Sci. Pollut. Res.* 28 (22), 28381–28390. doi:10.1007/s11356-020-11902-w

Liu, H. Y., Xie, Z. R., Chen, D. Y., Zhou, X. M., Feng, X. M., and Guo, K. Y. (2004). Preliminary assessment of soil environmental quality in Chengdu (in Chinese with English abstract) [J]. *J. Environ. Sci.* 24 (2), 297–303.

Loutfy, N., Fuerhacker, M., Tundo, P., Raccanelli, S., El Dien, A., and Ahmed, M. T. (2006). Dietary intake of dioxins and dioxin-like PCBs, due to the consumption of dairy products, fish/seafood and meat from Ismailia city, Egypt. *Sci. total Environ.* 370 (1), 1–8. doi:10.1016/j.scitotenv.2006.05.012

Loutfy, N., Mentler, A., Shoeab, M., Ahmed, M. T., and Füerhacker, M. (2012). Analysis and exposure assessment of some heavy metals in foodstuffs from Ismailia city, Egypt. *Toxicol. Environ. Chem.* 94 (1), 78–90. doi:10.1080/02772248.2011.638445

Masindi, V., and Muedi, K. L. (2018). Environmental contamination by heavy metals[J]. *Heavy met.* 10, 115–132.

Meng, W., Wang, Z., Hu, B., Li, H., and Goodman, R. C. (2016). Heavy metals in soil and plants after long-term sewage irrigation at tianjin China: A case study assessment. *Agric. water Manag.* 171, 153–161. doi:10.1016/j.agwat.2016.03.013

Ministry of Ecology and Environment of the PRC (2018). *Soil environmental quality Risk control standard for soil contamination of agricultural land (GB 15618-2018) (in Chinese) [S]*. Beijing: China Environmental Science Press.

Ministry of Health of the PRC (2017). *National food safety standard maximum Levels of pollutants in foods (GB 2762-2017) (in Chinese) [S]*.

Miranzadeh Mahabadi, H., Ramroudi, M., Asgharipour, M. R., Rahmani, H. R., and Afyuni, M. (2020). Assessment of heavy metals contamination and the risk of target hazard quotient in some vegetables in Isfahan[J]. *Pollution* 6 (1), 69–78. doi:10.22059/POLL.2019.285113.645

Nabulo, G., Young, S. D., and Black, C. R. (2010). Assessing risk to human health from tropical leafy vegetables grown on contaminated urban soils. *Sci. Total Environ.* 408 (22), 5338–5351. doi:10.1016/j.scitotenv.2010.06.034

Ouyang, W., Jiao, W., Li, X., Giubilato, E., and Critto, A. (2016). Long-term agricultural non-point source pollution loading dynamics and correlation with outlet sediment geochemistry. *J. Hydrology* 540, 379–385. doi:10.1016/j.jhydrol.2016.06.043

Pigna, M., Caporale, A. G., Cavalca, L., Sommella, A., and Violante, A. (2015). Arsenic in the soil environment: Mobility and phytoavailability. *Environ. Eng. Sci.* 32 (7), 551–563. doi:10.1089/ees.2015.0018

Qin, G., Niu, Z., Yu, J., Li, Z., Ma, J., and Xiang, P. (2021). Soil heavy metal pollution and food safety in China: Effects, sources and removing technology. *Chemosphere* 267, 129205. doi:10.1016/j.chemosphere.2020.129205

Qin, Y. S., Yu, H., Feng, W. Q., Wang, Z. Y., and Tu, S. H. (2013). Heavy metal content and potential ecological risk assessment in paddy soil in northern Chengdu Plain (in Chinese with English abstract) [J]. *Chin. J. Ecol.* 33 (19), 6335–6344.

Ren, L., Qin, B., Tang, W., Ma, Z., and Hu, Y. (2006). Analysis on the sources of mercury in soils in the chengdu basin, china (in Chinese with Englishabstract) [J]. *Chin. J. Geochem.* 25, 10–10. doi:10.1007/BF02839750

Reza, S. K., Baruah, U., Singh, S. K., and Das, T. H. (2015). Geostatistical and multivariate analysis of soil heavy metal contamination near coal mining area, Northeastern India. *Environ. Earth Sci.* 73 (9), 5425–5433. doi:10.1007/s12665-014-3797-1

Saha, N., Mollah, M. Z. I., Alam, M. F., and Safiur Rahman, M. (2016). Seasonal investigation of heavy metals in marine fishes captured from the Bay of Bengal and the implications for human health risk assessment. *Food control.* 70, 110–118. doi:10.1016/j.foodcont.2016.05.040

Sall, M. L., Diaw, A. K. D., Gningue-Sall, D., Efremova Aaron, S., and Aaron, J. J. (2020). Toxic heavy metals: Impact on the environment and human health, and treatment with conducting organic polymers, a review. *Environ. Sci. Pollut. Res.* 27 (24), 29927–29942. doi:10.1007/s11356-020-09354-3

Semenov, D. O., Fatjejev, A. I., Smirnova, K. B., Shemet, A. M., Lykova, O. A., Tyutyunnyk, N. V., et al. (2019). Geochemical and anthropogenic factors of variability of heavy metals content in the soils and crops of Ukraine at the example of copper[J]. *Environ. Monit. Assess.* 191 (8), 1–9. doi:10.1007/s10661-019-7622-x

SEPA (2018). *Soil environmental quality Risk control standard for soil contamination of agricultural land (GB15618-2018)[S]* (Beijing: China Environmental Science Press).

Setia, R., Dhaliwal, S. S., Singh, R., Kumar, V., Taneja, S., Kukal, S. S., et al. (2021). Phytoavailability and human risk assessment of heavy metals in soils and food crops around Sutlej river, India. *Chemosphere* 263, 128321. doi:10.1016/j.chemosphere.2020.128321

Shaheen, N., Ahmed, M., Islam, M., Habibullah-Al-Mamun, M., Tukun, A. B., Islam, S., et al. (2016). Health risk assessment of trace elements via dietary intake of 'non-piscine protein source' foodstuffs (meat, milk and egg) in Bangladesh. *Environ. Sci. Pollut. Res.* 23 (8), 7794–7806. doi:10.1007/s11356-015-6013-2

Sharma, P., Kumar, S., and Pandey, A. (2021). Bioremediated techniques for remediation of metal pollutants using metagenomics approaches: A review. *J. Environ. Chem. Eng.* 9 (4), 105684. doi:10.1016/j.jece.2021.105684

Singh, S. P., Tack, F. M., and Verloo, M. G. (1998). Heavy metal fractionation and extractability in dredged sediment derived surface soils[J. *Water Air Soil Pollut.* 102 (3), 313–328. doi:10.1023/a:1004916632457

Sodango, T. H., Li, X., Sha, J., and Bao, Z. (2018). Review of the spatial distribution, source and extent of heavy metal pollution of soil in China: Impacts and mitigation approaches. *J. health Pollut.* 8 (17), 53–70. doi:10.5696/2156-9614-8.17.53

Soil Survey Staff (1996). *Soil survey laboratory methods manual. Soil Survey Investigations Report, No. 42. Ver. 3.0.* Lincoln, NE: USDA-NRCS.

Tang, W. C., Zhang, X. Z., He, Y. S., and Qin, B. (2007). Distribution characteristics and origion of Cd, Pb and Zn in surface soil in the plain area of the Chengdu Basin (in Chinese with English abstract) [J]. *Geochem.* 36 (1), 89–97. doi:10.3321/j.issn:0379-1726.2007.01.010

Tapia-Gatica, J., González-Miranda, I., Salgado, E., Bravo, M. A., Tessini, C., Dovletyarova, E. A., et al. (2020). Advanced determination of the spatial gradient of human health risk and ecological risk from exposure to As, Cu, Pb, and Zn in soils near the Ventanas Industrial Complex (Puchuncaví, Chile). *Environ. Pollut.* 258, 113488. doi:10.1016/j.envpol.2019.113488

Timothy, N., and Tagui Williams, E. (2019). Environmental pollution by heavy metal: An overview. *Int. J. Environ. Chem.* 3 (2), 72–82. doi:10.11648/j.ijec.20190302.14

Udom, G. J., Obilor, O. F., Ise, U. P., Nkechi, O., Udoh, A., Aturamu, A., et al. (2022). Heavy metal content of a polyherbal drug: Any exposure-associated public health risks?[J]. *J. Health Sci. Surveillance Syst.* 10 (2), 189–196. doi:10.30476/JHSSS.2021.93527.1457

USEPA (2008). Child-Specific Exposure factors handbook (2008, Final Report). Available at: http://cfpub.epa.gov/ncea/cfm/recordisplay.cfm?deid=199243 (Accessed July 2, 2022).

USEPA (2012). *EPA region III risk-based concentration (RBC) table, region III.* Philadelphia, Pennsylvania: Environmental Protection Agency.

USEPA (2013). Regional Screening Levels (RSLs)-Generic Tables. Available at: https://www.epa.gov/risk/regional-screening-levels-rsls-generic-tables (Accessed July 2, 2022).

USEPA (2017). Mid atlantic risk assessment, regional screening levels (RSLs) - generic tables. Available at: http://www.epa.gov/region9/superfund/prg (Accessed May, 2017).

Violante, A., Cozzolino, V., Perelomov, L., Caporale, A. G., and Pigna, M. (2010). Mobility and bioavailability of heavy metals and metalloids in soil environments[J]. *J. soil Sci. plant Nutr.* 10 (3), 268–292. doi:10.4067/S0718-95162010000100005

Wang, G., Zhang, S., Xiao, L., Zhong, Q., Li, L., Xu, G., et al. (2017). Heavy metals in soils from a typical industrial area in sichuan, China: Spatial distribution, source identification, and ecological risk assessment. *Environ. Sci. Pollut. Res.* 24 (20), 16618–16630. doi:10.1007/s11356-017-9288-7

Wang, M., Chen, W., and Peng, C. (2016). Risk assessment of Cd polluted paddy soils in the industrial and township areas in Hunan, Southern China. *Chemosphere* 144, 346–351. doi:10.1016/j.chemosphere.2015.09.001

Wang, X., Bai, J., Wang, J., Le, S., Wang, M., and Zhao, Y. (2019). Variations in cadmium accumulation and distribution among different oilseed rape cultivars in Chengdu Plain in China. *Environ. Sci. Pollut. Res.* 26 (4), 3415–3427. doi:10.1007/s11356-018-3857-2

Wang, X., Yu, D., Li, C., Pan, Y., Pan, J., Wang, X., et al. (2016). Characteristics of variations in the organic carbon fractions in paddy soils. *Soil Sci. Soc. Am. J.* 80 (4), 983–991. doi:10.2136/sssaj2016.03.0063

Wang, Y., Duan, X., and Wang, L. (2020). Spatial distribution and source analysis of heavy metals in soils influenced by industrial enterprise distribution: Case study in Jiangsu Province. *Sci. Total Environ.* 710, 134953. doi:10.1016/j.scitotenv.2019.134953

Wu, X., Cobbina, S. J., Mao, G., Xu, H., Zhang, Z., and Yang, L. (2016). A review of toxicity and mechanisms of individual and mixtures of heavy metals in the environment. *Environ. Sci. Pollut. Res.* 23 (9), 8244–8259. doi:10.1007/s11356-016-6333-x

Yang, Y., Christakos, G., Guo, M., Xiao, L., and Huang, W. (2017). Space-time quantitative source apportionment of soil heavy metal concentration increments. *Environ. Pollut.* 223, 560–566. doi:10.1016/j.envpol.2017.01.058

Yao, T. S. (1987). Study on the background values of eleven chemical elements in alluvial paddy soils and grain crops (wheat, rice) in the agricultural economic natural area of the Western Sichuan Plain [J]. *J. Sichuan Normal Univ. Nat. Sci. Ed. (Res. Album Backgr. Value Elem. Soil Grain)*, 1–67. (in Chinese with English abstract).

Yaradua, A. I., Alhassan, A. J., Nasir, A., Matazu, S. S., Usman, A., Idi, A., et al. (2020). Human health risk assessment of heavy metals in onion bulbs cultivated in katsina state, north west Nigeria. *Archives Curr. Res. Int.* 20 (2), 30–39. doi:10.9734/acri/2020/v20i230175

Yuswir, N. S., Praveena, S. M., Aris, A. Z., Ismail, S. N. S., and Hashim, Z. (2015). Health risk assessment of heavy metal in urban surface soil (klang district, Malaysia). *Bull. Environ. Contam. Toxicol.* 95 (1), 80–89. doi:10.1007/s00128-015-1544-2

Zahedifar, M., Dehghani, S., Moosavi, A. A., and Gavili, E. (2017). Temporal variation of total and DTPA-extractable heavy metal contents as influenced by sewage sludge and perlite in a calcareous soil. *Archives Agron. Soil Sci.* 63 (1), 136–149. doi:10.1080/03650340.2016.1193164

Zhang, J., Gao, Y., Yang, N., Dai, E., Yang, M., Wang, Z., et al. (2021). Ecological risk and source analysis of soil heavy metals pollution in the river irrigation area from Baoji, China. *Plos one* 16 (8), e0253294. doi:10.1371/journal.pone.0253294

Zhao, F. J., Ma, Y., Zhu, Y. G., Tang, Z., and McGrath, S. P. (2015). Soil contamination in China: Current status and mitigation strategies. *Environ. Sci. Technol.* 49 (2), 750–759. doi:10.1021/es5047099

Zheng, S., Wang, Q., Yuan, Y., and Sun, W. (2020). Human health risk assessment of heavy metals in soil and food crops in the Pearl River Delta urban agglomeration of China. *Food Chem.* 316, 126213. doi:10.1016/j.foodchem.2020.126213

Zhu, H. D., Wang, J. X., and Chen, R. S. (2000). Study on element concentration and dietary intake in foods among Chinese residents (in Chinese with English abstract) [J]. *Chin. J. Radiat. Med. Prot.* 20 (6), 378–384. doi:10.3760/cma.j.issn.0254-5098.2000.06.002

Zhuang, P., McBride, M. B., Xia, H., Li, N., and Li, Z. (2009). Health risk from heavy metals via consumption of food crops in the vicinity of Dabaoshan mine, South China. *Sci. total Environ.* 407 (5), 1551–1561. doi:10.1016/j.scitotenv.2008.10.061

Zwolak, A., Sarzyńska, M., Szpyrka, E., and Stawarczyk, K. (2019). Sources of soil pollution by heavy metals and their accumulation in vegetables: A review. *Water Air Soil Pollut.* 230 (7), 164–169. doi:10.1007/s11270-019-4221-y

frontiers | Frontiers in Chemistry

TYPE Mini Review
PUBLISHED 08 September 2022
DOI 10.3389/fchem.2022.1008010

OPEN ACCESS

EDITED BY
Yaqiong Su,
Xi'an Jiaotong University, China

REVIEWED BY
Ya-Long Ding,
Huanghuai University, China
Hu Pan,
Jiaxing University, China

*CORRESPONDENCE
Tingting Li,
litt8293@163.com

SPECIALTY SECTION
This article was submitted to Green and Sustainable Chemistry, a section of the journal Frontiers in Chemistry

RECEIVED 31 July 2022
ACCEPTED 23 August 2022
PUBLISHED 08 September 2022

CITATION
Zheng Z, Dai A, Liu Y and Li T (2022), Sustainable alginate lyases catalyzed degradation of bio-based carbohydrates.
Front. Chem. 10:1008010.
doi: 10.3389/fchem.2022.1008010

Sustainable alginate lyases catalyzed degradation of bio-based carbohydrates

Zhiguo Zheng, Ali Dai, Yonggui Liu and Tingting Li*

State Key Laboratory Breeding Base of Green Pesticide and Agricultural Bioengineering, Key Laboratory of Green Pesticide and Agricultural Bioengineering, Ministry of Education, Guizhou University, Guiyang, China

Alginate is a water-soluble and acidic polysaccharide derived from the cell wall and intercellular substance of brown algae. It is widely distributed in brown algae, such as *Laminaria*, *Sargassum,* and *Macrocystis*, etc. Alginate lyase can catalytically degrade alginate in a β-eliminating manner, and its degradation product-alginate oligosaccharide (AOS) has been widely used in agriculture, medicine, cosmetics and other fields due to its wide range of biological activities. This article is mainly to make a brief introduction to the classification, source and application of alginate lyase. We hope this minireview can provide some inspirations for its development and utilization.

KEYWORDS

alginate lyase, Brown algae, AOS, agriculture, biological activity

Introduction

Alginate is the most abundant linear polysaccharide in brown algae (about 40% of dry weight). It is composed of two uronic acid monomers, β-D-mannuronic acid and C5-epimer α-L-guluronic acid, through α/β-1,4 glycosidic bonds in different combinations of poly-guluronic acid (poly-G), poly-mannuronic acid (poly-M), and hybrid fragments of random polymerization of G and M (poly-GM). (Gacesa, 1992; Lee and Mooney, 2012; Kurakake et al., 2017).

At present, the preparation of algal oligosaccharides mainly adopts three kinds of degradation methods: chemical, physical and biological. Chemical methods include acid hydrolysis, alkaline hydrolysis and oxidative degradation, and physical methods mainly include hydrothermal method, ultrasonic method and radiation method, but these two methods have many drawbacks, which are not conducive to large-scale production. Biological methods mainly use microbial fermentation or the action of enzymes to degrade the prepared enzymes. It has the advantages of mild conditions, easy control, and strong product specificity, which has attracted people's attention, it may be an important direction of industrial production. (Guo et al., 2016).

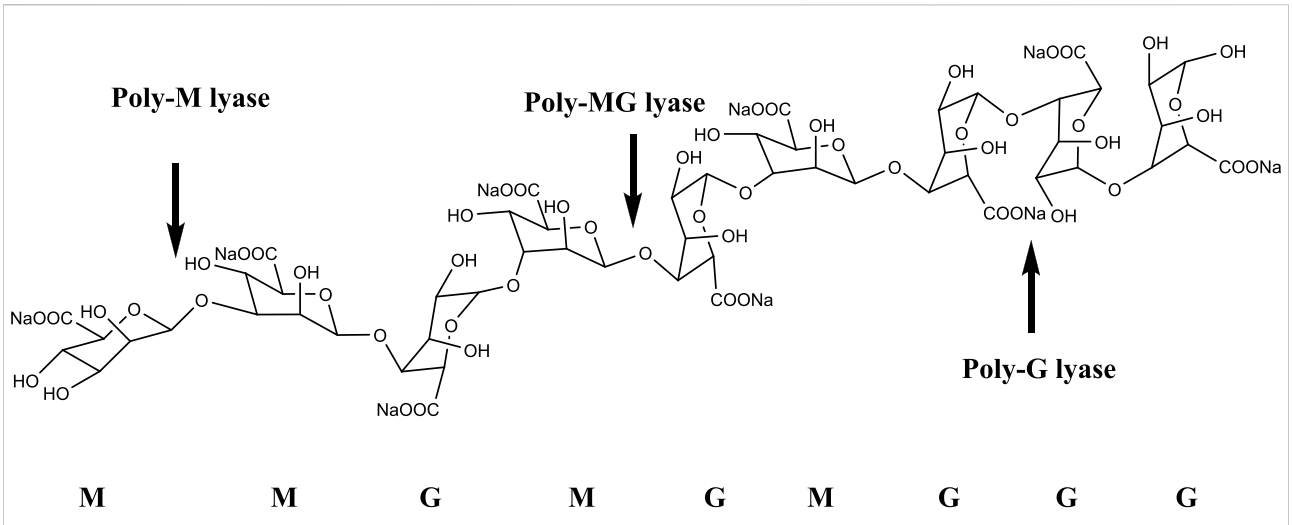

FIGURE 1
Degradation mode and site of alginate lyase.

Introduction and application of alginate lyase

Classification of alginate lyases

The alginate oligosaccharide produced by the enzymatic hydrolysis of alginate lyase has an unsaturated double bond between the C4 and C5 positions of the uronic acid unit at the non-reducing end, and it has a characteristic absorption peak at a specific wavelength of 235 nm. Alginate lyases can be divided into three groups based on substrate specificity, namely poly-G lyase (EC: 4.2.2.11), poly-M lyase (EC: 4.2.2.3), and displays both poly-G and poly-M lyase (Figure 1). In terms of the mode of action, alginate lyase can be divided into endonuclease and exonuclease (Wong et al., 2000). Endonuclease cleaves glycosidic bonds in algin and releases unsaturated oligosaccharides (disaccharides, trisaccharides and tetrasaccharides, etc.), while exonuclease can further degrade oligosaccharides into oligosaccharides. Monomer (Kim et al., 2012; Jagtap et al., 2014). Based on the amino acid sequence alignment, alginate lyases can be classified into different polysaccharide lyase (PL) families including PL5, PL6, PL7, PL8, PL14, PL15, PL17, PL18, PL31, PL32, PL34, PL36, PL39, and PL41 families, which are listed in the Carbohydrate-Active enzymes (CAZy) database (http://www.cazy.org/) (Barzkar et al., 2022).

Source of alginate lyase

The sources of alginate lyase are extensive, and it has been reported that the production of alginate lyase mainly comes from marine algae, marine mollusks and microorganisms (including bacteria, fungi and some viruses). Among them, there are the most reports on the source of microorganisms, including (*Pseudoalteromonas* sp.) (Ma et al., 2008) (*Vibrio* sp.), (Kawamoto et al., 2006) (*Flavobacterium* sp.) (An et al., 2009) (*Paenibacillus* sp.) (Zhu et al., 2020; Huang et al., 2022).

Application of alginate lyase

Alginate lyase is an important marine biological enzyme. AOS has various biological activities due to the differences in degradation mode, G content of degradation products (G/M ratio), molecular weight and spatial conformation. As an excellent natural antioxidant, alginate oligosaccharide has great application potential in the fields of human, animals and plants health (Yokose et al., 2009; Tondervik et al., 2014; Saberi Riseh, 2022). It can promote growth, improve stress resistance, increase yield, and inhibit fungal growth. With the implementation of the national strategy of regulating the use of chemical fertilizers and pesticides, it may become an environment-friendly bio-fertilizer and bio-pesticide in the future.

Alginate lyase is not only widely used in agriculture, but also in the fields of medicine and food. It can be used as a growth promoter for therapeutics such as antioxidants and tumor suppressors (Tusi et al., 2011; Hu et al., 2004), and can also induce cytokine production, regulate blood sugar and lipids (Iwamoto et al., 2005), which are widely used in the food and pharmaceutical industries. For example, *Pseudomonas aeruginosa* is one of the main pathogens of many chronic infectious diseases, such as chronic lung infection and urinary

tract infection (Jain and Ohman, 2005). The study found that algin is an important component of *Pseudomonas aeruginosa* biofilm, and Albrecht used lyase as an adjunct therapeutic agent together with antibiotics, which made the antibiotics come into direct contact with pathogenic bacteria to achieve the therapeutic effect (Albrecht and Schiller, 2005). This shows that the enzyme has great potential in the bactericidal application of biofilm pathogens.

Due to fuel consumption, researchers have begun to pay attention to the production of biofuel. At present, although chemical catalysis has high efficiency, its high cost, complex synthesis process, and high energy consumption under synthetic conditions limit its industrial application to a certain extent (Pan et al., 2022a; Pan et al., 2022b). Seaweed is considered an ideal source for bioethanol production due to its advantages of not occupying arable land and being non-polluting. According to reports, Wargacki et al. (2012) transformed *Escherichia coli* to establish a system for directly fermenting brown algae to produce ethanol. However, *Escherichia coli* has insufficient tolerance to ethanol, making it impossible for large-scale production. Sasaki et al. (2018) developed a co-cultivation platform for bioethanol production from brown algae, consisting of engineered yeast AM1 and CDY strains, which produced 2.1 g/L of ethanol when the brown algae *Ecklonia kurome* was used as the sole carbon source. This research has made significant progress in the biotechnology of brown algae to bioethanol, but it is still insufficient for industrial production. Studies have shown that the synergistic effect of multiple microorganisms on the ethanol fermentation system of macroalgae will be the trend of future research.

Conclusion and outlook

Alginate lyase has attracted the attention of researchers because of its unique properties and has great potential for application in various fields. At present, the related research on alginate lyase mainly focuses on the screening of strains, the mining of genes, and the analysis of the degradation substrate and product structure. With the continuous advancement of science and technology, people have gradually deepened the research on the analysis of alginate lyase protein crystal analysis, the catalytic mechanism of the active center and the transformation strategy. This will likely improve the problems of low enzyme-producing strains, low tolerance, and unstable properties in the large-scale industrial production process, and has great application potential in agricultural protection, biofuel production, and environmental protection.

Author contributions

ZZ and AD contributed equally to this work and drafted the manuscript. YL participated in some manuscript writing and checking. TL conceptualized and directed the whole project. All of the authors contributed to scientific discussions.

Funding

We acknowledge financial support from the Program of Introducing Talents of Discipline to Universities of China (111 Program, D20023), Frontiers Science Center for Asymmetric Synthesis and Medicinal Molecules, Department of Education, Guizhou Province [Qianjiaohe KY (2020)004], and Guizhou University.

Conflict of interest

The authors declare that the research was conducted in the absence of any commercial or financial relationships that could be construed as a potential conflict of interest.

Publisher's note

All claims expressed in this article are solely those of the authors and do not necessarily represent those of their affiliated organizations, or those of the publisher, the editors and the reviewers. Any product that may be evaluated in this article, or claim that may be made by its manufacturer, is not guaranteed or endorsed by the publisher.

References

Albrecht, M.-T., and Schiller, N.-L. (2005). Alginate lyase (AlgL) activity is required for alginate biosynthesis in *Pseudomonas aeruginosa*. *J. Bacteriol.* 187 (11), 3869–3872. doi:10.1128/jb.187.11.3869-3872.2005

An, Q.-D., Zhang, G.-L., Wu, H.-T., Zhang, Z.-C., Zheng, G.-S., Luan, L., et al. (2009). Alginate-deriving oligosaccharide production by alginase from newly isolated Flavobacterium sp. LXA and its potential application in protection against pathogens. *J. Appl. Microbiol.* 106 (1), 161–170. doi:10.1111/j.1365-2672.2008.03988.x

Barzkar, N., Sheng, R., Sohail, M., Jahromi, S.-T., Babich, O., Sukhikh, S., et al. (2022). Alginate lyases from marine bacteria: An enzyme ocean for sustainable future. *Molecules* 27 (11), 3375. doi:10.3390/molecules27113375

Gacesa, P. (1992). Enzymic degradation of alginates. *Int. J. Biochem.* 24 (4), 545–552. doi:10.1016/0020-711X(92)90325-U

Guo, J.-J., Ma, L.-L., Shi, H.-T., Zhu, J.-B., Wu, J., Ding, Z.-W., et al. (2016). Alginate oligosaccharide prevents acute doxorubicin cardiotoxicity by suppressing oxidative stress and endoplasmic reticulum-mediated apoptosis. *Mar. Drugs* 14 (12), 231. doi:10.3390/md14120231

Huang, H.-Q., Zheng, Z.-G., Zou, X.-X., Wang, Z.-X., Gao, R., Zhu, J., et al. (2022). Genome analysis of a novel polysaccharide-degrading bacterium paenibacillus algicola and determination of alginate lyases. *Mar. Drugs* 20 (6), 388. doi:10.3390/md20060388

Hu, X.-K., Jiang, X.-L., Hwang, H.-M., Liu, S.-L., and Guan, H.-S. (2004). Antitumour activities of alginate-derived oligosaccharides and their sulphated substitution derivatives. *Eur. J. Phycol.* 39 (1), 67–71. doi:10.1080/0967026031000163669 5

Iwamoto, M., Kurachi, M., Nakashima, T., Kim, D., Yamaguchi, K., Oda, T., et al. (2005). Structure-activity relationship of alginate oligosaccharides in the induction of cytokine production from RAW264. 7 cells. *FEBS Lett.* 579 (20), 4423–4429. doi:10.1016/j.febslet.2005.07.007

Jagtap, S.-S., Hehemann, J.-H., Polz, M.-F., Lee, J.-K., and Zhao, H. (2014). Comparative biochemical characterization of three exolytic oligoalginate lyases from *Vibrio splendidus* reveals complementary substrate scope, temperature, and pH adaptations. *Appl. Environ. Microbiol.* 80 (14), 4207–4214. doi:10.1128/aem.01285-14

Jain, S., and Ohman, D.-E. (2005). Role of an alginate llyase for alginate tansport in mucoid *Pseudomonas aeruginosa*. *Infect. Immun.* 73 (10), 6429–6436. doi:10.1128/iai.73.10.6429-6436.2005

Kawamoto, H., Horibe, A., Miki, Y., Kimura, T., Tanaka, K., Nakagawa, T., et al. (2006). Cloning and sequencing analysis of alginate lyase genes from the marine bacterium Vibrio sp. O_2. *Mar. Biotechnol.* 8 (5), 481–490. doi:10.1007/s10126-005-6157-z

Kim, H.-T., Chung, J.-H., Wang, D., Lee, J., Woo, H.-C., Choi, I.-G., et al. (2012). Depolymerization of alginate into a monomeric sugar acid using Alg17C, an exo-oligoalginate lyase cloned from *saccharophagus* degradans 2-40. *Appl. Microbiol. Biotechnol.* 93 (5), 2233–2239. doi:10.1007/s00253-012-3882-x

Kurakake, M., Kitagawa, Y., Okazaki, A., and Shimizu, K. (2017). Enzymatic properties of alginate lyase from *paenibacillus* sp. S29. *Appl. Biochem. Biotechnol.* 183 (4), 1455–1464. doi:10.1007/s12010-017-2513-5

Lee, K.-Y., and Mooney, D.-J. (2012). Alginate: Properties and biomedical applications. *Prog. Polym. Sci.* 37 (1), 106–126. doi:10.1016/j.progpolymsci.2011.06.003

Ma, L.-Y., Chi, Z.-M., Li, J., and Wu, L.-F. (2008). Overexpression of alginate lyase of Pseudoalteromonas elyakovii in Escherichia coli, purification, and characterization of the recombinant alginate lyase. *World J. Microb. Biot.* 24 (1), 89–96. doi:10.1007/s11274-007-9443-2

Pan, H., Xia, Q.-N., Wang, Y., Shen, Z.-F., Huang, H., Ge, Z., et al. (2022a). Recent advances in biodiesel production using functional carbon materials as acid/base catalysts. *Fuel Process. Technol.* 237, 107421. doi:10.1016/j.fuproc.2022.107421

Pan, H., Xia, Q.-N., Li, H., Wang, Y.-G., Shen, Z.-F., Wang, Y., et al. (2022b). Direct production of biodiesel from crude *Euphorbia lathyris* L. Oil catalyzed by multifunctional mesoporous composite materials. *Fuel* 309, 122172. doi:10.1016/j.fuel.2021.122172

Saberi Riseh, R., Gholizadeh Vazvani, M., Ebrahimi-Zarandi, M., and Skorik, Y.A. (2022). Alginate-induced disease resistance in plants. *Polymers* 14 (4), 661. doi:10.3390/polym14040661

Sasaki, Y., Takagi, T., Motone, K., Shibata, T., Kuroda, K., and Ueda, M. (2018). Direct bioethanol production from Brown macroalgae by Co-culture of two engineered *Saccharomyces cerevisiae* strains. *Biosci. Biotechnol. Biochem.* 82 (8), 1459–1462. doi:10.1080/09168451.2018.1467262

Tøndervik, A., Sletta, H., Klinkenberg, G., Emanuel, C., Powell, L.-C., Pritchard, M.-F., et al. (2014). Alginate oligosaccharides inhibit fungal cell growth and potentiate the activity of antifungals against *Candida* and *Aspergillus* spp. *PLoS One* 9 (11), e112518. doi:10.1371/journal.pone.0112518

Tusi, S.-K., Khalaj, L., Ashabi, G., Kiaei, M., and Khodagholi, F. (2011). Alginate oligosaccharide protects against endoplasmic reticulum-and mitochondrial-mediated apoptotic cell death and oxidative stress. *Biomaterials* 32 (23), 5438–5458. doi:10.1016/j.biomaterials.2011.04.024

Wargacki, A.-J., Leonard, E., Win, M.-N., Regitsky, D.-D., Santos, C.-N.-S., Kim, P.-B., et al. (2012). An engineered microbial platform for direct biofuel production from Brown macroalgae. *Science* 335 (6066), 308–313. doi:10.1126/science.1214547

Wong, T.-Y., Preston, L.-A., and Schiller, N.-L. (2000). Alginate lyase: Review of major sources and enzyme characteristics, structure-function analysis, biological roles, and applications. *Annu. Rev. Microbiol.* 54, 289–340. doi:10.1146/annurev.micro.54.1.289

Yokose, T., Nishikawa, T., Yamamoto, Y., Yamasaki, Y., Yamaguchi, K., and Oda, T. (2009). Growth-promoting effect of alginate oligosaccharides on a unicellular marine microalga, *Nannochloropsis oculata*. *Biosci. Biotechnol. Biochem.* 73 (2), 450–453. doi:10.1271/bbb.80692

Zhu, J., Mo, K.-L., Zheng, Z.-G., Wang, Z.-X., Hu, Y.-H., Zou, X.-X., et al. (2020). *Paenibacillus algicola* sp. nov., A novel alginate lyase-producing marine bacterium. *Int. J. Syst. Evol. Microbiol.* 70 (9), 5087–5092. doi:10.1099/ijsem.0.004385

frontiers | Frontiers in Chemistry

TYPE Mini Review
PUBLISHED 15 September 2022
DOI 10.3389/fchem.2022.1007707

OPEN ACCESS

EDITED BY
Yaqiong Su,
Xi'an Jiaotong University, China

REVIEWED BY
Qiuyun Zhang,
Anshun University, China
Jian He,
Jishou University, China

*CORRESPONDENCE
Hongguo Wu,
whg0408@126.com

SPECIALTY SECTION
This article was submitted to Green and Sustainable Chemistry, a section of the journal Frontiers in Chemistry

RECEIVED 30 July 2022
ACCEPTED 19 August 2022
PUBLISHED 15 September 2022

CITATION
Huang J, Jian Y, Zhou M and Wu H (2022), Oxidative C–C bond cleavage of lignin via electrocatalysis. *Front. Chem.* 10:1007707. doi: 10.3389/fchem.2022.1007707

Oxidative C–C bond cleavage of lignin *via* electrocatalysis

Jinshu Huang[1], Yumei Jian[1], Min Zhou[1] and Hongguo Wu[1,2]*

[1]State Key Laboratory Breeding Base of Green Pesticide and Agricultural Bioengineering, Key Laboratory of Green Pesticide and Agricultural Bioengineering, Ministry of Education, State-Local Joint Laboratory for Comprehensive Utilization of Biomass, Center for R&D of Fine Chemicals, Guizhou University, Guiyang, China, [2]College of Materials Science and Engineering, Guizhou Minzu University, Guiyang, China

Lignin, which is an important component of biomass in nature and is constantly produced in industry, becomes potential raw material for sustainable production of fine chemicals and biofuels. Electrocatalysis has been extensively involved in the activation of simple molecules and cleavage-recasting of complex scaffolds in an elegant environment. As such, electrocatalytic cleavage of C–C(O) in β-O-4 model molecules of lignin to value-added chemicals has received much attention in recent years. This mini-review introduces various anodes (e.g., Pb, Pt, Ni, Co., and Ir) developed for electro-oxidative lignin degradation (EOLD) under mild conditions. Attention was placed to understand the conversion pathways and involved reaction mechanisms during EOLD, with emphasis on the product distribution caused by different electrodes.

KEYWORDS

biomass conversion, lignin, biofuels, electrocatalysis, green chemistry

Introduction

Lignin, which is a large amount of biomass in nature and is constantly produced in industry, becomes potential raw material for sustainable production of fine chemicals, biofuels and functional materials, considering its polyphenolic structure and carbon-rich properties (Pardini et al., 2002; Li et al., 2019; Wu et al., 2021; Huang et al., 2022; Jian et al., 2022). Especially, catalytic cleavage of C–C(O) in β- O-4 model molecules has received much attention (Sun et al., 2018; Yu et al., 2022). Traditional β- O-4 model molecule degradation methods, including pyrolysis, catalytic hydrodeoxygenation, liquefaction, and oxidative cracking (Jia et al., 2018; Valle et al., 2013), can efficiently convert lignin into value-added fine chemicals (Figure 1A). Definitely, those methods have many areas to be improved, such as harsh conditions and non-specific selectivity. Alternatively, electro-oxidative lignin degradation (EOLD) is a mild and sustainable method that featured selective cleavage of the C–C bond (C_α–C_β bond and β- O-4 ether cleavage) using user-friendly electron while retaining the inherent aromatic structure (Figure 1B) (Liu et al., 2019; Di Fidio et al., 2021).

In 1946, Bailey and Brooks firstly illustrated that the metal materials (e.g., Pb, Cd, Pt, and Ag) serving as anodes for the electrocatalytic oxidation of alkali lignin or methylated butanol lignin could successfully furnish methyl ethyl ketone, acetone, and acetic acid

(Figueiredo et al., 2017). Since then, a growing number of researchers utilized metals such as Pb, Pt and Ni as anodes to conduct EOLD. The following sections are a detailed introduction to the classification of these anodic materials.

Lead/lead oxide electrodes

Lead/lead oxide electrodes are extensively used as anode materials for EOLD due to their superior chemical stability in aggressive media, high overpotentials in oxygen evolution reactions (competitive reactions), and low prices (Quiroz et al., 2005). In the presence of (+) (Pb/PbO_2)/SS (−) with an increased specific surface area, 4-methylanisole was mainly generated by the electrooxidation of lignin through C_α–C_β bond breaking with a free radical (·OH). When the current density was 50 mA/cm^2 at 50°C, the yield of product 4-methylanisole is the highest (Wang et al., 2015). It is worth noting that a high temperature will lead to the inactivation of the catalytic reaction free radical. In the same device, the cyclic voltammetry and cathodic polarization indicated that the copper electrode could reduce the hydrogenation rate and electrocatalytic hydrogenation rate of the hydrogen atom electrochemical solution (Liu et al., 2017). The yield of syringaldehyde was 57.30 g (kg-lignin)$^{-1}$, which is higher than that of vanillin and *p*-coumaric acid at a lower current density (20 mA/cm^2) and temperature (40°C). The same device could also be used to oxidize alkaline lignin to butyl hydroxytoluene (BHT) (Zhang et al., 2014). For the degradation process, electrochemical impedance spectroscopy and cyclic voltammetry show that the phenolic hydroxyl monomolecular structure in lignin is combined with sodium ions in the electrolyte to form sodium phenolate, and then the aromatic ring of the C–C bond was highly induced and selectively cleaved with superoxide anion radical ($O_2^{\bullet-}$) on the anodic surface of Pb/PbO_2, thus generating lignin superoxide anion radical. Finally, the branched chain of the benzene is cleaved, and then the intermediate is deoxygenated by cathodic protons. It was further converted into BHT by the electrophilic attack of *tert*-butyl carbophenyl ammonium ion with a final separation yield of 7.01% under constant current conditions (25 mA/cm^2), and the concentration of BHT was negatively correlated with the current

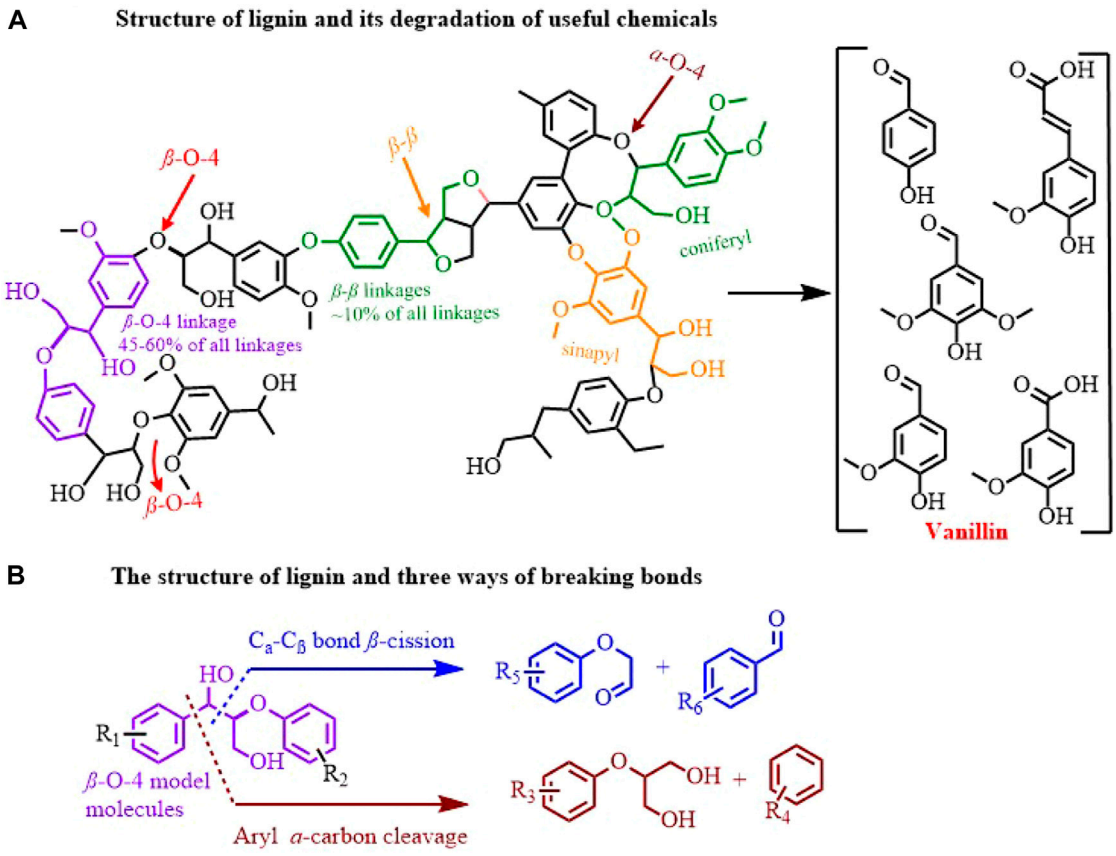

FIGURE 1
Schematic of the structure and bond cleavage position **(A)**, and fracture mode **(B)** of lignin..

density. When using Ti/PbO_2 and Ti/Sb-SnO_2 as electrocatalysts in the pre-degradation of sodium lignosulfonate solution (2000 ppm) (Shao et al., 2014), quinone and short-chain carboxylic acid are essential intermediates and primary products, respectively. The results showed that Ti/Sb-SnO_2 and Ti/PbO_2 had different advantages in their UV-visible absorption reduction, chemical oxygen demand (COD) removal capacity, and biodegradability. In the same device, the Ti/SnO_2-Sb_2O_3/α-Pb O $_2$/β-Pb O $_2$ electrode was prepared by further modification of Ti/Sb-SnO_2 and Ti/PbO_2 electrodes, and Ir or Ti-doped Ti/Cu/Sn electrode as a cathode. Interestingly, the products could be oriented toward aromatic ketone, aldehyde, or acid when Ti/Cu/Sn was used as the cathodic material, proving that cathodic materials with different titanium-based materials had important effects on the process and products of EOLD.

The lead oxide coating prepared by the conventional method is easy to peel off from the surface of the substrate owing to its relatively high interfacial resistance (Hao et al., 2015). This problem can be improved by photoelectrical deposition of lead oxide onto TiO_2 nanotubes (NTs) arrays. The NTs can increase the available surface area of the electrode, thus improving the load capacity of lead oxide (Pan et al., 2012). The prepared Ti/TiO_2NT/PbO_2 electrode showed a high electrochemical response and lasting stability, which was active for the crack of the C_α–C_β bonds of kraft lignin to give vanillin and vanillin acid. The $[Fe(CN)_6]^{3-}$ modified lead oxide electrode prepared by deposition method has a wider central active surface area, resulting in the formation of more OH radicals and their adsorption sites, closely correlated with significantly increased active sites (Hao et al., 2015). It is worth noting that implantation of $[Fe(CN)_6]^{3-}$ anion into the lead oxide matrix is beneficial to the growth of lead oxide crystals, thus optimizing the size and load capacity of lead oxide electrodes. Overall, the $[Fe(CN)_6]^{3-}$-modified lead oxide electrode can effectively reduce interfacial resistance and thus effectively prevent stripping. The accelerated life test data showed that the life of the modified PbO_2 electrode was 0.8 times longer than that of the bare PbO_2 electrode, and the degradation rate constant significantly increased from 0.00419 to 0.00609 min^{-1}, but the product category is not specified in this literature.

Platinum electrodes

Pt was usually developed as a hydrolysis catalyst and anodic electrode material to catalyze the electrically oxidative fracture of the C_α–C_β bond in the degradation and utilization of lignin (Liu et al., 2019). One-pot degradation of lignin by using hydrogen peroxide *tert*-butyl (*t*-BuOOH, 70%) as an oxidant, Pt as electrode material, where C_α–C_β bonds were cleaved specifically into functional aromatic hydrocarbons (e.g., 3-methoxy-benzaldehyde in 81% yield and phenol in 43% yield) (Ma et al., 2021). Mechanism studies show that the reaction pathway undergoes through forming *in situ* C_β-centered free radicals to produce peroxide intermediates and further inducing oxidative cleavage of C_α–C_β bond to give 3-methoxy-benzaldehyde. For highly dispersed single-atom Pt–N_3C_1 nanotubes, the increase in single-atom unsaturated coordination number results in the increase of the active sites, while the high degree of dispersion can improve the atomic utilization, thereby increasing the activity and yield per unit catalyst. The results of electrical experiments show that Pt_1/N-CNTs have high selectivity and activity for activating C_α–C_β bonds in lignin. Density functional theory (DFT) calculation proves that the C-center free-radical intermediate is formed in the degradation process, and the unstable C_β-radical undergoes a cross-coupling reaction to generate the peroxide intermediate. After the reaction, electron transfer results in C_α–C_β bond-breaking to provide benzaldehyde (81% yield) (Cui et al., 2021).

Nickel–, cobalt–, and nickel–cobalt–based electrodes

Ni-electrode has excellent chemical resistance and is widely used in EOLD. Ni is used as an anode and flow reactor (FM01) device to prepare vanillin (Masoumi et al., 2016). Control experiments showed that optimizing current density and adjusting the initial concentration of lignosulfonate can obviously improve the yield of vanillin, in which Ni as anode has two competitive reactions in lignin degradation. The reaction is oxidized by nickel (II) to the oxygen-containing nickel (III) species (Ni(III)OOH). A maximum vanillin yield of 7.4% w/w could be obtained from 1.5% w/v lignin at 130°C and 1.9 mA/cm^2. Unsatisfactorily, the complexity of the experimental device and the conditions of high temperature and high pressure hinder the development of this method. Instead, changing the simple device can make the reaction easy to operate, and the new device "Swiss coil" electrochemical reactor and Ni (foam) electrode using water as an electrolyte are applied to EOLD (Di Marino et al., 2019). Starting from lignin, the C–C bond is initially destroyed to form a carboxylic acid compound and then broken into a low molecular compound, such as vanillin. Free radicals can be reduced and generated by oxygen transfer from the anode to the cathode, which can promote the decrease of the average molecular weight of lignin to obtain value-added products. Di- and mono-carboxylic acids (e.g., ethanedioic acid, vinegar acid, and formic acid) have high reactivity, with the formic acid yield of 26.8%, which was higher than oxalic acid and acetic acid.

In the unstable electrochemical depolymerization process, a dynamic model was constructed to predict the formula weight change of the EOLD in the reaction device, and the simulation of the reaction (chain break, random recombination, and random fracture) is high similarity (Bawareth et al., 2018). After

introducing a contributor to the overall reaction, the model predicts the function of lignin degradation and product formation simultaneously, and the effect of the three major reactions is similar to the experimental data. It is further indicated that the reaction rate coefficient is linearly related to the initial multispecies and mean molecular weight of lignin. Also, a membrane reactor was applied to EOLD. The obtained results showed that when the membrane pore size was 1 nm, the aromatic hydrocarbon yield in the batch reactor could be increased from 0.01% to 11% (Bawareth et al., 2018). In general, the Ni-electrode is stable and does not fall off, but the activity is not ideal, which limits the application range of the Ni-based electrodes.

Cobalt oxide (CoO_x) electrodes show outstanding activity in EOLD and can significantly improve the yield of vanillin, but are easily detached from the electrolyte to lose the function of transferring electrons, which blocks its industrial applications. The stable Co. core/Pt shell structure is not only conducive to electron transport, but also effectively avoids the problem of easy shedding of exposed Co., and it was successfully prepared by the polyol method and applied for EOLD (Movil-Cabrera et al., 2016). The main products are heptane and apocynin, although the type and yield of the product vary with the electrode potential. Other oxidative products (e.g., 1,3-bis(1,1-dimethylethyl)-benzene and 1,4-di-*tert*-butyl phenol) may participate in the oxidative decomposition initiated by free radicals in an alkaline medium.

It has been shown that a variety of metal doping and multi-metal alloy electrode materials can not only avoid the inherent defects of the single metal itself, but also show the advantages of their respective metals (Cai et al., 2014). For example, Ni-Co co-based materials exhibited outstanding activity and excellent corrosion resistance. Waldvogel (Schmitt et al., 2015) and Zirbesl (Cai et al., 2014) both added a Co-based anode to a Ni-based anode for EOLD to improve the yield of vanillin. The former forms an electrochemically active NiOOH coating *in situ*, and the electrolysis conditions are optimized when the reaction temperature is lower than 100°C (Schmitt et al., 2015). The use of strongly basic anion exchange resin can selectively remove the low molecular weight of phenol in the strongly basic electrolyte, so it is unnecessary to acidify and precipitate the remaining lignin. Dissimilarly, Zirbes et al. (2019) electrochemically activated the electrode in black liquor, which was demonstrated to significantly increase the electrocatalytic activity and the Ni(foam)-electrode could be reused 6-times (Garedew et al., 2020). It was found that diaminotoluene was the main product in the adsorption layer, indicating that the compound was involved in the activation process to a certain extent. Else, the deposited organic surface layer can not only increase the lipophilicity of the electrode surface but also further promote the adsorption and oxidative degradation of lignin, thus obtaining a good yield (0.9 wt%) of vanillin. The mechanism of both sets of experiments was that in an alkaline electrolyte, an electrocatalytically active NiOOH layer was formed on the surface of the anode Ni (Schutyser et al., 2018), in which EOLD enhanced the oxidative activity of the electrode, while helping to avoid further peroxidation of the formed monomers (Smith et al., 2010), and thereby significantly increasing yield. Different from platinum and other expensive metal or large pieces of the metal electrode (e.g., large, and flat electrode), nanoparticle catalysts potentially show increased activity in electrically catalytic degradation of lignin, owing to a higher utilization rate of metal, which can promote the quality of the reactants and products through optimizing the structure of electrode materials.

Iridium oxide electrodes

The unexpected electrocatalytic selectivity and corrosion resistance of iridium oxide electrodes have attracted the wide attention of investigators (Trasatti, 2000). Different IrO_2-based electrodes (e.g., Ti/MO-IrO_2, MO = SnO_2, RuO_2, Ta_2O_5, and TiO_2) were prepared and applied to the EOLD (Tolba et al., 2010). The cyclic voltammetry curves show that the electrochemically active surface areas of the four metal/oxide species modified IrO_2 electrodes exhibit the following sequence: Ti/Ta_2O_5-IrO_2 > Ti/TiO_2-IrO_2 > Ti/SnO_2-IrO_2 > Ti/RuO_2-IrO_2. The good stability and highest reaction rate constant (apparent activation energy of electrochemical oxidation: 20 kJ/mol) indicate that the resulting hydroxyl radicals are advantageous for the break of the C–C bond in lignin. At 60°C, the optimum current density was 500 mA cm^{-2}, and the yield of vanilla and vanillic acid reached the maximum value (500 ppm lignin). A binary mixed metal oxide (MMO) ($Ru_{0.4}Ir_{0.6}O_x$) electrode derived from ruthenium and osmium oxide was successfully prepared and found to show good activity in electrocatalytic degradation of lignin to produce diaphylin (Zhu et al., 2014), but the decomposition of electrolyte causes electrochemical windows very narrow. Also, by using transition metals to modify the binary $Ru_{0.4}Ir_{0.6}O_x$-electrode for the preparation of three-membered MMO electrodes ($Ru_{0.2}M_{0.2}Ir_{0.6}O_x$; M = Mn, Pd, V, and Ti), the activity of $Ru_{0.2}M_{0.2}Ir_{0.6}O_x$-electrodes is higher than binary $Ru_{0.4}Ir_{0.6}O_x$-electrode, for example, the $Ru_{0.2}Mn_{0.2}Ir_{0.6}O_x$ has the highest electrocatalytic activity (11.5% yield) (Rauber et al., 2018). Moreover, the composition of the electrode also changes the number of cracking products and the selectivity of the break button. The reaction was carried out in ionic liquids ([Et_3NH][$MeSO_3$]) considering that [Et_3NH][$MeSO_3$] has quantitative turnover and no side reaction (Achinivu et al., 2014), as well as does not produce any contaminant, and shows high electrochemical windows through some synergy, such as the hydrophilicity of ILs and the hydrophobicity of the aromatic pyrolysis products allow the product to be separated from the untreated lignin. Lignin can be oxidized directly at the anode or

the cathode (Garedew et al., 2020). In a nondiaphragm cylindrical electrolytic cell, the graphite cathode is on the inside, and the RuO_2-IrO_2/Ti net anode is depolymerized in an alkaline aqueous solution on the outside. The by-product O_2 on the anode can be effectively reduced to H_2O_2 on the cathode. Also, ·OH, $\cdot O_2^-$ and OOH are decomposed into H_2O_2 (Moodley et al., 2012). As such, lignin is broken by these free radicals and the C–C bonds are anodized to produce aromatic products in different low molecular weights.

Lignin can directly form aromatic compounds by breaking the C–C bond. Some types of lignin can be oxidized into intermediates such as acids and ketones first, followed by decomposition of the C–C bond to generate vanillin (Schutyser et al., 2018), benzaldehyde, and other products. This class of lignin typically contains two hydroxyl groups at the β- O-4 position (Bosque et al., 2017), benzyl alcohol on C_α and aliphatic alcohol on C_γ. Such structures have a high degree of specificity of electron receptors, making the structure prone to highly selective rupture of the C_α–C_β bond (Karkas et al., 2016). Overall, the single alcohol in β- O-4 lignin can undergo highly selective oxidation to furnish oxidative intermediates, and these intermediates could proceed through C–C and/or C–O bonds cleavage to obtain single aromatic products.

Conclusion

In summary, a variety of electrode materials prepared with different advantages (e.g., high activity, good stability, easy availability, and high selectivity to C–C bonds break, and electrodes with multiple metals) are demonstrated to show unexpected comprehensive effects. Different reaction devices are also illustrated to have an impact on the product distribution and yield in the electrocatalytic degradation of lignin. The reaction mechanisms involve the generation of free radicals (e.g., $O_2\cdot^-$, andOH), and the formation of MOOH to induce the C–C bond breakage. The combination and development of the already well-established electrocatalytic cleavage technology and the much-touted biomass conversion are desired to usher another industrial renaissance in the domain of chemical synthesis.

Author contributions

JH, YJ, and MZ wrote the first draft of the manuscript. HW contributed to the supervision, reviewing, and editing of the manuscript. All authors read and approved the submitted version.

Conflict of interest

The authors declare that the research was conducted in the absence of any commercial or financial relationships that could be construed as a potential conflict of interest.

Publisher's note

All claims expressed in this article are solely those of the authors and do not necessarily represent those of their affiliated organizations, or those of the publisher, the editors and the reviewers. Any product that may be evaluated in this article, or claim that may be made by its manufacturer, is not guaranteed or endorsed by the publisher.

References

Achinivu, E. C., Howard, R. M., Li, G., Gracz, H., and Henderson, W. A. (2014). Lignin extraction from biomass with protic ionic liquids. *Green Chem.* 16, 1114–1119. doi:10.1039/c3gc42306a

Bawareth, B., Di Marino, D., Nijhuis, T. A., and Wessling, M. (2018). Unravelling electrochemical lignin depolymerization. *ACS Sustain. Chem. Eng.* 6, 7565–7573. doi:10.1021/acssuschemeng.8b00335

Bosque, I., Magallanes, G., Rigoulet, M., Karkas, M. D., and Stephenson, C. R. J. (2017). Redox catalysis facilitates lignin depolymerization. *ACS Cent. Sci.* 3, 621–628. doi:10.1021/acscentsci.7b00140

Cai, C., Zhang, H., Zhong, X., and Hou, L. (2014). Electrochemical enhanced heterogeneous activation of peroxydisulfate by Fe-Co/SBA-15 catalyst for the degradation of Orange II in water. *Water Res.* 66, 473–485. doi:10.1016/j.watres.2014.08.039

Cui, T., Ma, L., Wang, S., Ye, C., Liang, X., Zhang, Z., et al. (2021). Atomically dispersed Pt-N3C1 sites enabling efficient and selective electrocatalytic C–C bond cleavage in lignin models under ambient conditions. *J. Am. Chem. Soc.* 143, 9429–9439. doi:10.1021/jacs.1c02328

Di Fidio, N., Timmermans, J. W., Antonetti, C., Galletti, A. M. R., Gosselink, R. J., Bisselink, R. J., et al. (2021). Electro-oxidative depolymerisation of technical lignin in water using platinum, nickel oxide hydroxide and graphite electrodes. *New J. Chem.* 45, 9647–9657. doi:10.1039/d1nj01037a

Di Marino, D., Jestel, T., Marks, C., Viell, J., Blindert, M., Kriescher, S. M. A., et al. (2019). Carboxylic acids production via electrochemical depolymerization of lignin. *ChemElectroChem* 6, 1434–1442. doi:10.1002/celc.201801676

Figueiredo, M. C., Trieu, V., Eiden, S., and Koper, M. T. M. (2017). Spectro-electrochemical examination of the formation of dimethyl carbonate from CO and methanol at different electrode materials. *J. Am. Chem. Soc.* 139, 14693–14698. doi:10.1021/jacs.7b08208

Garedew, M., Lin, F., Song, B., DeWinter, T. M., Jackson, J. E., Saffron, C. M., et al. (2020). Greener routes to biomass waste valorization: Lignin transformation through electrocatalysis for renewable chemicals and fuels production. *ChemSusChem* 13, 4214–4237. doi:10.1002/cssc.202000987

Hao, X., Quansheng, Y., Dan, S., Honghui, Y., Jidong, L., Jiangtao, F., et al. (2015). Fabrication and characterization of PbO2 electrode modified with([Fe(CN)6]3-) and its application on electrochemical degradation of alkali lignin. *J. Hazard. Mat.* 286, 509–516. doi:10.1016/j.jhazmat.2014.12.065

Huang, J., Jian, Y., Li, H., and Fang, Z. (2022). Lignin-derived layered 3D biochar with controllable acidity for enhanced catalytic upgrading of Jatropha oil to biodiesel. *Catal. Today* (Online ahead of print). doi:10.1016/j.cattod.2022.04.016

Jia, Y., Wen, Y., Han, X., Qi, J., Liu, Z., Zhang, S., et al. (2018). Electrocatalytic degradation of rice straw lignin in alkaline solution through oxidation on a Ti/SnO2–Sb2O3/α-PbO2/β-PbO2 anode and reduction on an iron or tin doped titanium cathode. *Catal. Sci. Technol.* 8, 4665–4677. doi:10.1039/c8cy00307f

Jian, Y., Meng, Y., and Li, H. (2022). Selectivity control of C-O bond cleavage for catalytic biomass valorization. *Front. Energy Res.* 9, 827680. doi:10.3389/fenrg.2021.827680

Karkas, M. D., Matsuura, B. S., Monos, T. M., Magallanes, G., and Stephenson, C. R. (2016). Transition-metal catalyzed valorization of lignin: The key to a sustainable carbon-neutral future. *Org. Biomol. Chem.* 14, 1853–1914. doi:10.1039/c5ob02212f

Li, H., Guo, H., Su, Y., Hiraga, Y., Fang, Z., Hensen, E. J., et al. (2019). N-formyl-stabilizing quasi-catalytic species afford rapid and selective solvent-free amination of biomass-derived feedstocks. *Nat. Commun.* 10, 699. doi:10.1038/s41467-019-08577-4

Liu, C., Wu, S., Zhang, H., and Xiao, R. (2019). Catalytic oxidation of lignin to valuable biomass-based platform chemicals: A review. *Fuel Process. Technol.* 191, 181–201. doi:10.1016/j.fuproc.2019.04.007

Liu, M., Wen, Y., Qi, J., Zhang, S., and Li, G. (2017). Fine chemicals prepared by bamboo lignin degradation through electrocatalytic redox between Cu cathode and Pb/PbO2 anode in alkali solution. *ChemistrySelect* 2, 4956–4962. doi:10.1002/slct.201700881

Ma, L., Zhou, H., Kong, X., Li, Z., and Duan, H. (2021). An electrocatalytic strategy for C–C bond cleavage in lignin model compounds and lignin under ambient conditions. *ACS Sustain. Chem. Eng.* 9, 1932–1940. doi:10.1021/acssuschemeng.0c08612

Masoumi, F., Khadivinia, E., Alidoust, L., Mansourinejad, Z., Shahryari, S., Safaei, M., et al. (2016). Nickel and lead biosorption by Curtobacterium sp. FM01, an indigenous bacterium isolated from farmland soils of northeast Iran. *J. Environ. Chem. Eng.* 4, 950–957. doi:10.1016/j.jece.2015.12.025

Moodley, B., Mulholland, D. A., and Brookes, H. C. (2012). The chemical oxidation of lignin found in Sappi Saiccor dissolving pulp mill effluent. *Water sa.* 38, 1–8. doi:10.4314/wsa.v38i1.1

Movil-Cabrera, O., Rodriguez-Silva, A., Arroyo-Torres, C., and Staser, J. A. (2016). Electrochemical conversion of lignin to useful chemicals. *Biomass Bioenergy* 88, 89–96. doi:10.1016/j.biombioe.2016.03.014

Pan, K., Tian, M., Jiang, Z.-H., Kjartanson, B., and Chen, A. (2012). Electrochemical oxidation of lignin at lead dioxide nanoparticles photoelectrodeposited on TiO2 nanotube arrays. *Electrochim. Acta* 60, 147–153. doi:10.1016/j.electacta.2011.11.025

Pardini, V. L., Smith, C. Z., Utley, J. H. P., Vargas, R. R., and Viertler, H. (2002). Electroorganic reactions. 38. Mechanism of electrooxidative cleavage of lignin model dimers. *J. Org. Chem.* 56, 7305–7313. doi:10.1021/jo00026a022

Quiroz, M. A., Reyna, S., Martínez-Huitle, C. A., Ferro, S., and De Battisti, A. (2005). Electrocatalytic oxidation of p-nitrophenol from aqueous solutions at Pb/PbO2 anodes. *Appl. Catal. B Environ.* 59, 259–266. doi:10.1016/j.apcatb.2005.02.009

Rauber, D., Dier, T. K. F., Volmer, D. A., and Hempelmann, R. (2018). Electrochemical lignin degradation in ionic liquids on ternary mixed metal electrodes. *Z. Phys. Chem. (N F).* 232, 189–208. doi:10.1515/zpch-2017-0951

Schmitt, D., Regenbrecht, C., Hartmer, M., Stecker, F., and Waldvogel, S. R. (2015). Highly selective generation of vanillin by anodic degradation of lignin: A combined approach of electrochemistry and product isolation by adsorption. *Beilstein J. Org. Chem.* 11, 473–480. doi:10.3762/bjoc.11.53

Schutyser, W., Renders, T., Van den Bosch, S., Koelewijn, S. F., Beckham, G. T., and Sels, B. F. (2018). Chemicals from lignin: An interplay of lignocellulose fractionation, depolymerisation, and upgrading. *Chem. Soc. Rev.* 47, 852–908. doi:10.1039/c7cs00566k

Shao, D., Liang, J., Cui, X., Xu, H., and Yan, W. (2014). Electrochemical oxidation of lignin by two typical electrodes: Ti/SbSnO2 and Ti/PbO2. *Chem. Eng. J.* 244, 288–295. doi:10.1016/j.cej.2014.01.074

Smith, C. Z., Utley, J. H. P., and Hammond, J. K. (2010). Electro-organic reactions. Part 60[1]. The electro-oxidative conversion at laboratory scale of a lignosulfonate into vanillin in an FM01 filter press flow reactor: Preparative and mechanistic aspects. *J. Appl. Electrochem.* 41, 363–375. doi:10.1007/s10800-010-0245-0

Sun, Z., Fridrich, B., de Santi, A., Elangovan, S., and Barta, K. (2018). Bright side of lignin depolymerization: Toward new platform chemicals. *Chem. Rev.* 118, 614–678. doi:10.1021/acs.chemrev.7b00588

Tolba, R., Tian, M., Wen, J., Jiang, Z.-H., and Chen, A. (2010). Electrochemical oxidation of lignin at IrO2-based oxide electrodes. *J. Electroanal. Chem. (Lausanne).* 649 (1-2), 9–15. doi:10.1016/j.jelechem.2009.12.013

Trasatti, S. (2000). Electrocatalysis: Understanding the success of DSA®. *Electrochim. Acta* 45, 2377–2385. doi:10.1016/s0013-4686(00)00338-8

Valle, B., Remiro, A., Aguayo, A. T., Bilbao, J., and Gayubo, A. G. (2013). Catalysts of Ni/α-Al2O3 and Ni/La2O3-αAl2O3 for hydrogen production by steam reforming of bio-oil aqueous fraction with pyrolytic lignin retention. *Int. J. Hydrogen Energy* 38, 1307–1318. doi:10.1016/j.ijhydene.2012.11.014

Wang, Y.-S., Yang, F., Liu, Z.-H., Yuan, L., and Li, G. (2015). Electrocatalytic degradation of aspen lignin over Pb/PbO2 electrode in alkali solution. *Catal. Commun.* 67, 49–53. doi:10.1016/j.catcom.2015.03.033

Wu, H., Li, H., and Fang, Z. (2021). Hydrothermal amination of biomass to nitrogenous chemicals. *Green Chem.* 23, 6675–6697. doi:10.1039/d1gc02505h

Yu, H., Wang, S., Sun, Y., Zhang, W., Li, R., and Kang, X. (2022). Pyrolysis mechanism law of β-O-4 lignin dimer model compounds: A density functional theory study. *Ind. Crops Prod.* 180, 114746. doi:10.1016/j.indcrop.2022.114746

Zhang, Y.-M., Peng, Y., Yin, X.-L., Liu, Z.-H., and Li, G. (2014). Degradation of lignin to BHT by electrochemical catalysis on Pb/PbO2 anode in alkaline solution. *J. Chem. Technol. Biotechnol.* 89, 1954–1960. doi:10.1002/jctb.4282

Zhu, H., Wang, L., Chen, Y., Li, G., Li, H., Tang, Y., et al. (2014). Electrochemical depolymerization of lignin into renewable aromatic compounds in a non-diaphragm electrolytic cell. *RSC Adv.* 4, 29917–29924. doi:10.1039/c4ra03793f

Zirbes, M., Schmitt, D., Beiser, N., Pitton, D., Hoffmann, T., and Waldvogel, S. R. (2019). Anodic degradation of lignin at active transition metal-based alloys and performance-enhanced anodes. *ChemElectroChem* 6, 155–161. doi:10.1002/celc.201801218

frontiers | Frontiers in Chemistry

TYPE Mini Review
PUBLISHED 15 September 2022
DOI 10.3389/fchem.2022.999607

OPEN ACCESS

EDITED BY
Yaqiong Su,
Xi'an Jiaotong University, China

REVIEWED BY
Ling-Ping Xiao,
Dalian Polytechnic University, China
Yong Guo,
East China University of Science and Technology, China
Jianjian Wang,
Chongqing University, China

*CORRESPONDENCE
Yangang Wang,
ygwang8136@mail.zjxu.edu.cn
Xi Li,
xili21@mail.zjxu.edu.cn
Hu Pan,
hupand163@163.com

†These authors have contributed equally to this work

SPECIALTY SECTION
This article was submitted to Green and Sustainable Chemistry, a section of the journal Frontiers in Chemistry

RECEIVED 21 July 2022
ACCEPTED 02 August 2022
PUBLISHED 15 September 2022

CITATION
Zhang Q, Hu Y, Li S, Zhang M, Wang Y, Wang Z, Peng Y, Wang M, Li X and Pan H (2022), Recent advances in supported acid/base ionic liquids as catalysts for biodiesel production. *Front. Chem.* 10:999607. doi: 10.3389/fchem.2022.999607

Recent advances in supported acid/base ionic liquids as catalysts for biodiesel production

Qidi Zhang[1†], Yuxuan Hu[1†], Siying Li[1], Meiqi Zhang[1], Yangang Wang[1*], Ziheng Wang[1], Yixiang Peng[1], Meng Wang[1], Xi Li[1*] and Hu Pan[1,2*]

[1]College of Biological, Chemical Science and Engineering, Jiaxing University, Jiaxing, Zhejiang, China, [2]Key Laboratory for Power Machinery and Engineering of Ministry of Education, School of Mechanical Engineering, Shanghai Jiaotong University, Shanghai, China

Biodiesel is considered a potential substitute for fossil diesel because of its unique environmentally friendly and renewable advantages. The efficient and durable heterogeneous catalysts are vital to greenly and efficiently drive the biodiesel production process. The ionic liquid-functionalized materials, possessing the characteristics of both homogeneous and heterogeneous catalysts, are one of the promising substitutions for conventional homogeneous acid/base catalysts for producing biodiesel. This mini-review focuses on recent advances in supported acid/base ionic liquids to synthesize ionic liquid-functionalized materials for producing biodiesel. The methods of immobilizing ionic liquids on supports were summarized. The merits and demerits of various supports were discussed. The catalytic activities of the ionic liquid-functionalized materials for biodiesel production were reviewed. Finally, we proposed the challenges and future development direction in this area.

KEYWORDS

renewable oil, biodiesel production, heterogeneous catalysis, ionic liquid-functionalized material, solid acid/base catalyst

Introduction

The excessive consumption of fossil resources has brought a series of energy shortages and environmental pollution problems (Dong et al., 2019; Guo et al., 2022). It is desired to develop renewable and environmentally friendly alternatives to fossil fuels (Mao et al., 2022). Biodiesel is a well-known alternative to fossil diesel on account of its unique advantages, such as its renewability and environment-friendly nature. Biodiesel is mainly composed of long-chain fatty acid methyl esters. It is well known that biodiesel is mainly produced from renewable oil (e.g., vegetable oils and animal fats) through transesterification of triglycerides in oil and esterification of long-chain fatty acids in oil (Figure 1) (Pan et al., 2020). In this process, a catalyst plays a key role in influencing reaction conditions, the production efficiency of biodiesel, and biodiesel cost (Mukhtar et al., 2022). Ionic liquids (ILs), as a class of novel materials, are defined as organic salts

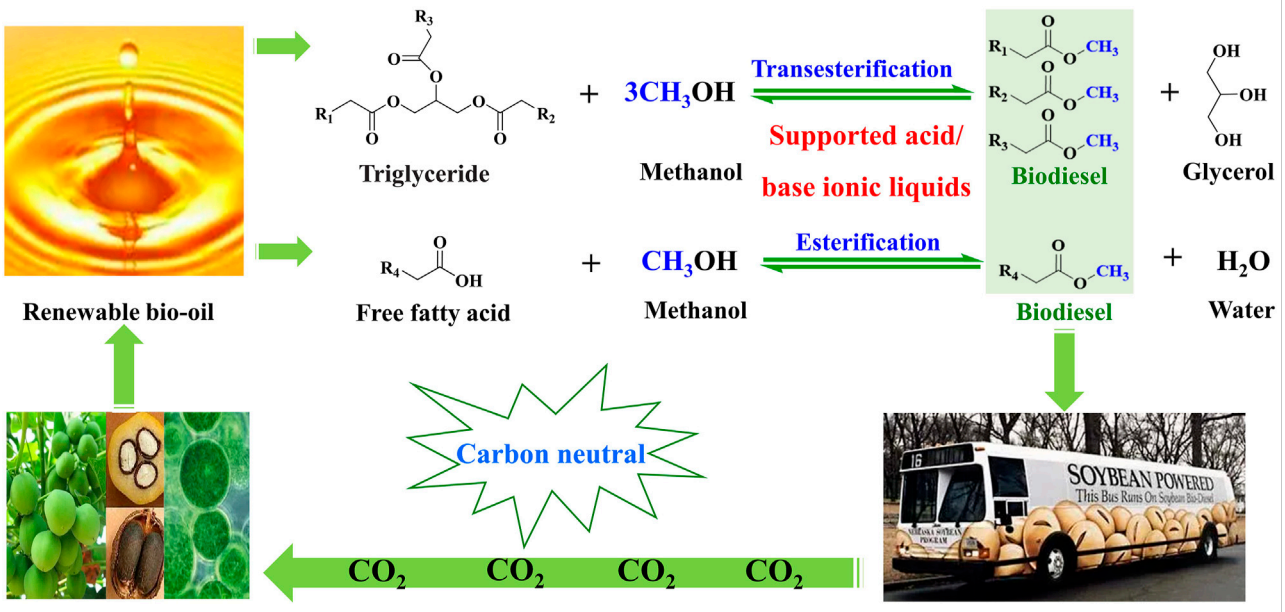

FIGURE 1
Biodiesel production cycle from renewable bio-oils *via* transesterification and esterification catalyzed by the supported acid/base ionic liquids.

with melting points below 100°C composed of anions and cations (Cheng et al., 2022). ILs utilized as catalysts have obtained enormous attention in the conversion of renewable oil to biodiesel, owing to their outstanding properties, such as ignored vapor pressure, strong solubility, wide liquid temperature, thermal and chemical stability, and low toxicity (Panchal et al., 2022). Meanwhile, physicochemical properties and functions of ILs can be designed and adjusted *via* changing the structure of anions and cations in ILs. Owing to these outstanding advantages of ILs, they have been employed for biodiesel production. For instance, SO_3H-functionalized ILs exhibited remarkable catalytic activity in the esterification of fatty acids to biodiesel (Han et al., 2022), and basic ILs afforded prominent catalytic performance in the transesterification of triglycerides to biodiesel (Panchal et al., 2022). However, ILs are usually soluble in polar solvents, resulting in their recycling difficulty in the process of biodiesel production. ILs also have a severe shortcoming of high viscosity, causing inconvenient operation. These deficiencies need to be solved to expand the application of ILs in the industrial production of biodiesel.

To deal with the aforementioned issues, the immobilization of ILs on solid supports to synthesize IL functionalized materials is a viable strategy. Ionic liquid-functionalized materials inherit the merits of ILs and supports, combining advantages of both homogeneous and heterogeneous catalysts; the former homogeneous characteristics come from highly soluble ILs on the support surface, and the latter heterogeneous characteristics originate from the solid support. Moreover, IL-functionalized materials are suitable for the continuous production of biodiesel on fixed-bed reactors. Therefore, various IL-functionalized materials have been developed for the catalytic synthesis of biodiesel production through immobilization of ILs on the supports, where various supports are utilized, including silica, magnetic nanomaterials, polymers, nitrogen-doped carbon, and metal–organic frameworks (MOFs) (Pan et al., 2016).

Although many high-quality reviews on ILs as catalysts or solvents for the synthesis of biodiesel have been published (Ong et al., 2021), a recent review focusing on heterogenization of ILs *via* immobilization of ILs on solid supports for biodiesel production is still required. Hence, we categorized and summarized recent developments in synthesizing IL-functionalized materials for producing biodiesel. The methods of immobilizing ILs onto various carriers, including silica, magnetic nanomaterials, polymers, nitrogen-doped carbon, and MOFs, are reviewed. The merits and demerits of various supports are discussed. The catalytic activities of the ionic liquid functionalized materials for biodiesel production are presented. Finally, the prospects and challenges of utilizing IL-functionalized materials as catalysts for biodiesel production are proposed.

Ionic liquid-functionalized silica

Silica materials are widely used catalyst carriers due to their distinct merits, such as low cost, thermal stability, and chemical inertness. Among them, mesoporous silica such as SBA-15 is the most popular, owing to its remarkable structural properties,

TABLE 1 Summary of carbon-supported metal oxides for biodiesel production.

Catalyst	Oil source	Reaction condition	Yield (%)	Reusability (time)	Reference
SBA- IL-3	Palmitic acid	9:1, 65°C, 15%, 8 h	88.1	80 (5)	Wang et al. (2018)
IL/Fe-SBA-15	Oleic acid	6:1, 90°C, 5%, 3 h	87.7[a]	80.8[a] (6)	Zhang et al. (2012)
PIL-3	Palmitic acid	6:1, 65°C, 3%,8 h	91.6	75 (5)	Wang et al. (2019)
P(VB-VS)HSO_4	Soapberry oil	29.1:1, 150°C, 8.7%, 8 h	95.2	90.9 (6)	Feng et al. (2017)
MIL-101(Cr)@ MBIAILs	Oleic acid	10:1, 67°C, 11%, 4 h	91.0	82.1 (6)	Han et al. (2018)
Fe_3O_4@HKUST-1	Soybean oil	30:1, 65°C, 1.2%, 3 h	92.3[a]	About 82[a] (5)	Xie and Wan, (2018)
AILs/HPW/UiO-66-2COOH	Acidic oil	35:1, 110°C, 10%, 6 h	95.8[a]	About 80[a] (5)	Xie and Wan., (2019)
FS-B-L-IL	*Koelreuteria integrifolia* oil	40:1, 160°C, 10%, 10 h	93.7	77.5 (5)	Zhang et al. (2017a)
$CoFe_2O_4$/MIL-88B(Fe)-NH_2/(Py-Ps)PMo	Acidic oil	30:1, 140°C, 8%, 8 h	95.6[a]	85.2 (5)	Xie and Wang., (2020)

[a]Conversion.

including high surface area, uniform hexagonal pores, large pore volume, and tailorable pore diameter (Ziarani et al., 2021). More importantly, abundant silanol groups on its surface enable grafting ILs *via* a covalent bond. For instance, phosphotungstic acid-based IL-functionalized SBA-15 was synthesized by post-modification of SBA-15 using the sulfhydryl reagent through the Si-O-Si- covalent bond, followed by grafting the acidic IL *via* the thiol-ene reaction (Wang et al., 2018). The acidic IL-functionalized SBA-15 was evaluated by esterification of palmitic acid to biodiesel production and exhibited an 88.1% yield using methanol to an acid molar ratio of 9:1 and 15 wt% catalyst dosage at 65°C for 9 h. The catalyst exhibited about 80% yield after being reused five times (Table 1, in supporting information).

To improve the acidity of the catalyst, Fe-incorporated SBA-15 (Fe-SBA-15) was utilized as a carrier for grafting sulfonic acid-functionalized IL. The acid catalyst (IL/Fe-SBA-15) is synthesized by immobilizing the sulfonic acid-functionalized IL on Fe-SBA-15 *via* a silylation reaction between alkoxy groups of IL and silanol groups of the support (Zhang et al., 2012). IL/Fe-SBA-15 showed 87.7% conversion of oleic acid using a catalyst amount of 5 wt% and methanol to an oleic acid molar ratio of 9:1 at 90°C for 3 h, which was ascribed to the synergistic effect of Lewis and Brønsted acidic sites. In addition to the loading acidic ILs, SBA-15 is also used to load basic ILs for producing biodiesel *via* transesterification. A series of basic catalysts were synthesized by immobilizing silane-based basic ILs on SBA-15 *via* a silylation reaction between alkoxy groups of silane-based basic ILs and silanol groups of SBA-15. The tetraalkylammonium hydroxides immobilized onto SBA-15 were fabricated and utilized for the conversion of soybean oil to biodiesel through transesterification (Xie and Fan., 2014). The basic catalyst exhibited a 99.8% yield with good reusability.

Although various acid or base ILs have been successfully immobilized onto mesoporous silica for the production of biodiesel, the following problems still need to be solved: 1) organosilicon reagents used to load ILs are usually expensive; 2) the -Si-O-Si- bond used to link ILs to mesoporous silica is unstable in the acidic or basic media; 3) the hydrophilicity of silica is not conducive to the contact between the substrate oil and catalyst and also easily causes catalyst deactivation by adsorption of by-products (water and glycerol) on the surface of the catalyst.

Ionic liquid-functionalized porous polymers

Porous polymers, featured with nanopore structures, large specific surface areas, high pore volumes, flexible chemical tenability, tunable wettability, and outstanding chemical stability, are remarkable carrier candidates for supported ILs (Mohamed et al., 2022). Porous polymers are mainly synthesized by the hard template method, soft template method, and template-free methods and functionalized with ILs using various methods, including self-polymerization of ILs, copolymerization of ILs with skeleton molecules, and post-modification (Zhang et al., 2022).

The acidic poly (ionic liquid) was synthesized by self-polymerization of the acidic IL monomer with the double bond group for esterification of palmitic acid to biodiesel with a 91.6% yield at 65°C for 8 h (Wang et al., 2019). The acidic ionic liquid polymer catalyst synthesized by self-polymerization usually exhibits low specific surface area and poor hydrophobicity. To improve the specific surface area and hydrophobicity of acidic ionic liquid polymers, copolymerization of the acid ionic liquid monomer and divinyl benzene (DVB) is a feasible synthetic method. The effect of DVB content in the catalyst on its specific surface area and hydrophobicity was investigated by Liang et al. (Li et al., 2016). The increase of the DVB content improves the hydrophobicity and specific surface area of the catalyst but reduces the acid density of the catalyst. Therefore, the physicochemical properties of the catalyst can be regulated by adjusting the content of DVB. Various ionic liquid polymers were

developed by copolymerization of various acidic ionic liquid monomers and DVB for biodiesel production. The poly (ionic liquid) was fabricated by copolymerization of the sulfonic acid ionic liquid monomer and DVB and possessed high surface areas with 100.1 m^2/g, rich meso-macropores, and acid density of 1.64 mmol/g (Feng et al., 2017). A 95.2% biodiesel yield was obtained from soapberry oil using a 29.1 methanol to oil molar ratio and an 8.7 wt% catalyst amount at 150°C for 8 h.

Condensation is also a method to synthesize acidic ionic liquid polymers. The poly ionic liquid was synthesized by phenolic condensation and exhibited high acidity with 4.5 mmol/g (Bian et al., 2019). Post-modification is a frequently used method to prepare acidic ionic liquid polymers. The mesoporous melamine-formaldehyde polymer was developed under solvothermal conditions using the soft template method (Pan et al., 2019). The nitrogen-rich polymer was used for immobilization of ILs through the chemical post-modification method. The resulting functional polymer exhibited multiple remarkable properties, including a rich mesoporous structure with a specific surface area of 283.0 m^2/g, high density (2.2 mmol/g), and strong acidity. These properties endowed high catalytic activity with 95% biodiesel yield from oleic acid. In addition, zirconium phosphonate and 2D-layered montmorillonite were also used to support acidic poly ILs for the synthesis of an acid catalyst (Liu et al., 2019; Pan et al., 2022). Polymers can also be used to synthesize basic catalysts for producing biodiesel. The basic poly (ionic liquid) was developed by copolymerization of the ionic liquid and subsequent ion exchange. The basic poly (ionic liquid) exhibited superhydrophobicity and porous structure with 103 m^2/g and 96.3% biodiesel yield from the conversion of soybean oil with methanol *via* transesterification (Jiang et al., 2017). Ionic liquid-functionalized porous polymers are potential catalysts for catalytic conversion of oils to biodiesel. However, its high cost and limited thermal stability should be paid close attention.

Ionic liquid-functionalized carbon

Owing to their obvious merits, including excellent thermal and chemical stability, controllable surface wettability, cheapness, availability, and no toxicity, carbonaceous materials offer promising supports for the synthesis of highly efficient and reusable catalysts (Dhawane et al., 2018). In particular, N-rich porous carbon contains a large number of N active sites, which can support ILs through chemical post-modification (Sun et al., 2019). In addition, N-rich porous carbon exhibits a high specific surface area, which promotes the reaction between active sites of carbon–nitrogen material and substrates, resulting in high IL loading.

Porous carbon nitrogen materials are mainly prepared using nitrogen-containing organic compounds (e.g., cyanamide, melamine, urea, etc.) or polymers (e.g., polypyrrole) as nitrogen and carbon sources. Meanwhile, doping fructose as a carbon source in nitrogenous organic compounds can adjust the carbon content in carbon–nitrogen materials. Carbonization and the solvothermal method are the main methods to convert organic compounds or polymers into carbon–nitrogen materials (Tang et al., 2018). To enhance the specific surface area of carbon–nitrogen materials, the template method is an effective technique for forming pore structures in carbon–nitrogen materials (Zhang et al., 2020). Common templates include potassium hydroxide (KOH), zinc chloride ($ZnCl_2$), and silicon dioxide (SiO_2). Porous structures of the materials are formed by removing the templates after carbonization, KOH and $ZnCl_2$ can be removed by washing, and SiO_2 is eliminated *via* corrosion using a strong base or hydrofluoric acid.

Ionic liquids' functional carbons were synthesized by quaternary ammonization of carbon–nitrogen materials with diverse quaternary ammonization reagents including iodomethane, 1,3-propane sultone, and 1,4-butanesultone, followed by strong acid treatment using acids such as $H_3PW_{12}O_{40}$, HSO_3CF_3, and H_2SO_4 (Liu et al., 2016). For instance, acid IL functional carbon was fabricated by quaternary ammonization of nanoporous carbon with 1,3-propanesultone and subsequent ion exchanging with HSO_3CF_3, where the nanoporous carbon was prepared from melamine and glucose through carbonization at 800°C. The resulting acid IL functional carbon exhibited 88.5% biodiesel yield *via* transesterification of tripalmitin with methanol at 65°C for 14 h (Liu et al., 2015). To reduce catalyst costs, waste cow manure was employed for the synthesis of N-rich nanoporous carbon through carbonization in the presence of $ZnCl_2$ and $FeCl_3$ templates. Subsequently, acid IL-functionalized carbon was developed by treating the N-rich nanoporous carbon with 1,4-butanesultone, followed by HSO_3CF_3 treatment. The resultant acid catalyst showed 88.5% biodiesel yield from tripalmitin at 65°C for 14 h, which even overmatched those of homogeneous $H_3PW_{12}O_{40}$ (Noshadi et al., 2016).

Ionic liquid-functionalized metal–organic frameworks

Metal–organic frameworks (MOFs) as a kind of inorganic–organic hybrid materials are constructed by coordination of metal ions or metal clusters with organic ligands (Zhang et al., 2019). MOFs have attracted tremendous interest in the immobilization of ILs for the synthesis of catalysts, owing to their remarkable advantages, including crystalline frameworks, high specific surface area, ordered pore structure, and uniform adjustable pore size (Cong et al., 2021). Meanwhile, compared with other porous materials, MOFs exhibit uniform porous structures with large specific surface areas, regular and adjustable pore, and versatile architecture (Wang et al., 2022).

Various IL-functionalized MOFs have been fabricated for the synthesis of catalysts. The IL-functionalized MOFs are synthesized

mainly through immobilization and encapsulation methods. The immobilization method mainly utilizes MOF as the carrier to load IL onto MOF through post-modification. For instance, the acidic IL-functionalized UiO-66 solid acids were synthesized by quaternization of the amino group originating from UiO-66 with 1,3-propane sultone, followed by an ion exchange with HSO_3CF_3, or H_2SO_4 (Peng et al., 2020). The prepared solid acids possessed high acid densities (3.27–3.33 mmol/g) and super acidity sites, where acidic ILs were immobilized on MOF *via* a covalent bond. The solid acids showed biodiesel yield of above 80% *via* transesterification of sunflower oil, which was superior to Amberlyst-15, Nafion NR50, and the homogeneous acid ionic liquid.

The acid–base interaction is another method of immobilizing ILs, in which acidic ILs are immobilized on MOF by the acid and base reaction between acidic IL and the amino group of MOF through the ionic bond. For example, the acidic IL-functionalized NH_2-UiO-66 was fabricated by the acid and base reaction between a sulfonic group from IL and an amino group from NH_2-UiO-66 (Lu et al., 2022). NH_2-UiO-66 and sulfonic acid IL are used as a carrier and catalytic active species, respectively. The obtained catalyst showed above 90% conversion of oleic acid and above 80% yield *via* transesterification of triglycerides. Using the same methods, the Brønsted IL was grafted in NH_2-MIL-88B (Fe) to synthesize the acid catalyst (Wu et al., 2016). The synthesized acid catalyst, exhibiting a specific surface area of 103.6 m^2/g and acidity of 1.76 mmol H^+ g^{-1}, showed 93.2% conversion using the ethanol to oil molar ratio of 10.5:1 and 8.5 wt% catalyst amount at 90°C for 4.5 h.

Except for MOF ligands, as bridge-supported ILs, unsaturated metal sites in MOF can also support ionic liquids *via* the coordination bond. MIL-101(Cr), as a stable MOF with 1809.1 m^2 g^{-1} surface area, was constituted by the interconnection of trimetric chromium and benzene-1,4-dicarboxylates *via* the coordination bond, possessing massive coordinatively unsaturated Cr (III) sites, which provides active sites for electron-rich group coordination. The thiol-functionalized ionic liquids were loaded on MIL-101(Cr) *via* coordination of electron-rich -SH groups from ILs and the unsaturated metal Cr sites (Han et al., 2018). MIL-101(Cr)@ MBIAILs exhibited a 91.0% conversion of oleic acid using the molar ratio of oleic acid to methanol 1:10 and 11 wt% catalyst amount at 67°C for 4 h. This method is also feasible for the synthesis of base catalysts. The amino-functional basic IL was attached to the Fe_3O_4@HKUST-1 carrier through coordination of the amino groups in the basic IL and unsaturated metal Cu^{2+} sites in HKUST-1, where HKUST-1 was synthesized from divalent copper and benzene-1,3,5-tricarboxylic acid by the solvothermal method (Xie and Wan., 2018). The solid base catalyst is used to produce biodiesel through transesterification of soybean oil and showed oil conversion of 92.3% under reaction conditions of 1.2 wt% catalyst dosage and a methanol/oil molar ratio of 30:1 at 65°C for 3 h.

Encapsulation is a novel strategy for heterogeneous ILs, where active species are physically accommodated in highly porous materials (Zheng et al., 2022). Compared with the immobilization method in which the active sites of the catalyst are fixed on the support, the active sites of the catalyst synthesized by the encapsulation strategy are flowable and free, which can promote the activity of the catalyst (Kong et al., 2016). The sulfonic acid IL is encapsulated into UiO-66-2COOH through the following two steps: 1) 12-tungstophosphoric acid (HPW) was encapsulated into UiO-66-2COOH *via* the *in situ* preparation strategy; 2) then, the sulfonic acid IL was encapsulated into HPW/UiO-66-2COOH *via* pairing PW anions with the sulfonic acid IL cations (Xie and Wan., 2019). The resultant acid catalyst with 3.40 mol/g acid density and 8.63 m^2/g specific surface area was used for the transformation of acidic vegetable oils into biodiesel through simultaneous esterification and transesterification, and 95.27% conversion was obtained using the methanol to oil molar ratio of 35:1 and catalyst amount of 10 wt% at 110°C for 6 h. Utilizing the same encapsulation strategy, sulfonic acid functionalized-IL was encapsulated within the cages of MIL-100 with a 0.83 mmol g^{-1} loading amount (Wan et al., 2015). The obtained acid catalyst with a surface area of 167 m^2 g^{-1} was used for catalytic esterification of oleic acid with ethanol to produce biodiesel. Conversion of 94.55 was realized using a 11:1 M ratio of ethanol to oleic acid and 15 wt% at 111°C for 5 h.

Ionic liquid-functionalized magnetic composites

Efficient recovery and reuse of catalysts are extremely important for industrial production of biodiesel because they can reduce the production cost of biodiesel and is environmentally friendly. Filtration and centrifugation are currently the main methods of separating catalysts from the reaction mixture (Li et al., 2020). Filtration is time-consuming and inefficient, especially for the separation of nano-catalysts (Krishnan et al., 2021). Meanwhile, for nano-catalysts with a very small size, filtration may be ineffective because they can pass through the filter paper during the filtration process. Centrifugation, as another separation method, helps overcome the defects of the filtration method and effectively separates nano-catalysts. Nevertheless, centrifugation is complex, energy consuming, and uneconomical, which limits its application in the industry (Quah et al., 2019).

Magnetic separation enables separation of catalysts simply and effectively from the reaction mixture by an external magnetic field, which offers a promising way to improve catalyst recovery (Chen et al., 2019). Various ionic liquid-functionalized magnetic composites were fabricated by immobilizing the functionalized ionic liquid on ferromagnetic materials including Fe_3O_4, γ-Fe_2O_3, Fe, Co, and Ni through post-modification. Among them, Fe_3O_4 nanoparticles are the most commonly used magnetic carrier, owing to their unique merits including small size, convenient synthesis, strong magnetism, and good dispersion (Wang et al., 2020). Fe_3O_4 nanoparticles are

mainly synthesized from divalent and trivalent iron salts by coprecipitation, hydrothermal, and reduction methods. Nevertheless, Fe_3O_4 nanoparticles are usually unstable and easily oxidized or hydrolyzed, especially in the presence of oxygen or acid, respectively. In addition, Fe_3O_4 nanoparticles are very easily agglomerated resulting in the formation of large particles, which greatly reduce their performance as a support. To overcome the aforementioned problems, coating Fe_3O_4 nanoparticles using organic or inorganic substrates is an effective and feasible strategy. Common coatings are silicon dioxide (SiO_2), polymers, and MOFs. For example, the Brønsted–Lewis acidic ionic liquid was supported on the carrier Fe_3O_4@SiO_2 to synthesize the magnetic acid catalyst for the one-pot transformation of *Koelreuteria integrifolia* oil with a high acid value into biodiesel (Zhang et al., 2017a). The obtained acid catalyst showed a core–shell structure and Fe_3O_4 as the core was coated with a 12–20 nm-thick SiO_2 shell through a Fe-O-Si bond. The acidic ionic liquid was immobilized on Fe_3O_4@SiO_2 *via* post-modification using an organosilicon reagent through the Si-O-Si-covalent bond. A 93.7% biodiesel yield was realized using a 10 wt% catalyst amount and 40:1 M ratio of methanol to oil at 160°C for 10 h. The catalyst could be quickly separated by magnetic force and was still able to maintain a 77.5% yield in the fifth run. Utilizing the same strategy, various acid or basic polyionic liquids have been immobilized on core–shell-structured Fe_3O_4@SiO_2 composites to synthesize magnetic acid or base catalysts for biodiesel production, where organosilicon reagents with double bond functional groups were the bridge between linking polyionic liquids and the Fe_3O_4@SiO_2 carrier (Zhang et al., 2017b; Ding et al., 2021). MOFs are another coating that enable encapsulation of Fe_3O_4 nanoparticles, playing a role in the isolation of nanoparticles. For instance, the magnetic support $CoFe_2O_4$/MIL-88B(Fe)-NH_2 was fabricated by encapsulation of magnetic $CoFe_2O_4$ particles in a cage of MIL-88B(Fe)-NH_2 with the amine functional group (Xie and Wang., 2020). Then, the acidic ionic liquid was immobilized on $CoFe_2O_4$/MIL-88B(Fe)-NH_2 by the acid and base reaction between the sulfonic acid functional group of the acidic ionic liquid and the amino group of MIL-88B(Fe)-NH_2 through the ionic bond. The obtained acid catalyst with an acid capacity of 4.37 mmol g^{-1} and a specific surface area of 35.44 m^2 g^{-1} exhibited oil conversion of 95.6% *via* transesterification under the condition of the methanol to oil molar ratio of 30:1 and catalyst amount of 8 wt% at 140°C for 8 h.

Summary and future perspectives

Acidic or basic ionic liquids (especially, sulfonic acid- and heteropoly acid-functionalized ionic liquids and quaternary ammonium hydroxide-based basic ionic liquids) have been proven to have excellent catalytic activity in the production of biodiesel. Nevertheless, shortcomings of ionic liquids, such as high cost, high viscosity, and recycling difficulty, limit their industrial application. To overcome the aforementioned shortcomings, immobilization of the ionic liquid on support is an effective strategy for the heterogeneous ionic liquid. Thus, this review primarily focuses on supported acid/base ionic liquids as catalysts for biodiesel production. The merits and demerits of various supports, including mesoporous silica, porous polymers, carbonaceous materials, MOFs, and ferromagnetic materials, are compared to immobilize ionic liquids for the production of biodiesel. The methods of immobilizing ionic liquids on supports were described for the synthesis of ionic liquid-functionalized materials.

Based on the green and efficient production of biodiesel, the following guidelines for the synthesis of efficient, stable, and low-cost ionic liquid-functionalized materials may still need to be taken into consideration:

(1) The support with excellent thermal and chemical stability would be highly desirable to improve the stability of ionic liquid-functionalized material. The reported supports such as mesoporous silica, MOFs, and ferromagnetic materials exhibit limited chemical stability. Specifically, in the presence of strong acid and base media, they are unstable. The polymer support exhibits excellent chemical stability, but its thermal stability is mediocre. Enormous effort should be devoted to develop suitable material with remarkable thermal and chemical stabilities for supporting ionic liquids.
(2) Compared with the immobilization of the ionic liquid on the support, encapsulation of the ionic liquid in the cage of the porous support is a superior strategy for the synthesis of ionic liquid-functionalized material with an outstanding catalytic activity. The active sites of the catalyst synthesized by encapsulation strategy are free and easily accessible to the substrate, which is beneficial to improve the catalytic activity of the catalyst.
(3) Although various ionic liquid-functionalized materials have been fabricated for the catalytic transformation of oil into biodiesel, their complex synthesis process and expensive raw materials inevitably lead to high catalyst costs. Hence, it is desirable to develop a simple method for the synthesis of ionic liquid-functionalized materials using cheap biomass.

Author contributions

QZ and YH jointly conceived the manuscript. SL and MZ collected the references. QZ, YH, ZW, YP, and MW wrote and edited the original draft. XL, YW, and HP revised the manuscript and provided financial support.

Funding

This work was funded by the Natural Science Foundation of Zhejiang Province (No. LQ22B060008), the National Key Research and Development Program of China (Grant No. 2018YFB1502900), the Innovation Jiaxing Elite Leadership Plan and Technology Development Project of Jiaxing University, the Research Startup Program of Jiaxing University, China (No.

CD70519067), and the First-class Course Program of Environmental Chemistry of Jiaxing University (No. 108542161).

Conflict of interest

The authors declare that the research was conducted in the absence of any commercial or financial relationships that could be construed as a potential conflict of interest.

Publisher's note

References

Bian, Y., Zhang, J., Zhang, S., Liu, C., and Zhao, D. (2019). Synthesis of polyionic liquid by phenolic condensation and its application in esterification. *ACS Sustain. Chem. Eng.* 7 (20), 17220–17226. doi:10.1021/acssuschemeng.9b03859

Chen, M. N., Mo, L. P., Cui, Z. S., and Zhang, Z. H. (2019). Magnetic nanocatalysts: Synthesis and application in multicomponent reactions. *Curr. Opin. Green Sustain. Chem.* 15, 27–37. doi:10.1016/j.cogsc.2018.08.009

Cheng, J., Mao, Y., Guo, H., Qian, L., Shao, Y., Yang, W., et al. (2022). Synergistic and efficient catalysis over Brønsted acidic ionic liquid [BSO_3HMIm] [HSO_4]-modified metal-organic framework (IRMOF-3) for microalgal biodiesel production. *Fuel* 322, 124217. doi:10.1016/j.fuel.2022.124217

Cong, W. J., Nanda, S., Li, H., Fang, Z., Dalai, A. K., and Kozinski, J. A. (2021). Metal-organic framework-based functional catalytic materials for biodiesel production: A review. *Green Chem.* 23 (7), 2595–2618. doi:10.1039/D1GC00233C

Dhawane, S. H., Kumar, T., and Halder, G. (2018). Recent advancement and prospective of heterogeneous carbonaceous catalysts in chemical and enzymatic transformation of biodiesel. *Energy Convers. Manag.* 167, 176–202. doi:10.1016/j.enconman.2018.04.073

Ding, J., Zhou, C., Wu, Z., Chen, C., Feng, N., Wang, L., et al. (2021). Core-shell magnetic nanomaterial grafted spongy-structured poly (ionic liquid): A recyclable brönsted acid catalyst for biodiesel production. *Appl. Catal. A General* 616, 118080. doi:10.1016/j.apcata.2021.118080

Dong, L., Lin, L., Han, X., Si, X., Liu, X., Guo, Y., et al. (2019). Breaking the limit of lignin monomer production via cleavage of interunit carbon-carbon linkages. *Chem* 5 (6), 1521–1536. doi:10.1016/j.chempr.2019.03.007

Feng, Y., Li, L., Wang, X., Yang, J., and Qiu, T. (2017). Stable poly (ionic liquid) with unique crosslinked microsphere structure as efficient catalyst for transesterification of soapberry oil to biodiesel. *Energy Convers. Manag.* 153, 649–658. doi:10.1016/j.enconman.2017.10.018

Guo, Y., Jing, Y., Xia, Q., and Wang, Y. (2022). NbO_x-based catalysts for the activation of C–O and C–C bonds in the valorization of waste carbon resources. *Acc. Chem. Res.* 55 (9), 1301–1312. doi:10.1021/acs.accounts.2c0.0097

Han, M., Li, Y., Gu, Z., Shi, H., Chen, C., Wang, Q., et al. (2018). Immobilization of thiol-functionalized ionic liquids onto the surface of MIL-101 (Cr) frameworks by SCr coordination bond for biodiesel production. *Colloids Surfaces A Physicochem. Eng. Aspects* 553, 593–600. doi:10.1016/j.colsurfa.2018.05.085

Han, S., Yang, J., and Huang, H. (2022). Novel self-solidifying double-site acidic ionic liquid as efficient and reusable catalyst for green biodiesel synthesis. *Fuel* 315, 122815. doi:10.1016/j.fuel.2021.122815

Jiang, B., Wang, Y., Zhang, L., Sun, Y., Yang, H., Wang, B., et al. (2017). Biodiesel production via transesterification of soybean oil catalyzed by superhydrophobic porous poly (ionic liquid) solid base. *Energy fuels.* 31 (5), 5203–5214. doi:10.1021/acs.energyfuels.7b00443

Kong, T., Guo, G., Pan, J., Gao, L., and Huo, Y. (2016). Polystyrene sulfonate threaded in MIL-101Cr (III) as stable and efficient acid catalysts. *Dalton Trans.* 45 (45), 18084–18088. doi:10.1039/C6DT03745C

Krishnan, S. G., Pua, F. L., and Zhang, F. (2021). A review of magnetic solid catalyst development for sustainable biodiesel production. *Biomass Bioenergy* 149, 106099. doi:10.1016/j.biombioe.2021.106099

Li, J., Zhang, S., Tian, W., and Liang, X. (2016). Novel polymer with ionic liquid moieties for biodiesel synthesis from waste oils. *RSC Adv.* 6 (111), 110454–110459. doi:10.1039/C6RA24596J

Li, X., Wang, C., Zhang, J., Liu, J., Liu, B., and Chen, G. (2020). Preparation and application of magnetic biochar in water treatment: A critical review. *Sci. Total Environ.* 711, 134847. doi:10.1016/j.scitotenv.2019.134847

Liu, F., Kong, W., Wang, L., Yi, X., Noshadi, I., Zheng, A., et al. (2015). Efficient biomass transformations catalyzed by graphene-like nanoporous carbons functionalized with strong acid ionic liquids and sulfonic groups. *Green Chem.* 17 (1), 480–489. doi:10.1039/C4GC01052C

Liu, F., Li, B., Liu, C., Kong, W., Yi, X., Zheng, A., et al. (2016). Template-free synthesis of porous carbonaceous solid acids with controllable acid sites and their excellent activity for catalyzing the synthesis of biofuels and fine chemicals. *Catal. Sci. Technol.* 6 (9), 2995–3007. doi:10.1039/C5CY01226K

Liu, F., Yi, X., Chen, W., Liu, Z., Qi, C. Z., Song, Y. F., et al. (2019). Developing two-dimensional solid superacids with enhanced mass transport, extremely high acid strength and superior catalytic performance. *Chem. Sci.* 10 (23), 5875–5883. doi:10.1039/C9SC01988J

Lu, P., Li, H., Li, M., Chen, J., Ye, C., Wang, H., et al. (2022). Ionic liquid grafted NH_2-UiO-66 as heterogeneous solid acid catalyst for biodiesel production. *Fuel* 324, 124537. doi:10.1016/j.fuel.2022.124537

Mao, Q., Guo, Y., Liu, X., Shakouri, M., Hu, Y., and Wang, Y. (2022). Identifying the realistic catalyst for aqueous phase reforming of methanol over Pt supported by lanthanum nickel perovskite catalyst. *Appl. Catal. B Environ.* 313, 121435. doi:10.1016/j.apcatb.2022.121435

Mohamed, M. G., El-Mahdy, A. F., Kotp, M. G., and Kuo, S. W. (2022). Advances in porous organic polymers: Syntheses, structures, and diverse applications. *Mat. Adv.* 3, 707–733. doi:10.1039/D1MA00771H

Mukhtar, A., Saqib, S., Lin, H., Shah, M. U. H., Ullah, S., Younas, M., et al. (2022). Current status and challenges in the heterogeneous catalysis for biodiesel production. *Renew. Sustain. Energy Rev.* 157, 112012. doi:10.1016/j.rser.2021.112012

Noshadi, I., Kanjilal, B., and Liu, F. (2016). Porous carbonaceous solid acids derived from farm animal waste and their use in catalyzing biomass transformation. *Appl. Catal. A General* 513, 19–29. doi:10.1016/j.apcata.2015.12.032

Ong, H. C., Tiong, Y. W., Goh, B. H. H., Gan, Y. Y., Mofijur, M., Fattah, I. R., et al. (2021). Recent advances in biodiesel production from agricultural products and microalgae using ionic liquids: Opportunities and challenges. *Energy Convers. Manag.* 228, 113647. doi:10.1016/j.enconman.2020.113647

Pan, H., Li, H., Liu, X. F., Zhang, H., Yang, K. L., Huang, S., et al. (2016). Mesoporous polymeric solid acid as efficient catalyst for (trans) esterification of crude Jatropha curcas oil. *Fuel Process. Technol.* 150, 50–57. doi:10.1016/j.fuproc.2016.04.035

Pan, H., Li, H., Zhang, H., Wang, A., and Yang, S. (2019). Acidic ionic liquid functionalized mesoporous melamine-formaldehyde polymer as heterogeneous catalyst for biodiesel production. *Fuel* 239, 886–895. doi:10.1016/j.fuel.2018.11.093

Pan, H., Liu, Y., Xia, Q., Zhang, H., Guo, L., Li, H., et al. (2020). Synergetic combination of a mesoporous polymeric acid and a base enables highly efficient heterogeneous catalytic one-pot conversion of crude Jatropha oil into biodiesel. *Green Chem.* 22 (5), 1698–1709. doi:10.1039/C9GC04135D

Pan, H., Xia, Q., Li, H., Wang, Y., Shen, Z., Wang, Y., et al. (2022). Direct production of biodiesel from crude Euphorbia lathyris L. Oil catalyzed by multifunctional mesoporous composite materials. *Fuel* 309, 122172. doi:10.1016/j.fuel.2021.122172

Panchal, B., Zhu, Z., Qin, S., Chang, T., Zhao, Q., Sun, Y., et al. (2022). The current state applications of ethyl carbonate with ionic liquid in sustainable biodiesel production: A review. *Renew. Energy* 181, 341–354. doi:10.1016/j.renene.2021.09.062

Peng, W. L., Mi, J., Liu, F., Xiao, Y., Chen, W., Liu, Z., et al. (2020). Accelerating biodiesel catalytic production by confined activation of methanol over high-

concentration ionic liquid-grafted UiO-66 solid superacids. *ACS Catal.* 10 (20), 11848–11856. doi:10.1021/acscatal.0c03261

Quah, R. V., Tan, Y. H., Mubarak, N. M., Khalid, M., Abdullah, E. C., and Nolasco-Hipolito, C. (2019). An overview of biodiesel production using recyclable biomass and non-biomass derived magnetic catalysts. *J. Environ. Chem. Eng.* 7 (4), 103219. doi:10.1016/j.jece.2019.103219

Sun, Y., Zhang, Q., Zhang, C., Liu, J., Guo, Y., and Song, D. (2019). *In situ* approach to dendritic fibrous nitrogen-doped carbon nanospheres functionalized by brønsted acidic ionic liquid and their excellent esterification catalytic performance. *ACS Sustain. Chem. Eng.* 7 (17), 15114–15126. doi:10.1021/acssuschemeng.9b03848

Tang, Z. E., Lim, S., Pang, Y. L., Ong, H. C., and Lee, K. T. (2018). Synthesis of biomass as heterogeneous catalyst for application in biodiesel production: State of the art and fundamental review. *Renew. Sustain. Energy Rev.* 92, 235–253. doi:10.1016/j.rser.2018.04.056

Wan, H., Chen, C., Wu, Z., Que, Y., Feng, Y., Wang, W., et al. (2015). Encapsulation of heteropolyanion-based ionic liquid within the metal–organic framework MIL-100 (Fe) for biodiesel production. *ChemCatChem* 7 (3), 441–449. doi:10.1002/cctc.201402800

Wang, A., Sudarsanam, P., Xu, Y., Zhang, H., Li, H., and Yang, S. (2020). Functionalized magnetic nanosized materials for efficient biodiesel synthesis via acid-base/enzyme catalysis. *Green Chem.* 22 (10), 2977–3012. doi:10.1039/D0GC00924E

Wang, K., Li, Y., Xie, L. H., Li, X., and Li, J. R. (2022). Construction and application of base-stable MOFs: A critical review. *Chem. Soc. Rev.* 23, 6417–6441. doi:10.1039/D1CS00891A

Wang, Y., Zhao, D., Chen, G., Liu, S., Ji, N., Ding, H., et al. (2019). Preparation of phosphotungsticacid based poly (ionic liquid) and its application to esterification of palmitic acid. *Renew. Energy* 133, 317–324. doi:10.1016/j.renene.2018.10.029

Wang, Y., Zhao, D., Wang, L., Wang, X., Li, L., Xing, Z., et al. (2018). Immobilized phosphotungstic acid based ionic liquid: Application for heterogeneous esterification of palmitic acid. *Fuel* 216, 364–370. doi:10.1016/j.fuel.2017.11.153

Wu, Z., Chen, C., Wan, H., Wang, L., Li, Z., Li, B., et al. (2016). Fabrication of magnetic NH_2-MIL-88B (Fe) confined Brønsted ionic liquid as an efficient catalyst in biodiesel synthesis. *Energy fuels.* 30 (12), 10739–10746. doi:10.1021/acs.energyfuels.6b01212

Xie, W., and Fan, M. (2014). Biodiesel production by transesterification using tetraalkylammonium hydroxides immobilized onto SBA-15 as a solid catalyst. *Chem. Eng. J.* 239, 60–67. doi:10.1016/j.cej.2013.11.009

Xie, W., and Wan, F. (2018). Basic ionic liquid functionalized magnetically responsive Fe_3O_4@ HKUST-1 composites used for biodiesel production. *Fuel* 220, 248–256. doi:10.1016/j.fuel.2018.02.014

Xie, W., and Wan, F. (2019). Immobilization of polyoxometalate-based sulfonated ionic liquids on UiO-66-2COOH metal-organic frameworks for biodiesel production via one-pot transesterification-esterification of acidic vegetable oils. *Chem. Eng. J.* 365, 40–50. doi:10.1016/j.cej.2019.02.016

Xie, W., and Wang, H. (2020). Synthesis of heterogenized polyoxometalate-based ionic liquids with brønsted-lewis acid sites: A magnetically recyclable catalyst for biodiesel production from low-quality oils. *J. Ind. Eng. Chem.* 87, 162–172. doi:10.1016/j.jiec.2020.03.033

Zhang, H., Li, H., Pan, H., Liu, X., Yang, K., Huang, S., et al. (2017a). Efficient production of biodiesel with promising fuel properties from Koelreuteriaintegrifoliola oil using a magnetically recyclable acidic ionic liquid. *Energy Convers. Manag.* 138, 45–53. doi:10.1016/j.enconman.2017.01.060

Zhang, H., Li, H., Pan, H., Wang, A., Xu, C. C., and Yang, S. (2017b). Magnetically recyclable basic polymeric ionic liquids for efficient transesterification of FirmianaplatanifoliaLf oil into biodiesel. *Energy Convers. Manag.* 153, 462–472. doi:10.1016/j.enconman.2017.10.023

Zhang, H., Li, H., Xu, C. C., and Yang, S. (2019). Heterogeneously chemo/enzyme-functionalized porous polymeric catalysts of high-performance for efficient biodiesel production. *ACS Catal.* 9 (12), 10990–11029. doi:10.1021/acscatal.9b0.2748

Zhang, L., Cui, Y., Zhang, C., Wang, L., Wan, H., and Guan, G. (2012). Biodiesel production by esterification of oleic acid over brønsted acidic ionic liquid supported onto Fe-incorporated SBA-15. *Ind. Eng. Chem. Res.* 51 (51), 16590–16596. doi:10.1021/ie302419y

Zhang, Q., Jiang, P., Nie, Z., and Zhang, P. (2020). Acidic ion functionalized N-doped hollow carbon for esterification of levulinic acid. *New J. Chem.* 44 (4), 1588–1593. doi:10.1039/C9NJ04752B

Zhang, Z., Jia, J., Zhi, Y., Ma, S., and Liu, X. (2022). Porous organic polymers for light-driven organic transformations. *Chem. Soc. Rev.* 51, 2444–2490. doi:10.1039/D1CS00808K

Zheng, W., Kan, X., Liu, F., Li, H., Song, F., Xia, G., et al. (2022). Ordered mesoporous carbon encapsulating KF: Efficient and stable solid base for biodiesel and fine chemical catalytic synthesis. *ACS Sustain. Chem. Eng.* 10 (11), 3477–3487. doi:10.1021/acssuschemeng.1c07157

Ziarani, G. M., Roshankar, S., Mohajer, F., and Badiei, A. (2021). The synthesis and application of functionalized mesoporous silica SBA-15 as heterogeneous catalyst in organic synthesis. *Curr. Org. Chem.* 25 (3), 361–387. doi:10.2174/1385272824.999201210194444

frontiers | Frontiers in Chemistry

TYPE Original Research
PUBLISHED 21 September 2022
DOI 10.3389/fchem.2022.1004925

OPEN ACCESS

EDITED BY
Hu Li,
Guizhou University, China

REVIEWED BY
Jianjian Wang,
Chongqing University, China
Jian He,
Jishou University, China
Heng Zhang,
Guizhou University, China

*CORRESPONDENCE
Chao Wang,
chao.wang@qdu.edu.cn
Qineng Xia,
xiaqineng159@163.com

SPECIALTY SECTION
This article was submitted to Green and Sustainable Chemistry, a section of the journal Frontiers in Chemistry

RECEIVED 27 July 2022
ACCEPTED 17 August 2022
PUBLISHED 21 September 2022

CITATION
Wang Y, Zhou Z, Wang C, Zhao L and Xia Q (2022), Hydrogenolysis of glycerol over TiO_2-supported Pt-WO_x catalysts: Effects of the TiO_2 crystal phase and WO_x loading.
Front. Chem. 10:1004925.
doi: 10.3389/fchem.2022.1004925

Hydrogenolysis of glycerol over TiO_2-supported Pt-WO_x catalysts: Effects of the TiO_2 crystal phase and WO_x loading

Yaju Wang[1,2], Zhiming Zhou[2], Chao Wang[3,4]*, Leihong Zhao[1] and Qineng Xia[1,2]*

[1]Key Laboratory of the Ministry of Education for Advanced Catalysis Materials, Institute of Physical Chemistry, Zhejiang Normal University, Jinhua, China, [2]College of Biological, Chemical Science and Engineering, Jiaxing University, Jiaxing, China, [3]College of Chemical Engineering, Qingdao University of Science and Technology, Qingdao, China, [4]Yankuang Technology Co., Ltd., Shandong Energy Group Co., Ltd., Jinan, China

The selective hydrogenolysis of glycerol to 1,3-propanediol (1,3-PDO) with high added value is attraction but challenging. Pt-WO_x-based catalysts have been extensively studied in the selective hydrogenolysis of glycerol. The catalyst support and the physicochemical state of WO_x play important roles on this reaction. In this paper, Pt-WO_x catalysts supported on TiO_2 with different crystal forms were prepared and studied for their catalytic performance in hydrogenolysis of glycerol. It was observed that the catalytic performance of anatase-type (A-type) TiO_2-supported catalyst (Pt/W/A-Ti) is much better than that of the rutile-type (R-type) TiO_2 catalyst (Pt/W/R-Ti) due to its higher stability. Furthermore, the influence of W loading amount and state were thoroughly investigated for the Pt/W/A-Ti catalysts, and Pt/W/A-TiO_2 with 5 wt% loading of WO_x achieved the best catalytic performance (100% conversion of glycerol and 41% yield of 1,3-PDO under the optimal reaction conditions), owing to the suitable WO_x domains and high dispersion of W species, as evidenced by XRD patterns and TEM images. Mechanism study by *in-situ* DRIFTS experiments indicated that glycerol was first converted to 3-hydroxypropanal and then converted to 1,3-PDO through subsequent reactions.

KEYWORDS

glycerol, hydrogenolysis, 1,3-propanediol, Pt-WO x based catalyst, TiO 2, crystal phase

Introduction

Biomass energy is currently receiving immense attention as a renewable energy source (ArthurRagauskas et al., 2006) (Pan et al., 2022). The production of glycerol is primarily associated with the process of biodiesel refining. Biodiesel refining of approximately 10 tons results in the production of approximately 1 ton of glycerol (Xu et al., 2021). Conversion of excess glycerol to value-added chemicals such as 1, 2- Propanediol (Dieuzeide et al., 2016), 1, 3- Propanediol (1,3-PDO) (Cheng et al., 2021), dihydroxyacetone (M. Walgode et al., 2021), acrolein (Talebian-Kiakalaieh & Amin,

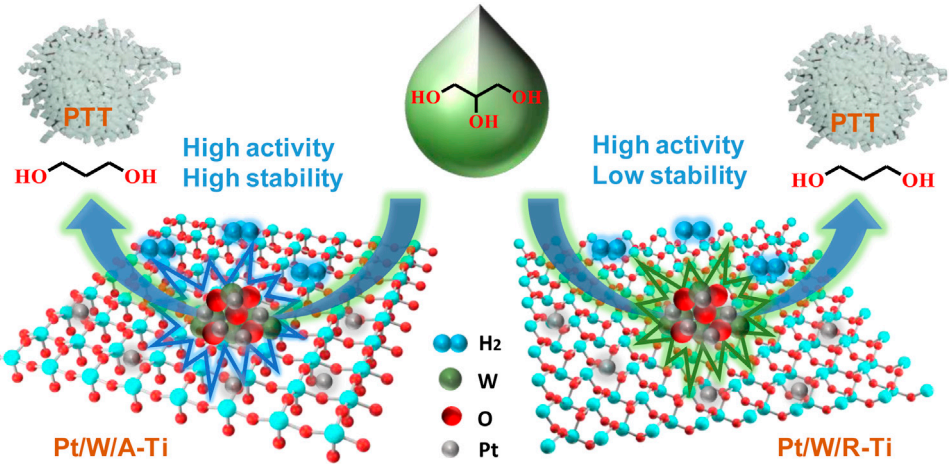

Table of Content

2017) and lactic acid (Arcanjo et al., 2019) has attracted extensive attention in recent years (Tadahiro Kurosaka et al., 2008). Among them, 1,3-PDO is an important bulk chemical feedstock which is industrially used to synthesize polytrimethylene terephthalate (PTT), polyurethanes, and cyclic compounds (Alvise Perosa, 2005). Besides, 1,3-PDO imparts various properties such as light stability, improved elasticity, and biodegradability to polymers (Julien Chaminand et al., 2004).

Efficient conversion of glycerol to 1,3-PDO through selective hydrogenolysis is attraction but challenging. Among the numerous catalysts studied so far, Ir-Re (Yoshinao Nakagawa et al., 2010) (Yasushi Amada et al., 2011) (Deng et al., 2015) (Liu et al., 2019) and Pt-W (Shi et al., 2018) (Jarauta-Córdoba et al., 2021) (Zhu et al., 2015) (Liu et al., 2020) bifunctional catalysts have been reported to exhibit the most promising performance. In particular, Pt-W-based catalysts are more durable and cost-competitive than Ir-Re-based catalysts. These catalysts have potential practical applications. Nonetheless, the activity and selectivity of the Pt-W catalysts seem to be lower than those of the Ir-Re catalysts, so there is an urgent need for the development of modification methods to improve the productivity of 1,3-PDO. In most modification studies, it is quite common to change the support to obtain highly active catalysts. Common supports such as ZrO_2 (Zhou et al., 2016), Al_2O_3 (Jarauta-Córdoba et al., 2021), SiO_2 (Zhou et al., 2020), TiO_2 (Zhang et al., 2013), etc., have been used to conduct the experiments. These supports can improve the activity of the Pt-W catalyst to a certain extent.

Among the above carriers, TiO_2 has become an excellent catalyst carrier attracting much attention due to its excellent chemical stability, non-toxicity and low cost (Xiaojie Zhang et al., 2017). Therefore, we introduced TiO_2 as a support into a Pt/W-based catalyst for the hydrogenolysis of glycerol. Before us, Zhang et al. (2013) prepared a Pt/W_n-$Ti_{(100-n)}$ catalyst using evaporation-induced self-assembly (EISA) strategy for hydrogenolysis of glycerol to 1,3-PDO, and 14.9% yield of 1,3-PDO was obtained. Herein, we prepared two TiO_2-supported Pt-WO_x catalysts with different crystal phases (anatase type and rutile type) and WO_x loading, and studied the effects of TiO_2 crystal phases and WO_x loading on the selective hydrogenolysis of glycerol to 1,3-PDO. A better 1,3-PDO yields (41% of anatase type Pt/W/Ti and 48% rutile type Pt/W/Ti) were obtained. It is found that the anatase-type Pt/W/A-Ti catalyst not only offer high catalytic activity with high 1,3-PDO yield (41%), but also exhibit excellent stability and can still maintain good catalytic activity after 5 cycles. However, the catalytic stability of rutile-type Pt/W/R-Ti is poor. Furthermore, for Pt/W/A-Ti catalysts, appropriate WO_x loading is also an important factor for the high catalytic selectivity of 1,3-PDO, and Pt/W/A-TiO_2 with 5 wt% loading of WO_x achieved the best catalytic performance, owing to the suitable WO_x domains and high dispersion of W species. At last, the reaction mechanism of the catalytic reaction was studied by the *In-situ* DRIFT technique.

Experimental

Chemicals and materials

$[(NH_4)_6(H_2W_{12}O_{40})\,nH_2O]$, (aladdin, ≥ 99.5%), TiO_2 (Rutile and Anatase, aladdin, ≥ 99.5%, Shanghai, China), Pt $(NO_3)_2$ (Xi'an Kaili new materials Co., Ltd., China, 0.15 g/ml Pt). All other chemicals and solvents (analytical grade) were purchased from Sinopharm Chemical Reagent Co., Ltd., China, SCRC.

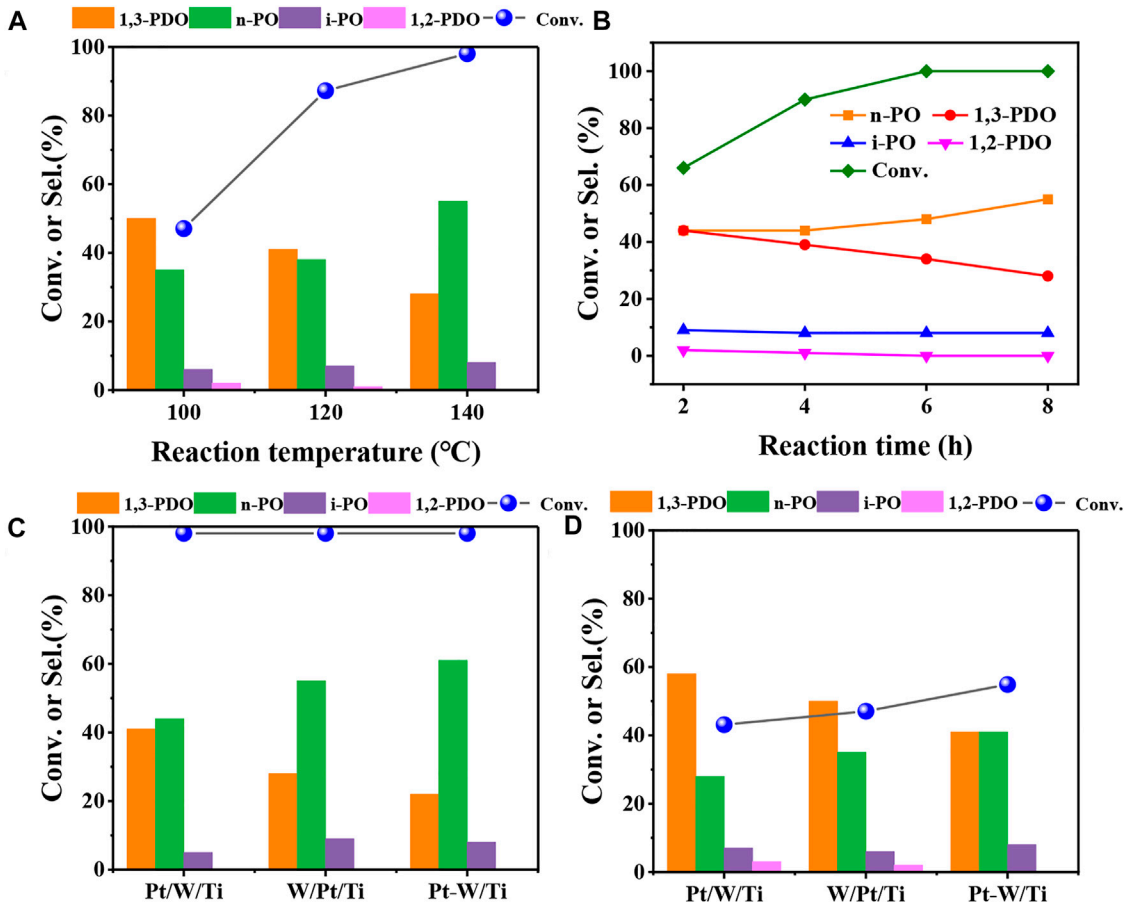

FIGURE 1
Catalytic results of glycerol hydrogenolysis at different reaction temperature **(A)** and different reaction time **(B)** over 5W/Pt/A-Ti catalyst; Catalytic results of glycerol hydrogenolysis over different catalysts at 140°C **(C)** and 100°C **(D)**. Reaction conditions: 0.3 g of catalyst (Support: A-Ti, WO_x: 5wt%) and 4.0 g of 10 wt% glycerol aqueous solution, 6 MPa H_2, **(B,C)** 140°C, 6 h (Pt/W/Ti means that W was loaded first, W/Pt/Ti means that Pt was loaded first and Pt-W/Ti means that Pt and W were loaded together).

Catalyst preparation

All catalysts with different WO_x loadings were prepared using a step-wise impregnation method, and the loading of Pt was 2 wt% unless otherwise specified. Take the preparation of Pt/2W/R-TiO_2 (R-TiO_2 refers to rutile TiO_2) as an example: Weigh 0.044 g of ammonium metatungstate $(NH_4)_6(H_2W_{12}O_{40})\cdot nH_2O$, (aladdin, ≥ 99.5%) into a 10 ml small beaker, add an appropriate amount of ultrapure water to dissolve, and weigh 1.92 g rutile-type TiO_2 (aladdin, ≥ 99.5%) was slowly added to the above small beaker, stirred until the mixture was initially wet, and the mixture was dried in a 110°C oven for 12 h. After drying, the powder was poured into a crucible and calcined in a muffle furnace. The calcination temperature and time were 450°C, 4 h, respectively. The sample obtained after calcination was named W/R-TiO_2. Then pipetting 133 μl of Pt $(NO_3)_2$ (0.15 g/ml Pt) solution into a 5 ml small beaker, add an appropriate amount of ultrapure water, weigh 0.98 g W/R-TiO_2 and slowly add it to the small beaker After stirring to the initial wet state, it was placed in an oven and dried at 110°C for 12 h. After calcination, the target catalyst Pt/2W/R-TiO_2 is finally obtained. For brevity, Pt/W/A-Ti and Pt/W/R-Ti are used to represent the anatase and rutile TiO_2 supported Pt-W series catalysts, respectively. The loadings of Pt and W appearing in the text are calculated according to the mass of Pt and WO_3, respectively.

Catalyst characterization

The specific surface area of the catalysts and support were measured by a Quantachrome Quadrosorb evo apparatus. The XRD patterns of the catalysts were recorded on a Bruker D8A A25 X-ray diffractometer with Cu Kα radiation source (λ = 0.15406 nm). The voltage was 40 kV, and the tube current used

was 40 mA. Ultraviolet-visible diffuse reflectance spectra (UV-vis DRS) were collected by a Cary 5000 UV-Vis-NIR spectrophotometer (Agilent, United States). The detector was a R928 PMT detector, the collection wavelength range was 200–800 nm, and the collection rate was 100 nm/min. The TEM and elemental mapping were obtained by a field emission electron microscope of the Talos F200S model from Thermo Fisher Scientific. The contents of W on the catalysts were determined using a Agilent 720/730 ICP-AES. The operating procedures of H_2-TPD test, NH_3-TPD test, CO-DRIFT absorption are shown in the experimental operation part of the Supplementary information.

In-situ DRIFT was performed on the same instrument for CO-DRIFT. The catalyst (50 mg) was milled and placed in the sample cell. Prior to the test, the catalyst was purged at 200°C for 1 h under He atmosphere, and the background was collected, and then reduced by introducing 10% H_2/He for 1 h. After the reduction, switch to He, cool down to room temperature, invoke the background, add glycerol dropwise, and quickly heat up to 200°C, and collect the adsorption state spectrum. Switch to 10% H_2/He to acquire reactive state spectra.

Catalytic tests

A stainless autoclave reactor (with a lining capacity of 25 ml) was used for the hydrogenolysis of glycerol. For a typical run, 0.3 g of catalyst and 4.0 g of 10 wt% glycerol aqueous solution were added into the reactor, sealed and purged with H_2 (3 MPa) for 4 times to exhaust the air in the autoclave, and then reacted at 6 MPa H_2 and 140°C for 6 h with 700 rpm magnetic stirring. After the reaction, the solid-liquid mixture in the lining of the reactor was taken out and weighed, and then a certain amount of 1,4-butanediol was added as an internal standard. Then the mixture was centrifuged to remove the catalyst for product analysis. The liquid product was analyzed by an Agilent 7890B gas chromatograph equipped with an HP-INNO Wax column (30 m × 0.32 mm × 0.50 μm) and a flame ionization detector (FID). The conversion (Conv.) of glycerol and the selectivity (Sel.) of each product are defined as follows:

$$\text{Conv. (\%)} = (\text{moles of glycerol converted})/(\text{moles of glycerol input}) \times 100\% \quad (1)$$

$$\text{Sel. (\%)} = (\text{moles of a specific product})/(\text{moles of glycerol converted}) \times 100\% \quad (2)$$

Results and discussion

Effects of reaction conditions and impregnation order of Pt and WO_x

The effect of reaction temperature was firstly investigated to determine the optimal reaction condition for glycerol hydrogenolysis with 5W/Pt/A-Ti as a probe catalyst. As the results shown in Figure 1A, it can be seen that the conversion of glycerol increased, while the selectivity of 1,3-PDO decreased with the increase of the reaction temperature. This result was in line with expectations because higher temperature speeds up the reaction rate for both glycerol hydrogenolysis to 1,3-PDO and further hydrogenolysis of 1,3-PDO to n-propanol (n-PO). Then, the reaction conducted for different reaction time at 140°C and 6 MPa shows that the conversion of glycerol reached 100% after reaction for 6 h (Figure 1B). It can be clearly seen that the selectivity of 1,3-PDO gradually declined and the selectivity of n-PO gradually increased as the reaction progress, while the selectivity of the other two by-products (1,2-PDO and i-PO) maintain almost unchanged. These results indicated that 1,3-PDO can further goes on hydrogenolysis to n-PO and therefore a proper reaction time is important.

We then explored the effects of impregnation order of Pt and WO_x on the glycerol hydrogenolysis and the results are displayed in Figures 1C,D. Here Pt/W/Ti means that W was loaded first, W/Pt/Ti means that Pt was loaded first and Pt-W/Ti means that Pt and W were loaded together. It can be seen that although all three catalysts achieved the full conversion of glycerol at 140°C, the selectivity of products were totally different. The Pt/W/Ti catalyst gave the highest yield (41%) of 1,3-PDO and Pt-W/Ti gave the lowest yield (21%) of 1,3-PDO. Since all three catalysts achieved the full conversion of glycerol and it is unreliable to compare the activity and selectivity at such a high conversion. We reduced the temperature to 100°C to lower the reaction rate and compare their activity and selectivity at a lower glycerol conversion (Figure 1D). It can be clearly seen that Pt/W/Ti offered the highest selectivity (58%) of 1,3-PDO, although the conversion of glycerol was slightly lower. Nevertheless, Pt/W/Ti catalyst gave the highest yield of 1,3-PDO. These results suggest that the impregnation order of Pt and WO_x has a great influence on the catalytic performance for glycerol hydrogenolysis, probably because different impregnation order of Pt and WO_x on TiO_2 surface gives the different Pt-W interface.

Effects of different crystal phases of TiO_2

We then explored the effects of different crystal phases of TiO_2 on the catalytic performance of glycerol hydrogenolysis. As shown in Figures 2A,B, we compared the catalytic performances of glycerol hydrogenolysis over two types of catalysts (i.e., Pt/W/A-Ti and Pt/W/R-Ti) with three different W loadings (i.e., 2%, 5%, and 10%). It is found that the initial activities of Pt/W/R-Ti catalysts were obviously better than the Pt/W/A-Ti catalysts for all 3 W loadings. Specifically, the yield of 1,3-PDO for Pt/5W/R-Ti (48%) was slightly higher than that for Pt/5W/A-Ti (41%) when the W loading was 5 wt%. However, the stability of Pt/5W/A-Ti catalyst was much better than that of the Pt/5W/R-Ti catalyst, as shown in Figures 2C,D, the Pt/5W/A-Ti maintain

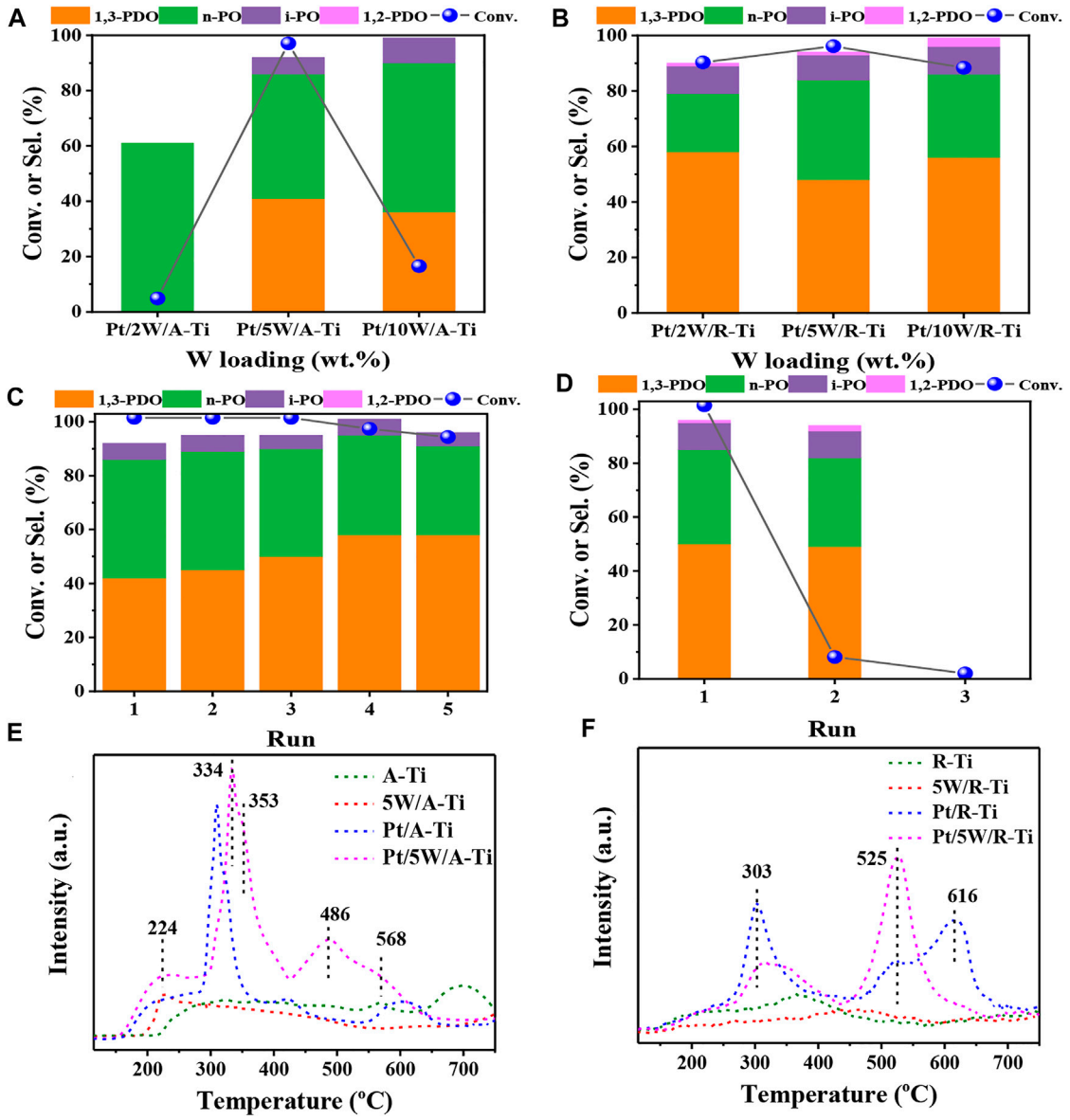

FIGURE 2
Comparative results obtained for the Pt/W/A-Ti **(A)** and Pt/W/R-Ti **(B)** fabricated under conditions of varying WO_x loadings. The cycle stability tests of Pt/5W/A-Ti **(C)** and Pt/5W/R-Ti **(D)**. NH_3-TPD profiles recorded for the catalysts and support A-Ti **(E)** and R-Ti **(F)**. Reaction conditions: 0.3 g of catalyst and 4.0 g of 10 wt% glycerol aqueous solution, 6 MPa H_2, 140°C, 6 h.

a very good catalytic activity after 5 cycles while Pt/5W/R-Ti almost completely lost its activity for the second run. The rapid deactivation of Pt/5W/R-Ti catalyst can be attributed to the severe leaching of the WO_x species, as we can visually see from Supplementary Figure S1 that the reaction solution became dark blue after reaction over Pt/5W/R-Ti, while the solution maintains colorless and transparent after reaction over Pt/5W/A-Ti. The severe leaching of WO_x species was also confirmed by ICP-AES measurements and results are shown in Supplementary Table S1. In addition, we also tried to change the durability of TiO_2 (R-type) by changing the calcination temperature during catalyst preparation. However, as shown in Supplementary Figure S2, the reaction results show that increasing the calcination temperature in the catalyst preparation process leads to lower catalytic activity.

To further compare the difference between these two types of catalysts, NH_3-TPD was used to investigate the acid strength and acidity of the two catalysts. Figure 2E reveals that the NH_3-TPD profile of 5W/A-Ti sample presents a desorption peak at 224°C, corresponding to weak acid site. NH_3-TPD profile of Pt/A-Ti

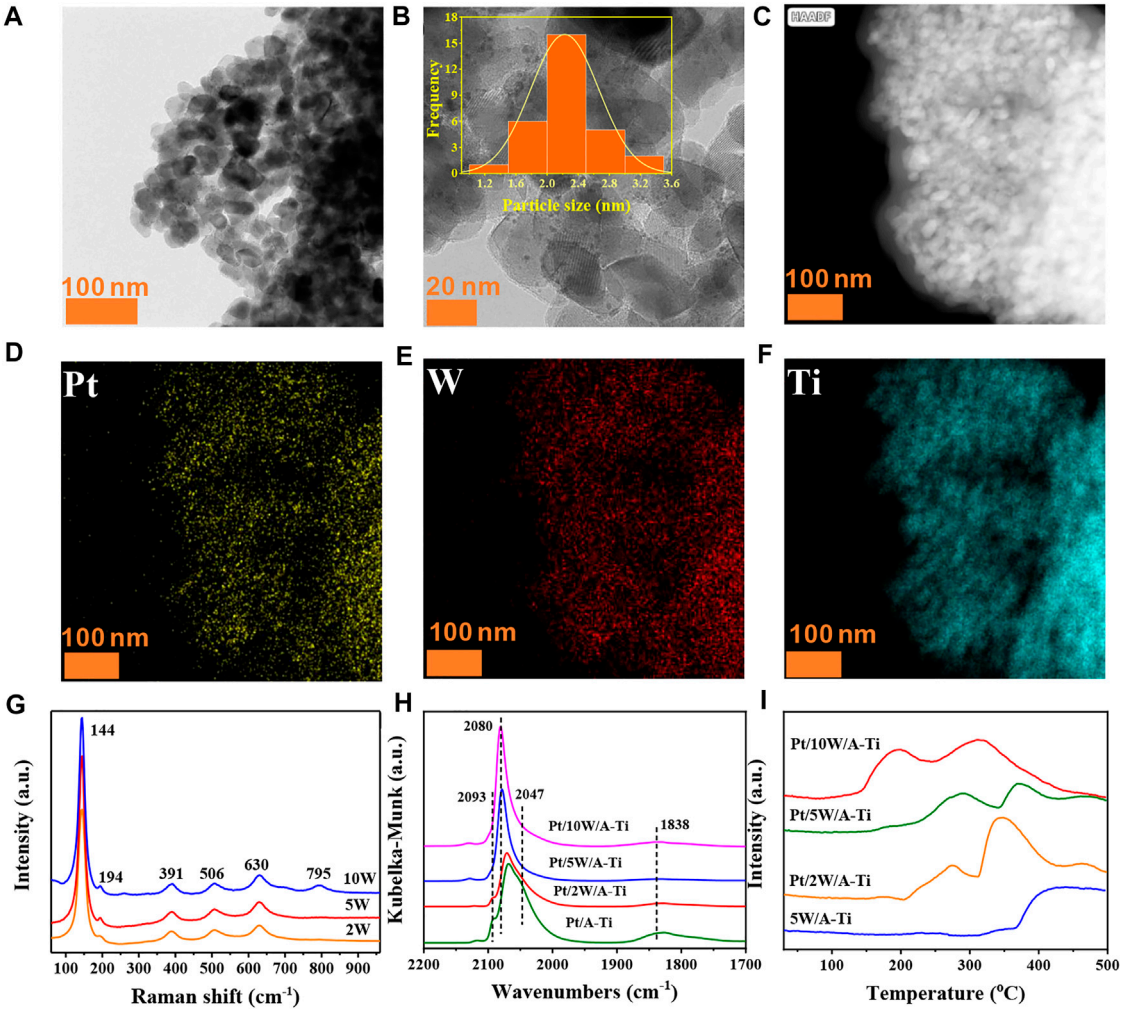

FIGURE 3
TEM image of the freshly reduced Pt/5W/A-Ti **(A,B)**, elemental mapping images of the freshly reduced Pt/5W/A-Ti **(C–F)**. Raman spectral profiles recorded for Pt/W/A-Ti **(G)**. DRIFTs of CO adsorption on the Pt/W/A-Ti catalysts prepared under conditions of varying W loadings **(H)**. H_2-TPD curves recorded for the Pt/W/A-Ti series catalysts **(I)**.

presents two desorption peaks in the range of 300°C–350°C, corresponding to the medium acid sites (Zhou et al., 2020) (Zhou et al., 2019) (Zhao et al., 2021). Compared to the peaks corresponding to 5W/A-Ti and Pt/A-Ti, the desorption peaks corresponding to the Pt/5W/A-Ti catalysts shifted toward the high-temperature region, indicating that the interaction between Pt, W, and Ti increased the acid strength of the catalyst. The information present in the NH_3-TPD profile of R-Ti type samples (Figure 2F) is different from the information present in A-Ti type samples (Figure 2E). The desorption peak at 616°C of Pt/R-Ti is shifted to 525°C in the profile recorded for Pt/5W/R-Ti. This can be potentially attributed to the interaction of Pt, W, and R-TiO_2 in Pt/5W/R-Ti catalyst. However, it can be seen that the acid strength of Pt/5W/R-Ti is higher than that of Pt/5W/A-Ti, and this can explain the higher initial activity of Pt/5W/R-Ti for glycerol hydrogenlysis to 1,3-PDO (Feng et al., 2019).

In order to better compare the difference of total acid amount among different samples, we used the integral peak area ratio (the 5W/R-Ti sample with the smallest integral peak area was taken as the benchmark, and the integral peak area of the NH_3-TPD curve desorption peak of other samples was compared with the integral peak area of the 5W/R-Ti sample) for semi-quantitative processing of the total acid content of each sample. The results were listed in Supplementary Table S2. Overall, the total acid content in A-Ti and the samples loaded with active components was higher than the total acid content recorded for the R-Ti counterparts. The effect of Pt on the acid content of the carrier is greater than the effect of W species, indicating that the presence of Pt results in the generation of additional acidic sites

on the TiO_2 support. From the acid content results of the two catalysts, it can be seen that the total acid amount of Pt/5W/A-Ti is higher than that of Pt/5W/R-Ti, but the initial yield of 1,3-PDO of Pt/5W/A-Ti is lower. This may suggest that only strong acid sites are responsible for glycerol hydrogenolysis of glycerol to 1,3-PDO. However, although the initial activity of Pt/5W/A-Ti is slightly lower, it has better application potential due to its ultra-high stability.

Effects of WO_x loading and chemical state

The catalytic results of the catalysts indicated that the appropriate loading of WO_x species is a key factor for the catalytic performance. Therefore, we further investigated the loading of WO_x on the Pt/5W/A-Ti catalyst. From the TEM and elemental mapping images, it can be concluded that the distribution of Pt and WO_x on the Pt/5W/A-Ti catalyst is highly uniform (Figures 3A–F). Texture analysis of the catalysts revealed that with an increase of the W loading, the specific surface area and pore volume of the Pt/W/A-Ti catalyst decreased, while the mean pore size remained constant (Supplementary Table S3). This is attributed to that W species is primarily loaded onto the pores of the TiO_2 support (García-Fernández et al., 2017). Raman spectroscopy was used to investigate the effect of W species on the catalyst. As shown in Figure 3G, the vibration peaks appearing at 144, 194, 391, 506, and 630 cm^{-1} were attributed to the anatase TiO_2 units. The peaks appearing at 391, 506, and 630 cm^{-1} correspond to the symmetrical bending vibration, antisymmetric bending vibration, and symmetrical stretching vibration of the O-Ti-O unit on the TiO_2 surface, respectively (Zhou et al., 2019) (He et al., 2018) (Xu et al., 2012) (Wachs, 2007) (Balta & Simsek, 2020) (Jia et al., 2021). Peak at 795 cm^{-1} was observed in the Raman spectral profile recorded for the Pt/10W/A-Ti catalyst. This peak can be attributed to the stretching vibration mode of W-O in bulk WO_3. In general, when the W content in the catalyst is > 5 wt%, vibration peaks attributable to bulk WO_3 are observed in the Raman spectral profiles recorded for the Pt/W/A-Ti catalysts. These results indicate that when the loading of W is higher than 5 wt%, bulk WO_3 is formed, resulting in a decrease in the catalytic activity. This is consistent with the results from XRD pattern (Supplementary Figures S3A, B). However, decreasing the W laoding to 2 wt% as Pt/2W/A-Ti catalyst results in the lack of WOx active species. These results show that 5 wt% is the best WO_x loading for Pt/W/A-Ti catalyst, consistent with the catalytic reaction results shown in Figure 2A. Analysis of Supplementary Table S4 and Supplementary Figure S4 revealed that the W species in these three different W supported catalysts are likely to exist in the form of W_{12} clusters because their spectral information and E_g values are similar with ammonium metatungstate (AMT) which exists as W_{12} clusters structure (Zhao et al., 2021) (Yang et al., 2022) (Xu et al., 2021).

To further explore the effect of WO_x loading on the chemical state of Pt, we used CO as a probe molecule to characterize a series of catalysts with different W contents. As shown in Figure 3H, the peaks in the range of 2000–2,100 cm^{-1} are attributed to the linear adsorption of CO on the Pt site, and the peak at 1838 cm^{-1} is attributed to the bridge adsorption of CO on the metallic Pt unit (Xin et al., 2021) (Zhou et al., 2021) (Botao Qiao et al., 2011). The profiles recorded for Pt/A-Ti and Pt/2W/A-Ti reveal the presence of a shoulder peak at 2093 cm^{-1}, which is attributed to the linear adsorption of CO on the surface of the PtO_x species. The molar ratio of CO to PtO_x is 1:1 in this case (Zhao et al., 2020). However, this peak was absent in the profiles recorded for the Pt/5W/A-Ti and Pt/10W/A-Ti samples, indicating that the PtO_x content in the catalysts fabricated under conditions of high WO_x loading was higher than the PtO_x content in the samples devoid of tungsten and fabricated under conditions of low WO_x content. The species are more easily reduced to Pt^0. The peaks at 2047 cm^{-1} and 2080 cm^{-1} in Figure 3H are attributed to the bonding of CO with the coordinatively unsaturated and coordinatively saturated Pt sites, respectively. The former appears in the spectral lines of the Pt/A-Ti and Pt/2W/A-Ti samples. The results reveal that with an increase in the W loading, the number of unsaturated Pt sites in the catalyst decrease. This can be explained by the coordination effect between the coordination-unsaturated Pt and W, which results in the conversion of these sites to coordination saturated sites. In addition, the peaks corresponding to CO adsorption on the coordination saturated Pt sites blue-shifted with an increase in the W loading. This indicated electron transfer (Pt→W) between Pt and W (Yang et al., 2018). More importantly, the strength of the CO bridge adsorption peaks corresponding to the three W-loaded samples was weaker than the strength of the peaks corresponding to the W-free Pt/A-Ti units. This indicates that W does interact with Pt to cover Pt to a certain extent. The number of adjacent Pt sites decreases, and among the three samples containing W, the bridge adsorption peak in Pt/5W/A-Ti is observed to be the weakest. This proves our finding that Pt/5W/A-Ti is the best catalyst as it is characterized by the maximum area of the Pt/WO_x interface, which is consistent with the catalyst characterization and catalytic reaction results.

Figure 3I presents the H_2-TPD diagram of the Pt/W/A-Ti series catalysts. Two desorption regions are observed in the H_2-TPD curves recorded for the catalysts prepared when the W loadings were 2 wt%, 5 wt%, and 10 wt%. Unlike the case of the 5W/A-Ti sample devoid of Pt, the desorption peak at higher temperature regions can be attributed to W/Ti, and the desorption peak at the lower temperature regions can be attributed to Pt-H. The desorption peak temperature corresponding to Pt/5W/A-Ti is higher than that of the samples corresponding to 2 wt% W and 10 wt% W, indicating that the strength of adsorption of H species on

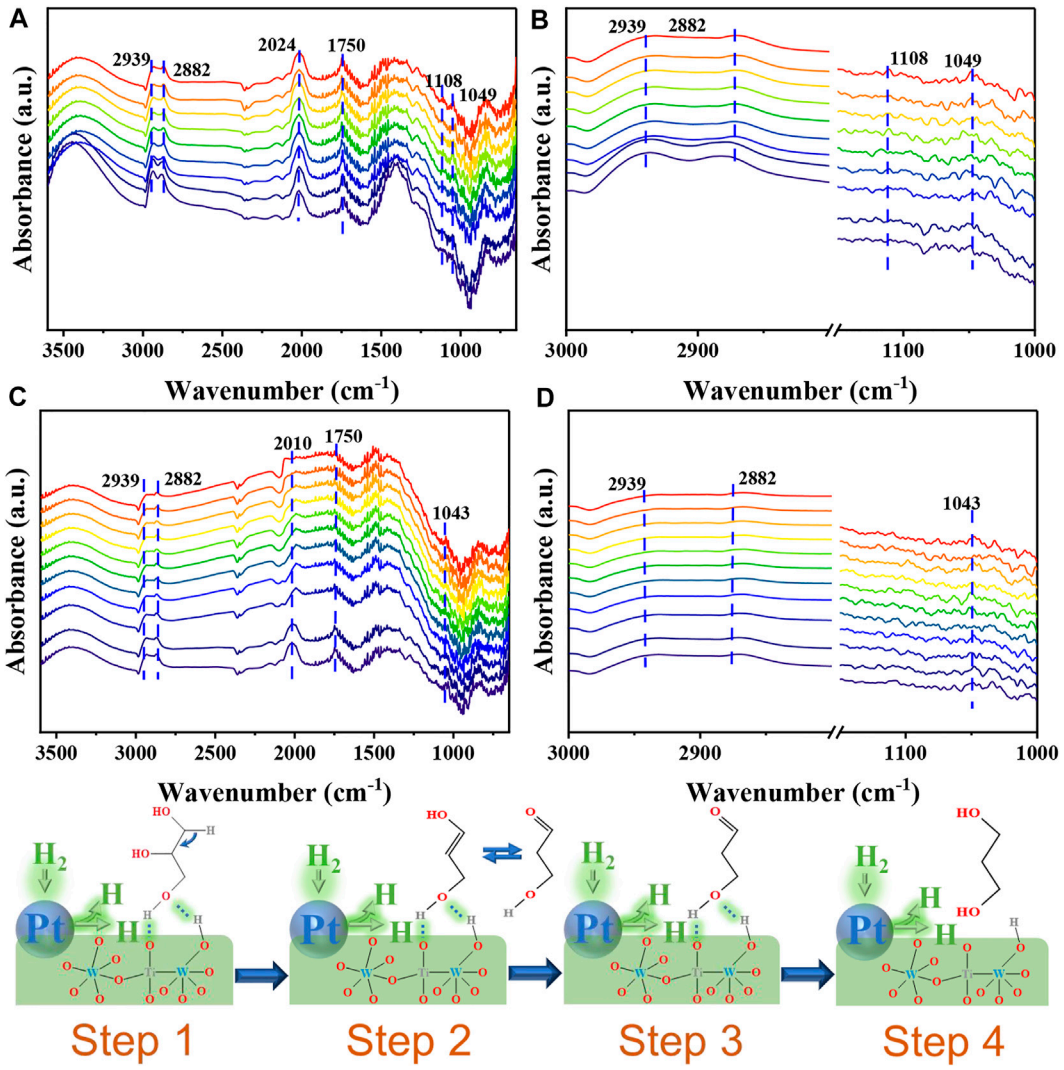

FIGURE 4
In-situ DRIFT profiles recorded for the adsorption of glycerol on Pt/5W/A-Ti studied within the investigated region **(A)**, and the adsorption state in the (C–H), 3,000–2,700 cm^{-1}, and (C–O), 1,150–950 cm^{-1}, regions **(B)**. Reactive state of glycerol on Pt/5W/A-Ti studied within the investigated region **(C)** and reactive state in the (C–H), 3,000–2,700 cm^{-1}, and (C–O), 1,150–950 cm^{-1}, regions **(D)**. Schematic diagram of the reaction mechanism (Step 1–4).

the surface of Pt/5W/A-Ti is the strongest (Kuang et al., 2020) (He et al., 2018).

Reaction mechanism study

There are many studies on the mechanism of glycerol hydrogenolysis to produce 1,3-PDO (Cheng et al., 2021) (Feng et al., 2019) (García-Fernández et al., 2017). However, we traced the reaction path by *in-situ* DRIFT and found that glycerol was first converted to enol form and then further converted to 1,3-propanediol. As shown in Figure 4A which is the adsorption state infrared spectrum of glycerol, an absorption peak appears at 1750 cm^{-1}, corresponding to the vibration of the C=O bond (García-Fernández et al., 2017), indicating that glycerol is converted to an enol-isomer when adsorbed on the catalyst which corresponds to step 1 and 2. Figures 4A–D all reveals the presence of two absorption peaks at 2,939 cm^{-1} and 2,882 cm^{-1}. These peaks correspond to the symmetric, and asymmetric vibrations of the C-H units present in glycerol, respectively (Juan del Pozo et al., 2017). The peak appearing in the range of 2,400–2000 cm^{-1} may

correspond to the absorption peak of CO_2 (García-Fernández et al., 2017). Peaks were also detected at 1,108 cm^{-1} and 1,049 cm^{-1}. These peaks corresponded to the (C-O) unit of the 2° and 1° OH groups in glycerol, respectively (JohnCopeland et al., 2013). Analysis of Figure 4C which is reaction state infrared spectrum of glycerol reveals that the peak at 1750 cm^{-1} is weak, indicating that enol glycerol is converted to 1,3-PDO following the passage of H_2. The strength of the absorption peak observed in Figure 4D is less than the strength of the absorption peak at 1,108 cm^{-1} appearing in Figure 4B which corresponds to step 3 and 4. This indicated that glycerol was successfully converted to 1,3-PDO.

Conclusion

In summary, Pt-WO_x catalysts supported on TiO_2 with different crystal forms and WO_x loadings were prepared and studied for their catalytic performance in hydrogenolysis of glycerol. The Pt-WO_x catalysts supported by different crystalline phases of TiO_2 exhibit completely different catalytic activities and catalytic stability. The Pt/W/A-Ti catalysts exhibit slightly lower initial catalytic activity than the Pt/W/R-Ti catalysts, but possess much higher stability owing to their excellent anti-leaching ability. Moreover, WO_x loading significantly influenced the catalytic performance and catalysts with moderate WO_x loading (5 wt%) exhibited the best catalytic performance. The results obtained using the CO DRIFT technique revealed the presence of special types of interactions between Pt and WO_x. WO_x covers Pt to a certain extent, and 5 wt % loading of WO_x at the Pt/WO_x interface help achieve the maximum catalytic activity for glycerol hydrogenolysis. The reaction mechanism associated with the conversion of glycerol on Pt/5W/A-Ti was discussed using the *in-situ* DRIFT technique, and the reaction path for the conversion of glycerol to 1,3-PDO was proposed.

Data availability statement

The original contributions presented in the study are included in the article/Supplementary Material, further inquiries can be directed to the corresponding authors.

Author contributions

YW: writing-original draft, writing-review and editing. ZZ: data curation, visualization. CW: methodology, writing-review and editing, funding acquisition. LZ: writing-review and editing. QX: conceptualization, supervision, writing-review and editing, funding acquisition.

Funding

This work was financially supported by the National Natural Science Foundation of China (No. 21972056), Natural Science Foundation of Zhejiang Province (No. LY21B030008), Natural Science Foundation of Shandong Province (No. ZR2020QB139) and Technology Development Project of Jiaxing University.

Conflict of interest

CW was employed by Yankuang Technology Co., Ltd., Shandong Energy Group Co., Ltd.

The remaining authors declare that the research was conducted in the absence of any commercial or financial relationships that could be construed as a potential conflict of interest.

Publisher's note

Supplementary material

The Supplementary Material for this article can be found online at: https://www.frontiersin.org/articles/10.3389/fchem.2022.1004925/full#supplementary-material

References

Alvise Perosa, P. T., and Tundo, P. (2005). Selective hydrogenolysis of glycerol with raney nickel. *Ind. Eng. Chem. Res.* 44, 8535–8537. doi:10.1021/ie0489251

Arcanjo, M. R. A., Silva, I. J., Cavalcante, C. L., Iglesias, J., Morales, G., Paniagua, M., et al. (2019). Glycerol valorization: Conversion to lactic acid by heterogeneous catalysis and separation by ion exchange chromatography. *Biofuel. Bioprod. Biorefin.* 14 (2), 357–370. doi:10.1002/bbb.2055

ArthurRagauskas, J., Davison, Brian H., George, Britovsek, Cairney, John, Eckert, Charles A., Frederick, William J., Jr., et al. (2006). The path forward for biofuels and biomaterials. *Science* 311 (5760), 484–489. doi:10.1126/science.1114736

Balta, Z., and Simsek, E. B. (2020). Insights into the photocatalytic behavior of carbon-rich shungite-based WO_3/TiO_2 catalysts for enhanced dye and pharmaceutical degradation. *New Carbon Mater.* 35 (4), 371–383. doi:10.1016/s1872-5805(20)60495-4

Botao Qiao, A. W., Yang, Xiaofeng, Allard, LawrenceF., Jiang, Zheng, Cui, Yitao, Liu, Jingyue, et al. (2011). Single-atom catalysis of CO oxidation using Pt_1/FeO_x. *Nat. Chem.* 3 (8), 634–641. doi:10.1038/nchem.1095

Cheng, S., Fan, Y., Zhang, X., Zeng, Y., Xie, S., Pei, Y., et al. (2021). Tungsten-doped siliceous mesocellular foams-supported platinum catalyst for glycerol hydrogenolysis to 1, 3-propanediol. *Appl. Catal. B Environ.* 297, 120428. doi:10.1016/j.apcatb.2021.120428

Deng, C., Duan, X., Zhou, J., Zhou, X., Yuan, W., and Scott, S. L. (2015). Ir–Re alloy as a highly active catalyst for the hydrogenolysis of glycerol to 1, 3-propanediol. *Catal. Sci. Technol.* 5 (3), 1540–1547. doi:10.1039/c4cy01285b

Dieuzeide, M. L., Jobbagy, Matías, and Amadeo, N. (2016). Vapor-phase hydrogenolysis of glycerol to 1, 2-propanediol over Cu/Al_2O_3 catalyst at ambient hydrogen pressure. *Ind. Eng. Chem. Res.* 55 (9), 2527–2533. doi:10.1021/acs.iecr.5b03004

Feng, S., Zhao, B., Liang, Y., Liu, L., and Dong, J. (2019). Improving selectivity to 1, 3-propanediol for glycerol hydrogenolysis using W- and Al-incorporated SBA-15 as support for Pt nanoparticles. *Ind. Eng. Chem. Res.* 58 (8), 2661–2671. doi:10.1021/acs.iecr.8b03982

García-Fernández, S., Gandarias, I., Requies, J., Soulimani, F., Arias, P. L., and Weckhuysen, B. M. (2017). The role of tungsten oxide in the selective hydrogenolysis of glycerol to 1, 3-propanediol over $Pt/WO_x/Al_2O_3$. *Appl. Catal. B Environ.* 204, 260–272. doi:10.1016/j.apcatb.2016.11.016

He, J., Burt, S. P., Ball, M., Zhao, D., Hermans, I., Dumesic, J. A., et al. (2018). Synthesis of 1, 6-hexanediol from cellulose derived tetrahydrofuran-dimethanol with $Pt\text{-}WO_x/TiO_2$ catalysts. *ACS Catal.* 8 (2), 1427–1439. doi:10.1021/acscatal.7b03593

Jarauta-Córdoba, C., Oregui Bengoechea, M., Agirrezabal-Telleria, I., Arias, P.-L., and Gandarias, I. (2021). Insights into the nature of the active sites of $Pt\text{-}WO_x/Al_2O_3$ catalysts for glycerol hydrogenolysis into 1, 3-propanediol. *Catalysts* 11 (10), 1171. doi:10.3390/catal11101171

Jia, A., Zhang, Y., Song, T., Zhang, Z., Tang, C., Hu, Y., et al. (2021). Crystal-plane effects of anatase TiO_2 on the selective hydrogenation of crotonaldehyde over Ir/TiO_2 catalysts. *J. Catal.* 395, 10–22. doi:10.1016/j.jcat.2020.12.012

John, R., Copeland, X.-R. S., Sholl, David S., and Sievers., Carsten (2013). Surface interactions of C_2 and C_3 polyols with $\gamma\text{-}Al_2O_3$ and the role of coadsorbed water. *Langmuir* 29 (2), 581–593. doi:10.1021/la304074x

Juan del Pozo, M. r.-I., Álvarez, Rosana, Lledós, Agustí, Casares, Juan A., Espinet, Pablo, and Espinet, P. (2017). Speciation of $ZnMe_2$, ZnMeCl, and $ZnCl_2$ in tetrahydrofuran (THF), and its influence on mechanism calculations of catalytic processes. *ACS Catal.* 7 (5), 3575–3583. doi:10.1021/acscatal.6b03636

Julien Chaminand, L. a. D., Gallezot, Pierre, Marion, Philippe, Pinel, Catherine, Rosier, Cécile, and Rosier, C. (2004). Glycerol hydrogenolysis on heterogeneous catalysts. *Green Chem.* 6 (8), 359–361. doi:10.1039/b407378a

Kuang, B., Zhang, Q., Fang, Y., Bai, Y., Qiu, S., Wu, P., et al. (2020). Ring opening of cyclic ether for selective synthesis of renewable 1, 5-pentanediol over $Pt/WO_3@SiO_2$ catalysts. *Ind. Eng. Chem. Res.* 59 (20), 9372–9381. doi:10.1021/acs.iecr.9b06790

Liu, L., Asano, T., Nakagawa, Y., Tamura, M., and Tomishige, K. (2020). One-pot synthesis of 1, 3-butanediol by 1, 4-anhydroerythritol hydrogenolysis over a tungsten-modified platinum on silica catalyst. *Green Chem.* 22 (8), 2375–2380. doi:10.1039/d0gc00244e

Liu, L., Kawakami, S., Nakagawa, Y., Tamura, M., and Tomishige, K. (2019). Highly active iridium–rhenium catalyst condensed on silica support for hydrogenolysis of glycerol to 1, 3-propanediol. *Appl. Catal. B Environ.* 256, 117775. doi:10.1016/j.apcatb.2019.117775

Pan, H., Xia, Q., Li, H., Wang, Y., Shen, Z., Wang, Y., et al. (2022). Direct production of biodiesel from crude Euphorbia lathyris L. Oil catalyzed by multifunctional mesoporous composite materials. *Fuel* 309, 122172. doi:10.1016/j.fuel.2021.122172

Shi, G., Cao, Z., Xu, J., Jin, K., Bao, Y., and Xu, S. (2018). Effect of WO_x doping into Pt/SiO_2 catalysts for glycerol hydrogenolysis to 1, 3-propanediol in liquid phase. *Catal. Lett.* 148 (8), 2304–2314. doi:10.1007/s10562-018-2464-7

Tadahiro Kurosaka, H. M., Naribayashi, Ikuya, Sasaki, Yoshiyuki, and Sasaki, Y. (2008). Production of 1, 3-propanediol by hydrogenolysis of glycerol catalyzed by $Pt/WO_3/ZrO_2$. *Catal. Commun.* 9 (6), 1360–1363. doi:10.1016/j.catcom.2007.11.034

Talebian-Kiakalaieh, A., and Amin, N. A. S. (2017). Coke-tolerant $SiW_{20}\text{-}Al/Zr_{10}$ catalyst for glycerol dehydration to acrolein. *Chin. J. Catal.* 38 (10), 1697–1710. doi:10.1016/s1872-2067(17)62891-2

Wachs, E. I. R.-M. a. I. E., and Wachs, I. E. (2007). Structural determination of bulk and surface tungsten oxides with UV-vis diffuse reflectance spectroscopy and Raman spectroscopy. *J. Phys. Chem. C* 111, 15089–15099. doi:10.1021/jp074219c

Walgode, M., Coelho, P., D., Coelho, Lucas C. D., Faria, V., Rodrigues, E., and Rodrigues, Alírio E. (2021). Dihydroxyacetone production: From glycerol catalytic oxidation with commercial catalysts to chromatographic separation. *Ind. Eng. Chem. Res.* 60 (29), 10551–10565. doi:10.1021/acs.iecr.1c00275

Xiaojie Zhang, G. Z., Lu, Xin, Tang, Changqing, Cao, Shuo, Yu, Miao, and Yu, M. (2017). Anatase TiO_2 sheet-assisted synthesis of Ti^{3+} self-doped mixed phase TiO_2 sheet with superior visible-light photocatalytic performance: Roles of anatase TiO_2 sheet. *J. Colloid Interface Sci.* 490, 774–782. doi:10.1016/j.jcis.2016.12.010

Xin, H., Zhang, W., Xiao, X., Chen, L., Wu, P., and Li, X. (2021). Selective hydrogenation of cinnamaldehyde with ni_x $Fe_{1\text{-}x}Al_2O_{4+\delta}$ composite oxides supported Pt catalysts: C=O versus C=C selectivity switch by varying the Ni/Fe molar ratios. *J. Catal.* 393, 126–139. doi:10.1016/j.jcat.2020.11.036

Xu, F., Fahmi, A., Zhao, Y., Xia, Y., and Zhu, Y. (2012). Patterned growth of tungsten oxide and tungsten oxynitride nanorods from Au-coated W foil. *Nanoscale* 4 (22), 7031–7037. doi:10.1039/c2nr32169f

Xu, W.-f., Niu, P.-y., Guo, H.-q., Jia, L.-t., and Li, D.-b. (2021). Study on the performance of platinum and tungsten bifunctional catalyst supported on Al_2O_3 in the hydrogenolysis of glycerol to 1, 3-propanediol. *J. Fuel Chem. Technol.* 49 (9), 1270–1280. doi:10.1016/s1872-5813(21)60101-9

Yang, C., Miao, Z., Zhang, F., Li, L., Liu, Y., Wang, A., et al. (2018). Hydrogenolysis of methyl glycolate to ethanol over a $Pt–Cu/SiO_2$single-atom alloy catalyst: A further step from cellulose to ethanol. *Green Chem.* 20 (9), 2142–2150. doi:10.1039/c8gc00309b

Yang, M., Wu, K., Sun, S., and Ren, Y. (2022). Regulating oxygen defects via atomically dispersed alumina on Pt/WO_x catalyst for enhanced hydrogenolysis of glycerol to 1, 3-propanediol. *Appl. Catal. B Environ.* 307, 121207. doi:10.1016/j.apcatb.2022.121207

Yasushi Amada, Y. S., Koso, Shuichi, Kubota, Takeshi, Yoshinao Nakagawa, K. T., Nakagawa, Y., and Tomishige, K. (2011). Reaction mechanism of the glycerol hydrogenolysis to 1, 3-propanediol over $Ir–ReO_x/SiO_2$ catalyst. *Appl. Catal. B Environ.* 105 (1-2), 117–127. doi:10.1016/j.apcatb.2011.04.001

Yoshinao Nakagawa, Y. S., Koso, Shuichi, Tomishige, Keiichi, and Tomishige, K. (2010). Direct hydrogenolysis of glycerol into 1, 3-propanediol over rhenium-modified iridium catalyst. *J. Catal.* 272 (2), 191–194. doi:10.1016/j.jcat.2010.04.009

Zhang, Y., Zhao, X.-C., Wang, Y., Zhou, L., Zhang, J., Wang, J., et al. (2013). Mesoporous Ti–W oxide: Synthesis, characterization, and performance in selective hydrogenolysis of glycerol. *J. Mat. Chem. A* 1 (11), 3724–3732. doi:10.1039/c3ta10217c

Zhao, B., Liang, Y., Yan, W., Liu, L., and Dong, J. (2021). A facile approach to tune WO_x species combining Pt catalyst for enhanced catalytic performance in glycerol hydrogenolysis. *Ind. Eng. Chem. Res.* 60 (34), 12534–12544. doi:10.1021/acs.iecr.1c02184

Zhao, P.-P., Chen, J., Yu, H.-B., Cen, B.-H., Wang, W.-Y., Luo, M.-F., et al. (2020). Insights into propane combustion over MoO_3 promoted Pt/ZrO_2 catalysts: The generation of $Pt\text{-}MoO_3$ interface and its promotional role on catalytic activity. *J. Catal.* 391, 80–90. doi:10.1016/j.jcat.2020.08.012

Zhou, W., Li, Y., Wang, X., Yao, D., Wang, Y., Huang, S., et al. (2020). Insight into the nature of Brönsted acidity of $Pt\text{-}(WO_x)_n\text{-}H$ model catalysts in glycerol hydrogenolysis. *J. Catal.* 388, 154–163. doi:10.1016/j.jcat.2020.05.019

Zhou, W., Luo, J., Wang, Y., Liu, J., Zhao, Y., Wang, S., et al. (2019). WOx domain size, acid properties and mechanistic aspects of glycerol hydrogenolysis over $Pt/WO_x/ZrO_2$. *Appl. Catal. B Environ.* 242, 410–421. doi:10.1016/j.apcatb.2018.10.006

Zhou, W., Zhao, Y., Wang, Y., Wang, S., and Ma, X. (2016). Glycerol hydrogenolysis to 1, 3-propanediol on $Pt/WO_3/ZrO_2$: Hydrogen spillover facilitated by Pt(111) formation. *ChemCatChem* 8 (23), 3663–3671. doi:10.1002/cctc.201600981

Zhou, Z., Jia, H., Guo, Y., Wang, Y., Liu, X., Xia, Q., et al. (2021). The promotional effect of sulfates on TiO_2 supported $Pt\text{-}WO_x$ catalyst for hydrogenolysis of glycerol. *ChemCatChem* 13 (18), 3953–3959. doi:10.1002/cctc.202100863

Zhu, S., Gao, X., Zhu, Y., and Li, Y. (2015). Promoting effect of WOx on selective hydrogenolysis of glycerol to 1, 3-propanediol over bifunctional $Pt–WO_x/Al_2O_3$ catalysts. *J. Mol. Catal. A Chem.* 398, 391–398. doi:10.1016/j.molcata.2014.12.021

frontiers | Frontiers in Chemistry

TYPE Original Research
PUBLISHED 29 September 2022
DOI 10.3389/fchem.2022.1022644

OPEN ACCESS

EDITED BY
Hu Li,
Guizhou University, China

REVIEWED BY
Peng Zheng,
Chongqing City Management College, China
Wei Hongbin,
Ministry of Natural Resources of the People's Republic of China, China

*CORRESPONDENCE
Wei Yang,
yangwei0928@163.com
Yutao Zhang,
zyt0516@126.com

SPECIALTY SECTION
This article was submitted to Green and Sustainable Chemistry, a section of the journal Frontiers in Chemistry

RECEIVED 18 August 2022
ACCEPTED 29 August 2022
PUBLISHED 29 September 2022

CITATION
Yang W, Li X, Li W, Zhang Y, Zhang H and Ran Y (2022), Carbon effect calculation and upgrading strategy of agricultural land consolidation project in urban edge of Three Gorges Reservoir Area. *Front. Chem.* 10:1022644. doi: 10.3389/fchem.2022.1022644

Carbon effect calculation and upgrading strategy of agricultural land consolidation project in urban edge of Three Gorges Reservoir Area

Wei Yang[1,2]*, Xiaohua Li[1,2], Weihua Li[2], Yutao Zhang[2,3]*, Haizhen Zhang[4] and Yuhe Ran[5]

[1]School of Resource and Environmental Engineering, Anshun University, Anshun, Guizhou, China, [2]College Rural Revitalization Research Center of Guizhou, Anshun University, Anshun, Guizhou, China, [3]School of Chemistry and Chemical Engineering, Anshun University, Anshun, China, [4]School of Continuing Education, Chongqing Vocational Institute of Engineering, Chongqing, China, [5]Administrative Committee of Anshun High tech Industrial Development Zone, Anshun, Guizhou, China

Under the background of promoting the construction of ecological civilization and the goal of carbon peak and carbon neutralization, it is of great significance to explore the measurement method and improvement strategy of the carbon effect of agricultural land consolidation. Based on a quantitative analysis and the whole life cycle of land consolidation, this study constructed a carbon effect accounting and analysis framework of agricultural land consolidation project from three stages of project initiation and design, project implementation, and operation management. Taking the agricultural land consolidation project in the Shiyan town on the urban edge of the Three Gorges Reservoir Area as a case, this study made empirical analysis and calculation and analyzed the carbon effect and influencing factors in different consolidation stages. The results showed that the overall carbon effect in the project area was a carbon source. The net carbon emission generated by the project construction was 8358t, which was mainly from workers input and concrete carbon emission; the carbon storage brought about by the adjustment of land use structure was 2,378.20t, which mainly came from the carbon storage increment of newly cultivated land; the carbon storage generated by the agricultural ecosystem was 1,100.04t, which was mainly based on the increase of cultivated land and the improvement of cultivated land quality; the carbon emission from agricultural production activities was 18.18t. Research conclusions: ① the carbon source effect of engineering construction is obvious. Artificial input and concrete are the main carbon sources in the hilly area at the edge of the metropolis; ② the adjustment of land use structure is manifested as a carbon sink effect, which mainly comes from the contribution of carbon storage of newly increased cultivated land; ③ the carbon effect of project operation and management may be a carbon source in the short term, and the long-term effect should be exerted; and ④ based on the concept of whole life cycle, promoting ecological land consolidation, optimizing project design, reasonably arranging consolidation projects, and strengthening operation management are

effective measures to improve the carbon effect of land consolidation projects, which are conducive to the realization of the "double carbon" goal.

KEYWORDS

agricultural land consolidation, ecosystem biomass, biomass carbon, carbon effect accounting, Shiyan town

1 Introduction

Global warming has led to a series of ecological and environmental problems, which have brought severe challenges to human survival and development. Greenhouse gas emission reduction has become a global issue (Dong et al., 2008). Under the goal of carbon peak and carbon neutrality, the implementation of carbon reduction is an important strategy for China's economy and society to achieve green and low-carbon development. The assessment report of the Intergovernmental Panel on Climate Change (IPCC) pointed out that the main cause of global warming was the greenhouse gas emissions from burning fossil fuels and land use by human activities (IPCC, 2001). According to the data released by the World Resources Research Institute and Climate Watch in 2016, 73.2% of global greenhouse gases came from energy consumption and 18.4% from agriculture, forestry, and land use (Wu et al., 2021). Some scholars estimated that the carbon emissions from land use and change, from 1850 to 1998, accounted for 1/3 of the total carbon emissions from human activities in the same period (Watson et al., 2000; Houghton et al., 2012); from 1850 to 2000, the net emission of CO_2 to the atmosphere due to land use change reached 156pg, of which 87% came from deforestation (Houghton et al., 1999; Watson et al., 2000). The impact of land use/land cover change (LUCC) on the carbon balance of terrestrial ecosystems has become the focus of research on global change and terrestrial carbon cycle (Gregorich et al., 1998). The carbon effect of land use and emission reduction measures are important ways to deal with global climate warming, which are of great concern to governments and scholars (Zhang et al., 2018).

Agricultural land consolidation is the reorganization of agricultural land use structure and ecosystem (Gao, 2003). It is an important way to coordinate the relationship between people and land, and one of the largest human activities to change the land use pattern and affect the terrestrial ecosystem in China (Zhang T et al., 2014; Wang et al., 2018), which directly affects the carbon cycle of the ecosystem. On the one hand, the strong disturbance of soil and the destruction of biomass caused by the project construction will directly affect the ecosystem in the project area. Meanwhile, the input of materials such as cement, steel and the consumption of energy such as gasoline and diesel will affect the carbon pool balance of the regional ecosystem.

China's rural land consolidation is developing rapidly and on a large scale, which has a prominent impact on the rural ecological environment, ecosystem biomass, and carbon emissions. According to the National Land Consolidation Plan (2016–2020), during the 13th Five-Year Plan period, 1.3333 million hm^2 of cultivated land will be replenished, 13.3333 million hm^2 of low and medium cultivated land will be transformed, and 400,000 hm^2 of rural construction land will be consolidated (The Ministry of Land and Resources of PRC The National Development and Reform Commission, 2017). Under the background of ecological civilization construction, the country has made great investment and continued promotion, which has made rural land consolidation a focus in the field of land resources management, and will continue to affect rural economic and social development and ecological environment construction.

At present, the planning, design, and construction practice of the agricultural land consolidation project pay more attention to the regional landscape pattern, soil erosion, and environmental pollution and pay less attention to the carbon effect of project implementation.

Domestic and foreign scholars have studied the carbon effect of agricultural land consolidation; one is to directly study the relationship between land use and carbon emissions, and the other is to indirectly study the carbon emissions caused by land use changes (Han et al., 2016), focusing on soil carbon content changes, energy, and material consumption, ecological compensation policies, and other contents (Tan et al., 2011; Guo et al., 2016; Zhang et al., 2016). Some scholars have also analyzed land consolidation types from the perspective of geomorphology types (Jin et al., 2013). In general, most of the existing studies are qualitative discussions and few quantitative calculations. The research on carbon emissions in different implementation stages of land consolidation projects and after the implementation of land consolidation projects is not enough. In addition, from the research area, there are few studies on the carbon effect of land consolidation in the Three Gorges Reservoir area, especially in the urban fringe. Therefore, this study reasonably absorbs the existing research results, takes the rural land consolidation project of the Shiyan town on the edge of the metropolitan area of the Three Gorges Reservoir Area in Chongqing as a case, adopts the quantitative method, and calculates the carbon effect and influencing factors at different stages based on the life cycle of agricultural land consolidation, so as to provide reference for the ecological transformation and development of agricultural

land consolidation in the metropolitan area edge. It provides a basis for the formulation of measures to reduce carbon emission and improve carbon effect in land consolidation regions, helps achieve the goal of carbon peak and carbon neutrality, and further enriches the theory and methods of low carbon and ecological land consolidation.

2 Overview of study area

The project area is located in Shiyan Town, Changshou District, Chongqing City, between 107°10′45″–107°14′08″E and 30°03′35″– 30°05′45″N, involving three villages including Muer, Zaojue, and Jianxin. The project area is located in the south of the parallel ridge Valley Liangping Syncline in the east of Sichuan Basin, mainly developed in the middle hilly terrain, and the micro landform is shallow hilly zone dam landform, with a relative height difference of 50–160 m and an average elevation of 370m; Longxi River in the area, with an average annual flow of 54 m^3/S; The groundwater has pressure bearing capacity and modulus is 27,000 m^3/km^2. It belongs to subtropical humid monsoon climate. The annual average temperature is 17.45°C, annual accumulated temperature of ≥0 °C is 6,423.7°C, annual accumulated temperature of ≥10°C is 5,783.75°C, frost free period is 331 days, average annual sunshine duration is 1,245.1 h, and average rainfall is 1117 mm, which is conducive to the growth of a variety of crops; the vegetation is mainly subtropical evergreen broad-leaved forest, with 184 tree species and 56 cultivated plants. The grain crops are mainly rice, corn, wheat, and sweet potato, and cash crops are mainly rapeseed and vegetables. The soil is brown purple soil and neutral purple mud paddy soil, with pH value of slightly acidic to slightly alkaline, and the thickness of soil layer ≥40 cm. Corn, sweet potato, and wheat can be planted in dry land three times a year; single cropping rice in the dam paddy field is mainly planted; and rice and wheat or rice and rapeseed planted in paddy fields in slope valley are mainly double cropping. The soil has high natural fertility, wide suitability for cultivation, and wide suitability for planting. The total area is 553.83 h m^2, population is 5,443, agricultural land is528.14 h m^2, unused land is 25.69 h m^2, and land reclamation rate is 64.63%. Land consolidation projects include land leveling, irrigation, drainage, field roads, farmland shelter forests, and other projects. The artificial leveling earthwork is 416,500 m^3, artificial tamping Earth barrier is 123,302 m^3, dry block stone sill 10090 m^3, new field road is 5 km, maintenance field road is 10.34 km, roads for production is 32.14 km, drainage and irrigation ditch are 28.083 km, new irrigation channel is 28.36 km, impounding reservoir is 67, desilting basin is 32,970, and shelter forest belt is 111.21 km.

3 Data sources and processing

3.1 Data sources

It mainly comes from the design report of the land consolidation project in Shiyan Town, Changshou District; the budget book of the land consolidation project in Shiyan Town, Changshou District; China Energy Statistics Yearbook; 2006 IPCC national greenhouse gas inventory Guide (IPCC, 2006); the budget quota of Chongqing land development and consolidation project; Changshou District Statistics Yearbook; the second national land survey data; and the relevant research literature on the carbon effect calculation of land consolidation projects.

3.2 Data processing

The material data of the consolidation project adopts the quantities and machine shifts in the project design report; energy consumption is obtained by conversion of the project budget quota standard. The carbon emission coefficients of different materials, energy, agricultural production inputs, and so on are modified based on relevant research results and combined with the actual situation of the study area. The carbon density parameters of soil and vegetation refer to the relevant data of similar remediation areas in the existing studies. The basic data such as crop yield are the average grain yield in the project area in the beginning year and 1 year after the completion and implementation of the agricultural land consolidation project.

4 Method

4.1 Logical framework of carbon effect accounting for agricultural land consolidation projects

Agricultural land consolidation has a profound impact on the carbon cycle and carbon storage in the project area, and the carbon effect is obvious. Based on the analysis of the whole life cycle, the agricultural land consolidation project has gone through such links as application, project approval, planning and design, engineering construction, completion acceptance, and operation. This study is simplified into three stages: project approval and design, project implementation, and operation and management. Agricultural land consolidation has an impact on biomass carbon, carbon cycle, and carbon pool reserves in the project area through disturbance of land and biomass, input of different materials, and use of mechanical fuel. The basic logic of three-stage carbon effect accounting was analyzed in the order of project life cycle (Figure 1): first, the carbon effect of land use structure change: the expected and actual land use structure

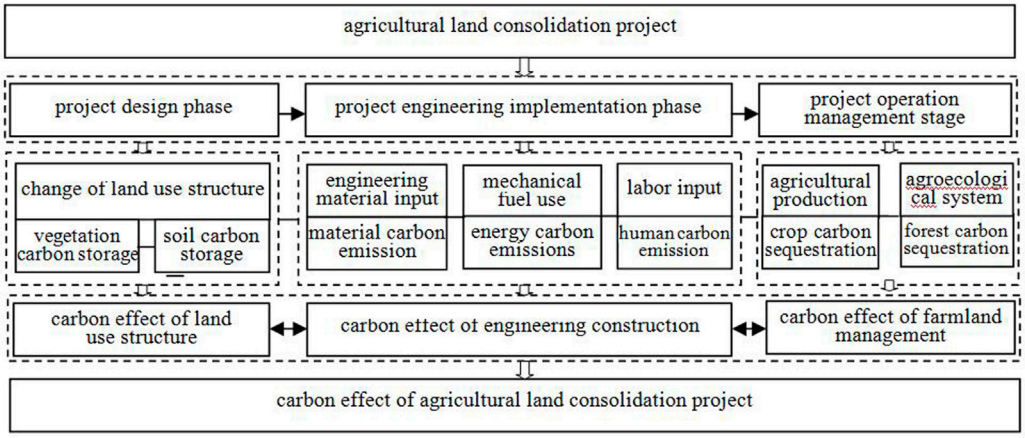

FIGURE 1
Logical framework of carbon effect accounting for agricultural land consolidation project.

change at the project approval and design stage and after completion and acceptance will lead to the change of the type and quantity of regional biomass and the disturbance of biomass carbon, resulting in the change of vegetation and soil carbon storage. Second, the carbon effect of project construction: the carbon cycle and carbon balance in the project area will be affected due to the disturbance of soil, biomass, and biomass carbon during the project construction and the disturbance of carbon balance in the project area caused by the input of a large amount of engineering materials, diesel and other fuels, and the CO_2 emissions of personnel. The third, the carbon effect of farmland operation and management: after the completion of the project, the change of agricultural production and ecosystem operation management and protection mode, such as the change of farming activities and farmland ecosystem on the type and quantity of biomass and biomass carbon in the project area will have an impact on the soil and vegetation carbon pool.

4.2 Accounting method for carbon effect of agricultural land consolidation projects

4.2.1 Calculation method of carbon effect in engineering construction

The engineering construction has the strongest disturbance on the soil, biomass and biomass carbon in the project area and the most direct impact on the carbon balance. One is to influence the carbon cycle in the project area by changing the land use structure and land use mode; Second, during the construction process, cement, stone, steel, concrete and other materials are put into use, diesel, electricity and other energy are consumed, and a large number of personnel are put into production, which will cause CO_2 emissions and affect the carbon balance of the project area. The use of gasoline, diesel and other energy sources directly generates CO_2 emissions; CO_2 emission of cement and other materials comes from the energy consumption in the production process; CO_2 emission of personnel input is generated from various production and construction activities. The influence of material transportation, wood and mortar plastering on carbon cycle is ignored in the carbon effect calculation, and river sand and water are partially reflected in concrete. According to this, the carbon emission during the construction of the project is the sum of the product of energy, materials, labor and its emission coefficient, the calculation model is as follows:

$$C_{eC} = \sum_{i=1}^{n} E_i \times f_{ie} + M_i \times f_{im} + P_i \times f_{ip}, \quad (1)$$

where C_{eC} is the total amount of carbon emissions from the construction of agricultural land consolidation projects; E_i, M_i, and P_i are the input amount of the *i*th energy, material, and personnel during construction; f_{ie}, f_{im}, and f_{ip} are the carbon emission coefficients corresponding to the *i*th energy, material, and personnel consumption, respectively. The existing research results (IPCC, 2006; Zhang et al., 2016; Cheng 2020; Zhai, 2017; He et al., 2018; Zhang et al., 2018) and the actual situation of the project area determine the carbon emission coefficient of each input material (Table 1).

4.2.2 Calculation method of carbon effect of land use structure change

The carbon effect of land use structure change is measured by the carbon storage change of the corresponding land use type before and after the consolidation. The implementation of agricultural land consolidation project will further develop and utilize some low-efficiency land such as bare land, grassland and ridge, merge small fields into large fields, level

TABLE 1 Carbon emission parameters of main materials/energy of agricultural land consolidation project in the project area.

Material type		Unit of measurement	Carbon emission coefficient	Data reference
Energy	Diesel oil	kg/kg	0.5927	IPCC (2006)
	Gasoline	kg/kg	0.5538	IPCC (2006); Cheng (2020)
	Electricity	kg/kw.h	0.9310	Cheng (2020)
Materials	Steel products	kg/kg	1.0600	Zhang et al. (2016); He et al. (2018)
	Cement	kg/kg	0.4598	Zhai (2017)
	Concrete	kg/m^3	231.50	He et al. (2018)
	Block stone	kg/m^3	2.3900	He et al. (2018)
Other	Workers	kg/人.d	18.9000	Zhang et al. (2018)
	Protection forest	kg/株.a	−23.6600	Zhang et al. (2016)

TABLE 2 Vegetation and soil carbon density parameters of different land types in the project area.

Land use type	Land type in the project area	Unit of measurement	Vegetation carbon density	Soil carbon density	Data reference
Cultivated land	Dry land and paddy field	t/hm^2	14.30	90.8	Chuai et al. (2012); Zhang et al. (2013)
Garden plot	Orchard garden	t/hm^2	25.10	84.3	Li et al. (2003)
Woodland	Protective forest land	t/hm^2	23.00	113.5	Zhang et al. (2013); Li et al. (2003)
Grassland	Other grassland	t/hm^2	10.31	109.39	Chen et al. (2021)
Land for transportation	Rural roads	t/hm^2	2.05	33.99	Xiang et al. (2022)
Land for water and water conservancy facilities	Pond surface and channel	t/hm^2	6.64	40.64	Cheng (2020)
Other agricultural land	Ridge of field	t/hm^2	1.59	62.95	Guo et al. (2015)
Unused land	Bare land	t/hm^2	1.50	55.45	Guo et al. (2015)

sloping farmland, build and maintain rural roads and irrigation and drainage channels, so as to adjust the land use structure and lay out of the project area, change the biomass type and production capacity, and CO_2 emissions of the ecosystem. Referring to the research results of scholars (Zhang et al., 2016; He et al., 2018; Zhang et al., 2018), the change of carbon storage of land use types is estimated by soil carbon storage and vegetation carbon storage, that is, the change area of each land use type in the project area is multiplied by the soil carbon density and vegetation carbon density per unit area of land. The calculation model is a follows:

$$CS_{ls} = CS_{lb} - CS_{lf} = \sum_{i=1}^{n} S_{ci} \times (CD_{vi}, +, CD_{si}), \quad (2)$$

where CS_{ls} is the total carbon storage change before and after the consolidation in the project area, CS_{lb} and CS_{lf} are the carbon storge after and before the consolidation, S_{ci} is the area change of the *i*th land use type, CD_{vi} and CD_{si} are the vegetation carbon density and soil carbon density of the *i*th land use type. The determination of relevant parameters (Li et al., 2003; Chuai et al., 2012; Zhang et al., 2013; Guo et al., 2015; Cheng, 2020; Chen et al., 2021; Xiang et al., 2022) is shown in Table 2.

4.2.3 Calculation method of carbon effect of project operation and management

The carbon effect of project operation and management is mainly reflected in the carbon storage of the farmland ecosystem and the carbon emission generated by the transformation of the farmland farming and management after consolidation. The carbon storage effect of farmland ecosystem lies in the increase of cultivated land area and the improvement of quality after the consolidation, which leads to the improvement of land utilization rate, crop yield, and the increase of biomass quantity and biomass carbon of crops and protective trees. The carbon sequestration capacity is calculated based on the average water content, economic coefficient, carbon absorption rate, and economic output of crops through crop biomass quantity and biochar (Zhang et al., 2016; Cheng, 2020). The calculation model of carbon absorption per unit output of crops is as follows:

TABLE 3 Carbon emission and absorption parameters of crops per unit yield in the project area.

Crops	Mean water Content/W_i	Economic coefficient of Crops/H_i	Carbon uptake rate of Crops/f_{ia}	Carbon uptake per unit of crop Yield/C_{ia}	Data reference
Paddy	0.14	0.45	0.41	0.783	Zhao and Qin, (2007); Zhang et al. (2018)
Corn	0.13	0.40	0.47	1.065	Cheng (2020); Zhang et al. (2018)
Wheat	0.13	0.40	0.49	1.066	Zhang et al. (2016); Zhang et al. (2018)
Rapeseed	0.09	0.25	0.45	1.638	Cheng (2020); Zhang T et al. (2014)

TABLE 4 Main carbon emission parameters of agricultural production activities in the project area.

Agricultural production activities	Carbon emission coefficient	Unit of measurement	Data reference
Agricultural irrigation	266.48	kg/hm^2	Duan et al. (2011); Zhao and Qin, (2007)
Land cultivation	218.82	kg/km^2	Zhang et al. (2018); Wu et al. (2007)
Fertilizer application	0.8956	kg/kg	Zhang T et al. (2014); Zhang et al. (2018)
Pesticide spraying	4.9341	kg/kg	Zhang Z et al. (2014); Zhang et al. (2018)
Agricultural film mulching	5.18	kg/kg	Zhang Z et al. (2014); Zhang et al. (2018)

$$CU_a = \sum_{i=1}^{n} C_{ia} = \sum \left[(1 - W_i) \times \frac{1}{H_i} \times f_{ia} \right], \quad (3)$$

where CU_a is the carbon uptake of crops per unit output (kg/kg), C_{ia} is the carbon uptake per unit crop of class i (kg/kg), W_i and H_i is the average water content of crops (kg/kg) and economic coefficient, and f_{ia} is the carbon uptake rate (%) of class i crops. Based on the research results of scholars (Zhao and Qin 2007; Zhang Z et al., 2014; Zhang et al., 2016; Cheng, 2020; Zhang et al., 2018) and the actual situation of the project area, the relevant parameters of carbon emission are determined (Table 3).

During the operation and management of the project, various agricultural production activities will inevitably produce CO_2 emissions. First, the carbon emissions from agricultural production links, such as the CO_2 emissions from energy consumption of farming machinery, crop irrigation and drainage, and the use of fertilizers and pesticides. The second is the emission of greenhouse gases from farmland ecosystems, such as soil respiration and CH_4 emissions from paddy fields. In practice, material balance algorithm and farmland greenhouse gas flux are usually used to estimate (Cheng (2020); Song, 2017). The calculation formula is as follows:

$$CE = \sum_{i=1}^{n} CE_i = \sum_{i=1}^{n} E_i \times \gamma_i, \quad (4)$$

where CE is the total amount of carbon emissions from agricultural cultivation in the project area, CE_i is the carbon emission of agricultural farming activities or agricultural inputs of type i, E_i is the amount of agricultural activities or agricultural inputs of type i, and γ_i is the carbon emission coefficient of different agricultural activities. The corresponding carbon emission coefficient is determined according to the research of scholars (Zhang T et al., 2014; Zhao and Qin (2007); Song, 2017; Duan et al., 2011; Wu et al., 2007) and the actual situation of the project area (Table 4).

5 Results and analysis

5.1 Carbon effect of project construction

The calculation results showed that the carbon emission of the project construction was 10,493.5t, and the carbon sink is 2135t, On the whole, it was shown as carbon source, and the net carbon emission was 8358t (Table 5). The emission of energy was 72.06t, accounting for 0.69% of the total carbon emission, gasoline 4.82t, diesel 19.27t, and electricity 47.97t, accounting for relatively low. The emission of materials was 2,410.87t, accounting for 22.97%, steel 25.20t, cement 344.98t, concrete 1,598.8t, block stone 441.89t, concrete was the most. Other categories: first, artificial emission of 8010.6T, accounting for 76.34% of the total, which is the main body of carbon emission. The second is the shelter forest project, which stores 2135t carbon, which can offset 20.35% of the total carbon emission. In terms of project type, the carbon emission from land leveling is

10.3389/fchem.2022.1022644

TABLE 5 Construction materials, energy input, and carbon emission results of the project area.

Material type		Land leveling		Irrigation and drainage		Field road		Farmland protection		Total	
		Consumption	Carbon emission	Consumption	Carbon emission	Consumption	Carbon emission	Consumption	Carbon emission	Consumption	Carbon emission
Energy	Diesel oil	0.40	0.24	9.86	5.84	22.26	13.19	0.00	0.00	32.52	19.27
	Gasoline	0.00	0.00	7.31	4.05	1.39	0.77	0.00	0.00	8.70	4.82
	Electricity	0.00	0.00	26.47	24.64	25.05	23.32	0.00	0.00	51.52	47.97
Materials	Steel products	0.00	0.00	23.77	25.20	0.00	0.00	0.00	0.00	23.77	25.20
	Cement	0.00	0.00	495.0	227.6	255.3	117.4	0.00	0.00	750.3	344.98
	Concrete	0.00	0.00	4,974	1,151	1928	446	0.00	0.00	6,902	1,598.8
	Block stone	100.9	241	22.01	52.61	61.99	148.1	0.00	0.00	184.9	441.89
Other	Worker	31.78	6,007	3.59	678.9	7.01	1,325	0.00	0.00	42.38	8010.6
	Protection forest	0.00	0.00	0.00	0.00	0.00	0.00	90,230	−2,135	90,230	−2,135
小计			6,249		2,170		2074		−2,135		8358

Unit of measurement: Electricity 1000Kw.h, concrete block stone 1000m^3, worker/10000, shelterbelt/plant, steel products, diesel oil, gasoline, cement, carbon emission/t.

6249t, accounting for 59.55% of the total carbon emission; Irrigation and water conservancy 2170t, accounting for 20.68%; and field road 2074t, accounting for 19.77%. Farmland protection works are carbon sinks (Figure 2). If the impact of artificial carbon emission is not included, the total carbon emission is 2,481.97t, including 1,491.36t for farmland water conservancy projects, 749.23t for field road projects and 241.38t for land leveling projects (Figure 3).

The project area is located in the hilly area on the edge of the metropolitan area of the Three Gorges Reservoir area. The project construction involves a lot of labor, with a total of 423,800 people per day, and less machinery. Therefore, different from many existing scholars, this study fully considered artificial carbon emission during construction. At the same time, the farmland protection project will be included in the carbon effect accounting of the project construction stage, and the carbon sink function will be played through the accumulation of biomass quantity and biomass carbon.

5.2 Carbon effect of land use structure change

After renovation, the cultivated land in the project area has increased by 54.15 h m^2, including 37.05 h m^2 of dry land, 2.36 h m^2 of paddy field, 2.36 h m^2 of garden land, 4.28 h m^2 of rural road land, the water surface of pit pond remains unchanged, 1.36 h m^2 of ditch, 0.48 h m^2 of other grassland, and 36.94 h m^2 and 25.69 h m^2 of ridge and bare land (Table 6). Rural residential areas, roads and woodlands are not included in the project area.

The calculation results showed that the carbon storage increment generated by the change of land use structure was 2,378.20t, which was a carbon sink in general. On the change of carbon storage of different land use types, the carbon storage of cultivated land increased by 5,691.17 t (3,893.96 t for dry land and 1797.21 t for paddy field), 258.19 t for garden land, 154.25 t for rural roads, 64.30 t for irrigation and drainage ditches, 57.46 t for grassland. The carbon storage of the ridge of field is reduced by 2384t, and the unused land is reduced by 1463t (Table 6). Increase of carbon reserves in the project area is mainly due to the increase of land use types such as dry land, paddy field, garden land and rural roads due to the improvement of other agricultural land and the development of unused land, thus increasing the biomass production, soil organic matter and biomass charcoal in the project area.

5.3 Carbon effect of project operation and management

5.3.1 Carbon sink effect of farmland ecosystem

The main grain crops in the project area are paddy, wheat and corn, and the major cash crops are rapeseed and some

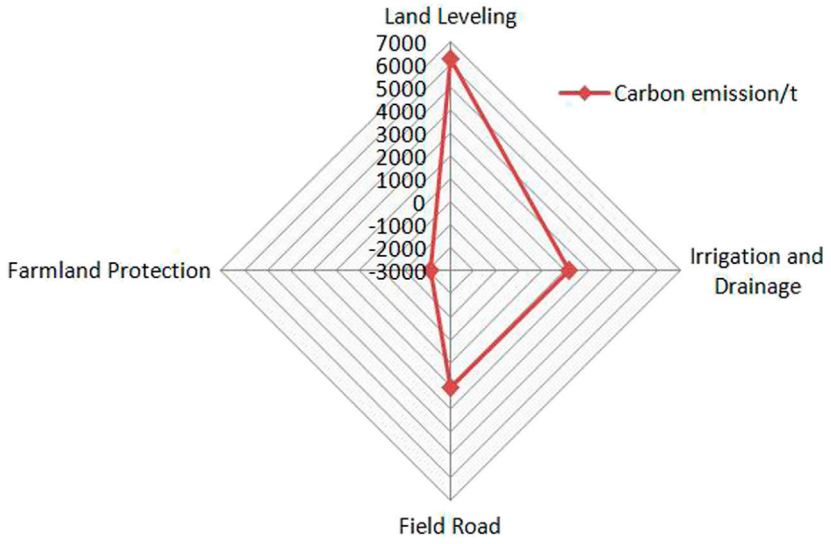

FIGURE 2
Carbon effect structure of different land consolidation projects (including personnel).

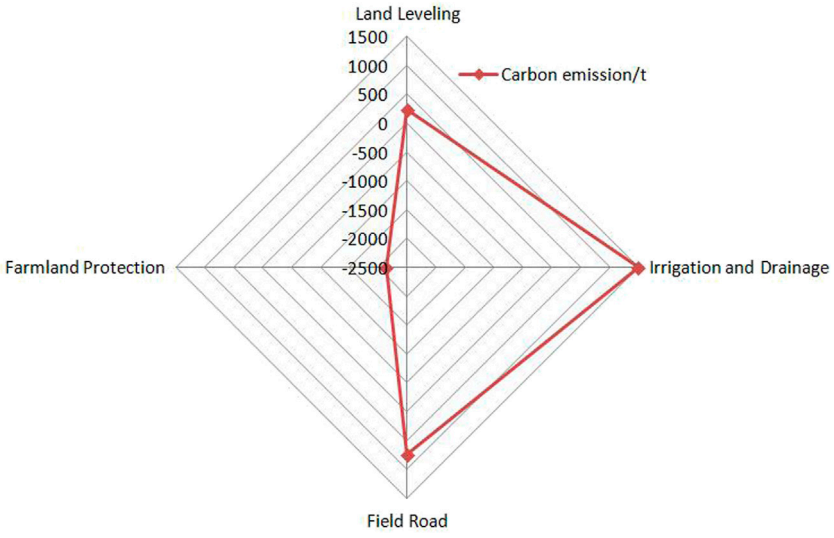

FIGURE 3
Carbon effect structure of different remediation projects (excluding personnel).

vegetables. In agricultural production, the rotation of corn and wheat is adopted in dry land, and paddy and rapeseed are rotated in paddy field. After the implementation of the project, firstly, the increase of the amount of arable land leads to the increase of grain output; secondly, the improvement of the medium and low yield fields leads to the improvement of the quality of arable land and the increase of crop output. Both of them work together to increase the overall biomass, biomass carbon and carbon reserves in the project area due to the increase of grain output. According to the calculation results, the newly increased cultivated land and grain yield: paddy field 17.1 h m^2, dry land 37.5 h m^2, rice 128.76t, rapeseed 38.48t, corn 161.17t, wheat 84.47t, a total of 412.88t; Arranging medium and low yield fields and increasing

TABLE 6 Carbon storage change for land use structure adjustment in the project area.

Land type		Before consolidation	After consolidation	Land type change	Carbon storage change		
					Soil	Vegetation	Subtotal
Cultivated land	Dry land	180.32	217.37	37.05	3,364.14	529.82	3,893.96
	Paddy field	177.61	194.71	17.10	1,552.68	244.53	1797.21
Garden plot	Orchard garden	0.00	2.36	2.36	198.95	59.24	258.19
Land for transportation	Rural roads	5.29	9.57	4.28	145.48	8.77	154.25
Land for water and water conservancy facilities	Pond surface	1.72	1.72	0.00	0.00	0.00	0.00
	Channel	0.51	1.87	1.36	55.27	9.03	64.30
Grassland	Other grassland	0.00	0.48	0.48	52.51	4.95	57.46
Other agricultural land	Ridge of field	162.69	125.75	−36.94	−2,325	−58.73	−2,384
Unused land	Bare land	25.69	0.00	−25.69	−1,424	−38.53	−1,463
Total		553.83	553.83	0.00	1,619.14	−59.06	2,378.20

Unit of measurement: land type/hm^2, soil, and vegetation carbon storage/t.

TABLE 7 Change of crop yield and carbon storage after consolidation in the project area.

Crops	Grain output of newly increased cultivated land		Increase grain yield by arranging medium and low yield fields		Carbon storage
	Cultivated land area	Grain yield	Renovation area	Grain production increase	
Paddy	17.1	128.76	177.61	213.13	267.70
Rapeseed		38.48		119.89	259.41
Corn	37.05	161.17	180.32	143.35	324.31
Wheat		84.47		148.76	248.62
合计	54.15	412.88	357.93	625.13	1,100.04

Unit of measurement: area/hm^2, grain yield, grain production increase, and carbon storage/t.

grain yield: arranging 180.32 h m^2 of dry land and 177.76 h m^2 of paddy fields, increasing the yield of rice by 213.3t, rapeseed by 259.41t, corn by 143.76t and wheat by 148.76t, totaling 625.13t (Table 7).

The results showed that the increase of crop biomass production in the project area increased the total carbon storage by 1,100.04t, including 267.70t of rice, 259.41t of rapeseed, 324.31t of corn and 248.62t of wheat. In general, the proportion of carbon storage increase caused by the consolidation of medium and low yield fields in the project area was larger (Table 7), and the carbon sink effect of agricultural ecosystem was obvious.

5.3.2 Carbon source effect of agricultural production activities

After the implementation of the consolidation in the project area, the amount of fertilizer, pesticide, agricultural film and other materials invested in agricultural farming activities is adjusted every year, and the area of agricultural irrigation and land cultivation is increased, resulting in the change of carbon balance in the project area. The results showed that the agricultural irrigation area increased by 46.33 h m^2, the land plowing increased by 0.57 km^2, the use of agricultural film increased by 4.49t, and the carbon emission increased by 12.35 t, 0.12 t and 23.26 t respectively in 1 year; The amount of pesticide application was reduced by 0.55t and the amount of fertilizer was reduced by 16.56t. The annual carbon emissions in the project area are reduced by 2.71t and 14.83 T respectively. In general, the annual net carbon emission of agricultural production activities in the project area after consolidation was 18.18t, which was shown as carbon source effect (Table 8).

5.4 Carbon effect balance analysis in the project area

The carbon effect of the three stages of the agricultural land consolidation project is different. During the

TABLE 8 Agricultural production activities and carbon emissions after consolidation in the project area.

Agricultural production activities	Unit of measurement	Before consolidation	After consolidation	Quantity change	Carbon Emissions/t.a
Agricultural irrigation	hm^2	221.63	267.96	46.33	12.35
Land cultivation	km^2	3.57	4.14	0.57	0.12
Fertilizer application	t	268.45	251.89	−16.56	−14.83
Pesticide spraying	t	3.98	3.43	−0.55	−2.71
Agricultural film mulching	t	20.4	24.89	4.49	23.26
Total		518.03	552.31	34.28	18.18

implementation stage of the agricultural land improvement project, due to various materials input, machinery use, energy consumption, labor input and other reasons, the ecosystem, biomass production and biomass carbon in the project area are destroyed, resulting in a large amount of carbon emissions, affecting the regional carbon cycle and carbon balance. The carbon emission in this stage is short-term and one-time, and the project area is a carbon source; In the stage of operation management and conservation, due to the increase of cultivated land area, quality improvement, biomass production of crops and biomass carbon, it is manifested as a carbon sink, which is a long-term carbon effect with an annual cycle. At the same time, in the stage of operation and management, agricultural production activities increased, and the overall carbon emissions increased accordingly. In this cycle, after a certain period of operation, the carbon emissions from the project construction will be gradually digested by the agricultural ecosystem to achieve carbon balance. The time to achieve carbon balance is determined by the carbon emission of project construction, the carbon storage of land use structure adjustment, the carbon storage of agroecosystem and the carbon emission of agricultural production activities. The calculation formula is as follows:

$$T_{cb} = \frac{C_{eC} - CS_{ls}}{CU_a - CE}, \quad (5)$$

where T_{cb} is the time to achieve carbon effect balance in the project area, C_{eC} is the total amount of carbon emissions from the construction of agricultural land consolidation project, CS_{ls} is the total carbon storage change before and after the consolidation in the project area, CU_a is the carbon uptake of crops per unit output, and CE is the total amount of carbon emissions from agricultural cultivation in the project area.

The carbon emissions of the project construction are 8358t, the carbon reserves of land use structure adjustment are 2,378.20t, the carbon reserves of agricultural ecosystem in the project area are 1,100.04t, and the carbon emissions of agricultural production activities are 18.18t. It is estimated that the time to achieve carbon balance is 5.53 years.

6 Conclusion and discussion

6.1 Conclusion

Based on the historical background of promoting the construction of ecological civilization and achieving the goal of carbon peak and carbon neutralization, this study took the life cycle of agricultural land consolidation project as the clue, and adopted quantitative analysis method to construct the carbon effect accounting and analysis framework of agricultural land consolidation project from three stages of project approval design, project implementation and operation and management. Taking the agricultural land consolidation project in Shiyan town on the edge of the Three Gorges Reservoir Area as the research case, this study made empirical analysis and calculation, and explored the influencing factors of carbon storage in different life cycle stages. The main conclusions were as follows:

(1) The overall carbon effect of the project area was measured as the carbon source state. The net carbon emissions generated by the project construction were 8358t, the carbon reserved generated by the land use structure adjustment were 2,378.20t, the carbon reserved generated by the agricultural ecosystem were 1,100.04t, and the carbon emissions from agricultural production activities were 18.18t.

(2) The project area was located in the hilly area on the edge of the metropolitan area of the Three Gorges Reservoir area, and the carbon source effect of the project construction was obvious. Among them, the carbon emission of artificial input was 8010.6t, and the land leveling project in the project category was 6249t, accounting for 59.55% of the total carbon emission; excluding the carbon emission of artificial input, the total carbon emission was 2,481.97t, of which 1,598.8t was from concrete, accounting for 64.42%, followed by 441.89t from block stone and 344.98t from cement. In the project category, 1491.36t was from farmland water conservancy, 749.23t was from field roads and 241.38t was from land leveling. The farmland shelter

forests were carbon sinks, increasing carbon reserves by 2135t.

(3) The carbon effect of land use structure adjustment was generally shown as carbon sink. Among them, the newly increased cultivated land in the project area increases the carbon reserved by 5,691.17t, which was the main body of the increase in carbon reserves; As the area of ridge of field and bare land decreases, the carbon reserves were reduced by 2384t and 1463t.

(4) The calculation results of the carbon protection effect of the project operation and management were generally shown as carbon sinks. The carbon reserved of farmland ecosystem increased by 1,100.04t due to the increase of cultivated land area and the improvement of cultivated land quality, and the carbon reserved increased more due to the improvement of cultivated land quality. The total carbon emission from agricultural production activities was 18.18t.

6.2 Discussion and suggestions

Under the background of vigorously promoting the construction of ecological civilization, rural land consolidation will pay more and more attention to the goal of low carbon emission and high carbon sink. Rural land consolidation will certainly have a certain reverse effect on ecosystem structure and carbon sequestration effect in the project area. Therefore, it is inevitable to explore and promote low carbon and ecological land consolidation.

(1) Ecological land consolidation is an important means to promote the construction of ecological civilization and the realization of the "double carbon" goal. The research shows that the different stages of agricultural land consolidation, especially the engineering construction, have strong disturbance on the soil and vegetation in the project area, and great influence on the biomass production of the ecosystem, which directly affects the regional carbon cycle and carbon balance. Therefore, exploring and promoting ecological land consolidation with low carbon emission and high carbon sink is an important carrier to achieve the "double carbon" goal and an important means to promote the construction of ecological civilization.

(2) Based on the concept of life cycle, optimizing project design, reasonably arranging consolidation projects and strengthening operation management and protection are effective measures to improve the carbon effect of land consolidation projects.

Project approval and design stage: revise the policy standards for land consolidation project approval, and take the potential of carbon sequestration and sink increase as an important indicator for project approval and storage. In the operation, the change of carbon storage in vegetation and soil and carbon effect accounting of the project area before and after the consolidation are taken as the necessary contents of the project feasibility study, and the projects with good carbon effect and strong implement ability are preferentially selected for storage and filing.

Construction stage of the project: ecological engineering materials such as ecological bricks are mostly selected. The layout of the project is adapted to local conditions to reduce unnecessary or small projects. The projects that are unreasonable or have a great impact on the ecological environment of the project area are canceled according to the actual situation. The terrain and landform of the project area are mostly kept, and the demolition and construction are not large, so as to reduce the engineering disturbance to the project area.

Project operation and management stage: establish and adjust the acceptance and assessment standards for agricultural land consolidation projects, and take the achievement degree and stability of carbon reduction and sink increase of newly added cultivated land, farmland water conservancy projects, field road projects and farmland shelter forest projects before and after the implementation of the project as important indicators. Regional standards and incentives for farmland cultivation, seed selection, irrigation and drainage, fertilizer and pesticide application should be established to reduce carbon emission and increase carbon storage, so as to improve the carbon storage and carbon effect of the project area through a perfect operation management and conservation policy system.

Data availability statement

The original contributions presented in the study are included in the article/Supplementary Material; further inquiries can be directed to the corresponding authors.

Author contributions

WY was in charge of designing the experiments and writing the manuscript; XL,WL, HZ, YR, and YZ was in charge of revising the manuscript; YZ was in charge of project administration.

Funding

This work was supporting by the Guizhou Province Theoretical Innovation Project (GZLCZB-2023-28-5), Anshun City Land Space Planning and Resource Efficient Utilization of Science and Technology Innovation Talent Team ([2022]4), the Creative Research Groups Support Program of Guizhou Education Department (KY [2017]049), and Research project

of Humanities and social sciences of Chongqing Education Commission(21SKGH352).

Conflict of interest

The authors declare that the research was conducted in the absence of any commercial or financial relationships that could be construed as a potential conflict of interest.

Publisher's note

References

Chen, M. J., Wang, Q. R., and Bai, Z. K., (2021). Transition of "production-living-ecological" Space and its carbon storage effect under the vision of carbon neutralization: A case study of Guizhou Province. *China Land Sci.* 35 (11), 101–111. doi:10.27175/d.cnki.gjxcu.2020.001450

Cheng, Y. Q. (2020). *Reserch on carbon effect calculation and decision optimization of land remidiation projects-taking the project area of zhongbu town, leoing city as an example*. Nanchang, Jiangxi: Jiangxi University of Finance and Economics.

Chuai, X. W., Lai, L., Huang, X. J., Zhao, R., Wang, W., and Chen, Z. (2012). Temporospatial changes of carbon footprint based on energy consumption in China. *J. Geogr. Sci.* 22 (1), 110–124. doi:10.1007/s11442-012-0915-4

Dong, H. M., Li, Y. E., Tao, X., Peng, X., Li, N., and Zhu, Z. (2008). China greenhouse gas emissions from agricultural activities and its mitigation strategy. *Trans. CSAE* 24 (10), 269–273.

Duan, H. P., Zhang, Y., and Zhao, J. B., (2011). Carbon footprint analysis of farmland ecosystem in China. *J. Soil Water Conservation* 25 (05), 203–208. doi:10.13870/j.cnki.stbcxb.2011.05.020

Gao, X. J. (2003). *Theory and practice of land consolidation*. Beijing: Geological Publishing House.

Gregorich, E. G., Rochette, P., McGuire, S., Liang, B. C., and Lessard, R. (1998). Soluble or-ganic carbon and carbon dioxide fluxes in maize fields receiving spring applied manure. *J. Environ. Qual.* 27, 209–214. doi:10.2134/jeq1998.00472425002700010029x

Guo, X. H., Dun, Y. L., and Bo, G. T., (2015). Study on effect of land consolidation project on carbon emission in plain area-taking the land consolidation of hebei Province as an example. *Res. Soil Water Conservation* 22 (3), 241–246. doi:10.13869/j.cnki.rswc.2015.03.043

Guo, Y. Q., Yun, W. J., and Huang, N., (2016). The effect of land consolidation projects on soil carbon emissions. *Chin. J. Soil Sci-ence* 47 (1), 36–41. doi:10.19336/j.cnki.trtb.2016.01.006

Han, J., Zhou, X., and Xiang, W. N. (2016). Progress in research on land use effects on carbon emissions and low carbon management. *Acta Ecol. Sin.* 36 (4), 1152–1161. doi:10.5846/stxb201406271334

He, D. W., Jin, G., and Wang, Y. Q., (2018). Carbon emissions accounting for construction of different types of land consolidation projects in Hubei Province. *J. Hubei Univ. Sci.* 40 (6), 568–573. doi:10.3969/j.issn.1000-2375.2018.06.004

Houghton, R. A., Hackler, J. L., and Lawrence, K. T. (1999). The U.S.carbon budget:contributions from land-use change. *Science* 285 (5427), 574–578. doi:10.1126/science.285.5427.574

Houghton, R. A., Vander Werf, G. R., Defries, R. S., van der Werf, G. R., and Hansen, M. C., (2012). Carbon emissions from land use and land-cover change. *Biogeosciences* 9 (1), 5125–5142. doi:10.5194/bg-9-5125-2012

IPCC (2006). *2006 IPCC guidelines for national greenhouse gas inventories*. Kanagawa: IGEC.

IPCC (2001). *Climate change 2001-synthesis repoet: Third assessment report of the intergovernmental Panel on climate change*. New York: Cambridge University Press.

Jin, G., Wang, Z. Q., and Chong, D., (2013). Categorizing of land consolidation engineering zones in Tibet. *Sci. Techno-logical Manag. Land Resour.* 30 (5), 21–27. doi:10.3969/j.issn.1009-4210.2013.05.004

Li, K. R., Wang, S. Q., and Cao, M. K. (2003). Vegetation and soil carbon storage in China. *Sci. China (Series D)* (01), 72–80.

Song, D. (2017). *Analysis of low-carbon land use and research on structure optimization in changchun city*. Changchun, Jilin: Jilin University.

Tan, M., Huang, X. J., and Zhong, T. Y., (2011). Impacts of land consolidation on soil organic carbon conten. *Trans. CSAE* 27 (8), 324–329. doi:10.3969/j.issn.1002-6819.2011.08.057

The Ministry of Land and Resources of PRC The National Development and Reform Commission (2017). *The national land con-solidation planning*. Beiging: The National Development and Reform Commission. EB/OL]. (2017-01-10) [2017-08-28 http:/www.mlr.gov.cn/zwgk/zytz/201702/t20170215_1440315.htm.

Wang, J., Zhong, L. N., and Ying, L. X. (2018). Review on the study of the impacts of land consolidation on ecosystem services. *J. Ecol. Rural Environ.* 34 (9), 803–812. doi:10.11934/j.issn.1673-4831.2018.09.006

Watson, R. T., Noble, I. R., and Bolin, B., (2000). *Land use, land use change, and forestry*. Cambridge, UK: Cambridge University Press.

Wu, F. L., Li, L., and Zhang, H. L., (2007). Effects of conservation tillage on net carbon flux from farmland ecosystems. *Chin. J. Ecol.* 26 (12), 2035–2039. 10.13292j.1000-4890.2007.0360

Wu, J. L., Su, M. Y., and Su, S. Q., (2021). Research on the path of comprehensive land management in the whole region under the goal of "double carbon. *Nat. Resour. Econ. China* 34 (12), 77–83. doi:10.19676/j.cnki.1672-6995.000672

Xiang, S. J., Zhang, Q., Wang, D., Wang, S., Wang, Z. f., Xie, Y. q., et al. (2022). Response and vulnerability analysis of carbon storage to LUCC in the main urban area of Chongqing during 2000-2020. *J. Nat. Resour.* 37 (5), 1198–1213. doi:10.31497/zrzyxb.20220507

Zhai, H. B. (2017). *Determination of carbon emission of land consolidation project in taihang mountains in shijiazhuang west*. Shijiazhuang, Hebei: Hebei University of Economics and Business.

Zhang, L. G., Wang, Z. Q., and Li, B. Q. (2018). Carbon effect accounting and analysis of land consolidation in hubei Province. *J. Nat. Resour.* 33 (11), 2006–2019. doi:10.31497/zrzyxb.20171141

Zhang, M., Lai, L., and Huang, X. J., (2013). The carbon emission intensity of land use conversion in different regions of China. *Resour. Sci.* 35 (4), 792–799.

Zhang, S., Jin, X. B., and Yang, X. H., (2016). Determining and estimating impacts of farmland consolidation projects on the regional carbon effects. *Resour. Sci.* 38 (1), 93–101. doi:10.18402/resci.2016.01.10

Zhang, T. T., Cai, H. S., and Zhang, X. L. (2014). Spatial-temporal dynamics of famland and ecosystem carbon souce/sink based on carbon footprint in JiangXi Province. *Resour. Environ. Yangtze Basin* 23 (06), 767–773. doi:10.18402/resci.2016.01.10

Zhang Z, Z. F., Zhao, W., and Gu, X. K. (2014). Changes resulting from a land consolidation project (lcp) and its resource–environment effects: A case study in tianmen city of hubei Province, China. *Land Use Policy* 40, 74–82. doi:10.1016/j.landusepol.2013.09.013

Zhao, R. Q., and Qin, M. Z. (2007). Temporal spatial viriation of partial carbon source/sink of farm land ecosystem in coastal Chi-na. *J. Ecol. Rural Environ.* 23 (2), 1–6.

frontiers | Frontiers in Chemistry

TYPE Original Research
PUBLISHED 11 October 2022
DOI 10.3389/fchem.2022.1041843

OPEN ACCESS

EDITED BY
Hu Li,
Guizhou University, China

REVIEWED BY
Qingping Ke,
Anhui University of Technology, China
Guoqiang Wu,
Jiangxi Agricultural University, China
Zhisheng Shi,
Anhui Polytechnic University, China

*CORRESPONDENCE
Zeying Wu,
wuzy@czu.cn
Jiancheng Zhou,
jczhou@seu.edu.cn

SPECIALTY SECTION
This article was submitted to Green and Sustainable Chemistry, a section of the journal Frontiers in Chemistry

RECEIVED 11 September 2022
ACCEPTED 26 September 2022
PUBLISHED 11 October 2022

CITATION
Xiang M, Gao Z, Ji X, Li D, Deng Y, Ding Y, Yu C, Zhang W, Zhang Z, Wu Z and Zhou J (2022), Boosting CO_2 hydrogenation to methane over Ni-based ETS-10 zeolite catalyst. *Front. Chem.* 10:1041843. doi: 10.3389/fchem.2022.1041843

Boosting CO_2 hydrogenation to methane over Ni-based ETS-10 zeolite catalyst

Mei Xiang[1,2], Zhangxi Gao[3], Xiaonan Ji[1], Dantong Li[1], Yaoyao Deng[1], Yalong Ding[4], Chi Yu[5], Wei Zhang[1], Zhenwei Zhang[1], Zeying Wu[1]* and Jiancheng Zhou[2]*

[1]Research Center of Secondary Resources and Environment, School of Chemical Engineering and Materials, Changzhou Institute of Technology, Changzhou, China, [2]Department of Chemical Engineering, School of Chemistry and Chemical Engineering, Southeast University, Nanjing, China, [3]Jiangsu Key Laboratory of Advanced Catalytic Materials and Technology, Changzhou University, Changzhou, China, [4]College of Chemistry and Pharmaceutical Engineering, Huanghuai University, Zhumadian, China, [5]Zhongyi Testing and Research Institute Co, Ltd., Huzhou, China

The activation and conversion of the CO_2 molecule have always been the most vexing challenge due to its chemical inertness. Developing highly active catalysts, which could overcome dynamic limitations, has emerged as a provable and effective method to promote CO_2 activation–conversion. Herein, ETS-10 zeolite–based catalysts, with active nickel species introduced by *in situ* doping and impregnation, have been employed for CO_2 methanation. Conspicuous CO_2 conversion (39.7%) and perfect CH_4 selectivity (100%) were achieved over the Ni-doped ETS-10 zeolite catalyst at 280°C. Comprehensive analysis, which include X-ray diffraction, N_2 adsorption–desorption, SEM, TEM, H_2 chemisorption, CO_2 temperature programmed desorption, and X-ray photoelectron spectroscopy, was performed. Also, the results indicated that the resultant hierarchical structure, high metal dispersion, and excellent CO_2 adsorption–activation capacity of the Ni-doped ETS-10 zeolite catalyst played a dominant role in promoting CO_2 conversion and product selectivity.

KEYWORDS

CO_2 hydrogenation, methane, ETS-10 zeolite, *in situ* doping, Ni-based catalyst

1 Introduction

As one of the major greenhouse gases, CO_2 has commanded the attention of the whole world due to its increasing emission that results in a series of critical environmental problems (Saeidi et al., 2021). While being not blamed for the ecological concern, CO_2 is in fact quite an important C1 source to produce high value–added chemicals, such as CH_4, CH_3OH, HCOOH, CH_3CH_2OH, and other C^{2+} products (Wang et al., 2021; Zhu et al., 2022). Hence, extensive and continuous efforts have been made to reduce CO_2 emissions, among which catalytic hydrogenation has been proved to be an attractive and promising process in which the required hydrogen is produced renewably by water electrolysis (Meng et al., 2022). In particular, the hydrogenation of CO_2 into methane has been identified as one of the most important and economically feasible strategies, during which

the produced simplest C-H molecule has high gravimetric/volumetric energy density and is easily liquefied and safely transported by means of the existing natural gas infrastructure (Zhao et al., 2022). However, due to the chemical inertness of the CO_2 molecule, its activation and conversion have always been the most vexing challenges. The current solutions cannot be divorced from the use of high energy consumption and an efficient catalyst. Therefore, a wide range of studies have been focused on developing highly active catalysts that are conducive in overcoming dynamic limitations and promoting CO_2 activation–transformation (Gao et al., 2022; Liu et al., 2022; Song et al., 2022).

Bifunctional catalysts, consisting of active metal components and supports, are the most widely employed and investigated for CO_2 methanation. Among these catalysts, the Ni-based catalytic system has been proven to be the most prominent because of the corresponding extraordinary activities and selectivity, as well as the relative lower costs (Gonçalves et al., 2022; Italiano et al., 2022; Ren et al., 2022; Xie et al., 2022). Nevertheless, the agglomeration of Ni metallic particles at a high temperature that inevitably results in catalyst deactivation has always been the bottleneck. Besides, at a low temperature, thermal sintering can also take place by reason of the interactions between Ni and CO, leading to the formation of nickel carbonyls followed by an increase in deactivation. Furthermore, there is a general consensus that the Ni-based catalysts are actually unfit for low-temperature hydrogenation reactions. However, for CO_2 hydrogenation to methane, the process is in fact highly exothermic and profoundly affected by pressure and temperature, giving rise to contradictory requirements of reaction conditions for achieving both high CO_2 conversion and methane selectivity (Boukha et al., 2022; Makdee et al., 2022; Pu et al., 2022). Consequently, in order to effectively keep from the thermodynamics and kinetics equilibrium limitations, a breakthrough in design and development of Ni-based catalysts with a conspicuous catalytic performance and robust stability at a low temperature is necessary and much awaited. Strategies with an eye on active metal, supports, and catalyst preparation methods have been frequently reported and have mainly included metal doping, encapsulation and alloying, metal–support interaction regulation, support design, modification, and morphology engineering, among which supports have carried considerable weightage in catalyst construction and fabrication, maximizing the corresponding catalytic performances and anti-sintering abilities without doubt (Yang et al., 2021). Oxide supports, for example, Al_2O_3, TiO_2, SiO_2, MgO, CeO_2, ZrO_2, and Nb_2O_5, have been widely investigated and proved to be very active because of their characteristics, such as enhanced Ni dispersion, stable anchoring sites, suitable acid/basic properties, and an appropriate amount of structural defects (Zhou et al., 2016; Wang L. et al., 2020; Wang L. X. et al., 2020; Hu et al., 2021; Wang Z. M. et al., 2022; Zafar et al., 2022). Even though these advantages have indeed made contributions in regulating and controlling the compositions and structures of catalysts, the resulting catalytic activities and thermal stabilities can only be promoted to a limited extent. Thus, it is still highly desirable to keep digging into fairly promising Ni-based catalysts so as to boost the corresponding CO_2 methanation activities and stabilities.

As one of the most popular supports for metal-based catalysts, zeolites with high specific surface areas, hydrothermal stabilities, regular channels, and typical ion-exchange and adsorption properties are of great academic and practical importance in catalysis (Wang X. Y. et al., 2022). For CO_2 methanation reactions, certain kinds of zeolites have been reported, which include ZSM-5, USY, BEA, and MCM-41 adopted zeolites (Graca¸ et al., 2014; Gac et al., 2021; Hussain et al., 2021; Uttamaprakrom et al., 2021; Cui et al., 2022), in which a series of transition metals have been incorporated by means of co-crystallization, recrystallization, inter-zeolite transformation, encapsulation, and two-step post-synthesis preparation methods (Franken et al., 2020; Ra et al., 2020; Fan and Tahir, 2021; Frei et al., 2021; Hwang et al., 2021; Skrypnik et al., 2022). According to the encouraging results, the use of zeolite support for CO_2 hydrogenation to methane did improve metal dispersion, metal–support interactions, and CO_2 adsorption activations, resulting in promoted low-temperature kinetics and remarkable methane selectivity (Azzolina-Jury et al., 2017; Upasen et al., 2022). However, the evaluated zeolite catalysts were mostly treated with surface modifications, and their catalytic promotion have always been backed with other additives and metal promoters (Kosinov and Hensen, 2020; Liu et al., 2020; Zhang et al., 2020; Yang et al., 2021). Hence, there is plenty of scope for the development of zeolite-based catalysts with the inherent framework and physicochemical properties that are useful in and highly compatible with CO_2 methanation processes.

ETS-10 zeolite, different from other widely used aluminosilicate zeolites such as MFI, FAU, and LTA, is a titanosilicate zeolite that is characterized by the unique three-dimensional 12-membered ring network and intrinsic Lewis basicity, which is derived from the specific corner sharing TiO_6^{2-} octahedra with two negative charges (Xiang and Wu, 2019a; Chen et al., 2022). Besides, the interconnected channels of ETS-10 present a free entrance of about 0.8 × 0.5 nm, enabling the easy adsorption and diffusion of small molecules such as CO_2, CO, CH_4, H_2, and H_2O (Fu et al., 2018). As a result, due to the peculiar framework architectures and chemical compositions, as well as the relatively wide pore dimensions, ETS-10 has gained more and more attention and acquitted itself admirably in adsorption, ion exchange, and shape-selective catalysis. Actually, in previously published reports, the Ni-based ETS-10 catalyst has been employed for a hydrogenation process and proved to be conspicuously catalytically active with excellent selectivity and extraordinary stability in heterogeneous catalysis

(Chen et al., 2016). Furthermore, considering the electron acceptor characteristics and geometric construction of the CO_2 molecule, the typical structural unit of the -Ti-O-Ti- chain in ETS-10 that is characterized by extraordinary and strong electron donor capability deserves to place great expectations on boosting CO_2 activation and conversion.

Hence, the main goal of this work was to construct catalysts made up of Ni active phased and structurally unique ETS-10 zeolite that is a self-contained Lewis base and can be highly envisioned to make an indispensable contribution to the selective conversion of CO_2 into methane. Specifically, when compared to previously reported studies on the popular USY, ZSM-5, and beta zeolite-based catalysts, as well as those well-reviewed rare earth oxides catalysts, the prepared ETS-10 zeolite catalyst herein has been proven to be more potential in adsorption and activation of CO_2. To account for this, intensive characterizations and measurements were carried out, which further helped to get deep insights into the corresponding catalysis promotion mechanisms. Furthermore, the impact of different Ni incorporation methods on catalyst stabilities has also been evaluated by relevant techniques.

2 Experimental

2.1 Catalyst preparation

A hydrothermal method was used with a molar composition of 1.0 TiO_2: 7.1 SiO_2: 4.4 Na_2O: 1.9 K_2O: 0.4 NiO: 160.0 H_2O according to our previous studies (Xiang and Wu, 2019a). Typically, 6.0 ml of 6.67 mol/L aqueous NaOH was added into 10.0 ml aqueous water glass solution [SiO_2/Na_2O (molar ratio): 3.67] under vigorous stirring. Afterward, the mixed solution composed of 0.5 g nickel (II) nitrate hexahydrate and 7.0 g of $TiCl_3$ solution (17 wt% in HCl) was introduced by slow dropwise addition. Then, 7.6 ml of 3.62 mol/L KF aqueous solution was added, followed by continuous stirring for 1.5 h. The obtained gel was subsequently transferred into a Teflon-coated stainless steel autoclave for crystallization (230°C, 64 h). The resulting product was then filtered, washed, and dried at 100°C overnight before being calcined in air at 450°C for 5 h. For comparison, incipient wetness impregnation was also performed with the ETS-10 zeolite prepared in the same way as abovementioned and by using parallel amounts of nitrate precursor. The resulting catalyst sample was named Ni/ETS-10. Other ETS-10-based catalysts with various metal species introduced by the doping method were also prepared and named M-ETS-10 (M refers to metal species).

Besides, a series of common zeolite supports was used to prepare Ni-based catalysts, which included Ni-ZSM-5, Ni-beta, Ni-SAPO-56, Ni-Y, and Ni-X. They were all prepared by the same method mentioned above, among which the ZSM-5, beta, Y, and X zeolite support were synthesized following previous works (Xiang et al., 2017; Vosoughi et al., 2021; Yu et al., 2022). For the Ni-SAPO-56 catalyst sample, its zeolite support was synthesized with a molar composition of 0.8 Al_2O_3: 0.9 SiO_2: 1.0 P_2O_5: 40 H_2O: 2.0 TMHD (template: N,N,N′,N′-tetramethyl-1,6-hexanediamine). The pseudoboehmite, phosphoric acid solution (85 wt%), and fumed silica were adopted as the aluminum, phosphorous, and silicon sources, respectively. Ni/SiO_2 and Ni/Al_2O_3 were prepared by an incipient-impregnation method using parallel amounts of nitrate precursor.

2.2 Catalyst characterization

Powder X-ray diffraction (XRD) measurements were performed on a Rigaku powder X-ray diffractometer using Cu Kα radiation (λ = 0.1542 nm), and the scan range was from 5° to 45°. The actual Ni contents were determined by inductively coupled plasma optical emission spectrometry (ICP-OES) on a PerkinElmer 3300 DV emission spectrometer. N_2 adsorption–desorption experiments were conducted on a Micromeritics ASAP 2020 M apparatus at −196°C. The samples were degassed at 300°C for at least 8 h prior to characterization. The specific surface area was calculated from the adsorption data using the Brunauer–Emmett–Teller (BET) equation. The pore size distribution was also obtained by using adsorption data and calculated according to the Barrett–Joyner–Halenda (BJH) model. The scanning electron microscopy (SEM) method was performed using an FEI Inspect F50. Transmission electron microscope (TEM) images were collected using a JEM-2100F.

The basicity of the catalysts was measured using temperature-programmed desorption of carbon dioxide (CO_2-TPD) on a Micromeritics ASAP 2920 instrument, by which the corresponding CO_2 adsorption capacity was also evaluated. A 200 mg sample was placed in a quartz tube and pretreated in a helium stream at 450°C for 2 h, and then cooled to 100°C to allow the CO_2 gas to be passed over for 30 min. After the physically adsorbed CO_2 was removed by flowing helium for 2 h at 100°C, the total flow rate of the gas was fixed at 10 m^3/min, and the spectra were recorded from 100 to 650°C at a heating rate of 10°C/min. Similarly, H_2-TPR measurements were also taken on this chemical adsorption instrument with the sample first being pretreated under Ar gas flow at 120°C for 1 h before being cooled down to room temperature. Then, a reducing gas of 10 vol% H_2 in Ar reducing gas was introduced into the system, and the sample was heated to 600°C at a heating rate of 10°C/min. For the CO chemisorption experiment, the pretreatment process was carried out at 400°C in an H_2 atmosphere for 2 h, after which He was purged and maintained for 1 h before the system was cooled to room temperature. Subsequently, a 10 vol % CO-He pulse was introduced and the corresponding CO uptake was measured by a TCD detector based on which the metal dispersion (*D*) was calculated using a previously reported equation (Xiang and Wu, 2019b).

Quasi in situ X-ray photoelectron spectroscopy (XPS) experiments were performed under vacuum on a Thermo Scientific ESCALAB 250Xi spectrometer with an Al Kα X-ray resource (hν = 1,486.6 ev). To avoid oxidization, a pretreatment with hydrogen at 400°C for all the samples in the reaction chamber was employed.

2.3 CO_2 hydrogenation to methane

The catalytic performance evaluation of ETS-10–based catalysts for CO_2 hydrogenation to methane was evaluated in a fixed bed reactor at atmospheric pressure. Before the reaction, the catalyst was reduced *in situ* in the H_2 flow at 450°C for 3 h, after which the activated catalyst was exposed to the mixed reactant gas (CO_2:H_2:N_2 = 1:4:1, molar ratio). The gas hourly space velocity (GHSV) was kept at 7,500 ml•g_{cat}^{-1}•h^{-1}. The products were analyzed online by a GC-2060 gas chromatograph equipped with a flame ionization detector (FID) and a thermal conductivity detector (TCD). N_2 was used as the internal standard for quantitative analysis. The CO_2 conversion (X_{CO2}) was calculated by using Eq 1:

$$X_{CO_2} = \frac{n_{CO_{2in}} - n_{CO_{2out}}}{n_{CO_{2in}}} \times 100\%, \quad (1)$$

where n_{CO2in} and n_{CO2out} are the moles of CO_2 at the inlet and outlet, respectively. Also, the selectivity of CH_4, CH_3OH, and CO were calculated by the internal standard method based on Eqs 2–4:

$$S_{CH_3OH} = \frac{n_{CH_3OH_{out}}}{n_{CO_{2in}} - n_{CO_{2out}}} \times 100\%, \quad (2)$$

$$S_{CH_4} = \frac{n_{CH_{4out}}}{n_{CO_{2in}} - n_{CO_{2out}}} \times 100\%, \quad (3)$$

$$S_{CO} = \frac{n_{CO_{out}}}{n_{CO_{2in}} - n_{CO_{2out}}} \times 100\%, \quad (4)$$

where $n_{CH3OHout}$, n_{CH4out}, and n_{COout} refer to moles of CH_3OH, CH_4, and CO at the outlet, respectively.

The space–time yield (*STY*) of CH_4 was expressed as grams of CH_4 per hour and per gram of metal. The STY_{CH4} was calculated by the following equation:

$$STY_{CH4} = \frac{n_{CO_2in} \times X_{CO_2} \times S_{CH4} \times M_{CH4}}{m_{Ni} \times t}, \quad (5)$$

where m_{Ni} is the mass of the Ni-based catalyst.

3 Results and discussion

3.1 Structure characteristics of ETS-10–based catalyst

As can be seen from Figure 1A, the XRD patterns of Ni-ETS-10 and Ni/ETS-10 display well-resolved peaks associated with the ETS structure in the range of 5°–45°, which is similar to that of the pristine ETS-10 sample but obviously with lower peak intensities. Indeed, by combining these results with N_2 adsorption–desorption analysis data (Table 1), the decreased BET-specific area further confirms that the introduction of nickel species did threaten the framework integrity, leading to material crystallinity being reduced to different degrees. However, it is worth noting that the Ni particles were not presented in the XRD patterns for the two Ni-based ETS-10 catalyst samples, while according to the ICP analysis, the actual Ni contents were 3.7 wt% and 4.2 wt%, respectively, indicating the high dispersion of Ni species. Moreover, based on the CO-TPD results, the calculated dispersion of nickel species for Ni-ETS-10 and Ni/ETS-10 is 37.4% and 27.2%, which is no worse than that widely reported for Ni-based catalysts. Besides, when comparing Ni-ETS-10 with Ni/ETS-10, although both the calculated crystallinity and BET surface area were at a disadvantage, the introduced mesopores with a pore size distribution centered at 10 nm (Figure 1B) prove that they deserve the attention.

Figure 1C shows the SEM image of Ni-ETS-10 with smooth spherical particles of uniform size (17–21 μm). In addition, the obvious surface defect gives a visual illustration that the direct doping of Ni species influences the structural integrity of ETS-10 zeolite, leading to apparently declined crystallinity and BET-specific area, but with the hierarchical pores being formed. The high-magnification TEM image of the thin-sectioned Ni-ETS-10 is shown in Figure 1D. As can be seen, the numerous light areas strongly evidence the presence of abundant hierarchical pores, and the corresponding size range is also visibly uniform and in line with the pore size distribution resulting from N_2 adsorption–desorption. On the other hand, the lattice fringes of Ni-ETS-10 crystals are basically intact, indicating that the native microporous structure delightfully survived the ravages of forming hierarchical pores.

The basic properties of ETS-10, Ni-ETS-10, and Ni/ETS-10 were explored by CO_2-TPD, and the results are shown in Figure 2A and Table 2. For all the three samples, even though the peak intensities were relatively weak, there is a non-negligible peak in the temperature range of 100°C and 150°C, which has resulted from the interactions between CO_2 and the weak basic surface hydroxyl groups on ETS-10 zeolite-based samples. When comparing the results of ETS-10 and Ni/ETS-10, the significant difference was the dramatic shift of base strength distribution to high temperature rather than the modestly increased CO_2 adsorption capacity, demonstrating that there are more high-strength basic sites in Ni/ETS-10 than that in the pristine ETS-10 sample. When it comes to the catalyst with nickel species introduced by *in situ* doping, not only did the total CO_2 adsorption rise sharply to 1.29 mmol/g but it also presents mainly strong basic sites with the CO_2 desorption being concentrated in the temperature range higher than 500°C. This corresponds well to our previous study that shows, other

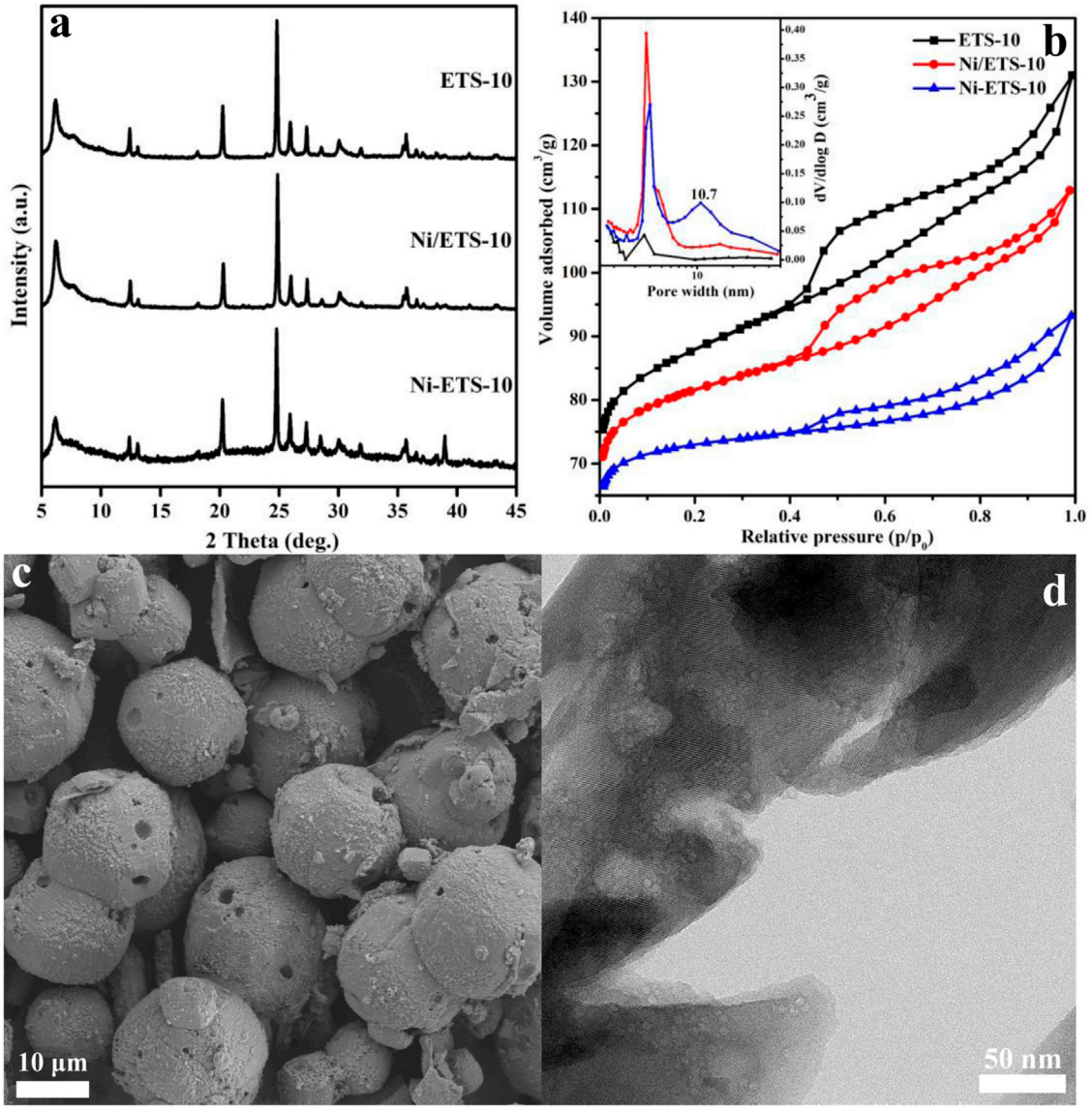

FIGURE 1
(A) XRD patterns and **(B)** N_2 adsorption–desorption isotherm and pore size distribution (insert, calculated using desorption branch) of ETS-10–based samples; **(C)** and **(D)** SEM and TEM images of the Ni-ETS-10 sample.

than the structure and pore topology, the presence of transition metal species and their composition, as well as the interaction with the zeolite support, all make significant contributions to enhance the basicity of ETS-10 zeolite–based catalysts (Xiang and Wu, 2018). Moreover, according to the comparison between Ni/ETS-10 and Ni-ETS-10, though with the same metal active phase, a definite edge in CO_2 adsorption for the latter exists, especially in the high-temperature region, that further confirms the resultant hierarchical structure, the optimized metal dispersion (37.4% *vs.* 27.2%), and the interactions with zeolite supports which definitely endow Ni-ETS-10 with a great potential for CO_2 methanation. In particular, the hierarchical structure existing in the zeolite channel system had long been considered as a promoter for exposing more catalytic active sites and offering easy access for metal species to zeolite supports. Thus, it is fair to say that the significantly improved basic strength of Ni-ETS-10 herein owed much to the introduced hierarchical structure.

The X-ray photoelectron spectroscopy (XPS) spectra were collected to investigate the surface composition and chemical bonding states of the active sites on the reduced Ni-based catalysts. As shown in Figure 2B, there are six characteristic peaks from the Ni 2p XPS spectra of both Ni-ETS-10 and Ni/

TABLE 1 Physicochemical properties of ETS-10–based samples.

Sample	Ni contents[a]	C[b]	S_{BET}[c]	S_{mic}[d]	S_{ext}[e]	V_{micro}[f]	V_{meso}[g]	D[h]	d[i]
ETS-10	—	98.2	337	291	46	0.12	0.01	4	-
Ni/ETS-10	4.2	91.9	312	280	32	0.11	0.02	4	27.2
Ni-ETS-10	3.7	83.6	287	204	83	0.10	0.10	10	37.4

[a]The actual Ni contents detected by ICP (wt%).
[b]Crystallinity calculated by the Scherrer equation (%).
[c]BET, surface area (m^2/g).
[d]Microporous surface area (m^2/g).
[e]External surface area, obtained from the *t*-plot method (m^2/g).
[f]Microporous pore volume, obtained from the *t*-plot method (cm^3/g).
[g]Mesoporous pore volume, obtained from BJH adsorption cumulative volume of pores between 1.7 and 300 nm in diameter (cm^3/g).
[h]Mean pore diameter (nm).
[i]Dispersion of supported metal particles (%).

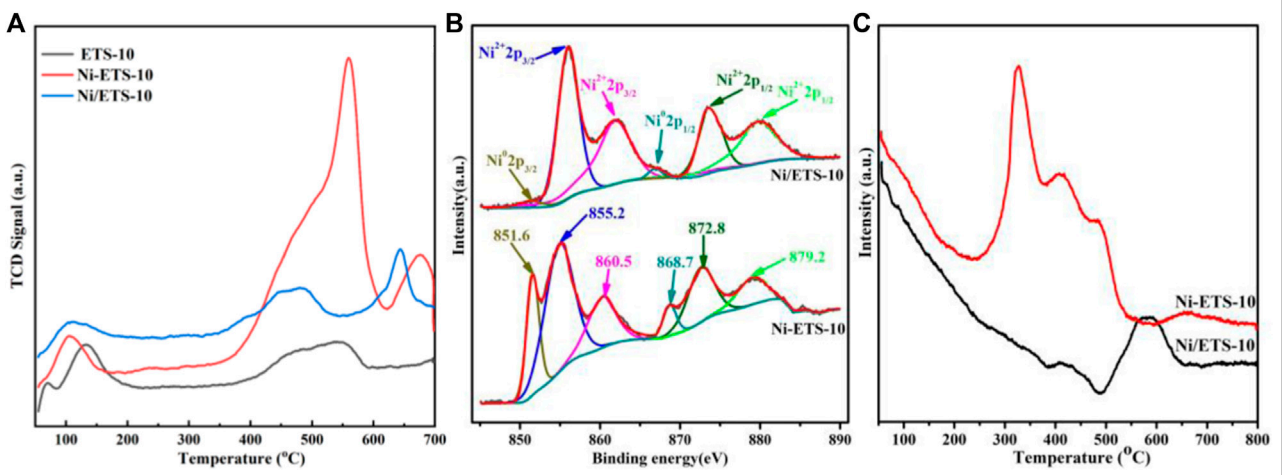

FIGURE 2
(A) CO_2-TPD profiles of ETS-10, Ni-ETS-10, and Ni/ETS-10 samples; **(B)** XPS spectra of Ni 2p for Ni-ETS-10 and Ni/ETS-10 samples; **(C)** H_2-TPR profiles of Ni-METS-10 and Ni/ETS-10 samples.

TABLE 2 Basic properties of the ETS-10 zeolite samples.

Sample	Temperature of peak (°C)				CO_2 adsorption (mmol/g)
ETS-10	68	129	478	540	0.76
Ni/ETS-10	109	469	644		0.86
Ni-ETS-10	106	506	562	677	1.29

ETS-10 catalysts. The peaks around 868.7 and 851.6 eV can be assigned to Ni^0 $2p_{1/2}$ and $2p_{3/2}$ phases, respectively. The peaks appearing near 855.2 and 872.8 eV can be attributed to the presence of Ni^{2+} species at the zeolite exchange sites that strongly interacted with support. The other two multi-split peaks at ~860.5 and 879.2 eV fell to the shake-up satellite peaks, which further indicate the location of Ni^{2+} species at the zeolite exchange sites. Besides, according to the Ni^0/Ni^{2+} ratio of the summarized XPS results, Ni-ETS-10 unquestionably contained more Ni^0 (26.1%) than Ni/ETS-10 (3.8%), indicating the presence of stronger metal–support interactions.

H_2-TPR was used to further explore the behavior of surface Ni species and their interactions with the ETS-10 zeolite support.

TABLE 3 Hydrogenation of CO_2 on different catalysts[a].

Catalyst	C^b (%)	$S_{CH4}{}^c$ (%)	$S_{CO}{}^d$(%)	$S_{methanol}{}^e$(%)
Blank	0	0	0	0
ETS-10	1.48	1.33	95.14	3.53
Ni/ETS-10	5.19	12.36	74.79	12.85
Ni-ETS-10	6.21	16.44	70.66	12.90

[a]Reaction conditions: 0.2 g catalyst, 200°C, 3 h, CO_2:H_2:N_2 = 1:4:1 (molar ratio), 3.0 MPa, and GHSV = 7,500 ml●g_{cat}^{-1}●h^{-1}.
[b]Conversion of CO_2.
[c,d,e]Selectivity of CH_4, CO and methanol, respectively.

According to the H_2-TPR results, there were three salient peaks around 327°C, 414°C, and 489°C for Ni-ETS-10, with a total H_2 consumption of 0.69 mmol/g (Figure 2C). As reported previously, the reduction took place at relatively low temperatures, which can be assigned to those NiO species on the surface of ETS-10 being reduced to metallic Ni, illustrating their weak interactions with the zeolite support (Vosoughi et al., 2021). The peaks near 400°C were due to the moderately reduced NiO species deposited inside the porous structure of the ETS-10 zeolites. The peaks at higher reduction temperatures may be related to Ni^{2+} species that strongly interacted with the zeolite support. While for Ni/ETS-10, the reduction peak shifted to a higher temperature of 580°C with the onset temperature of 410°C with a total H_2 consumption of 0.26 mmol/g, indicating its poorer reducibility and declined hydrogen dissociation ability. As a result, it can be concluded that doping can benefit the reducibility of nickel species, which is in line with the results obtained from the XPS spectra.

3.2 Catalytic activity

Three catalysts, ETS-10, Ni-ETS-10, and Ni/ETS-10, were first tested, and the results are listed in Table 3. Besides, a blank experiment with no presence of any catalyst was also conducted. The results showed that it failed to convert CO_2 to methane under certain reaction conditions. When it came to those catalytic runs, it was obvious that the existence of catalysts did play a part in promoting CO_2 activation and conversion. Furthermore, it seemed that except for the desired product methane, CO and methanol were the main interferential factors that went against the improvement of selectivity.

Compared with the pristine ETS-10 catalyst sample, the introduction of Ni species was definitely beneficial to both CO_2 conversion and product selectivity. Meanwhile, according to the comparison between Ni-ETS-10 and Ni/ETS-10, the superiority of Ni-ETS-10 in facilitating CO_2 transformation and methane production was noticeable, which can be attributed to the enhanced molecule transfer, exposure of active sites, and metal dispersion that resulted from the hierarchical structures. Thus, Ni-ETS-10 was chosen for further investigating the processes of CO_2 hydrogenation to methane in the following experiments.

Figure 3 shows the CO_2 conversion, product selectivity, and *STY* value as a function of reaction pressure, temperature, and catalyst dosage and types. Considering that hydrogenation of CO_2 to methane is in fact a molecule-reducing reaction, increasing the pressure is theoretically in favor of CO_2 conversion. Indeed, based on the experimental data shown in Figure 3A, not only CO_2 conversion but also methane selectivity increased with the increase of pressure. When the pressure was increased to 3.0 Mpa, the conversion of CO_2 went up to 6.21%, and the selectivity of methane rose to 16.44%, after which a deceleration of growth took place. Consequently, as the reaction pressure continued to be increased to 3.5°Mpa, only 0.46% more CO_2 conversion and 0.79% more methane selectivity were obtained. That is to say, when the pressure is over 3.0°MPa, further optimization is conducive but makes little sense in practice, especially taking the security and cost requirements into account.

As a typical exothermic reaction, the hydrogenation of CO_2 to methane deservedly benefits from elevated temperature, which can contribute to the activation of those molecules with low energy. Thus, effective collision and bonding among reactant molecules can be greatly enhanced, giving rise to an accelerated reaction rate. It can be seen from Figure 3B that the transformation of CO_2 to methane could be markedly boosted with a higher temperature. And notably, when it rose to 280°C, CO_2 was transformed to methane completely, leading to the desired selectivity of 100%. More importantly, the selectivity is maintained at 100% when the reaction temperature is raised to 300°C and then to 320°C. Meanwhile, the continuous growth of both CO_2 conversion and space–time yield of CH_4 are observed in the temperature range of 200°C–320°C. However, considering the actual energy consumption required for a high operating temperature, a comparatively low temperature (<300°C) seems to be more suitable. Thus, the following experiments were carried out under 280°C.

It is well known that the amount of catalyst definitely plays a part in improving the catalytic performance by adjusting its active sites. Typically, the more the catalysts are added, the more the active sites become available for reactants' adsorption. As shown in Figure 3C, increasing the catalyst dosage from 0.05 to 0.20 g can bring about a growth leap in CO_2 conversion and STY_{CH4}, after which the rising tendency begins to level off. This can be demonstrated as access to more and more indispensable active sites that significantly promotes the activation of CO_2 and facilitates subsequent combinations between the activated-CO_2 intermediates and the adsorbed-dissociated H_2, and then accelerates the formation of methane. Despite being conducive to enhancing catalytic activities, there appears no need to blindly increase the quantity of catalysts once it has reached up to 0.2 g, where the catalytic active sites in the reaction system are

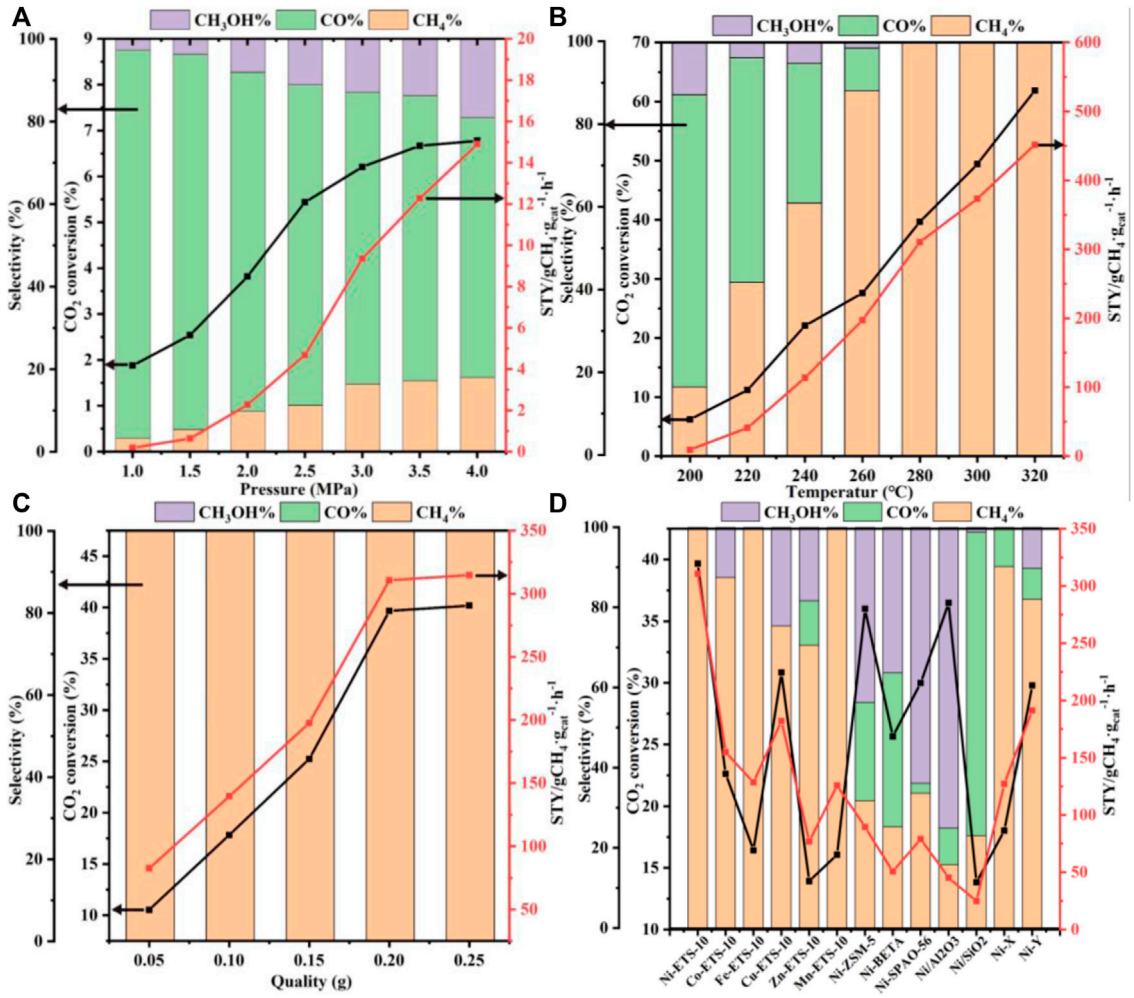

FIGURE 3
Activity of CO_2 hydrogenation into methane over Ni-ETS-10 as a function of **(A)** pressure, **(B)** temperature, **(C)** catalyst quality, and **(D)** the activity of different catalysts for CO_2 methanation (reaction conditions: 280°C, 3 MPa, 7,500 ml•g_{cat}^{-1}•h^{-1}, 3 h, and 0.2 g catalyst).

saturated. What is noteworthy is that no matter how the catalyst quality is regulated, the resulting methane selectivity remains stable at 100% under the current reaction conditions.

The impact of the catalyst types involving different supports and active metal species on CO_2 conversion and methane selectivity was also taken into consideration and explored under the reaction conditions of 280°C, 3 MPa, 7,500 ml•g_{cat}^{-1}•h^{-1}, 3 h, and 0.2 g catalyst. According to the comparison between the Ni-ETS-10 and other catalysts (Figure 3D), the superiority in CO_2 conversion (39.7%) and methane selectivity (100%) was distinct. For Cu-ETS-10, though it gave good results in CO_2 activation and transformation, the moderate H_2 adsorption–dissociation capacity of copper species resulted in a relatively strong appetite for methanol formation. On the contrary, both Fe-ETS-10 and Mn-ETS-10 catalysts were highly enthusiastic about producing methane but failed to effectively promote the transformation of CO_2. For the remaining two ETS-10 zeolite–based catalysts, Co-ETS-10 and Zn-ETS-10, their catalytic performances were too common to be on par with others. Apart from the reactivity discrepancies caused by various active metals, the differences caused by diverse catalyst supports, such as ZSM-5, beta, SAPO-56, X, Y, Al_2O_3, and SiO_2 that have been widely reported and used for CO_2 conversion were investigated. Ni-ZSM-5 and Ni/Al_2O_3 were undoubtedly two of the best for CO_2 activation, which shows comparative CO_2 conversion with Ni-ETS-10. However, there was still an obvious imperfection of product selectivity, which appeared in the intensive formation of CO and methanol. Ni-X was better in obtaining target product methane with a higher selectivity of 90.2%, but unfortunately, it could not activate CO_2 effectively. Also for the Ni-Y catalyst, the corresponding catalytic performance was a middle case with the CO_2 conversion

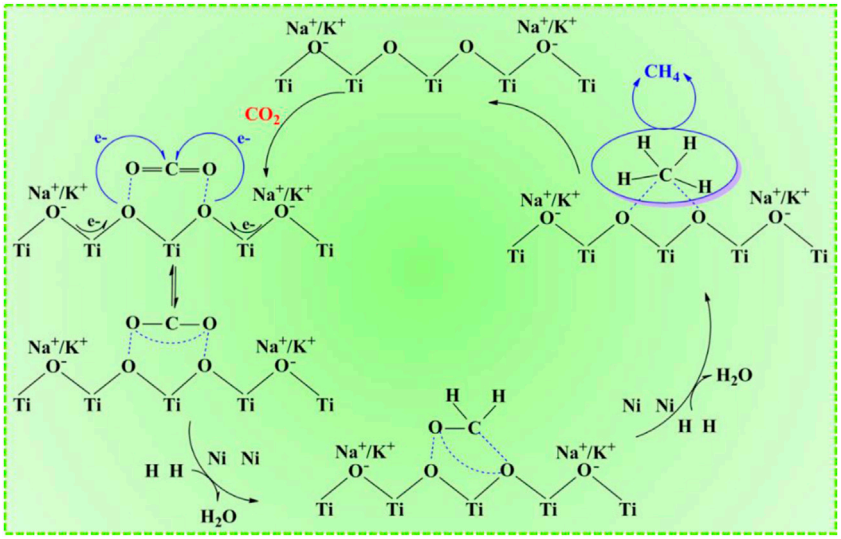

SCHEME 1
Possible reaction mechanism for CO_2 hydrogenation into methane over Ni-ETS-10.

approaching 30% (29.8%) and methane selectivity just above 80% (82.0%). Even though Ni-beta and Ni-SAPO-56 did not seem good for the catalytic conversion of CO_2 to methane, they were still superior to Ni/SiO_2, over which only a small amount of CO_2 (13.8%) was converted and the main product was CO. So, there are reasons to believe that the employment of a suitable catalyst support is of great importance for CO_2 activation and oriented

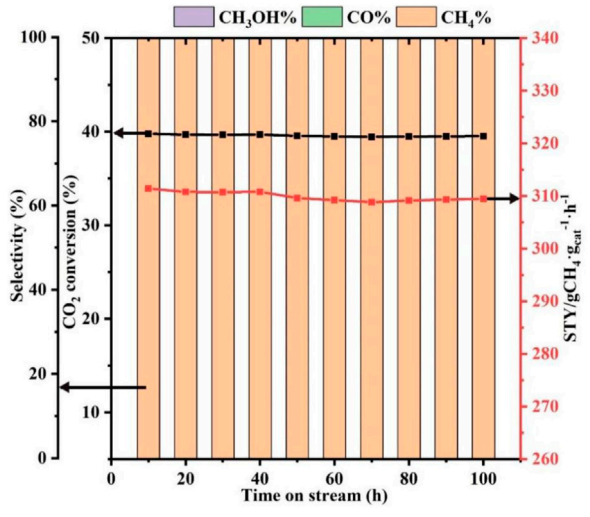

FIGURE 4
Stability of Ni-ETS-10 catalyst (reaction conditions: 280°C, 3 MPa, 7,500 ml•g_{cat}^{-1}•h^{-1}, 3 h, and 0.2 g catalyst).

conversion. The three most common aluminosilicate zeolite catalysts, ZSM-5, beta, and Y, which are characterized by strong surface Brønsted acidity/basicity, have been widely used in various catalytic reactions, especially hydrogenation reactions. However, precisely because of this typical feature, product selectivity is always the key bottleneck for further applications. As for the two representative commercial catalysts, Ni/Al_2O_3 clearly outperforms Ni/SiO_2 due to the presence of abundant surface Lewis acid that endows it with excellent capability for CO_2 adsorption and activation. Being different from those conventional silicon aluminum zeolites, X zeolite with inherent basicity is more prone to methane formation. However, the base strength is far from enough for high efficiency. Thus, it follows that the ability and method of CO_2 adsorption–activation are the determinants for the succeeding hydrogenation process and producing methane, which are closely linked to the physicochemical properties and structure of the catalyst supports. Besides, the active metal species and their composition, dispersion, and corresponding interaction with the support all dominated the catalytic performance. Herein, Ni-ETS-10 is, of course, the most outstanding catalyst for the hydrogenation of CO_2 to methane. This can be due to the unique 3D pore structure and framework of ETS-10 zeolite, especially the peculiar structure unit of the -Ti-O-Ti- chain that is characterized by extraordinary and strong donor capability. Furthermore, the constructed multiple catalytic active centers those resulted from the desired interactions between the Ni species and ETS-10 framework do meet the demands of CO_2 activation, which in fact can be promoted by

making full use of its electron acceptor characteristic and geometric construction (Scheme 1).

3.3 Catalyst stability

Catalyst stability is an important basis for practical applications. Hence, the stability of the Ni-ETS-10 catalyst after 100 h of reaction under the desired conditions was evaluated. As revealed in Figure 4, Ni-ETS-10 is proven to be reasonably stable at 280°C for 100 h with less than 5% decline in CO_2 conversion and *STY*. More importantly, the methane selectivity can be sustained at a consistent level of 100% throughout the process under the optimized reaction conditions.

4 Conclusion

In conclusion, ETS-10 zeolite–based catalysts were used to investigate the process of methane formation from CO_2 hydrogenation in detail. For comparison, different metal species and supports were studied, among which the Ni-ETS-10 catalyst prepared by the *in situ* doping method presented obvious advantages in both CO_2 conversion and methane selectivity. This can be due to the exposure of more basic sites and the absence of porous blockage and structural damage by metal incorporation to a great extent, which is because of the introduced hierarchical pores. More importantly, the presence of more highly dispersed Ni^0 species is vital for accelerating the access of reactants to the Lewis basic sites (TiO_6^{2-}). As a result, the reduced Ni-ETS-10 with better metal dispersion, advantageous hierarchical structure, and stronger Lewis basic strength has been proven to be highly reactive among the studied catalysts for CO_2 hydrogenation, giving a 39.7% CO_2 conversion and 100% methane selectivity under mild conditions. Last but not least, the catalytic performance of Ni-ETS-10 that was maintained at 280°C for 100 h with only less than 5% decline in CO_2 conversion and *STY* indicated its excellent stability and reusability.

Data availability statement

The original contributions presented in the study are included in the article/Supplementary Material; further inquiries can be directed to the corresponding authors.

Author contributions

ZW and JZ: conceptualization and supervision; MX: investigation and original draft; ZG, XJ, and DL: methodology; YD, YD, CY, WZ, and ZZ: investigation, review, and editing. All authors contributed to the manuscript and approved the submitted version.

Funding

The Natural Science Foundation of the Jiangsu Higher Education Institutions of China (Nos. 20KJB530006 and 20KJB150044), Science and Technology Foundation of Changzhou (No. CJ20200042), and Jiangsu Key Laboratory of Advanced Catalytic Materials and Technology (No. BM2012110).

Acknowledgments

The authors thank the Natural Science Foundation of the Jiangsu Higher Education Institutions of China (No. 20KJB530006, 20KJB150044), Science and Technology Foundation of Changzhou (No. CJ20200042), and Jiangsu Key Laboratory of Advanced Catalytic Materials and Technology (No. BM2012110).

Conflict of interest

CY was employed by Zhongyi Testing and Research Institute Co, Ltd.

The remaining authors declare that the research was conducted in the absence of any commercial or financial relationships that could be construed as a potential conflict of interest.

Publisher's note

References

Azzolina-Jury, F., Bento, D., Henriques, C., and Thibault-Starzyk, F. (2017). Chemical engineering aspects of plasma-assisted CO_2 hydrogenation over nickel zeolites under partial vacuum. *J.CO₂ Util.* 22, 97–109. doi:10.1016/j.jcou.2017.09.017

Boukha, Z., Bermejo-López, A., Pereda-Ayo, B., González-Marcos, J. A., and González-Velasco, J. R. (2022). Study on the promotional effect of lanthana addition on the performance of hydroxyapatite-supported Ni catalysts for the CO_2 methanation reaction. *Appl. Catal. B Environ.* 314, 121500. doi:10.1016/j.apcatb.2022.121500

Chen, S. C., Shao, Z., Fang, Z. X., Chen, Q., Tang, T., Fu, W. Q., et al. (2016). Design and synthesis of the basic Cu-doped zeolite X catalyst with high activity in oxidative coupling reactions. *J. Catal.* 338, 38–46. doi:10.1016/j.jcat.2016.01.030

Chen, Z. M., Chen, W., Zhang, L., Fu, W. Q., Cai, G. R., Zheng, A. M., et al. (2022). Acidic hierarchical porous ZSM-5 assembled palladium catalyst: A green substitute to transform primary amides to nitriles. *Appl. Catal. B Environ.* 302, 120835. doi:10.1016/j.apcatb.2021.120835

Cui, Y., Qiu, J., Chen, B., Xu, L. L., Chen, M. D., Wu, C. E., et al. (2022). CO_2 methanation over Ni/ZSM-5 catalysts: the effects of support morphology and La_2O_3 modification. *Fuel* 324, 124679. Part B. doi:10.1016/j.fuel.2022.124679

Fan, W. K., and Tahir, M. (2021). Recent trends in developments of active metals and heterogenous materials for catalytic CO2 hydrogenation to renewable methane: A review. *J. Environ. Chem. Eng.* 9 (4), 105460. doi:10.1016/j.jece.2021.105460

Franken, T., Terreni, J., Borgschulte, A., and Heel, A. (2020). Solid solutions in reductive environment-A case study on improved CO_2 hydrogenation to methane on cobalt based catalysts derived from ternary mixed metal oxides by modified reducibility. *J. Catal.* 382, 385–394. doi:10.1016/j.jcat.2019.12.045

Frei, M. S., Mondelli, C., García-Muelas, R., Morales-Vidal, J., Philipp, M., Safonova, O. V., et al. (2021). Nanostructure of nickel-promoted indium oxide catalysts drives selectivity in CO_2 hydrogenation. *Nat. Commun.* 12, 1960. doi:10.1038/s41467-021-22224-x

Fu, W. Q., Shen, R. S., Bai, E. H., Zhang, L., Chen, Q., Fang, Z. X., et al. (2018). Reaction route and mechanism of the direct N-alkylation of sulfonamides on acidic mesoporous zeolite β-Catalyst. *ACS Catal.* 8 (10), 9043–9055. doi:10.1021/acscatal.8b02030

Gac, W., Zawadzki, W., Słowik, G., Kuśmierz, M., and Dzwigaj, S. (2021). The state of BEA zeolite supported nickel catalysts in CO_2 methanation reaction. *Appl. Surf. Sci.* 564, 150421. doi:10.1016/j.apsusc.2021.150421

Gao, M. T., Zhang, J., Zhu, P. Q., Liu, X. C., and Zheng, Z. F. (2022). Unveiling the origin of alkali metal promotion in CO_2 methanation over Ru/ZrO_2. *Appl. Catal. B Environ.* 314, 121476. doi:10.1016/j.apcatb.2022.121476

Gonçalves, L. P. L., Mielby, J., Soares, S. G. P., Sousa, J. P. S., Petrovykh, D. Y., Lebedev, O. I., et al. (2022). *In situ* investigation of the CO_2 methanation on carbon/ceria-supported Ni catalysts using modulation-excitation DRIFTS. *Appl. Catal. B Environ.* 312, 121376. doi:10.1016/j.apcatb.2022.121376

Graca , I., González, L. V., Bacariza, M. C., Fernandes, A., Henriques, C., Lopes, J. M., et al. (2014). CO_2 hydrogenation into CH_4 on NiHNaUSY zeolites. *Appl. Catal. B Environ.* 147, 101–110. doi:10.1016/j.apcatb.2013.08.010

Hu, F. Y., Chen, X. H., Tu, Z. A., Lu, Z. H., Feng, G., and Zhang, R. B. (2021). Graphene aerogel supported Ni for CO_2 hydrogenation to methane. *Ind. Eng. Chem. Res.* 60 (33), 12235–12243. doi:10.1021/acs.iecr.1c01953

Hussain, I., Jalil, A. A., Hassan, N. S., and Hamid, M. Y. S. (2021). Recent advances in catalytic systems for CO_2 conversion to substitute natural gas (SNG): Perspective and challenges. *J. Energy Chem.* 62, 377–407. doi:10.1016/j.jechem.2021.03.040

Hwang, S. M., Han, S. J., Park, H. G., Lee, H., An, K., Jun, K. W., et al. (2021). Atomically alloyed Fe-Co catalyst derived from a N-coordinated Co single-atom structure for CO_2 hydrogenation. *ACS Catal.* 11 (4), 2267–2278. doi:10.1021/acscatal.0c04358

Italiano, C., Ferrante, G. D., Pino, L., Laganà, M., Ferraro, M., Antonucci, V., et al. (2022). Silicon carbide and alumina open-cell foams activated by Ni/CeO_2-ZrO_2 catalyst for CO_2 methanation in a heat-exchanger reactor. *Chem. Eng. J.* 434, 134685. doi:10.1016/j.cej.2022.134685

Kosinov, N., and Hensen, E. J. M. (2020). Zeolite-based catalysts: Reactivity, selectivity, and stability of zeolite-based catalysts for methane dehydroaromatization (adv. Mater. 44/2020). *Adv. Mater.* 32, 2070332. doi:10.1002/adma.202070332

Liu, Y. T., Deng, D. H., and Bao, X. H. (2020). Catalysis for selected C1 chemistry. *Chem* 6 (10), 2497–2514. doi:10.1016/j.chempr.2020.08.026

Liu, Z. H., Gao, X. H., Liu, B., Ma, Q. X., Zhao, T. S., and Zhang, J. L. (2022). Recent advances in thermal catalytic CO_2 methanation on hydrotalcite-derived catalysts. *Fuel* 321, 124115. doi:10.1016/j.fuel.2022.124115

Makdee, A., Kidkhunthod, P., Poo-arporn, Y., and Chanapattharapol, K. C. (2022). Enhanced CH_4 selectivity for CO_2 methanation over Ni-TiO_2 by addition of Zr promoter. *J. Environ. Chem. Eng.* 10 (3), 107710. doi:10.1016/j.jece.2022.107710

Meng, X. Y., Peng, C., Jia, J. P., Liu, P., Men, Y. L., and Pan, Y. X. (2022). Recent progress and understanding on In_2O_3-based composite catalysts for boosting CO_2 hydrogenation. *J. CO_2 Util.* 55, 101844. doi:10.1016/j.jcou.2021.101844

Pu, T. C., Chen, J. C., Tu, W. F., Xu, J., Han, Y. F., Wachs, I. E., et al. (2022). Dependency of CO_2 methanation on the strong metal-support interaction for supported Ni/CeO_2 catalysts. *J. Catal.* 413, 821–828. doi:10.1016/j.jcat.2022.07.038

Ra, E. C., Kim, K. Y., Kim, E. H., Lee, H., An, K., and Lee, J. S. (2020). Recycling carbon dioxide through catalytic hydrogenation: Recent key developments and perspectives. *ACS Catal.* 10 (19), 11318–11345. doi:10.1021/acscatal.0c02930

Ren, J., Zeng, F., Mebrahtu, C., and Palkovits, R. (2022). Understanding promotional effects of trace oxygen in CO_2 methanation over Ni/ZrO_2 catalysts. *J. Catal.* 405, 385–390. doi:10.1016/j.jcat.2021.12.017

Saeidi, S., Najari, S., Hessel, V., Wilson, K., Keil, F. J., Concepción, P., et al. (2021). Recent advances in CO_2 hydrogenation to value-added products-Current challenges and future directions. *Prog. Energy Combust. Sci.* 85, 100905. doi:10.1016/j.pecs.2021.100905

Skrypnik, A. S., Petrov, S. A., Kondratenko, V. A., Yang, Q. X., Lund, H., Matvienko, A. A., et al. (2022). Descriptors affecting methane selectivity in CO_2 hydrogenation over unpromoted bulk iron (III)-based catalysts. *ACS Catal.* 12, 11355–11368. doi:10.1021/acscatal.2c03375

Song, M., Shi, L. L., Xu, X. N., Du, X. H., Chen, Y., Zhuang, W. C., et al. (2022). Ni/M/SiO_2 catalyst (M=La, Ce or Mg) for CO_2 methanation: Importance of the Ni active sites. *J. CO_2 Util.* 64, 102150. doi:10.1016/j.jcou.2022.102150

Upasen, S., Sarunchot, G., Srira-ngam, N., Poo-arporn, Y., Wattanachai, P., Praserthdam, P., et al. (2022). What if zeolite LTA4A and zeolite LTA5A used as Nickel catalyst supports for recycling carbon dioxide to green fuel methane. *J. CO_2 Util.* 55, 101803. doi:10.1016/j.jcou.2021.101803

Uttamaprakrom, W., Reubroycharoen, P., Charoensiritanasin, P., Tatiyapantarak, J., Srifa, A., Koo-Amornpattana, W., et al. (2021). Development of Ni-Ce/Al-MCM-41 catalysts prepared from natural kaolin for CO_2 methanation. *J. Environ. Chem. Eng.* 9 (5), 106150. doi:10.1016/j.jece.2021.106150

Vosoughi, M., Maghsoudi, H., and Gharedaghi, S. (2021). Ion-exchanged ETS-10 adsorbents for CO_2/CH_4 separation: IAST assisted comparison of performance with other zeolites. *J. Nat. Gas. Sci. Eng.* 88, 103862. doi:10.1016/j.jngse.2021.103862

Wang, D., Xie, Z. H., Porosoff, M. D., and Chen, J. G. G. (2021). Recent advances in carbon dioxide hydrogenation to produce olefins and aromatics. *Chem* 7 (9), 2277–2311. doi:10.1016/j.chempr.2021.02.024

Wang, L., Hu, J., Liu, H., Wei, Q., Gong, D., Mo, L., et al. (2020). Three-dimensional mesoporous Ni-CeO_2 catalysts with Ni embedded in the pore walls for CO_2 methanation. *Catalysts* 10 (5), 523. doi:10.3390/catal10050523

Wang, L. X., Guan, E. J., Wang, Z. Q., Wang, L., Gong, Z. M., Cui, Y., et al. (2020). Dispersed nickel boosts catalysis by copper in CO_2 Hydrogenation. *ACS Catal.* 10 (16), 9261–9270. doi:10.1021/acscatal.0c00907

Wang, X. Y., Ma, Y., Wu, Q. M., Wen, Y. Q., and Xiao, F. S. (2022). Zeolite nanosheets for catalysis. *Chem. Soc. Rev.* 51, 2431–2443. doi:10.1039/d1cs00651g

Wang, Z. M., Xiao, M. Q., Wang, X. X., Wang, H., Chen, X., Dai, W. X., et al. (2022). Thermo-driven photocatalytic CO_2 hydrogenation over NiOx/Nb_2O_5 via regulating the electron transfer behavior of reactant gas adsorption. *Appl. Surf. Sci.* 592, 153246. doi:10.1016/j.apsusc.2022.153246

Xiang, M., and Wu, D. F. (2018). Transition metal-promoted hierarchical ETS-10 solid base for glycerol transesterification. *RSC Adv.* 8, 33473–33486. doi:10.1039/c8ra06811a

Xiang, M., and Wu, D. F. (2019a). Facile preparation of pore- and morphology-controllable ETS-10 zeolite with enhanced biomass hydrogenation activity. *Chem. Eng. J.* 369, 180–194. doi:10.1016/j.cej.2019.03.058

Xiang, M., and Wu, D. F. (2019b). Highly selective catalytic conversion of lignin-derived phenolic compounds to cycloalkanes over a hierarchically structured zeolite catalyst. *J. Mater. Sci.* 54, 2940–2959. doi:10.1007/s10853-018-3057-y

Xiang, M., Liu, J. N., Fu, W. Q., Tang, T. D., and Wu, D. F. (2017). Improved activity for cellulose conversion to levulinic acid through hierarchization of ETS-10 zeolite. *ACS Sustain. Chem. Eng.* 5 (7), 5800–5809. doi:10.1021/acssuschemeng.7b00529

Xie, Y., Chen, J. J., Wu, X., Wen, J. J., Zhao, R., Li, Z. L., et al. (2022). Frustrated Lewis pairs boosting low-temperature CO_2 methanation performance over Ni/CeO_2 nanocatalysts. *ACS Catal.* 12 (17), 10587–10602. doi:10.1021/acscatal.2c02535

Yang, Y. J., Zhang, J. C., Liu, J., Wu, D. W., Xiong, B., Yang, Y. C., et al. (2021). Nickel nanoparticles encapsulated in SSZ-13 cage for highly efficient CO_2 hydrogenation. *Energy F* 35 (16), 13240–13248. doi:10.1021/acs.energyfuels.1c01881

Yu, Y. X., Li, X. H., Min, X. B., Shang, M. Y., Tao, P., and Sun, T. J. (2022). Influences of channel morphology and Brønsted acidity on ETS-10, ZSM-5, and SSZ-13 for xenon and krypton separation. *J. Environ. Chem. Eng.* 10 (1), 106982. doi:10.1016/j.jece.2021.106982

Zafar, F., Zhao, R., Ali, M., Park, Y. M., Roh, H. S., Gao, X. H., et al. (2022). Unprecedented contributions of In_2O_3 promoter on ordered mesoporous Cu/Al_2O_3 for CO_2 hydrogenation to oxygenates. *Chem. Eng. J.* 439, 135649. doi:10.1016/j.cej.2022.135649

Zhang, Q., Yu, J., and Corma, A. (2020). Applications of zeolites to C1 chemistry: Recent advances, challenges, and opportunities. *Adv. Mater.* 32, 2002927. doi:10.1002/adma.202002927

Zhao, T. T., Yang, Z. Y., Tang, Y. X., Liu, J. R., and Wang, F. L. (2022). Advances and perspectives of photopromoted CO_2 hydrogenation for methane production: Catalyst development and mechanism investigations. *Energy Fuels.* 36 (13), 6711–6735. doi:10.1021/acs.energyfuels.2c01507

Zhou, R., Rui, N., Fan, Z., and Liu, C. J. (2016). Effect of the structure of Ni/TiO_2 catalyst on CO_2 methanation. *Int. J. Hydrogen Energy* 41, 22017–22025. doi:10.1016/j.ijhydene.2016.08.093

Zhu, J., Wang, P., Zhang, X. B., Zhang, G. H., Li, R. T., Li, W. H., et al. (2022). Dynamic structural evolution of iron catalysts involving competitive oxidation and carburization during CO_2 hydrogenation. *Sci. Adv.* 8 (5), eabm3629. doi:10.1126/sciadv.abm3629

frontiers | Frontiers in Environmental Science

TYPE Mini Review
PUBLISHED 20 October 2022
DOI 10.3389/fenvs.2022.1029510

OPEN ACCESS

EDITED BY
Hu Li,
Guizhou University, China

REVIEWED BY
Yutao Zhang,
Anshun University, China
Rongguo Sun,
Guizhou Normal University, China

*CORRESPONDENCE
Yuchi Yang,
yangyuchi@tongji.edu.cn

SPECIALTY SECTION
This article was submitted to Land Use Dynamics,
a section of the journal
Frontiers in Environmental Science

RECEIVED 27 August 2022
ACCEPTED 03 October 2022
PUBLISHED 20 October 2022

CITATION
Yang Y (2022), Research hotspots and evolution trends of rural resilience in the perspective of biodiversity—Based on citeSpace's visual analysis of bibliometrics.
Front. Environ. Sci. 10:1029510.
doi: 10.3389/fenvs.2022.1029510

Research hotspots and evolution trends of rural resilience in the perspective of biodiversity —Based on citeSpace's visual analysis of bibliometrics

Yuchi Yang*

College of Architecture and Urban Planning, Tongji University, Shanghai, China

Strengthening the construction of rural resilience and improving the rural ecotope and biodiversity are of great significance to improving the governance's abilities of rural areas to resist external disturbances and various crises. Based on the 1786 documents which are associated with the research topics collected in the "Web of Science" database from 1992 to 2022, this study uses the visualization analysis method of the "CiteSpace document" to focus on the rural resilience from the ecosystem perspective, sort out the hotspots of rural resilience construction research, and study and judge the future development tendencies. It pertinently put forward the research evolution trends of "bottom–up ecological restoration" and "top–down planning improvement." The research results are beneficial to provide useful references and direction enlightenment for the sustainable research of rural resilience and the formulation of planning strategies from the perspectives of biodiversity.

KEYWORDS

rural resilience, biodiversity, ecosystem biomass, CiteSpace, sustainable development

1 Introduction

The continuous advancement of industrialization and urbanization has led to the overall reconstruction of rural areas and has been facing a series of problems such as industrial decline, population decline, and ecological decline. The instability and fragility of rural areas have become increasingly prominent and inhibited the sustainable development of rural areas (McManus P et al., 2012; Modica M et al., 2015; Pandey R et al., 2017). How to strengthen the rural resilience construction, improve the governance abilities of rural areas to resist natural disasters, instability, and various crises caused by external disturbances, improve the quality of the rural ecological environment (Qiu et al., 2021), and promote the high-quality development of rural areas remains unclear. It has been highly valued by the countries over the world and has also attracted extensive attention from the academic communities (Center and Garden,2009; Chaigneau, T et al., 2022; Ekblom et al., 2020; Li et al.,

2022). Regarding the cognition of resilience theory, Western scholars have two perspectives: one is the equilibrium theory based on engineering resilience and ecological resilience (Rigg et al., 2015; Roberts et al., 2017), and the other is the evolution theory based on evolutionary resilience (Chen, 2007;Chen et al., 2017; Hennebry, 2020; Huang, et al., 2020; Li et al., 2014; Li et al., 2020). Following this logic, the academic research has been deepened gradually, and the concept and connotation of resilience have been evolving and developing from focusing on the resilience of research objects to focusing on biological and ecological sustainability (Wang et al., 2021; Li Y,2022) and then to long-term adaptability; it has been constantly evolving and developing.

Wilson took the lead in introducing resilience theory into the research on rural multi-functional transformation, which has better explained many problems faced in rural transformation and development (Wilson, 2012; Li, 2020). Scholars have found that rural resilience is mainly reflected in the rural disturbance and instability caused by natural disasters (Cutter et al., 2016), climate change, sustainable utilization of biomass energy (Emmanuel et al., 2012), and social–economic changes (Tebboth et al., 2019; Yang, et al., 2020). At present, the research on rural resilience mainly focuses on the prevention and control of rural natural disasters (M.F.MFirdhous et al., 2018; Mohamed et al., 2014; Babulo et al., 2008), community construction and governance (Philp, 2008; Bjorna and Aarseether., 2009; Marsden and Sonnino., 2008), farmers' livelihood (M.F. MFirdhous et al., 2018), infrastructure construction (Elisabeth et al., 2017; Nguyen et al., 2017), and resilience evaluation (Mazur et al., 2018; Wilson et al., 2018; Scott, 2013). With the connotation of resilience becoming an important aspect of biological sustainability, rural resilience is widely understood as the ability of rural systems to cope with changes (Kilkenny, et al., 2008; Koning, et al., 2021), adapt, and continue to develop in the uncertain environment of unexpected shocks and challenges (Folke et al., 2010; Pain and Levine, 2012; Brown, 2017; Folke, et al., 2016). The concept and connotation of rural resilience have also gradually shifted from the equilibrium theory to evolution theory (Scott, 2013; Qiu et al., 2021; Wang et al., 2021).

Over the years, the research on resilience theory mainly focuses on urban areas, while the research on rural biodiversity (especially rural biodiversity) is not enough and systematic. The unbalanced development between urban and rural areas has made the rural infrastructure backward and the flood control and drought relief facilities weak, thus reducing the ability of disaster prevention (Cutter et al., 2010) and risk resistance in rural areas (Mazur et al., 2018), and the living environment in rural areas has become increasingly worse. In this research, resilience is defined as the ability of the rural regional system to maintain relative stability through comprehensive means such as social, economic, and ecological relative stability (Holladay and Power., 2013). It realizes the transition from the original equilibrium state to a new equilibrium state and emphasizes the characteristics of the system by actively adapting and maintaining sustainable development (Heijman Hagelaar, 2007; Li et al., 2021). Therefore, it is significant and necessary to gradually analyze the research results of rural resilience, promote the construction of rural resilience, improve the ability of rural areas to cope with various crises (Al-Zubaidy.,2015), and promote the construction of the beautiful ecological environment (Huang X, et al., 2019), biodiversity, and sustainable development in rural areas (McManus et al., 2012; Dai Qi., 2015). Based on the "Web of Science" database and utilizing CiteSpace document visualization analysis software, this study focuses on the research on rural resilience from the ecosystem perspective, discusses and analyzes the hotspots of rural resilience construction research, and studies and judges the future development and evolution trend, thus guiding the direction for further research on it. The innovation lies in focusing on the rural resilience research from the perspective of the ecosystem, discussing and analyzing the hotspots of rural resilience construction research, with judging the future development trend from the perspective of biodiversity, so as to guide the direction for further research on rural resilience. Literature visualization software helps sort out the salience time, salience intensity, and the important literature of various keywords and is more beneficial to understand the research progress.

2 Research data and analysis methods

2.1 Research data

The research data are obtained from the "Web of Science" literature database. Here, "rural resilience" and "rural resilience" are selected as the main topic words, respectively, and they are set as TS = ("rural resilience") or TS = ("rural-resilience") through the advanced search of the WOS database; time expand = "1992–2022." The conference contributions, the opening remarks of the volume, and introduction of personal academic achievements in the search results were deleted completely, and the duplicate literature was eliminated, and 1786 relevant literature reports were finally determined. Through the function of year per slices *via* "CiteSpace," all the literature studies are departed to a cycle of 3 years. Among them, the number of relevant literature has increased significantly year by year, with only two literature studies from 1992 to 1994, 72 literature studies from 2007 to 2009, and 249 literature studies from 2019 to 2021.

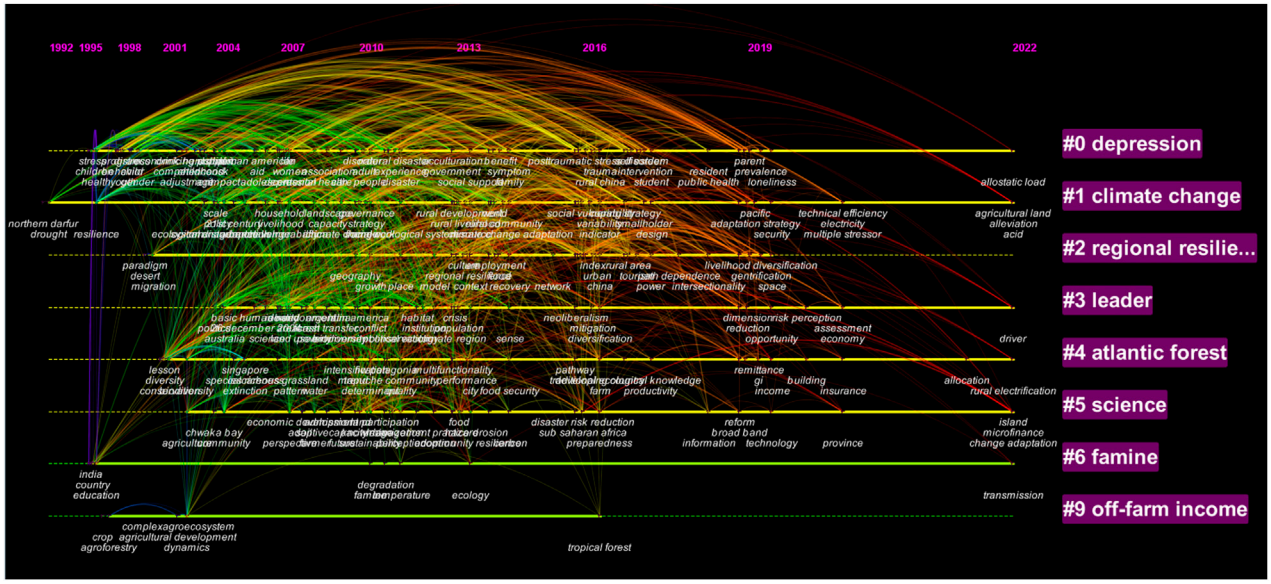

FIGURE 1
Evolution analysis of theme words of rural resilience in the Wos database.

2.2 Analysis method

"CiteSpace bibliometric visualization analysis" describes the main content of the literature, analyzes, and builds the correlation relationship between knowledge with the help of statistical methods, which can effectively provide important technical support for mining-related research progress (Chen et al., 2009; Hu et al., 2018). It is extensively used in the research and analysis of the existing literature (LI Jie et al., 2016; Yue, 2009). Therefore, this research adopted CiteSpace software analysis, combined with association analysis and cluster analysis, to import the literature data retrieved and sorted out from 1992 to 2022 into "CiteSpace 6.1." Through debugging the setting of relevant parameters, the keyword co-occurrence network graph and subject salient word graph are drawn completely.

3 Research hotspots and evolution analysis

The research is based on the time zone function of the CiteSpace 6.1 software platform to search for mutant words and analyze mutant words through literature keywords, aiming to explore the current top keywords with the strongest citation bursts. A burstness model was used to calculate words and sudden mutation in the rural resilience–related literature. The burstness model is used to calculate the mutant words and literature in the related research of rural resilience. The mutant detection algorithm of the computing party thinks that the emerging and rising mutant literature are frontier and timely in revealing the new tendency in the scientific field. In order to ensure the number of mutant words in the calculation, the threshold value was adjusted from 1 to 0.8, and 20 mutant words were detected with the help of software, among which the highest intensity was "Africa, biodiversity, environment, support," etc.

3.1 Research on mutation words and their evolution

The academic research on rural resilience has a wide range of perspectives and methods. The evolution analysis graph of rural resilience subject words in the Wos database (Figure 1) reveals that 20 mutant words have appeared in the past 30 years. In terms of the mutant words' intensity, the highest value is "Africa," and the frequency intensity is 4.4869, which appeared in 2007 and ended in 2015 with a moderate occurrence cycle. The second is "biodiversity" with a frequency intensity of 4.3301, which appeared in 2001 and ended in 2015, and the occurrence cycle was relatively long. From the point of view of the intensity of the mutant word, the highest value was "Africa" and the frequency intensity was 4.4869, which appeared in 2007 and ended in 2015, and the occurrence cycle was moderate. The high-frequency literature mainly researches the persistence and resistance to human

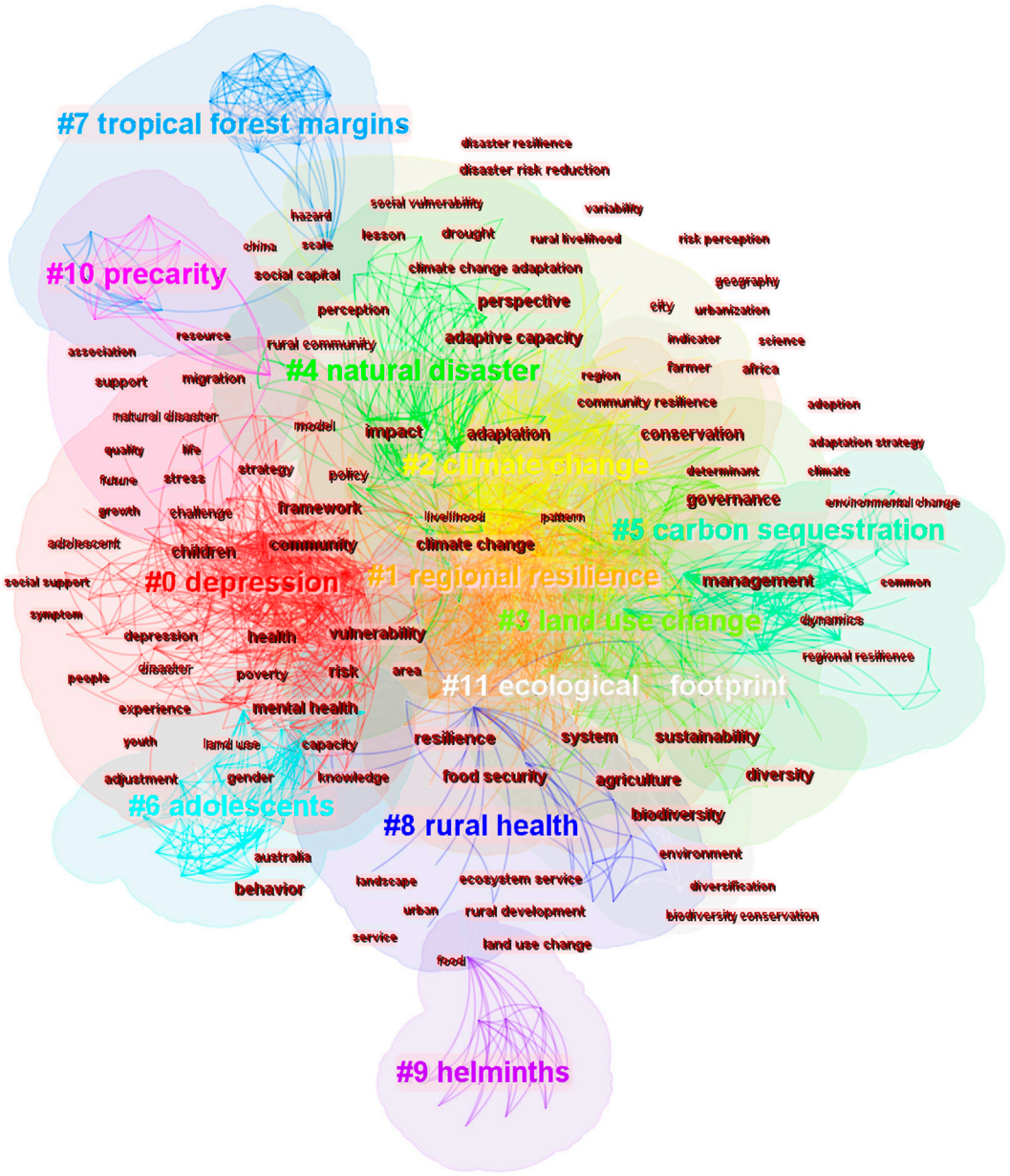

FIGURE 2
Clustering diagram of rural resilience keywords in the Wos database.

disturbance of rainforest birds in plantations and primary forests of Peninsular Malaysia (Kelvin, 2005).

The high-frequency word from 2010 to 2015 was the social ecological system (SES), with a frequency intensity of 3.6702. It mainly includes a social ecological system framework proposed by Ostrom, which is mainly used in ecological restoration projects, biomass energy, ecological vulnerability assessment, etc. From 2010 to 2015, the high-frequency word was "Social Ecological System (SES)" with a frequency intensity of 3.6702. It mainly includes a social ecological system framework proposed by Ostrom, which is mainly used in ecological restoration projects, biomass energy, ecological vulnerability assessment, etc. The high-frequency literature mainly researches the resilience and vulnerability of remote rural communities to global climate and ecological environment changes (Scott et al., 2013; Bailey et al., 2016; Douglas et al., 2019; Peng et al., 2017). The frequency intensity of the mutant word "adaptivity" was 3.0606, which appeared in 2013 and ended in

2018. It is mostly used for resilience and adaptability to cope with biomass and biodiversity changes. The high-frequency literature mainly researches the adaptability and resilience of rural households to cope with climate changes and carbon dioxide emission reduction (Angeler et al., 2018).

The mutant words mainly indicate the concern about biomass energy, biodiversity, climate change, and ecological environment in the research topics of rural resilience. In part, vulnerability assessment, optimal utilization of resources, ecological planning, and other methods are widely used to improve the level of rural resilience. For the resilience measurement in the ecosystem, the quantitative measurement and diversity characteristics are reflected in the landscape heterogeneity (Liu et al., 2015), landscape diversity (Yang et al., 2021), and biodiversity (Schwarz et al., 2011).

The biomass content can further reflect the threshold level of numerous elements of the rural ecosystem and can explain the motivations and influencing factors in the evolution of the ecosystem.

3.2 Research keywords and evolution

The clustering nodes are set as keywords by CiteSpace 5.8 software, and the keyword co-occurrence relationship graph based on the Wos database is obtained after eliminating the words with low relevance and low frequency to the subject words (Figure 2). It reveals that the research topics of "rural resilience" are relatively concentrated, and the keywords are closely connected. Among them, the keywords with high frequency are "region resilience," "climate change," "land use change," "natural disaster," "carbon sequestration," "traditional forest margins," "rural health," "precarity," and "ecological footprint." The analysis shows that the impact of climate change is being felt globally. To a large extent, climate change is regarded as the greatest threat to people's lives. It is expected that the impact of climate change will be greater in the future (IPCC, 2014). According to the World Bank (2010), the total loss caused by all disasters during 1970–2008 was about $230 billion. Some highly cited keywords revealed in the figure indicate the concern about climate changes, natural disasters, biological sustainability, carbon storage, etc., emphasizing the ability level of the rural social–ecological system to maintain a relatively stable state and sustainable development.

The results obtained by keyword cluster analysis show that the research topic pays attention to external factors such as "climate change," "natural disaster," and "ecological footprint" that affect the resilience and stability of rural ecosystems. Meanwhile, it combines the internal elements of the system such as "land use change," "carbon sequestration," and "rural health." Numerous research studies have been conducted on the external and internal factors that affect the stability of the system and cope with changes. From the research on internal and external systems, influencing factors to the rural human settlement environment, we pay attention to the living conditions, environmental quality, and climate conditions of rural residents. The biomass content not only affects the stability and diversity of the rural social–ecological system but also directly or indirectly affects various physiological and psychological states of people in the system and the threshold level and evolution trend of some elements.

4 Main research contents

The theory of rural resilience has a pluralistic essence, highlighting the interaction between elements, the form, coupling structure, and the non-equilibrium evolution path of rural material elements (Li et al., 2019). Rural transformation in the new period often adopts a new development mode to improve its ability to resist the impact and maintain a stable state. Combined with the sorting and quantitative analysis of the high-frequency mutation words and keywords in the research on rural resilience, it is found that the research content of rural resilience based on the perspective of biodiversity focuses on the biodiversity and external climate change in the rural ecosystem and their interaction modes and conditions on rural resilience. Scholars believe that the spatial promotion of rural resilience through social spatial reproduction (Westlund H, 2006) can improve the biomass content in rural ecosystems and enrich the organizational structure to maintain relative stability.

4.1 Resilience and biodiversity

Biodiversity can reflect the multiple characteristics of rural resilience, and the influencing factors are relatively complex and comprehensive. Scholars at home and abroad have carried out a series of studies on this issue. For example, Nivaldo Peroni et al. (2002) put forward a theoretical model focusing on biodiversity and resource resilience to explain the impact factors of biodiversity decline: the rural population outflow, increase in tourism, and changes in production and lifestyle, aiming at the interspecific and intraspecific diversity of cultivated crops. Kelvin S.H (2005) studied the composition and structure of virgin forests, artificial forests, and birds in rural areas, proposed that the abundance of material resources and factors closely related to forest disturbance affect biodiversity, and explored resilience of rural areas from the perspective of ecosystem stability and sustainability. Peng et al. (2017) quantitatively analyzed the internal relationship between regional ecosystem health assessment, biodiversity, and rural land use and land cover change through quantitative indicators and explored the mutual relationship between the model and process and rural resilience. Marleen Schouten (2013) explained the interrelation between biodiversity and rural resilience at the landscape level through the

theoretical construction and scheme experiment of the rural environmental agency model and proposed that the top–down government investment aimed at improving the public value of the rural society ecosystem and improving rural resilience. M.G.Sorice (2012) studied the land ownership patterns in three counties in central Texas. Through interviews with 767 owners and questionnaire data, he found that changes in land owners and their ideas may bring about changes in the land cover, thus affecting ecological diversity and resilience.

Biodiversity assessment is the ecological basis for assessing the resilience level of rural areas. How to conduct rural scale assessment requires comprehensive consideration of the land cover, landscape vegetation, biological composition and structure, and other factors. As for the rural "social–ecology–economic" system, existing research mainly focuses on landscape diversity, landscape fragmentation degree, coverage, etc., without comprehensive and systematic consideration of rural social–ecology–economic factors. In recent years, with the rise of spatial quantitative analysis and the improvement of the availability of remote sensing data in villages, many scholars have paid attention to the quantitative measurement of biodiversity and ecosystem assessment. Future research needs to pay attention to the soil carbon content, biomass carbon dioxide, etc., and effectively link up with the double carbon targets of carbon neutralization and carbon peak.

4.2 Resilience and climate change

Climate changes affect various elements of the rural ecosystem and their relationships at the macro scale. For example, drought can easily lead to the loss of rural crops and the reduction of biomass in soil. Soil and water loss affect the content of soil biomass and the spatial pattern of soil and water. The research by Elisabeth Simelton (2009) shows that the size of rural population and the amount of agricultural input are negatively correlated with drought vulnerability, and the vulnerability is negatively correlated with land abundance. Loring and Gerlach (2009) addressed the complex ecological environment and climate change by studying rural food security and sustainable development of food resources. Nguyen et al., (2017) researched the rural land-use decision-making factors represented by land-use selection decisions and crop diversity. He found that they are closely associated with the ability to cope with the impact of climate change, economic life expectations, and living environment characteristics and discussed the rural resilience shown by coping with climate change and measures on how to improve rural resilience.

In the background of urban sprawl, population expansion, and climate change, Kristine Lien Skog (2016) researched the conversion of the rural arable land and the protection of the arable land by quantitative measures. Taking Norway as an example, he discussed the influence mode and mechanism of soil attachments on rural resilience from the perspective of conversion of the arable land to a construction land. Barrett, C (2015) researched the correlation between rural economic conditions and soil quality and proposed the importance of soil fertility for rural resilience and resistance to climate change. As the spatial carrier of biomass coverage and bearing, the land provides material conditions for rural adaptation to climate change, and the level of the land itself has a positive impact on resilience. In his speech on the International Year of Soil in 2015, the UN Secretary-General Ban Ki Moon believed that "A healthy life is not possible without healthy soils."

In summary, the richness and quality of the land, the rationality of spatial distribution, the content of soil biomass, artificial agricultural production, and non-agricultural behavior play a decisive role in rural resilience under the background of climate change. Climate changes have a direct impact on the rural ecological environment, affect the stability of the rural social–economic system, and play a role in its ability to cope with occasional shocks and complex risk changes.

5 Development trend of rural resilience research

5.1 Research results

Based on the perspective of biodiversity, this study adopted the CiteSpace document visualization analysis method to analyze the mutation words, keywords, and evolution trend of rural resilience research from 1992 to 2022 using the knowledge map. The main conclusions are as follows: first, more and more attention is paid to rural resilience; second, the high-frequency mutation words in rural resilience research mainly include "Africa, biodiversity, social ecological system and adaptability," which reflect that biomass energy, biodiversity, climate change, and ecological environment have received high attention in the study of rural resilience. The high-frequency keywords mainly include "region resilience, climate change, land use change, natural disaster, carbon sequestration," etc., indicating the concern about climate change, natural disasters, biological sustainability, carbon storage, etc. Third, the research content mainly focuses on resilience and biodiversity, and resilience and climate change; the fourth conclusion is made to analyze and judge the development trend of promoting the research and construction of rural resilience from the aspects of ecological restoration and rural planning.

5.2 Development trend

In combination with the main research contents, relevant research progress, and the two main research hotspots

mentioned earlier, the author made the following prediction and conclusion on the development trend of the interdisciplinary research on the combination of rural resilience and biodiversity: 1) with the in-depth implementation of the strategies such as "beautiful countryside, carbon peak, and carbon neutralization," the importance of rural ecological environment protection and biomass diversity protection will become more and more prominent in rural resilience construction and research. 2) Carrying out bottom–up ecological restoration and top–down planning improvement will be an important development trend and research direction for the future development of rural resilience construction. This point will be emphatically discussed later.

5.2.1 Bottom–up ecological restoration

In response to biodiversity changes, rural resilience emphasizes the mode, extent, and direction of adaptation formed by resisting external environmental changes, which are affected by natural, economic, social, and other factors. Rural resilience from the perspective of biodiversity needs to consider the rural regional ecosystem and its evolution process from the perspective of spatial–temporal changes and factor transmission, and accurately recognize and evaluate the resilience level and capacity of the rural system from a dynamic perspective. It is proposed that the bottom–up ecological restoration mode is a path of self-restoration and improvement based on the evolution and coordination perspective with rural space as the carrier and the land as the cell under the existing framework of rural resilience identification, measurement, and research. It can effectively promote the richness of land biomass, sustainable development of the rural spatial system, realize the goal of individual cognition, network social association, human–earth system co-existence, and improve biodiversity in practice. In further research, we should pay attention to the combination of theory and empirical cases.

5.2.2 Top–down planning improvement

In response to global climate change, rural resilience emphasizes on coping with complex change scenarios and optimizing sustainable development paths. Based on the perspective of climate adaptation and climate change, it is necessary to emphasize the top–down planning promotion path. From the perspective of a more macroscopic spatial scale and time evolution, it is necessary to systematically sort out and think about the whole elements of the land space in the village and propose planning strategies, planning paths, and spatial layout optimization methods. Starting from the complex relationship and interaction between various related elements of rural resilience, it is considered to dock territorial space planning, construct village territorial space planning, optimize the layout of the village territorial space from the top to the bottom, and promote the integration and improvement of biological resources. Dynamic monitoring and follow-up are carried out according to the evolution trend of rural resilience, and new spatial adjustments are constantly made to optimize the rural social–economic–ecological system so as to better improve the biomass content of land resources and carry rural production and life. Scholars should pay attention to the applicability of planning improvement in different spatial scales and time conditions in further research studies.

Author contributions

YY was in charge of designing the experiments and writing the manuscript; YY was in charge of revising the manuscript; YY was in charge of project administration.

Conflict of interest

The author declares that the research was conducted in the absence of any commercial or financial relationships that could be construed as a potential conflict of interest.

Publisher's note

References

Al-Zubaidy, M. S. K. (2015). A literature evaluation of the energy efficiency of leadership in energy and environmental design (LEED)—certified buildings[J]. *Am. J. Civ. Eng. Archit.* 3 (1), 1–7. doi:10.12691/ajcea-3-1-1

Angeler, D. G., Allen, C. R., Garmestani, A., Pope, K. L., Twidwell, D., and Bundschuh, M. (2018). Resilience in environmental risk and impact assessment: Concepts and measurement. *Bull. Environ. Contam. Toxicol.* 101, 543–548. doi:10.1007/s00128-018-2467-5

Babulo, B., Muys, B., Nega, F., Tollens, E., Nyssen, J., Deckers, J., et al. (2008). Household livelihood strategies and forest dependence in the highlands of Tigray, Northern Ethiopia. *Agric. Syst.* 98 (2), 147–155. doi:10.1016/j.agsy.2008.06.001

Bailey, I., and Buck, L. E. (2016). Managing for resilience: A landscape framework for food and livelihood security and ecosystem services. *Food Secur.* 8, 477–490. doi:10.1007/s12571-016-0575-9

Barrett, C., and Bevis, L. (2015). The self-reinforcing feedback between low soil fertility and chronic poverty. *Nat. Geosci.* 8, 907–912. doi:10.1038/ngeo2591

Bjorna, H., and Aarsæther, N. (2009). Combating depopulation in the northern periphery: Local leadership strategies in two Norwegian municipalities. *Local Gov. Stud.* 35 (2), 213–233. doi:10.1080/03003930902742997

Brown, K. (2017). Book review: Brown, katrina. 2016: Resilience, development and global change. *Prog. Dev. Stud.* 17 (1), 90–92. doi:10.1177/1464993416672302

Center, L. B. J. W., and Garden, U. S. B. (2009). The sustainable sites initiative: Guidelines and performance benchmarks[J]. *Environ. Policy Collect.*

Chaigneau, T., Coulthard, S., Daw, T. M., Szaboova, L., Camfield, L., Chapin, F. S., et al. (2022). Reconciling well-being and resilience for sustainable development. *Nat. Sustain.* 5, 287–293. doi:10.1038/s41893-021-00790-8

Chen, C. M., Chen, Y., and Hou, J. (2009). CiteSpace II: Identification and visualization emerging trends and transient patterns in scientific literature[J]. *J. China Soc. Sci. Inf.* 28 (3), 401–21. doi:10.1002/asi.20317

Chen, C. M. (2009). Citespace II:detecting and visualizing emerging trends and transient patterns in scientific literature. *J. China Soc. Sci. Tech. Inf.* doi:10.1002/asi.20317

Chen, M., and Mengyuan, C. (2017). Aninternational literature review of regional economic resilience:Theories and practices based on the evolutionary perspective. *Progress. Geogr.* 36 (11), 1435–1444. doi:10.18306/dlkxjz.2017.11.012

Cutter, S. L., Burton, C. G., and Emrich, C. T. (2010). Disaster resilience indicators for benchmarking baseline conditions. *J. Homel. Secur. Emerg. Manag.* 7 (1). doi:10.2202/1547-7355.1732

Cutter, S. L., Ash, K. D., and Emrich, C. T. (2016). Urban–rural differences in disaster resilience[J]. *Ann. Am. Assoc. Geogr.* 106 (6), 1236–1252. doi:10.1080/24694452.2016.1194740

Dai, D., and Qi, C. (2015). Cases and enlightenments of sustainable landscape architecture in the United States[J]. *China Urban For.* 13 (1), 33–37.

Ekblom, A. (2020). Livelihood security, vulnerability and resilience: A historical analysis of chibuene, southern Mozambique. *AMBIO* 41, 479–489. doi:10.1007/s13280-012-0286-1

Emmanuel, R., and Krüger, E. (2012). Urban heat island and its impact on climate change resilience in a shrinking city: The case of Glasgow, UK. *Build. Environ.* 53, 137–149. doi:10.1016/j.buildenv.2012.01.020

Folke, C., Carpenter, S. R., Walker, B., Scheffer, M., Chapin, T., and Rockstr€om, J. (2010). Resilience thinking:integrating resilience, adaptability and transformability. *Ecol. Soc.* 15 (4), 20. available at:. doi:10.5751/es-03610-150420http://www.ecologyandsociety.org/vol15/iss4/art20/

Folke, C. (2016). Resilience (republished). *Ecol. Soc.* 21 (4), 44. doi:10.5751/ES-09088-210444

Heijman, W. J. M., and Hagelaar, J. L. F. (2007). Rural resilience as a new development concept[C]//DENILO T,MILANDIN M. 100th seminar of the EAAE: Development of agriculture and rural areas in central and eastern europe. *NoviSad, Serbia Montenegro Eur. Assoc. Agric. Econ.*, 383–396.

Hennebry, B. (2020). The determinants of economic resilience in rural regions. An examination of the Portuguese case. *Misc. Geogr.* 24 (1), 24–29. doi:10.2478/mgrsd-2020-0001

Holladay, P. J., and Powell, R. B. (2013). Resident perceptions of social–ecological resilience and the sustainability of community-based tourism development in the Commonwealth of Dominica[J]. *J. Sustain. Tour.* 21, 1188–1211. doi:10.1080/09669582.2013.776059

Hu, K. F., and Zheng, X. (2018). Literature review of key areas and frontier trends in landscape performance research based on citespace bibliometric analysis[J]. *Landsc. Archit.* 25 (11), 84–89. doi:10.14085/j.fjyl.2018.11.0084.06

Huang, J., and Waibel, H. (2021). Location and economic resilience in rubber farming communities in southwest China. *China Agric. Econ. Rev.* 13 (2), 367–396. doi:10.1108/CAER-06-2020-0153

Huang, X., Li, H., Zhang, X., Hu, K. F., and Zheng, X. (2018). Land use policy as an instrument of rural resilience – the case of land withdrawal mechanism for rural homesteads in China. *Ecol. Indic.* 87, 47–55. doi:10.1016/j.ecolind.2017.12.043

IPCC (2014). *Climate change 2014: Impacts, adaptation, and vulnerability.Part A: Global and sectoral aspects. Contribution of working group II to the fifth assessment report of the intergovernmental panel on climate*. Cambridge, United Kingdom and New York, USA: Cambridge University Press.

Júnior, W. S. F., Ladio, A. H., and Albuquerque, U. P. D. (2011). Resilience and adaptation in the use of medicinal plants with suspected anti-inflammatory activity in the Brazilian Northeast. *J. Ethnopharmacol.* 138 (1), 238–252. doi:10.1016/j.jep.2011.09.018

Kelvin, S. H. P., Johnny, D. J., Navjot, S. S., Susan, L. H. L., Yap, C. A. M., Lim, S. L. H., et al. (2005). Lowland rainforest avifauna and human disturbance: Persistence of primary forest birds in selectively logged forests and mixed-rural habitats of southern peninsular Malaysia. *Biol. Conserv.* 123 (4), 489–505. doi:10.1016/j.biocon.2005.01.010

Kilkenny, M. (2008). Social capital in the knowledge economy: Theory and empirics – by hans westlund. *Pap. Reg. Sci.* 87 (1), 149–152. doi:10.1111/j.1435-5957.2007.00157.x

Koning, J. D., Hobbis, S. K., Mcneill, J., and Prinsen, G. (2021). Vacating place, vacated space? A research agenda for places where people leave. *J. Rural Stud.* 82 (1), 271–278. doi:10.1016/j.jrurstud.2021.01.026

Li, H., Jin, X., Liu, J., Feng, D., Xu, W., and Zhou, Y. (2022). Analytical framework for integrating resources, morphology, and function of rural system resilience—an empirical study of 386 villages. *J. Clean. Prod.* 365, 132738. doi:10.1016/j.jclepro.2022.132738

Li, H., Li, Y., Huang, H., and Song, C. (2020). Rural settlements research from the perspective of resilience theory. *Sci. Geogr. Sin.* 40 (4), 556–562. doi:10.13249/j.cnki.sgs.2020.04.007

Li, J., and Chen, C. (2016). *Citespace: Scientific text mining and visualization[M]*. Beijing: Capital University of Economics and Business Press.

Li, T., Niu, P., and Gu, C. (2014). Research on framework of resilient cities. *Urban Plan. Forum* (5), 23–31. https://kns.cnki.net/kcms/detail/detail.aspx?dbcode=CJFD&dbname=CJFDLAST2015&filename=CXGH201405008&uniplatform=NZKPT&v=8v9R6NbfdyWOFA6jUiTczhrVqFcFpbqDCNdJOFpEK4doLawN3y9bzyJ1TZcdVJzj.

Li, Y., Huang, H., Song, C., et al. (2020). The spatiotemporal evolution ofChina's rural resilience and the key factors detection. *Actageogr. Sin.* 2020-06-15. [2020-09-28] http://kns.cnki.net/kcms/detail/11.1856.P.20200615.0835.002.html.

Li, Y. (2022). A systematic review of rural resilience. *China Agric. Econ. Rev.* ahead-of-print No. ahead-of-print. doi:10.1108/CAER-03-2022-0048

Li, Y., Westlund, H., and Liu, Y. (2019). Why some rural areas decline while some others not: An overview of rural evolution in the world. *J. Rural Stud.* 68, 135–143. doi:10.1016/j.jrurstud.2019.03.003

Li, Y., Wu, W., and Wang, Y. (2021). Global poverty dynamics and resilience building for sustainable poverty reduction. *J. Geogr. Sci.* 31 (8), 1159–1170. doi:10.1007/s11442-021-1890-4

Lien Skog, K., and Steinnes, M. (2016). How do centrality, population growth and urban sprawl impact farmland conversion in Norway? *Land Use Policy* 59, 185–196. doi:10.1016/j.landusepol.2016.08.035

Liu, Y. X., Peng, J., Wang, A., Xie, P., and Han, Y. N. (2015). New research progress and trends in ecosystem health. *Acta Ecol. Sin.* 35 (18), 5920–5930. doi:10.5846/stxb201401060032

Loring, P. A., and Gerlach, S. C. (2009). Food, culture, and human health in Alaska: An integrative health approach to food security. *Environ. Sci. Policy* 12, 466–478. doi:10.1016/j.envsci.2008.10.006

Marsden, T., and Sonnino, R. (2008). Rural development and the regional state: Denying multifunctional agriculture in the UK. *J. Rural. Stud.* 24 (4), 422–431. doi:10.1016/j.jrurstud.2008.04.001

Mazur, C., Hoegerle, Y., Brucoli, M., van Dam, K., Guo, M., Markides, C. N., et al. (2018). A holistic resilience framework development for rural power systems in emerging economies. *Appl. Energy* 235. doi:10.1016/j.apenergy.2018.10.129

McManus, P., Walmsley, J., Argent, N., Baum, S., Bourke, L., Martin, J., et al. (2012). Rural Community and Rural Resilience: What is important to farmers in keeping their country towns alive?[J]. *J. Rural Stud.* Vol. 28, 20–29. doi:10.1016/j.jrurstud.2011.09.003

Mfirdhous, M. F., and Mkaruratane, P. (2018). A model for enhancing the roleof information and communication technologies for improving the resilience of rural communities to disasters. *Procedia Eng.* 212, 707–714. doi:10.1016/j.proeng.2018.01.091

Modica, M., and Reggiani, A. (2015). Spatial economic resilience: Overview and perspectives. *Netw. Spat. Econ.* 15 (2), 211–233. doi:10.1007/s11067-014-9261-7

Mohamed, A., Nguyen, C., and Ben Youssef, A. (2015). Natural disasters, household welfare, and resilience:evidence from rural vietnam. *World Dev.* 70, 59–77. doi:10.1016/j.worlddev.2014.12.017

Nguyen, T. T., Nguyen, L. D., Lippe, R. S., and Grote, U. (2017). Determinants of farmers' land use decision-making: Comparative evidence from Thailand and vietnam. *World Dev.* 89, 199–213. doi:10.1016/j.worlddev.2016.08.010

On first World Soil Day (2014). *Secretary-General says in message, sustainable management should be universal priority, as healthy planet requires healthy soils*. Tokyo: United Nations Press Release. doi:10.1016/S0167-8809(01)00298-5

Pain, A., and Levine, S. (2012). A conceptual analysis of livelihoods and resilience: Addressing. *Theinsecurity agency*.

Pandey, R., Jha, S. K., Alatalo, J. M., Archie, K. M., and Gupta, A. K. (2017). Sustainable livelihood framework-based indicators for assessing climate change vulnerability and adaptation for Himalayan communities[J]. *Ecol. Indic.* 79, 338–346. doi:10.1016/j.ecolind.2017.03.047

Peng, J., Liu, Y., Li, T., and Wu, J. (2017). Regional ecosystem health response to rural land use change: A case study in lijiang city, China. *Ecol. Indic.* 72, 399–410. doi:10.1016/j.ecolind.2016.08.024

Peroni, N., and Hanazaki, N. (2002). Current and lost diversity of cultivated varieties, especially cassava, under swidden cultivation systems in the Brazilian Atlantic Forest. *Agric. Ecosyst. Environ.* 92 (2–3), 171–183. doi:10.1016/S0167-8809(01)00298-5

Qiu, M. L., Liu, D. F., and Liu, Y. L. (2021). Review on theoretical framework and evaluation system of rural resilience[J]. *China Land Sci.* 35 (8), 107–114. doi:10.11994/zgtdkx.20210812.094413

Rigg, J., and Oven, K. (2015). Building liberal resilience? A critical review from developing rural asia[J]. *Glob. Environ. Change* 32, 175–186. doi:10.1016/j.gloenvcha.2015.03.007

Roberts, E., Beel, D., Philip, L., and Townsend, L. (2017). Rural resilience in a digital society: Editorial. *J. Rural Stud.* 54, 355–359. doi:10.1016/j.jrurstud.2017.06.010

Schouten, M., Paul, O., Polman, N., and Westerhof, E. (2013). Resilience-based governance in rural landscapes: Experiments with agri-environment schemes using a spatially explicit agent-based model. *Land Use Policy* 30, 934–943. doi:10.1016/j.landusepol.2012.06.008

Schwarz, A-M., Bene, C., Bennett, G., Boso, D., Hilly, Z., Paul, C., et al. (2011). Vulnerability and resilience of remote rural communities to shocks and global changes: Empirical analysis from Solomon Islands[J]. *Glob. Environ. Change* 21, 1128–1140. doi:10.1016/j.gloenvcha.2011.04.011

Scott, M. (2013). Resilience: A conceptual lens for rural studies? *Geogr. Compass. Geogr. Compass* 7, 597–610. doi:10.1111/gec3.12066

Shoemaker, D. A., BenDor, T. K., and Meentemeyer, R. K. (2019). Anticipating trade-offs between urban patterns and ecosystem service production: Scenario analyses of sprawl alternatives for a rapidly urbanizing region. *Comput. Environ. Urban Syst.* 74, 114–125. doi:10.1016/j.compenvurbsys.2018.10.003

Simelton, E., Evan, D., Fraser, G., Termansen, M., Piers, M., and Andrew, J. (2009). Dougill(2008).Typologies of crop-drought vulnerability: An empirical analysis of the socio-economic factors that influence the sensitivity and resilience to drought of three major food crops in China (1961–2001). *Environ. Sci. Policy* 12, 438–452. doi:10.1016/j.envsci.2008.11.005

Sorice, M. G., Kreuter, U. P., Wilcox, B. P., and Fox, W. E. (2012). Classifying land-ownership motivations in central, Texas, USA: A first step in understanding drivers of large-scale land cover change. *J. Arid Environ.* 80, 56–64. doi:10.1016/j.jaridenv.2012.01.004

Tebboth, M. G. L., Conway, D., and Adger, W. N. (2019). Mobility endowment and entitlements mediate resilience in rural livelihood systems. *Glob. Environ. Change* 54, 172–183. doi:10.1016/j.gloenvcha.2018.12.002

Wang, C., Ren, M., Hu, Q., and Li, Q. (2021). Rural production space system resilience and its research domains. *Prog. Geogr.* 40 (1), 85–94. doi:10.18306/dlkxjz.2021.01.008

Wang, J., and Zigang, C. (2021). Resilient rural construction: Conceptual connotation and logical approach [J]. *Acad. Exch.*, 140–151.

Westlund, H. (2006). *Social capital in the knowledge economy: Theory and empirics*. Cheltenham: Edward Elgar.

Wilson, G. A. (2012). Community resilience, globalization, and transitional pathways of decision-making. *Geoforum* 43 (6), 1218–1231. doi:10.1016/j.geoforum.2012.03.008

Wilson, G. A., Hu, Z., and Rahman, S. (2018). Community resilience in rural China: The case of Hu village, sichuan province. *J. Rural Stud.* 60, 130–140. doi:10.1016/j.jrurstud.2018.03.016

Wilson, G. (2010). Multifunctional 'quality' and rural community resilience. *Trans. Inst. Br. Geogr.* 35 (3), 364–381. doi:10.1111/j.1475-5661.2010.00391.x

World Bank (2010). *Natural hazards, unnatural disasters, the economics of effective prevention*. Washington, DC, USA: The World Bank.

Yang, B., Feldman, M. W., and Li, S. (2020). The status of perceived community resilience in transitional rural society: An empirical study from central China. *J. Rural Stud.* 80, 427–438. doi:10.1016/j.jrurstud.2020.10.020

Yang, T., Chen, H., Liu, D., Zhang, H., and Shi, Q. (2021). Spatiotemporal change of rural community resilience in loess hilly-gully region and influencing factors: A case study of gaoqu township in mizhi county, shannxi province. *Prog. Geogr.* 40 (2), 245–256. doi:10.18306/dlkxjz.2021.02.006

frontiers | Frontiers in Chemistry

TYPE Mini Review
PUBLISHED 29 November 2022
DOI 10.3389/fchem.2022.1078170

OPEN ACCESS

EDITED BY
Hu Li,
Guizhou University, China

REVIEWED BY
Cheng Zhang,
Southwest University, China
Jinshan Zhu,
Yangtze Normal University, China

*CORRESPONDENCE
Yuchi Yang,
yangyuchi@tongji.edu.cn

SPECIALTY SECTION
This article was submitted to Green and Sustainable Chemistry, a section of the journal Frontiers in Chemistry

RECEIVED 24 October 2022
ACCEPTED 07 November 2022
PUBLISHED 29 November 2022

CITATION
Yang Y (2022), Improvement of rural soil properties and states by biomass carbon under the concept of sustainability: A research progress.
Front. Chem. 10:1078170.
doi: 10.3389/fchem.2022.1078170

Improvement of rural soil properties and states by biomass carbon under the concept of sustainability: A research progress

Yuchi Yang*

College of Architecture and Urban Planning, Tongji University, Shanghai, China

Biomass carbon is a highly aromatic carbonaceous solid obtained by thermochemical reaction of biomass raw materials. It is frequently used in the research and application of soil properties and states improvement. Biomass carbon has abundant porous structure, high specific surface area and surface functional groups. After being applied to the soil, it has a significant impact on manipulating the physichemical properties of the soil, enhancing the microbial environment and remediating soil pollutants, which is conducive to the resource utilization of agricultural wastes and the long-term preservation of the environment. Based on 328 moderately to highly relevant literatures on biomass carbon and rural soil property improvement since 2010, this paper reviewed the contemporary research progress of biomass carbon application in soil property improvements utilizing the concept of sustainable development. In order to provide beneficial illumination for the complete implementation of biomass carbon in improving rural soil properties, this paper primarily evaluated the principle as well as mechanism of promoting sustainable soil properties. It tends to prospect the application and development aspirations of biomass carbon in soil ecological restoration, crop growth, development.

KEYWORDS

biomass carbon, soil properties and states improvement, soil pollution, rural sustainable development, research progress

1 Introduction

In recent years, the research on the application of biomass carbon in soil properties and states improvement has attracted much attention from the academic community. Recent increases in industrialization and urbanization have resulted in significant CO_2 emissions, global warming, sewage and other pollutants. As more than just a result, enormous rural regions have unavoidably become the emission receptors for numerous pollutants. Rural soil has become the first place to absorb some heavy metals and toxic chemical elements, so point pollution and non-point source pollution flowing one after another. The rural soil ecological environment has become increasingly worse as a result,

TABLE 1 Research Frontiers of biomass carbon application in soil improvement.

Research topics	Research contents	Researchers	Key words
Biochars' influence on soil reclaimarion	Research status of biochar for soil improvement and outstanding advantages of carbonization technology	Wang et al. (2014)	biochar; soil reclaimarion; soil ecosystem
Slow-release property and soil remediation mechanism of biochar-based fertilizers	Slow release mechanism and influencing factors of biomass carbon based fertilizer	Zhao et al. (2021)	biochar-based fertilizers; slow-release property; soil improvement
Biochar on transport of inorganic pollutants in soil	the basic characteristics, carbon content and structure of biomass carbon are affected by the properties of source materials	Zhang et al. (2021)	Biochar; adsorbent; Heavy metals; Soil; repair
Soil Physiochemical Properties and Nitrogen Transformation	Changes and response mechanism of nitrogen cycle, nitrogen fixation reaction, ammonification reaction and nitrification reaction driven by soil microorganism	Wang et al. (2019)	Soil physical properties; Soil chemical properties; Microorganism
Effect of biochar on soil physical characteristics improvement	Effect of biochar addition on soil physical characteristics, the best application rate of biochar	Deng et al. (2020)	land consolidation; fertility betterment
Effects of biochar on remediation of heavy metal containeated soil	Application of biochar in remediation of heavy metal contaminated soil	Yang et al. (2020)	Soil heavy metal; mechanism; remediation effect
Remediation of As and Cd contamination by calcium-based magnetic biochar	Solution to the problem of remediation of As and Cd contaminated soil	Wu (2020)	calcium-based magnetic biochar; Cd As co-contamination; bioavailability; paddy soil
Effects of biochar on remediation of heavy metal containeated soil	Application of biochar in remediation of heavy metal contaminated soil	Yang et al. 2020	Soil heavy metal; mechanism; remediation effect
Biochar Behavior in Soil Environment	Behavior of biochar in soil environment and effects of biochar improvement on soilphysihemical properties and crop growth	Zhang et al. (2021)	biochar; soil; environmental behavior; pollutants
Heavy metal contaminated soil using modified biochar	Preparation and properties of biochar and effects of different modification methods on the structural characteristics of biochar	Zhang et al. (2021)	Soil, heavy metals; modified biochar; adsorption
Biochar remediation of petroleum contaminated soil	Physicochemical properties of biochar and biochar remediation of petroleum contaminated soil	Song et al. (2021)	petroleum pollution; remediation technology; soil
Biochar from constructed wetland biomass waste	Characteristics of wetland plant derived biochar, and its utilization in soil improvement, carbon sequestration	Cui et al. (2022)	Aquatic plant Carbon sequestration Sorption Soil improvement
Characteristics of biochar and its effects and mechanism on soil properties	The role of biochar addition in improving soil structure, soil fertility, adjusting soil pH, repairing contaminated soil	Chen F et al. (2022)	biochar; soil properties; influence mechanism; remediation
Effects of biochar addition on nutrient levels and its components in dry farmland soils	The application of biomass carbon in soil improvement and fertility improvement in dry farming areas of the Loess Plateau	Pan et al. (2022)	Loess Plateau; soil nutrient; organic carbon fraction; humic substance

which has aroused widespread concern and high attention from the government and academics. Over the years, rural soil has been carrying the important mission of increasing biomass carbon production, absorbing CO_2 and other carbon containing substances. Improvement of rural soil properties, research and application of sustainable development of soil ecosystems have recently become hot topics in the academic community due to the crisis of heavy metals, toxic chemical element accumulation, as well as changes in soil physichemical structure. The biomass carbon rich in organic carbon has naturally entered the public's consciousness due to its effective soil improvement performance.

The Amazon basin is where American Indians first applied black carbon to soil to produce fertile black soil known as "Terra Preta" and this is where the phrase "biomass carbon" first appeared (Goldberg, 1985; Lehmann et al., 2003; Lehmann et al., 2008). According to Jiang et al. (2017) and Kong et al. (2015), biomass carbon is the carbonaceous solid product of the high-temperature pyrolysis and carbonization from organic biomass materials including wood, straw, fruit shells in an atmosphere with little to no oxygen. At a relatively modest preparation temperature (<700°C), biomass carbon might well be pyrolyzed to produce valuable carbon-containing compounds (Ahmad et al., 2014; Wang et al., 2022). The characteristics of biomass carbon include high pH, adsorption capacity, abundant nutritional content, large specific surface area, pore structure, stable physichemical properties, and abundant surface functional groups, etc.It may enhance soil, promote soil fertility, encourage crop development and increase soil nitrogen on the impact of chemical circulation because of its unique physichemical properties (Wang et al., 2019; He et al., 2021). High pH, nutritional content, pollutant adsorption ability, rich pore structure, large specific surface area, stable physichemical properties, and a richness of surface functional groups are all features of biomass carbon. When applied to farmland, its unique physical and chemical characteristics can enhance soil, increase soil fertility, encourage crop development, and influence the chemical cycle of soil nitrogen (Wang et al., 2019; Raza et al., 2022).

According to research, biomass carbon improves soil's physical structure and physichemical properties, which can be utilized as an organic remediation agent in soil systems for carbon sequestration and emission reduction (Wang et al., 2019; Chen F et al., 2022), making it a suitable substance for water and soil remediation (Beesley et al., 2011; Dey et al., 2014; Wu, 2020). According to Spokas et al. (2012), enhancing soil fertility and carbon sequestration, recovering reclaimed land and lowering greenhouse gas emissions from farms are all potential applications for biomass carbon in terrestrial ecosystems (Harter et al., 2014; Troy et al., 2013; Cayuela et al., 2014). Research by academics indicates that biomass carbon can effectively promote the improvement of agricultural soil, the growth and development of crops (Table 1). The expense of preparation is also significantly lower than that of activated carbon, which mostly consumes wood and coal as raw materials. At the same time, its preparation materials originate from a wide range of sources. The application of biomass carbon to enhance soil characteristics will definitely become the primary concern of upcoming researches as a consequence of the progressively severe soil pollution situation.

This paper is based on the concept of sustainable development and does use the literature research method. It typically analyzes 328 highly relevant literatures on the topics of biomass carbon and rural soil property improvement since 2010, including 181 Chinese journal literatures in CNKI database and 147 English review journal literatures in WOS database. The production of raw materials, fundamental characteristics, preparation factors, principle and mechanism of biomass carbon to improve rural soil properties are almost all reviewed and analyzed in this paper. The findings are summarized in Table 1 in conjunction with the great potential applications and future development direction of biomass carbon in soil ecological restoration, crop growth and development, research development trend.

2 Summary of research progress

The scholars' research on the improvement of rural soil properties by biomass carbon mainly concentrated on the production of raw materials, basic properties, influencing factors of preparation, the principle and mechanism of biomass carbon to improve rural soil properties and states by sorting out the results of the existing internal and external research.

2.1 Raw materials and basic properties of biomass carbon

There are a wide range of raw materials for biomass carbon preparation, such as straw, manure, grass, wood, etc. (Jiang et al., 2017; Liu et al., 2009; Cantrell et al., 2012). Generally, they can be divided into traditional (such as agricultural, forestry wastes and urban wastes) and non-traditional biomass carbon (Zhang et al., 2021; Hossain et al., 2011). There are apparent differences in composition, structure and element types, etc. (Rego et al., 2019; Cao et al., 2022). The physicochemical properties of biomass carbons produced from different raw materials or under different preparation environmental conditions have significant differences and diversity (Aller, 2016), so the impact on crop growth is also very different (Liu et al., 2013; Jeffery et al., 2011). The chemical effects of the same kind of biomass carbons at different temperatures are also different. The differences in specific surface area, cation exchange capacity, the proportions and contents of biomass carbon with different degrees of dissolution of biomass carbon prepared at the same time show significant differences in physical and chemical properties.

Biomass carbon is an important measure for the resource utilization of soil biomass waste and the realization of farmland carbon management. Biomass carbon contains a large number of nutrient elements such as N, P, and K, as well as medium and micronutrient elements such as Ca, S, Fe, and Si, which are used to reduce pests, diseases and ensure the normal growth of soil crops (Zhang, 2017). Researches have shown that biomass carbon is mainly composed of aromatic hydrocarbons, elemental carbon or carbon combinations with graphite-like structure (Chen et al., 2013). Its surface physical and chemical characteristics are of great significance for its potential production and application, which are mainly affected by the temperature of the thermal reaction and raw materials (Chen Y et al., 2022).

Biomass carbon is a solid substance with rich carbon content generated from the pyrolysis of agricultural wastes such as straw (Zhang, 2017). Its carbon fixation and emission reduction effect in farmland soil are mainly due to its high carbon content and highly stable structure (Keiluweit and Johnson 2010). The characterization of biomass carbon is of great significance for its potential applications. Its physical and chemical properties are mainly affected by the thermal treatment temperature and raw materials. Biomass carbon applied to soil can increase soil carbon storage and slow down the carbon cycle process of terrestrial ecosystem (Lehmann et al., 2006; Lehmann et al., 2008; Weng et al., 2017; Zhang, 2017).

2.2 Factors affecting the preparation of biomass carbon

Biomass carbon is rich in organic carbon, which is often compared with activated carbon. Activated carbon is mainly made from coal, wood and other materials through high-temperature carbonization reaction, activation and condensation by various preparation methods (Wu et al., 2014; Ahmed et al., 2019). The preparation of raw materials is relatively simple and the source is relatively limited. Biomass

carbon is prepared by pyrolysis reaction at low temperature. Its raw materials come from a wide range of sources, such as cheap and rich traditional agricultural wastes (Zhou et al., 2021) and non-traditional biomass (Inyang et al., 2016), such as straw, fruit shells, peanut shells, walnut shells, poultry manure, etc. The preparation cost of biomass carbon is significantly lower than that of activated carbon.

Biomass carbon is a carbon rich solid mixture formed by pyrolysis of biomass wastes such as straw under the condition of oxygen limitation, with an obvious aromatic structure (Raveendran et al.,1995; Brodowski et al., 2005). The constituent elements of biomass carbon are closely related to the preparation temperature in the carbon production process. Specifically, with the increase of carbonization reaction temperature within a certain controllable range, the hydrogen and oxygen content decreases while the carbon and ash contents increase significantly, (Schmidt and Noack 2000; Chen et al., 2013). It is mainly used for recycling agricultural and forestry waste resources or improving farmland soil properties (Liu et al., 2020; Zhang et al., 2021).

2.3 Principle and mechanism of improving rural soil properties and states by biomass carbon

2.3.1 Effects of biomass carbon on soil physicochemical properties

The improvement of soil properties by biomass carbon has widely aroused extensive research in academia. The principle of improving soil physical and chemical properties is mainly to affect the soil nitrogen cycle, promote soil carbon sequestration and emission reduction, reduce soil nutrient loss, affect the distribution of soil components and other direct or indirect ways of action. Due to its high pH value, loose porous structure, available carbon nutrient content, biomass carbon plays an important role in mitigating soil acidification, reducing nutrient loss, promoting carbon fixation and emission reduction (Ogura and Date 2016; Ali et al., 2017). Most of the existing researches focus on the overall changes of soil caused by the uniform mixing of biomass carbon and soil, ignoring the spatial heterogeneity and variability of the impact of biomass carbon on the distribution of soil components (Yu and Meng 2019; Wang et al., 2019). Akhtar et al. (2014) finds that biomass carbon is beneficial from improving chlorophyll content, photosynthesis rate (Pn), stomatal conductance (Gs), relative water content (Rwc) and photosynthesis efficiency of tomato leaves. Shafaqat et al. (2017) reveals that the physical and biological characteristics of soil strengthened by biomass carbon under drought conditions improved water conservation capacity, regulated stomatal conductance, plant hormone content, specifically decreased Na^+, K^+ absorption of plants. The surface cationic adsorption capacity of biomass carbon can improve the soil cationic exchange capacity. Wang et al. (2019) reveals the different porosity and structure of different soil components are important reasons for the variation of soil water content, rich porous structure, large specific surface area (SSA) and particle mechanical strength could affect the soil water permeability. Biomass carbon is a stable inert substance, which mainly depends on its highly carbonized and aromatic molecular structure (Yu and Meng 2019; Yu, 2021). However, instability phenomena such as aging and decomposition of biomass carbon may occur as time goes by.

Biomass carbon can improve soil by affecting nitrogen transformation. The application of biomass carbon to soil changes the N element cycle, adsorbs and retains N element to a greater extent through its porous characteristics or affects the microbial environment (biodiversity, richness and vitality) in the process of N element cycle. It cannot directly increase the content of N element in soil and mineral N element which are conducive to crop growth and development. Instead, it affects the cycling process of N elements (Wu et al., 2014). Asada et al. (2002) finds that the higher temperature of biomass carbon preparation, the lower number of acid functional groups attached to the surface, and the ability to react to NH_3 or NH_4^+ will be weakened. At the same time, the addition of biomass carbon to the soil will increase the abundance of ammonia oxidizing bacteria, promote the conversion of NH_4^+ into NO_3^- in soil (Nelissen et al., 2012), or adsorb phenolic compounds that inhibit nitrification indirectly promoting nitrification (Deluca et al., 2006). Taghizadeh Toosi et al. (2012) focuses on the isotope labeling experiment of N element, the results shows that N element are stable and non-volatile in air, and it could be used by plants after being applied to soil, which reduces the loss of N elements and improves the utilization efficiency. Biomass carbon actually enhanced the nitrogen fixation capacity of soil and enhanced the nitrogen cycle process in soil.

2.3.2 Effects of biomass carbon on soil microbial environment

Biomass carbon improves the soil microecosystem. Its principle is to indirectly promote crop governors by optimizing microbial growth conditions, increasing microbial content, enriching microbial community structure or affecting soil physichemical properties. The uniform and dense pores of biomass carbon can be retained in the soil and form a large number of micropores, which provides a suitable material carrier for the reproduction of microorganisms and the enrichment of community structure. Within a certain range, with the increase of biomass carbon application rate, the number and activity of soil microorganisms significantly increased (Steiner et al., 2007; Simone et al., 2009). Microbial growth requires certain water and temperature conditions, such as drought stress conditions that have a negative impact on crop growth and nutrient absorption (Robertso and Thorbum 2006). These microorganisms can adapt to environmental changes and

produce enzymes that decompose soil exogenous substances to promote degradation or transformation of pollutants (Song et al., 2021).

The effects of biomass carbon on soil physichemical properties and states can be divided into direct effects on the growth and development of microorganisms or indirect enhancement of the microbial carrier material richness of physichemical reactions. The influence of biomass carbon on the physichemical properties and states of soil will directly affect the growth and development of microorganisms, which are also important catalysts for soil physichemical reactions and complement to each other. Yu (2021) researches the migration and distribution of biomass carbon in soil, carbon effect, soil microbial diversity and community structure characteristics, nitrogen transformation functional microorganisms in the intercarboniferous microdomain. Yu (2021) researches the effects of biomass carbon on the chemical properties, microbial richness, community structure, soil fertility, crop growth and nitrification of acidified soil, effects on nitrification of acidified soil. Zhang (2017) researches the impact of biomass carbon on agricultural crop productivity, land carbon fixation, emission reduction in different ecosystems, and the impact of biomass carbon application on soil nutrient element rotation (turnover of P, C, and N elements). Zhao et al. (2021) finds that the effect of biomass carbon on crop productivity i significantly different under different soil conditions.

2.3.3 Ecological remediation effect of biomass carbon on soil pollution

Biomass carbon can be used as a functional adsorption material and mixed into soil as a remediation agent. There are many articles on remediation of petroleum soil pollution and heavy metal pollution (Zhang et al., 2021; Erin et al., 2017; El Rasafi and Haddioui 2020). The pollutants are mainly removed through chemical reaction and physical adsorption. Methods used for soil pollution remediation include chemical precipitation, ion exchange, redox and adsorption methods (Xu et al., 2020; Zhang et al., 2021; Wang et al., 2020). Compared with other methods, adsorption method is widely used due to its simple operation, high efficiency, low cost, etc. The research of Bird et al. (1999) and Dai et al. (2005) reveals that under the long-term effect, biomass carbon can physically migrate or decompose to a certain extent, redistribute in the vertical direction of soil and better adsorb pollutants. Xiao et al. (2021) suggest that wetland plant biomass carbon has strong adsorption capacity for various inorganic, organic pollutants and significant effect on soil improvement. Kambo et al. (2015) researches and recognizes the physichemical properties of plant biomass carbon, such as high water content, low calorific value, high volatile components which greatly limits its further application in soil remediation.

The potential toxic substances in soil such as heavy metal ions and polycyclic aromatic hydrocarbons are important material to which need to be paid attention. Biomass carbon can enhance the ability of soil microorganisms to metabolize organic matter, complete the overall adsorption process in order to realize the interaction of all aspects of remediation. At the same time, pollutants may be degraded autonomously in soil as time goes by which also affects the growth and development of soil microorganisms.

3 Research conclusion and prospects

In recent years, biomass carbon has become a soil improvement material of great concern. Meanwhile, the widespread application of biomass energy will contribute to a reduction in the consumption of fossil fuels and environmental pollution. It does have valuable characteristics such a potent ability for adsorption, simple preparation requirements, low pollution risk and sustainable utility. The resource utilization of agricultural production wastes can be accomplished through the production from several forms of biomass carbon. Regarding soil improvement and restoration, current research primarily concentrates on improving the physichemical characteristics of rural soil, increasing soil fertility and enriching soil microbial communities. The preparation of different types of biomass carbon can realize the resource utilization of agricultural production wastes. Existing researches mainly focus on the improvement of physichemical properties of rural soil, the improvement of soil fertility and the enrichment of soil microbial communities to achieve soil improvement and restoration. Despite the existence of multiple breakthroughs when field experiments are combined with biomass carbon, there are still many issues that need to be resolved before biomass carbon could be extensively used for rural soil improvement, remediation, and establishing standardized approaches. During the long-term application process in actual agricultural production, it is critical to take the environment's dangers into account as well as the biomass carbon's appropriate environment. Following is an extensive description of the crucial challenges and emerging trends in research on enhancing rural soil properties by biomass carbon based on an analysis of academics' research results and contemporary development demands (Figure 1).

3.1 Research defects

Biomass carbon can not only improve rural soil environment, but also be used as slow release pesticide and growth fertilizer in agricultural production process. Existing researches are deficient in the following aspects. The existing researches are insufficient in the following aspects: 1) How to standardize the combined

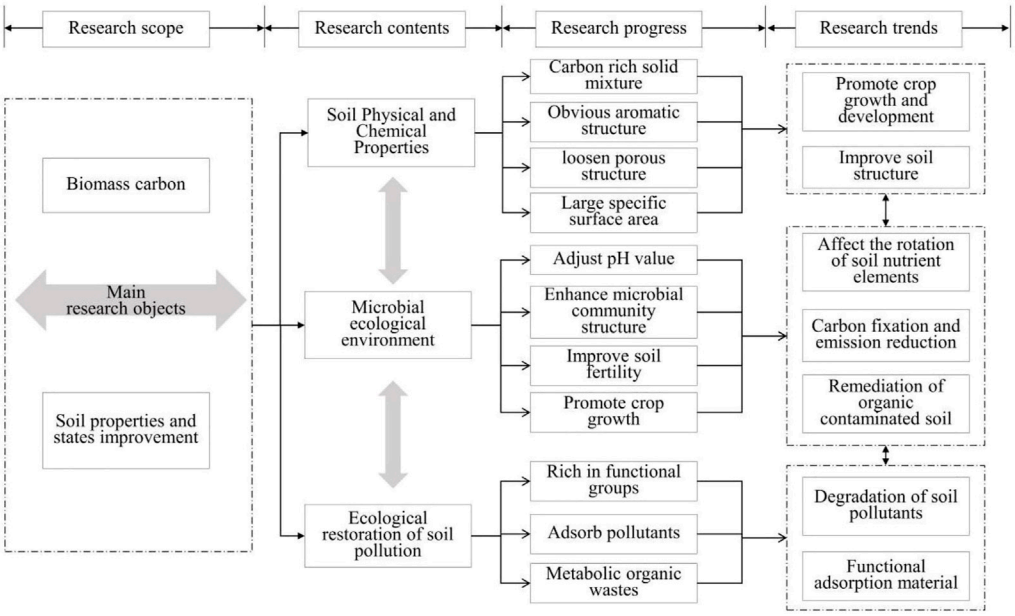

FIGURE 1
Research progress on improving rural soil properties by biomass carbon.

application of biomass carbon with different content, type, proportion to cope with specific soil improvement process and take enduring effect quickly. 2) How does the biomass carbon cope with the soil improvement process under different climate, temperature, humidity conditions, realize the long-term carbon fixation and emission reduction of farmland. 3) During the standardized preparation of biomass carbon, we should pay attention to the process conditions, original sources and relatively stable components to minimize the potential environmental risks of biomass carbon as much as possible. 4) When biomass carbon was applied to soil, unknown organic matter would be released during the aging process, and its long-term harmfulness to the environment needs further attention in a long time. 5) The biomass carbon to soil pollutants should be repair for single contaminant to compound pollutants, from a single biomass carbon to a variety of biomass carbon synergy mechanism researches and an extensive experiment. 6) Biomass carbon can not only be used as soil improvement and pollution remediation, but also as slow release pesticide and fertilizer application in the fields together. 7) From the macroscopic action process of biomass carbon to the microscopic in-depth research process of biomass carbon. To research the free radicals on the surface of biomass carbon material, the functional structure of molecules, the efficiency of action, effectiveness, etc. At the same time, it should be shifted from the research of short-term effects to the comprehensive application and in-depth tracking research of long-term environmental benefits. 8) Biomass carbon has a broad development prospect in the future, 1 combination is further broaden its applications such as in the village planning, such as in village planning, rural community construction, regional carbon reduction and emission reduction, and rural revitalization. So as to continue to expand its research and attention to environmental protection and economic applications.

3.2 Research prospects

The focus as well as objectives of economic and social development in the new era are always to prevent global warming, reduce CO_2 and other greenhouse gas emissions, develop circular and sustainable agriculture, construct green and low-carbon communities, implement rural revitalization strategies, encourage sustainable land spatial patterns, and create ecological civilizations. The capacity to guarantee food security and maintain sustainable development of rural soil are both important goals. Additional researches will concentrate on the potential of biomass carbon for crop growth and development as well as its application to the ecological rehabilitation of rural soil. How to batch and modularize the preparation of different kinds of biomass carbon, and actively invest in the process of rural soil environmental restoration. How to determine appropriate means and pathway of improving soil with biomass carbon according to different types of pollutants, so as to maintain a more stable remediation niche. In the process of further research and

practice, more stable application of multiple biomass carbon in rural soil remediation such as content needs to be emphatically considered in the future application.

3.2.1 Methods and efficiency of biomass carbon for ecological restoration of rural soil

Biomass carbon remediation of organically polluted soil is mainly achieved through adsorption, and the adsorption mechanism mainly includes three ways such as distribution, surface adsorption, pore interception. Due to the increase in the types and quantities of organic pollutants in recent years, the remediation process of soil ecological restoration has become more complex, and the adsorption of pollutants is more difficult. So it is necessary to pay attention to the joint application of multiple adsorption methods. Single biomass carbon is difficult to effectively solve the problem of soil ecological restoration, which needs to be used together with other remediation measures such as organic fertilizer. According to the systematic principle, different types, dosage and ratio of biomass carbon combined use, application conditions, environment and other relevant reference standards for future applications need to be referred to in the future. Biomass carbon which has emerged in recent years shows great adsorption performance for heavy metals due to its rich functional groups and high specific surface area, which can effectively reduce the bioavailability and mobility of heavy metals in soil. For different types of pollutants, how to determine the most appropriate way to improve biomass carbon needs further research, and the adsorption efficiency and action intensity of different types of biomass carbon need to be concerned. It is necessary to turn short-term laboratory experiments into long-term integrated field experiments, systematically consider the remediation and application effects of biomass carbon in different soil types, establish long-term location tracking experiments or isotope experiments. Focusing on the advantages of modified biomass carbon, we need to be cautious about its negative effects in the repair process. During the repair process, potential hazardous substances may be released and there is a risk of secondary pollution at the same time. Under the concept of sustainable development, it is necessary to fully consider the safety of biomass carbon and give full attention to the biomass charcoal degradation ability of soil pollutants, which is of great practical significance to improve the functional characteristics of biomass carbon.

3.2.2 Effects of biomass carbon on crop growth and yield

Biomass carbon affects plant growth and photosynthetic efficiency by improving soil phychemical properties and increasing plant water content. The influence of biomass carbon on soil water retention rate is different due to the content, source, application amount of biomass carbon and other pertinent factors. The activity and retention efficiency of biomass carbon are affected by the preparation method and process. The external surface of biomass carbon has oxidation capacity and can adsorb more metal cations such as Al^{3+}, H^{+}. It contains Ca^{2+}, K^{+}, Mg^{2+}, Na^{+} and other salt ions, which can improve the exchange capacity and frequency of cations in soil. The research found that the effects of biomass carbon on crop growth, development and yield are mainly focused on as follows: Biomass carbon by improving soil phychemical properties and states, increase water content of plants to affect plant growth, photosynthesis efficiency. Biomass carbon to soil water retention effect because of factors such as biomass carbon content, source and find the differences. The influence of biomass carbon on soil water retention rate is different due to the content, source and application amount of biomass carbon. The activity and retention efficiency of biomass carbon are affected by the preparation method and process. The outer surface of biomass carbon has oxidation ability, which can absorb more metal cations such as Al^{3+} and H^{+}. It contains Ca^{2+}, K^{+}, Mg^{2+}, Na^{+} and other salt ions, which can improve the exchange capacity and frequency of cations in soil. This research actually finds that the effects of biomass carbon on crop growth, development and yield are mainly concerned as follows: 1) The multi-microporous structure of biomass carbon provides the content of bacteria in the soil which is conducive to growth and enriches the growth environment. 2) Enhancing soil available nutrients content such as porosity, water retention, pH, salinity, electrical conductivity (EC), cation exchange capacity (CEC) and other physicochemical properties. 3) Biomass carbon contains rich trace elements such as N, P, K which can effectively exchange with metal cations in the soil to provide more growth elements, etc. 4) Impact on soil carbon cycle, carbon sequestration and emission reduction: carbon sequestration and storage in soil can improve soil structure, nutrient content and reduce greenhouse gas emissions such as CO_2. 5) To promote the growth of seed germination plants and increase crop yield. It is noteworthy that the porous structure and alkalinity of biomass carbon play an important role in improving the properties of acid soil and increasing crop yield. However, biomass carbon with high soil pH value will lead to poor crop growth. Tar and resin which are generated in the preparation process will inhibit crop growth. In further research, the focus should be on the pollution recovery of large-scale application of biomass carbon in the ecosystem, the adsorption and transport of natural organic matter on biomass carbon. How to maintain the same growth efficiency and improve crop yield in soil crops with different environmental conditions such as pH, temperature, etc.

In summary, in order to better comprehend how biomass carbon affects soil quality, several large-scale and long-term

field application research involving biomass carbon should be undertaken in the future. It must emphasize the breadth, depth, or application of development. Pay sincere attention to how it is used in the processes of improving the soil and eradicating pollution, as well as the long-term, short-term effects (both positive and negative effects). The latest research results will be widely used in crop practice.

Author contributions

YY was in charge of designing the experiments and writing the manuscript; YY were in charge of revising the manuscript; YY was in charge of project administration.

Conflict of interest

The author declares that the research was conducted in the absence of any commercial or financial relationships that could be construed as a potential conflict of interest.

Publisher's note

All claims expressed in this article are solely those of the authors and do not necessarily represent those of their affiliated organizations, or those of the publisher, the editors and the reviewers. Any product that may be evaluated in this article, or claim that may be made by its manufacturer, is not guaranteed or endorsed by the publisher.

References

Ahmad, M., Rajapaksha, A. U., Lim, J. E., Zhang, M., Bolan, N., Mohan, D., et al. (2014). Biochar as a sorbent for contaminant management in soil and water: A review. *Chemosphere* 99, 19–33. doi:10.1016/j.chemosphere.2013.10.071

Ahmed, M., Johir, M. A. H., Zhou, J., Ngo, H. H., Nghiem, L. D., Richardson, C., et al. (2019). Activated carbon preparation from biomass feedstock: Clean production and carbon dioxide adsorption. *J. Clean. Prod.* 225, 405–413. doi:10.1016/j.jclepro.2019.03.342

Akhtar, S. S., Li, G., Andersen, M. N., and Liu, F. (2014). Biochar enhances yield and quality of tomato under reduced irrigation. *Agric. Water Manag.* 138, 37–44. doi:10.1016/j.agwat.2014.02.016

Ali, S., Rizwan, M., Qayyum, M. F., Ok, Y. S., Ibrahim, M., Riaz, M., et al. (2017). Biochar soil amendment on alleviation of drought and salt stress in plants: A critical review. *Environ. Sci. Pollut. Res.* Res24, 12700–12712. doi:10.1007/s11356-017-8904-x

Aller, M. F. (2016). Biochar properties: Transport, fate, and impact. *Crit. Rev. Environ. Sci. Technol.* 46 (14-15), 1183–1296. doi:10.1080/10643389.2016.1212368

Asada, T., Ishihara, S., Yamane, T., Toba, A., Yamada, A., and Oikawa, K. (2002). Science of bamboo charcoal: Study on carbonizing temperature of bamboo charcoal and removal capability of harmful gases. *J. Health Sci.* 48 (6), 473–479. doi:10.1248/jhs.48.473

Beesley, L., Moreno-Jimenez, E., Gomez-Eyles, J., Harris, E., Robinson, B., and Sizmur, T. (2011). A review of biochars' potential role in the remediation, revegetation and restoration of contaminated soils. *Environ. Pollut.* 159 (12), 3269–3282. doi:10.1016/j.envpol.2011.07.023

Bird, M. I., Moyo, C., Veenendaal, E. M., Lloyd, J., and Frost, P. (1999). Stability of elemental carbon in a savanna soil. *Glob. Biogeochem. Cycles* 13 (4), 923–932. doi:10.1029/1999GB900067

Brodowski, S., Amelung, W., Haumaier, L., Abetz, C., and Zech, W. (2005). Morphological and chemical properties of black carbon in physical soil fractions as revealed by scanning electron microscopy and energy-dispersive X-ray spectroscopy. *Geoderma* 128 (1), 116–129. doi:10.1016/j.geoderma.2004.12.019

Cantrell, K. B., Hunt, P. G., Uchimiya, M., Novak, J. M., and Ro, K. S. (2012). Impact of pyrolysis temperature and manure source on physicochemical characteristics of biochar. *Bioresour. Technol.* 107, 419–428. doi:10.1016/j.biortech.2011.11.084

Cao, T. T., Zhou, D.-D., Wang, X.-D., and Cui, C. (2022). Photocatalytic degradation of bisphenol A over Co-BiOCl/biochar hybrid catalysts: Properties, efficiency and mechanism. *J. Mol. Liq.* 362, 119622. doi:10.1016/j.molliq.2022.119622

Cayuela, M. L., Van Zwieten, L., Singh, B. R., Jeffery, S., Roig, A., and Sanchez-Monedero, M. (2014). Biochar's role in mitigating soil nitrous oxide emissions: A review and meta-analysis. *Agric. Ecosyst. Environ.* 191, 5–16. doi:10.1016/j.agee.2013.10.009

Chen F, F. J., Xia, H. J., and Liu, F. D., (2022). Characteristics of biochar and its effects and mechanism on soil properties. *J. Environ. Eng. Technol.* 12 (1), 161–172. doi:10.12153/j.issn.1674-991X.20210067

Chen, W., Zhang, W., and Meng, J. (2013). Advances and prospects in research of biochar utilization in agriculture. *Sci. Agric. Sin.* 46 (16), 3324–3333. doi:10.3864/j.issn.0578-1752.2013.16.003

Chen Y, Y., Syed-Hassan, S. S. A., Li, Q., Deng, Z., Hu, X., Xu, J., et al. (2022). Effects of temperature and aspect ratio on heterogeneity of the biochar from pyrolysis of biomass pellet. *Fuel Process. Technol.* 235, 107366. doi:10.1016/j.fuproc.2022.107366

Cui, X., Wang, J., Wang, X., Khan, M. B., Lu, M., Khan, K. Y., et al. (2022). Biochar from constructed wetland biomass waste: A review of its potential and challenges. *Chemosphere* 287, 132259. doi:10.1016/j.chemosphere.2021.132259

Dai, X., Boutton, T. W., Glaser, B., Ansleyc, R. J., and Zech, W. (2005). Black carbon in a temperate mixed-grass savanna. *Soil Biol. Biochem.* 37, 1879–1881. doi:10.1016/j.soilbio.2005.02.021

Deluca, T. H., Mac Kenziea, M. D., and Gundale, M. J., (2006). Wildfire-produced charcoal directly influences nitrogen cycling in ponderosa pine forests. *Soil Sci. Soc. Am. J.* 70 (2), 448–453. doi:10.2136/sssaj2005.0096

Dey, A., Singh, R., and Purkait, M. K. (2014). Cobalt ferrite nanoparticles aggregated schwertmannite: A novel adsorbent for the efficient removal of arsenic. *J. Water Process Eng.* 3, 1–9. doi:10.1016/j.jwpe.2014.07.002

El Rasafi, T., and Haddioui, A. (2020). Growth, survival and biomass production of barley in a polluted mine soil amended with biochar and animal manure. *Bull. Environ. Contam. Toxicol.* 105, 155–165. doi:10.1007/s00128-020-02914-w

Erin, M. K., Katherine, J. S., Richard, E. F., and Siciliano, S. D. (2017). Petroleum hydrocarbon remediation in frozen soil using a meat and bonemeal biochar plus fertilizer. *Chemosphere* 173, 330–339. doi:10.1016/j.chemosphere.2017.01.016

Goldberg, E. D. (1985). "Black carbon in the environment," in *Properties and distribution* (New York: John Wiely).

Harter, J., Krause, H. M., Schuettler, S., Ruser, R., Fromme, M., Scholten, T., et al. (2014). Linking N2O emissions from biochar-amended soil to the structure and function of the N-cycling microbial community. *ISME J.* 8 (3), 660–674. doi:10.1038/ismej.2013.160

He, M., Xiong, X., Wang, L., Hou, D., Bolan, N. S., Ok, Y. S., et al. (2021). A critical review on performance indicators for evaluating soil biota and soil health of biochar-amended soils. *J. Hazard. Mater.* 414, 125378. doi:10.1016/j.jhazmat.2021.125378

Hossain, M. K., Strezov, V., Chan, K. Y., Ziolkowski, A., and Nelson, P. F. (2011). Influence of pyrolysis temperature on production and nutrient properties of wastewater sludge biochar. *J. Environ. Manag.* 92 (1), 223–228. doi:10.1016/j.jenvman.2010.09.008

Inyang, M., Gao, B., Yao, Y., Xue, Y., Zimmerman, A., Mosa, A., et al. (2016). A review of biochar as a low-cost adsorbent for aqueous heavy metal removal. *Crit. Rev. Environ. Sci. Technol.* 46 (4), 406–433. doi:10.1080/10643389.2015.1096880

Jeffery, S., Verheijen, F., Van Der Velde, M., and Bastos, A. (2011). A quantitative review of the effects of biochar application to soils on crop productivity using meta-analysis. *Agric. Ecosyst. Environ.* 144 (1), 175–187. doi:10.1016/j.agee.2011.08.015

Jiang, Q., Liu, J., and Zhang, Y. (2017). Research progress on improvement soil by Biochar. *Gansu Agr.Sci.and Techn* 2017 (06), 68–71. doi:10.3969/j.issn.1001-1463.2017.06.023

Keiluweit, N. P. S., Johnson, M. G., and Kleber, M. (2010). Dynamic molecular structure of plant biomass-derived black carbon (biochar). *Environ. Sci. Technol.* 44 (4), 1247–1253. doi:10.1021/es9031419

Kong, S., Yao, X., and Zhang, J., (2015). Review of characteristics of biochar and research progress of its applications. *Ecol. Environ. Sci.* 24 (4), 716–723. doi:10.16258/j.cnki.1674-5906.2015.04.025

Lehmann, J., Gaunt, J., and Rondon, M. (2006). Bio-char sequestration in terrestrial ecosystems – a review. *Mitig. Adapt. Strat. Glob. Change* 11 (2), 403–427. doi:10.1007/s11027-005-9006-5

Lehmann, J., Skjemstad, J., Sohi, S., Carter, J., Barson, M., Falloon, P., et al. (2008). Australian climate–carbon cycle feedback reduced by soil black carbon. *Nat. Geosci.* 1 (12), 832–835. doi:10.1038/ngeo358

Lehmann, J., Pereira da Silva, J., Steiner, C., Nehls, T., Zech, W., and Glaser, B. (2003). Nutrient availability and leaching in an archaeological anthrosol and a ferralsol of the central Amazon basin: Fertilizer, manure and charcoal amendments. *Plant Soil249* 249, 343–357. doi:10.1023/A:1022833116184

Liu, G. J., Zhou, D. D., and Li, L. N., (2020). Effects of citric acid on the stability of immobilizaed heavy metals by biochar in contaminatedsoil. *Environ. Chem.* 39 (2), 43–351. doi:10.7524/j.Issn.0254-6108.2019021906

Liu, X., Zhang, A., Ji, C., Joseph, S., Bian, R., Li, L., et al. (2013). Biochar's effect on crop productivity and the dependence on experimental conditions—A meta-analysis of literature data. *Plant Soil* 373 (1-2), 583–594. doi:10.1007/s11104-013-1806-x

Liu, Y., Liu, W., Wu, W., Zhong, Z. K., and Chen, Y. X. (2009). Environmental behavior and effect of biomass derived black carbon in soil A review. *Chin. J. Appl. Ecol.* 20 (4), 977–982. doi:10.13287/j.1001-9332.2009.0124

Nelissen, V., Rütting, T., Huygens, D., Staelens, J., Ruysschaert, G., and Boeckx, P. (2012). Maize biochars accelerate short-term soil nitrogen dynamics in a loamy sand soil. *Soil Biol. Biochem.* 55, 20–27. doi:10.1016/j.soilbio.2012.05.019

Ogura, T., Date, Y., Masukujane, M., Coetzee, T., Akashi, K., and Kikuchi, J. (2016). Improvement of physical, chemical and biological properties of aridisol from Botswana by the incorporation of torrefied biomass. *Sci. Rep.* 6, 28011. doi:10.1038/srep28011

Raveendran, K., Ganesh, A., and Khilar, K. C. (1995). Influence of mineral matter on biomass pyrolysis characteristics. *Fuel* 74 (12), 1812–1822. doi:10.1016/0016-2361(95)80013-8

Raza, S. T., Zhu, Y., Wu, J., Rene, E. R., Ali, Z., Feyissa, A., et al. (2022). Different ratios of canna indica and maize–vermicompost as biofertilizers to improve soil fertility and plant growth: A case study from southwest China. *Environ. Res.* 215, 114374. doi:10.1016/j.envres.2022.114374

Rego, F., Soares Dias, A. P., Casquilho, M., Rosa, F. C., and Rodrigues, A. (2019). Fast determination of lignocellulosic composition of poplar biomass by thermogravimetry. *Biomass Bioenergy* 122, 375–380. doi:10.1016/j.biombioe.2019.01.037

Robertso, F. A., and Thorbum, P. J. (2006). Management of sugarcane harvest residues: Consequences for soil carbon and nitrogen. *Soil Res.* 45 (1), 13–23. doi:10.1071/sr06080

Schmidt, M. W. I., and Noack, A. G. (2000). Black carbon in soils and sediments: Analysis, distribution, implications, and current challenges. *Glob. Biogeochem. Cycles* 14 (3), 777–793. doi:10.1029/1999gb001208

Simone, E. K., Kevin, J. F., and Mathew, E. D. (2009). Effect of charcoal quantity on microbial biomass and activity in temperate soils. *Soil Sci. Soc. Am. Joumal* 73 (4), 1173–1181. doi:10.2136/sssaj2008.0232

Song, S., Xu, J., and Song, X., (2021). Research progress of biochar remediation of petroleum contaminated soil. *Appl. Chem. Ind.* 50 (12), 3402–3406+3410. doi:10.16581/j.cnki.issn1671-3206.20210928.002

Spokas, K. A., Cantrell, K. B., Novak, J. M., Archer, D. W., Ippolito, J. A., Collins, H. P., et al. (2012). Biochar: A synthesis of its agronomic impact beyond carbon sequestration. *J. Environ. Qual.* 41 (4), 973–989. doi:10.2134/jeq2011.0069

Steiner, C., Teixeira, W. G., Lehmann, J., Nehls, T., de Macedo, J. L. V., Blum, W. E. H., et al. (2007). Long term effects of manure, charcoal, and mineral: Fertilization on crop production and fertility on a highly weathered central amazonian upland soil. *Plant Soil* 291, 275–290. doi:10.1007/s11104-007-9193-9

Taghizadeh Toosi, A., Clough, T. J., Sherlock, R., and Condron, L. M. (2012). Biochar adsorbed ammonia is bioavailable. *Plant Soil* 350 (1/2), 57–69. doi:10.1007/s11104-011-0870-3

Troy, S. M., Lawlor, P. Q., O'Flynn, C. J., and Healy, M. G. (2013). Impact of biochar addition to soil on greenhouse gas emissions following pig manure application. *Soil Biol. Biochem.* 60 (60), 173–181. doi:10.1016/j.soilbio.2013.01.019

Wang, J., Wang, Y., Wang, J., Du, G., Khan, K. Y., Song, Y., et al. (2022). Comparison of cadmium adsorption by hydrochar and pyrochar derived from Napier grass. *Chemosphere* 308 (3), 136389. doi:10.1016/j.chemosphere.2022.136389

Wang, L., Ding, S., and Liu, G. (2014). Progress of the research on biochars' influence on soil reclaimarion. *soil fertilizer Sci. china* (03). doi:10.11838/sfsc.20140301

Wang, T., Duan, J. D., and Wang, J. X., (2020). Research progress on remediation effect of biochar on heavy metals in soil. *Hunan Journalof Ecol. Sci.* 7 (3), 55–65. doi:10.3969/j.issn.1001-3601.2020.04.032

Wang, Z., Li, Y., and Xu, Z., (2019). Research progresses in effects of biochar on soil physiochemical properties and nitrogen transformation. *Soils* 51 (05), 835–842. doi:10.13758/j.cnki.tr.2019.05.001

Weng, Z. H., Van Zwieten, L., Singh, B. R., Tavakkoli, E., Joseph, S., and Macdonald, L. M., (2017). Biochar built soil carbon over a decade by stabilizing rhizodeposits. *Nat. Clim. Change* 7, 371–376. doi:10.1038/nclimate3276

Wu, J. (2020). *The remediation of as and Cd co-contamination by a novel calcium-based magnetic biochar and involving mechanism*. China: Zhe Jiang University. doi:10.27461/d.cnki.gzjdx.2020.001799

Wu, Y., XuG.and Lü, Y., (2014). Effects of biochar amendment on soil physical and chemical properties: Current status and knowledgegaps. *Adv. Earth Sci.* 29 (1), 68–79. doi:10.11867/j.issn.1001-8166.2014.01.0068

Xu, D. M., Fu, R. B., Liu, H. Q., and Guo, X. P. (2020). Current knowledge from heavy metal pollution in Chinese smelter contaminated soils, health risk implications and associated remediation progress in recent decades: A critical review. *J. Clean. Prod.* 286, 124989. doi:10.1016/j.jclepro.2020.124989

Yu, M. (2021). *Charosphere effects of biochar and its associated key processes of soil nitrogen transformation*. China: Zhe Jiang University. doi:10.27461/d.cnki.gzjdx.2021.000439

Yu, M., Meng, J., Yu, L., Su, W., Afzal, M., Li, Y., et al. (2019). Changes in nitrogen related functional genes along soil pH, C and nutrient gradients in the charosphere. *Sci. Total Environ.* 650, 626–632. doi:10.1016/j.scitotenv.2018.08.372

Zhang, B., Chen, L., and Han, L., (2021). Review on the remediation of heavy metal contaminated soil using modified biochar. *Environ. Chem.* 40 (9), 2693–2703. doi:10.7524/j.issn.0254-6108.2020122302

Zhang, D. (2017). *Effect of biochar amendment on crop Productivity,Greenhouse gases emission and soil nutrients transformation*. Nanjing, China: NanJing Agricultural University. Available at: https://kns.cnki.net/KCMS/detail/detail.aspx?dbname=CDFDLAST2019&filename=1019154304.

Zhao, Z., Wang, X., and Li, H., (2021). Slow-release property and soil remediation mechanism of biochar-based fertilizers. *J. Plant Nutr. Fertilizers* 27 (05), 886–897. doi:10.11674/zwyf.20472

Zhou, W. Y., Liang, H. T., Lu, Y. Y., Xu, H., and Jiao, Y. (2021). Adsorption of gold from waste mobile phones by biochar and activated carbon in gold iodized solution. *Waste Manag.* 120, 530–537. doi:10.1016/j.wasman.2020.10.017

frontiers | Frontiers in Chemistry

TYPE Mini Review
PUBLISHED 02 December 2022
DOI 10.3389/fchem.2022.1084089

OPEN ACCESS

EDITED BY
Hu Li,
Guizhou University, China

REVIEWED BY
Qiuyun Zhang,
Anshun University, China
Yang Wei,
Anshun University, China
Xiufang Cui,
Harbin Engineering University, China

*CORRESPONDENCE
Can Li,
lican790108@163.com

SPECIALTY SECTION
This article was submitted to Green and Sustainable Chemistry, a section of the journal Frontiers in Chemistry

RECEIVED 30 October 2022
ACCEPTED 16 November 2022
PUBLISHED 02 December 2022

CITATION
Liu X, Luo H, Yu D, Pei Z, Zhang Z and Li C (2022), The development of novel ionic liquid-based solid catalysts and the conversion of 5-hydroxymethylfurfural from lignocellulosic biomass. *Front. Chem.* 10:1084089. doi: 10.3389/fchem.2022.1084089

The development of novel ionic liquid-based solid catalysts and the conversion of 5-hydroxymethylfurfural from lignocellulosic biomass

Xiaofang Liu, Hangyu Luo, Dayong Yu, Zhengfei Pei, Zhuangzhuang Zhang and Can Li*

Guizhou Provincial Key Laboratory for Rare Animal and Economic Insects of the Mountainous Region, College of Biology and Environmental Engineering, Guiyang University, Guiyang, China

Ionic liquids have attracted attention due to their excellent properties and potential for use as co-solvents, solvents, co-catalysts, catalysts, and as other chemical reagents. This mini-review focuses on the properties and structures of ionic liquids, the pretreatment of lignocellulosic biomass, and the development of novel ionic liquid-based solid catalysts for cellulose and hemicellulose derived HMF production.

KEYWORDS

5-hydroxymethylfurfural, ionic liquids, lignocellulosic biomass, cellulose, hemicellulose

Introduction

As reported, lignocellulosic biomass is abundant (Zabed et al., 2017), has carbon–neutral properties, and is a sustainable and non-edible green feedstock (Hoang et al., 2021) that is a potential source material for the production of valuable biofuels and chemicals. The percentage of each constituent is determined by the wood/plant species, but, in general, is composed of cellulose (40%–50%), hemicellulose (25%–30%), and lignin (15%–20%), as well as small amounts of pectin, nitrogen compounds, and inorganic compounds (Kumar A. A. et al., 2020). The compound 5-hydroxymethylfurfural (HMF) is known as the "sleeping giant" of renewable intermediate chemicals, with derivatives that can be used in applications such as pesticides, medicines, and biofuel chemistry (Osatiashtiani et al., 2015; Le et al., 2022; Nasrollahzadeh et al., 2022). With current energy shortages and environmental pollution, it is critical that we seek green, sustainable, and alternative solutions.

Properties and structures of ionic liquids

Ethyl ammonium nitrate, which is a liquid at ambient temperature and pressure, was the first described ionic liquid (IL) in 1914 (Walden, 1914; Angell et al., 2012). ILs have been widely identified as green substitutes for organic solvents based on their near-zero vapor pressures, high thermal stability and devisable polarity, hydrophobicity, and excellent capacity as solvents through modification of cations and anions (Zhang et al., 2014; Amarasekara, 2016). To the best of our knowledge, whether ILs can be recognized as green depends on approaches to synthesis and internal physico-chemical properties.

An IL can also be regarded as a salt, depending on whether its melting point is below 100°C, as salts consist of large and asymmetrical ions that typically have lower melting points (Berthod et al., 2017). Generally, the melting temperature, Tm, decreases with increased size, anisotropy, and internal flexibility of the ions; however, Tm increases with enhanced alkyl chain interaction (Weingärtner, 2008). Viscosity is one of the most significant material properties of ILs. High values for viscosity limit applications of ILs in various areas, since it reduces rate of reaction and molecule diffusion by forming a circulation barrier (Weingärtner, 2008). Tests of the thermal stability of ILs have shown that decomposition happens slowly at nearly 200°C (Berthod et al., 2017) in a process that hinges on the unique cation and corresponding anion association. The thermal stability of the imidazolium salts, along with the growth of the number of alkyl substitutions, has been demonstrated (Ngo et al., 2000). ILs involving linear side chains are more thermally stable than comparable branched monocationic ones (Xue et al., 2016). Halide anions can also decrease thermal stability to a certain extent. Generally, cations account for viscosity, melting point, and electrochemical stability, whereas anions are responsible for hydrogen bonding and miscibility with other solvents or water (Puripat et al., 2016).

The first-generation ILs defined dialkylimidazolium and alkylpyridinium as cations and metal halide ($FeCl_4^-$ and $Al_2Cl_7^-$) as anions sensitive to water and air. Cations of quaternary ammonium and phosphonium containing dialkylimidazolium, alkylpyridinium, ammonium, and phosphonium, along with the classic anions tetrafluoroborate (BF_4^-) and hexafluorophosphate (PF_6^-) made up the second generation of ILs, which are not sensitive to either water or air. Unfortunately, slow hydrolysis of these anions with increased temperature leads to the production of hazardous and ecotoxic hydrogen fluoride (HF). From a green, sustainability perspective, second-generation ILs also show poor biodegradability, and are neither cost-effective nor green (Deetlefs and Seddon, 2010). Third-generation ILs are biodegradable cations and anions, and natural compounds containing choline, amino acids, or carbohydrates have been developed for IL production (Egorova et al., 2017). Widespread commercial application of ILs in various fields has been studied on account of these attributes (Figure 1).

Because of the above-mentioned characteristics, ILs have been identified as excellent solvents and catalysts for the synthesis of HMF from biomass and associated derivatives (Jiang et al., 2016; Li et al., 2018). Among IL cations, the mono-imidazole type has exhibited excellent performance. To facilitate the interaction between ILs and biomass or carbohydrates, di-/tri-cationic ILs with higher density and more hydrogen bonding were developed (Marullo et al., 2019; Rathod et al., 2019; Prasad et al., 2021).

Catalytic transformation of lignocellulosic biomass in IL-based catalysts

Lignocellulosic biomass pretreatment is a significant process in the production of biofuels and value-added chemicals, the degradation of which is hindered by chemical properties, chemical structure, and microscopic complexity. Therefore, new approaches and reaction parameters are determined by attributes such as the degree of crystallization and polymerization of cellulose and the percentage of hemicellulose and lignin (Mood et al., 2013; Abraham et al., 2020) (Figure 2). Various ILs have been investigated to determine their effectiveness in lignocellulose dissolution and degradation to main compounds (Bian et al., 2014), although without the desired target HMF yield due to the multiple steps necessary to isolate HMF from raw materials.

Kahani et al. (2017) synthesized N-allyl-N-methylmorpholinium acetate ([AMMorph][Ac]) and successfully introduced it for the pretreatment of rice straw. Compared to the most efficient solvent imidazolium liquids, the morpholinium liquids are less toxic and less expensive, while providing glucose yields of 98.4 ± 1.3% using mixtures of [AMMorph][Ac]-DMSO (70:30, v/v) and N-methylmorpholine-N-oxide (NMMO), [Bmim][Ac], and NaOH at 120°C. Furthermore, using DMSO as a co-solvent could minimize IL usage and enhance pretreatment efficiency by reducing viscosity (Kahani et al., 2017).

Use of a novel integrated $-SO_3H$ functionalized IL catalyst [IL-SO_3H][Cl] and nickel sulfate ($NiSO_4.6H_2O$) co-catalyst resulted in a maximum glucose conversion of 99.92%, with 21.80% HMF yield when incubated at 175°C for 1.5 h in the aqueous phase (Kumar K. et al., 2020). According to the pseudo-first-order kinetic equations, the activation energy (E_a) and pre-exponential factor (A) was confirmed to be 47.45 kJ/mol and 7.9×10^3 min^{-1}, respectively, for conversion of glucose into HMF. The research demonstrated an effective synergistic effect of the IL catalyst and Lewis acidic co-catalyst in clean synthesis of HMF from waste biomass derived glucose, providing a promising pathway for the preparation of vital platform chemicals and renewable fuels.

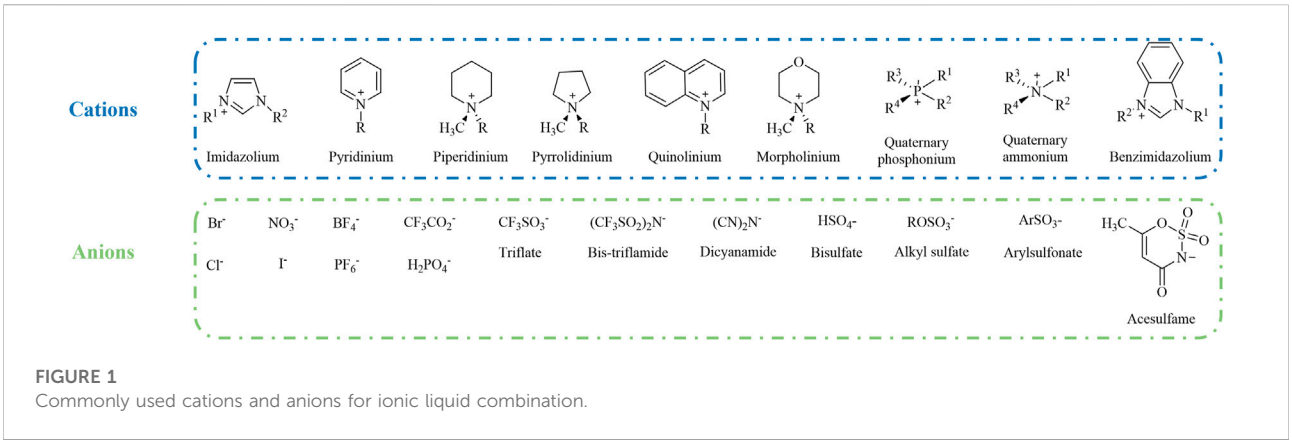

FIGURE 1
Commonly used cations and anions for ionic liquid combination.

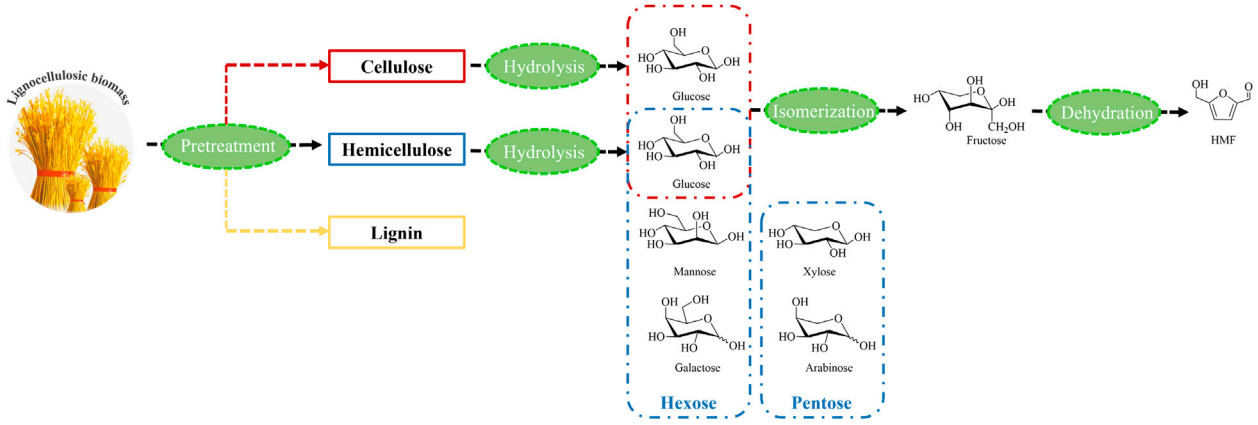

FIGURE 2
Different components of lignocellulosic biomass and the degradations.

Conversion of cellulose with IL-based catalysts

The synthesis of HMF derived from cellulose involves several steps: depolymerization, hydrolysis, isomerization and, ultimately, dehydration (Tyufekchiev et al., 2018; Zhang et al., 2018a; Zhang et al., 2018b; Naz et al., 2021). For different processes, catalyst properties vary depending on the reactions.

Excessive Brønsted acid or Lewis acid can accelerate the side reactions that produce by-products. Therefore, the "tailor-made" development of satisfactory catalyst processing with the appropriate ratio of Lewis acid to Brønsted acid is crucial for increasing HMF yield. In addition, allylimidazole-type ILs have strong advantages in cellulose dissolution (Liu et al., 2012).

At the beginning of the instantiation phase, metallic ILs (i.e., $Cr([PSMIM]HSO_4)_3$ and $CuCr([PSMIM]SO_4)_5$) were designed and applied to the cellulose-HMF system (Zhou et al., 2013). $Cr([PSMIM]HSO_4)_3$ demonstrated higher catalytic performance in the production of HMF, with 53% yield ascribed to the bifunctionality and higher Brønsted acidity at 120°C.

Liu et al. (2022) prepared a series of reactions with different proportions of Brønsted acid and Lewis acid ILs for the degradation of cellulose to produce HMF. Among these, $[(HSO_3\text{-}P)_2im]Cl{\cdot}ZnCl_2$ exhibited excellent catalytic performance, with an HMF yield of 65.66% at 140°C for 3 h. This study facilitated directional optimization of the catalyst. The quantum chemical calculation method for molecular design was used to predict the catalytic effect (different ratios of Brønsted acid to Lewis acid) and investigate the catalytic mechanism. Therefore, the solvation model density (SMD) model was proposed in combination with Frontier orbital theory. In addition, cellulose degradation experiments were performed to verify the simulation results and inform discussion of the catalytic mechanism (Liu et al., 2022).

Conversion of hemicellulose by IL-based catalysts

As the second most predominant component of lignocellulosic biomass, hemicellulose is composed of pentoses like xylose, arabinose, and hexose, including glucose, mannose, galactose, and the amorphous polymer xylan (Ruiz et al., 2013). There are few developments in the production of HMF derived from mannose and galactose. Researchers demonstrated that mannose is predominantly isomerized to fructose, which can be efficiently converted into HMF, while galactose primarily isomerizes to tagatose, which is the C-4 epimer of fructose and weaker than fructose in yielding HMF (van Putten et al., 2013).

When lignocellulosic biomass was employed as raw material, cellulose with higher HMF yield than hemicellulose was preferentially chosen for the synthesis of HMF, as the research was aimed at improving the conversion efficiency of cellulose (Menegazzo et al., 2018). Considering the complex components involved, the conversion conditions for HMF are difficult to control.

Conclusion and outlook

HMF yield close to 100% will eventually be achieved by adjusting the approach to isolation of the compound from feedstock and optimizing IL-based catalyst reaction conditions. This cost-effective, green, sustainable catalyst system, which inhibits by-products, is easily functionalized, and has no adverse environmental impact, will lead to significant advances in future industrial-scale HMF production. Density functional theory (DFT) and molecular dynamics should be applied in biomass conversion to aid in the development of reliable reaction pathways.

Author contributions

XL conceived the article and discussed the outline. XL wrote the manuscript. HL, DY, ZP, and ZZ made preliminary revisions to the manuscript. CL and XL coordinated the content of the manuscript and made detailed revisions.

Funding

This work was financially supported by the Technical Talent Support Program of Guizhou Education Department ([2022]087), the Guizhou Provincial Key Laboratory for Rare Animal and Economic Insects of the Mountainous Region ([2018]5102), the National Natural Science Foundation of China (22065004), and the Guizhou Science and Technology Foundation ([2020]1Y054).

Conflict of interest

The authors declare that the research was conducted in the absence of any commercial or financial relationships that could be construed as a potential conflict of interest.

The handling editor declared a past co-authorship with the authors XL and CL.

Publisher's note

References

Abraham, A., Mathew, A. K., Park, H., Choi, O., Sindhu, R., Parameswaran, B., et al. (2020). Pretreatment strategies for enhanced biogas production from lignocellulosic biomass. *Bioresour. Technol.* 301, 122725. doi:10.1016/j.biortech.2019.122725

Amarasekara, A. S. (2016). Acidic ionic liquids. *Chem. Rev.* 116, 6133–6183. doi:10.1021/acs.chemrev.5b00763

Angell, C. A., Ansari, Y., and Zhao, Z. (2012). Ionic liquids: Past, present and future. *Faraday Discuss.* 154, 9–27. doi:10.1039/C1FD00112D

Berthod, A., Ruiz-Ángel, M. J., and Carda-Broch, S. (2017). Recent advances on ionic liquid uses in separation techniques. *J. Chromatogr. A* 1559, 2–16. doi:10.1016/j.chroma.2017.09.044

Bian, J., Peng, F., Peng, X. P., Xiao, X., Peng, P., Xu, F., et al. (2014). Effect of [Emim]Ac pretreatment on the structure and enzymatic hydrolysis of sugarcane bagasse cellulose. *Carbohydr. Polym.* 100, 211–217. doi:10.1016/j.carbpol.2013.02.059

Deetlefs, M., and Seddon, K. R. (2010). Assessing the greenness of some typical laboratory ionic liquid preparations. *Green Chem.* 12, 17–30. doi:10.1039/B915049H

Egorova, K. S., Gordeev, E. G., and Ananikov, V. P. (2017). Biological activity of ionic liquids and their applicationin pharmaceutics and medicine. *Chem. Rev.* 117, 7132–7189. doi:10.1021/acs.chemrev.6b00562

Hoang, A. T., Ong, H. C., Fattah, I. M. R., Chong, C. T., Cheng, C. K., Sakthivel, R., et al. (2021). Progress on the lignocellulosic biomass pyrolysis for biofuel production toward environmental sustainability. *Fuel Process. Technol.* 223, 106997. doi:10.1016/j.fuproc.2021.106997

Jiang, Y., Zang, H., Han, S., Yan, B., Yu, S., and Cheng, B. (2016). Direct conversion of chitosan to 5-hydroxymethylfurfural in water using Brønsted-Lewis acidic ionic liquids as catalysts. *RSC Adv.* 6, 103774–103781. doi:10.1039/c6ra21289a

Kahani, S., Shafiei, M., Abdolmaleki, A., and Karimi, K. (2017). Enhancement of ethanol production by novel morpholinium ionic liquids. *J. Clean. Prod.* 168, 952–962. doi:10.1016/j.jclepro.2017.09.008

Kumar, A. A., Rapoport, A., Kunze, G., Kumar, S., Singh, D., Singh, B., et al. (2020). Multifarious pretreatment strategies for the lignocellulosic substrates for the generation of renewable and sustainable biofuels: A review. *Renew. Energy* 160, 1228–1252. doi:10.1016/j.renene.2020.07.031

Kumar, K., Pathak, S., and Upadhyayula, S. (2020). 2nd generation biomass derived glucose conversion to 5-hydroxymethylfurfural and levulinic acid catalyzed by ionic liquid and transition metal sulfate: Elucidation of kinetics and mechanism. *J. Clean. Prod.* 256, 120292. doi:10.1016/j.jclepro.2020.120292

Le, H. S., Said, Z., Pham, M. T., Le, T. H., Veza, I., Nguyen, V. N., et al. (2022). Production of HMF and DMF biofuel from carbohydrates through catalytic pathways as a sustainable strategy for the future energy sector. *Fuel* 324, 124474. doi:10.1016/j.fuel.2022.124474

Li, X. C., Zhang, Y. Y., Xia, Q. N., Liu, X. H., Peng, K. H., Yang, S. H., et al. (2018). Acid-free conversion of cellulose to 5-hydroxymethyl-furfural catalyzed by hot seawater. *Ind. Eng. Chem. Res.* 57, 3545–3553. doi:10.1021/acs.iecr.8b00443

Liu, D. T., Xia, K. F., Cai, W. H., Yang, R. D., Wang, L. Q., and Wang, B. (2012). Investigations about dissolution of cellulose in the 1-allyl-3-alkylimidazolium chloride ionic liquids. *Carbohydr. Polym.* 87 (2), 1058–1064. doi:10.1016/j.carbpol.2011.08.026

Liu, S. Y., Zheng, W. W., Wen, X. F., Fang, Z. Q., Li, H., Li, C. L., et al. (2022). Molecular design and experimental study of cellulose conversion to 5-hydroxymethylfurfural catalyzed by different ratios of Brønsted/Lewis acid ionic liquids. *Carbohydr. Polym.* 278, 118936. doi:10.1016/j.carbpol.2021.118936

Marullo, S., Rizzo, C., and Anna, F. D'. (2019). Task-specific organic salts and ionic liquids binary mixtures: A combination to obtain 5-hydroxymethylfurfural from carbohydrates. *Front. Chem.* 7, 134–215. doi:10.3389/fchem.2019.00134

Menegazzo, F., Ghedini, E., and Signoretto, M. (2018). 5-Hydroxymethylfurfural (HMF) production from real biomasses. *Molecules* 23 (9), 2201. doi:10.3390/molecules23092201

Mood, S. H., Golfeshan, A. H., Tabatabaei, M., Jouzani, G. S., Najafi, G. H., Gholami, M., et al. (2013). Lignocellulosic biomass to bioethanol, a comprehensive review with a focus on pretreatment. *Renew. Sustain. Energy Rev.* 27, 77–93. doi:10.1016/j.rser.2013.06.033

Nasrollahzadeh, M., Nezafat, Z., Momenbeik, F., and Orooji, Y. (2022). Polystyrene immobilized Brønsted acid ionic liquid as an efficient and recyclable catalyst for the synthesis of 5-hydroxymethylfurfural from fructose. *J. Mol. Liq.* 345, 117811. doi:10.1016/j.molliq.2021.117811

Naz, S., Uroos, M., and Muhammad, N. (2021). Effect of molecular structure of cation and anions of ionic liquids and co-solvents on selectivity of 5-hydroxymethylfurfural from sugars, cellulose and real biomass. *J. Mol. Liq.* 334, 116523. doi:10.1016/j.molliq.2021.116523

Ngo, H. L., LeCompte, K., Hargens, L., and McEwen, A. B. (2000). Thermal properties of imidazolium ionic liquids. *Thermochim. Acta* 357, 97–102. doi:10.1016/S0040-6031(00)00373-7

Osatiashtiani, A., Lee, A. F., Granollers, M., Brown, D. R., Olivi, L., Morales, G., et al. (2015). Hydrothermally stable, conformal, sulfated zirconia monolayer catalysts for glucose conversion to 5-HMF. *ACS Catal.* 5, 4345–4352. doi:10.1021/acscatal.5b00965

Prasad, D., Patil, K. N., Manoorkar, V. K., Dateer, R. B., Nagaraja, B. M., and Jadhav, A. H. (2021). Sustainable catalytic process for fructose dehydration using dicationic ionic liquid assisted ZSM-5 zeolite. *Mater. Manuf. Process.* 36 (13), 1571–1578. doi:10.1080/10426914.2021.1905828

Puripat, A. M., Yokogawa, D., Parasuk, V., and Irle, S. (2016). Glucose transformation to 5-hydroxymethylfurfural in acidic ionic liquid: A quantum mechanical study. *J. Comput. Chem.* 37 (3), 327–335. doi:10.1002/jcc.24214

Rathod, P. V., Mujmule, R. B., Chung, W. J., Jadhav, A. R., and Kim, H. (2019). Efficient dehydration of glucose, sucrose, and fructose to 5-hydroxymethylfurfural using tri-cationic ionic liquids. *Catal. Lett.* 149 (3), 672–687. doi:10.1007/s10562-019-02667-0

Ruiz, H. A., Cerqueira, M. A., Silva, H. D., Rodríguez-Jasso, R. M., Vicente, A. A., and Teixeira, J. A. (2013). Biorefinery valorization of autohydrolysis wheat straw hemicellulose to be applied in a polymer-blend film. *Carbohydr. Polym.* 92, 2154–2162. doi:10.1016/j.carbpol.2012.11.054

Tyufekchiev, M., Duan, P., Schmidt-Rohr, K., Focil, S. G., Timko, M. T., and Emmert, M. H. (2018). Cellulase-inspired solid acids for cellulose hydrolysis: Structural explanations for high catalytic activity. *ACS Catal.* 8, 1464–1468. doi:10.1021/acscatal.7b04117

van Putten, R. J., Soetedjo, J. N. M., Pidko, E. A., van der Waalet, J. C., Hensen, E. J. M., Jong, E. D., et al. (2013). Dehydration of different ketoses and aldoses to 5-hydroxymethyl furfural. *ChemSusChem* 6 (9), 1681–1687. doi:10.1002/cssc.201300345

Walden, P. (1914). Ueber die Molekulargrösse und elektrische Leitfähigkeit einiger geschmolzenen Salze. *Bull. Acad. Imp. Sci. Petersbg.* 8, 405–422.

Weingärtner, H. (2008). Understanding ionic liquids at themolecular level: Facts, problems, and controversies. *Angew. Chem. Int. Ed.* 47, 654–670. doi:10.1002/anie.200604951

Xue, L. J., Gurung, E., Tamas, G., Koh, Y. P., Shadeck, M., Simon, S. L., et al. (2016). Effect of alkyl chain branching onphysicochemical properties of imidazolium-based ionic liquids. *J. Chem. Eng. Data* 61, 1078–1091. doi:10.1021/acs.jced.5b00658

Zabed, H., Sahu, J. N., Suely, A., Boyce, A. N., and Faruq, G. (2017). Bioethanol production from renewable sources: Current perspectives and technological progress. *Renew. Sustain. Energy Rev.* 71, 475–501. doi:10.1016/j.rser.2016.12.076

Zhang, S., Sun, J., Zhang, X., Xin, J., Miao, Q., and Wang, J. (2014). Ionic liquid-based green processes for energy production. *Chem. Soc. Rev.* 43, 7838–7869. doi:10.1039/C3CS60409H

Zhang, Y. L., Liu, M., Zhao, J. J., Wang, K., Meng, M. J., and Yan, Y. S. (2018a). Halloysite nanotubes templated acid-base bi-functional hollow polymeric solids for select conversion of cellulose to 5-hydroxymethylfurfural. *ChemistrySelect* 3, 5950–5959. doi:10.1002/slct.201800829

Zhang, Y. L., Xiong, Q., Chen, G. Y., Liu, M., Jin, P., Yan, Y. S., et al. (2018b). Synthesis of Ceria and sulfated zirconia catalysts supported on mesoporous SBA-15 toward glucose conversion to 5-hydroxymethylfurfural in a green isopropanol-mediated system. *Ind. Eng. Chem. Res.* 57, 1968–1979. doi:10.1021/acs.iecr.7b04671

Zhou, L., Liang, R., Ma, Z., Wu, T., and Wu, Y. (2013). Conversion of cellulose to HMF in ionic liquid catalyzed by bifunctional ionic liquids. *Bioresour. Technol.* 129, 450–455. doi:10.1016/j.biortech.2012.11.015

frontiers | Frontiers in Chemistry

TYPE Mini Review
PUBLISHED 10 January 2023
DOI 10.3389/fchem.2022.1106426

OPEN ACCESS

EDITED BY
Hu Li,
Guizhou University, China

REVIEWED BY
Jian He,
Jishou University, China
Hu Pan,
Jiaxing University, China

*CORRESPONDENCE
Yutao Zhang,
zyt0516@126.com
Qiuyun Zhang,
sci_qyzhang@126.com

SPECIALTY SECTION
This article was submitted to Green and Sustainable Chemistry, a section of the journal Frontiers in Chemistry

RECEIVED 23 November 2022
ACCEPTED 06 December 2022
PUBLISHED 10 January 2023

CITATION
Zhang Y, Li W, Wang J, Jin J, Zhang Y, Cheng J and Zhang Q (2023), Advancement in utilization of magnetic catalysts for production of sustainable biofuels.
Front. Chem. 10:1106426.
doi: 10.3389/fchem.2022.1106426

Advancement in utilization of magnetic catalysts for production of sustainable biofuels

Yutao Zhang[1,2,3]*, Weihua Li[1], Jialu Wang[3], Jiaxing Jin[2], Yixi Zhang[1], Jingsong Cheng[2] and Qiuyun Zhang[1,2,3]*

[1]Engineering Technology Center of Control and Remediation of Soil Contamination of Guizhou Science and Technology Department, Anshun University, Anshun, Guizhou, China, [2]School of Chemistry and Chemical Engineering, Anshun University, Anshun, Guizhou, China, [3]College Rural Revitalization Research Center of Guizhou, Anshun University, Anshun, Guizhou, China

In this study, we summarize recent advances in the synthesis of magnetic catalysts utilized for biodiesel production, particularly focusing on the physicochemical properties, activity, and reusability of magnetic mixed metal oxides, supported magnetic catalysts, ionic acid-functionalized magnetic catalysts, heteropolyacid-based magnetic catalysts, and metal–organic framework-based magnetic catalysts. The prevailing reaction conditions in the production of biodiesel are also discussed. Lastly, the current limitations and challenges for future research needs in the magnetic catalyst field are presented.

KEYWORDS

magnetic, heterogeneous catalysis, reusability, esterification, transesterification, biodiesel

1 Introduction

With the rapidly expanding economy and high energy demand, the over-consumption of fossil fuels and fossil fuel usage has led to severe effects on the environment (e.g., global warming), creating wide attention among researchers (Li et al., 2023; Pan et al., 2022a; Zhang et al., 2022a; Pan et al., 2022b). Thus, seeking a sustainable energy resource is a high priority. To date, various types of biofuels, such as biodiesel, bioethanol, and aviation biofuels, have been considered as fossil fuel replacements. Among them, biodiesel (fatty acid alkyl ester, FAME) has been getting significant interest as an alternative fuel because of its safety, biodegradability, and carbon-neutrality (Zhang et al., 2020; Hoang et al., 2021). Currently, biodiesel is synthesized from free fatty acids (FFAs) and various oils mixed with short-chain alcohols, using homogeneous, heterogeneous, or enzymatic catalysts to promote the reaction (Figure 1) (Zhang et al., 2023). However, the homogeneous catalysis system exhibits numerous disadvantages, such as the fact that homogeneous catalysts (e.g., NaOH, KOH, H_2SO_4, etc.) are non-recyclable and cause pollution (Zhang et al., 2021; Liu et al., 2022). In contrast, heterogeneous catalysts (e.g., zeolites, heteropolyacids, metal

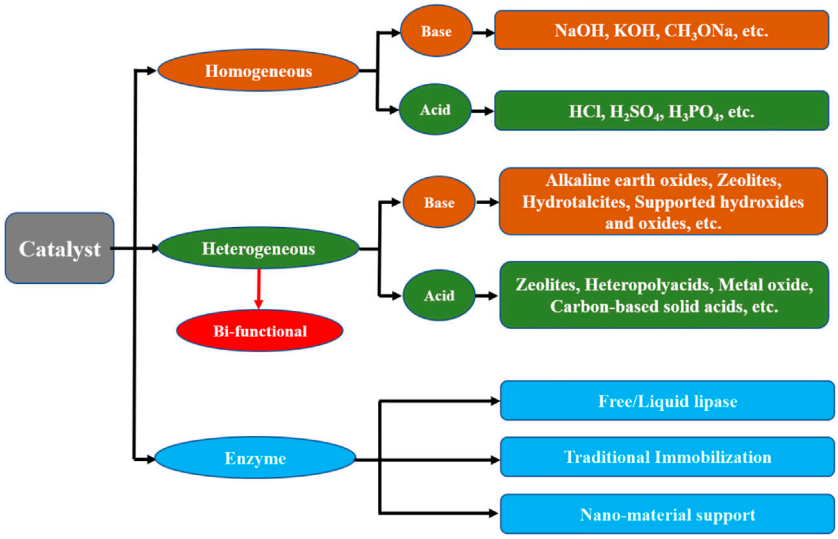

FIGURE 1
Classification of catalysts for biodiesel production.

oxides, etc.) have attracted growing interest owing to their low pollution and easy recovery (Woo et al., 2021; Zhang et al., 2022b; Paiva et al., 2022; Ul Islam et al., 2022). However, high-efficiency separation of the catalyst from the liquid phase and reduction of catalyst loss remain challenges. The use of magnetic separation techniques is an interesting approach to solving these problems (Chen et al., 2022).

In recent times, magnetic solid acid/base catalysts have been widely applied for esterification and transesterification reactions as compared to other heterogeneous catalysts because they are environmentally friendly and cheap, and their highly magnetic nature allows efficient separation with an external magnetic field (Shylesh et al., 2010; Zhang et al., 2014). The present work reviews recent applications of different types of magnetic catalysts and their functionalized magnetic composites employed in biodiesel production, including magnetic mixed metal oxides, supported magnetic catalysts, ionic acid-functionalized magnetic catalysts, heteropolyacid-based magnetic catalysts, and MOF-based magnetic catalysts, among others. The physicochemical properties, activity, and reusability of these magnetic catalysts are evaluated and discussed. Lastly, a brief conclusion and summary on the outlook for designing magnetic catalysts with high catalytic activity is presented.

2 Magnetic catalysts

In general, Fe-, Co-, and Ni-based catalysts exhibit permanent magnetism and can be used as magnetic materials; Fe-based catalysts have been especially widely studied. According to their characteristics, magnetic catalysts can be roughly classified into five types, namely, magnetic mixed metal oxides, supported magnetic catalysts, ionic acid-functionalized magnetic catalysts, heteropolyacid-based magnetic catalysts, and MOF-based magnetic catalysts.

2.1 Magnetic mixed metal oxides

Recently, spinel ferrites, MFe_2O_4 (where *M* indicates a transition metal atom of Cu, Zn, Mo, Co, or Mn) have been widely researched for applications as heterogeneous catalysts due to their thermal stability and ease of separation by using an external magnet. Luadthong et al. (2016) investigated the transesterification of palm oil using a copper ferrite spinel oxide ($CuFe_2O_4$) catalyst. The characterization results revealed that the major active species of $CuFe_2O_4$ were the Cu^{2+} and Fe^{2+}. Optimal reaction conditions of 220°C, 1 g of catalyst, a methanol: oil molar ratio of 1:18, and a high FAME content of >90% were determined. A similar study was conducted by Ali et al. (2020), in which a cuprospinel $CuFe_2O_4$ catalyst was used for the transesterification of waste frying oil with methanol at 60°C, giving a 90.24% yield. Kinetic results showed that the transesterification reaction followed pseudo-first-order kinetics, and the activation energy was found to be 37.64 kJ/mol. AlKahlaway et al. (2021) prepared ferric molybdate, $Fe_2(MoO_4)_3$, nanoparticles for biodiesel synthesis and the catalytic conversion of oleic acid was 90.5%.

In addition, some magnetic mixed metal oxides including $MoO_3/SrFe_2O_4$ (Gonçalves et al., 2021), $MnFe_2O_4$/GO (Bai et al., 2021), $MgFe_2O_4$@OA@CRL (Iuliano et al., 2020), $NaFeTiO_4$/Fe_2O_3–$FeTiO_3$ (Gutierrez-Lopez et al., 2021), Mg^{2+}-doped

$ZnFe_2O_4$ (Ashok et al., 2021), and waste chalk/$CoFe_2O_4$/K_2CO_3 (Foroutan et al., 2022) have been explored for their application largely due to their unique magnetism. Gonçalves et al. (2021) prepared a magnetic catalyst, MoO_3/$SrFe_2O_4$, for the transesterification of waste cooking oil, and results confirmed the success of MoO_3 anchorage of the $SrFe_2O_4$ material. The activity test showed that a biodiesel yield of 95.4% was obtained in 4 h at 164°C. The MoO_3/$SrFe_2O_4$ catalyst could be easily separated by a permanent magnet and showed high stability with a yield of 84% after five cycles. Bai et al. (2021) investigated the catalytic performance of a $MnFe_2O_4$/graphene oxide catalyst for biodiesel production from waste edible oil. The $MnFe_2O_4$/graphene oxide catalyst had a high basicity of 3978.6 mmol/g, and in transesterification reactions, a high biodiesel yield of 96.47% was achieved. Moreover, the physical properties of the synthetic biodiesel were within the ASTM D6751 and EN 14214 standard range. A K_2CO_3 modification to the waste chalk/$CoFe_2O_4$ was developed by Foroutan et al. (2022), and the characterization results showed that the composite catalyst had a lower surface area due to the introduction of K_2CO_3. The highest biodiesel yield of 98.87% was obtained under optimized conditions, and the activation energy and frequency factor of the reaction system was found to be 11.8 kJ/mol and 0.78 min^{-1}, respectively.

Rezania et al. (2021) synthesized a heterogeneous magnetic MGO@MMO nanocatalyst via the ultra-sonication procedure for biodiesel production from waste frying oil. From the results, a high biodiesel yield of 94% was achieved with a 1.5 h reaction at 60°C; the catalyst could be separated and recycled four times, achieving an 86% biodiesel yield. However, after the eighth cycle, the biodiesel yield decreased significantly, possibly due to leaching of the active components or active site blocking. In a more recent study by Hanif et al. (2022), a magnetic Fe/SnO nanocatalyst supported on feldspar was synthesized for the transesterification of various non-edible oils. The magnetic catalyst exhibited a high catalytic activity with more than 97% yield for all the tested non-edible oils. A highly active bifunctional Na–Fe–Ca nanocatalyst was developed by Wang et al. (2022). The catalytic activity of the magnetic Na–Fe–Ca nanocatalyst in biodiesel production was evaluated at low temperatures. Interestingly, with a 500°C calcination temperature, the catalyst reached a 95.84% biodiesel yield with 16 cycles via magnetic separation. In conclusion, magnetic mixed metal oxides have been used successfully as acid/base catalysts or supports in the catalysis industry, and the design and composition of cheap, magnetic composite nanocatalysts is a highly desirable goal in the future.

2.2 Supported magnetic catalysts

Apart from magnetic spinel ferrite catalysts, supported magnetic acid/base catalysts have also attracted significant interest for biofuels production in recent years. At present, Fe_3O_4 magnetic particles do not commonly exhibit good catalytic activity, although they are easily separated and reused. Magnetic Fe_3O_4 is often used as a carrier, and the catalytic system is cost-effective and environment-friendly. Joorasty et al. (2021) prepared NaOH/clinoptilolite–Fe_3O_4 for the transesterification reaction of *Amygdalus scoparia* oil, and the highest biodiesel yield by the catalyst was 91%. The kinetics of NaOH/clinoptilolite–Fe_3O_4-catalyzed transesterification were also explored, and the activation energy was determined to be 9.21 kJ/mol. Xia et al. (2022) prepared bifunctional Co-doped Fe_2O_3–CaO nanocatalysts (Co/Fe_2O_3–CaO) and studied their catalytic performance in soybean oil transesterification. It was reported that the Co/Fe_2O_3–CaO catalyst had good ferromagnetism (26.2 emu/g) after the Co doping, and could be efficiently separated. In another study by Nizam et al. (2022), magnetic Fe_2O_3 immobilized on microporous molecular sieves (Fe_2O_3/MS) was developed using a plant extract-mediated method. In the catalytic reaction, the Fe_2O_3/MS catalyst exhibited excellent applicability in the esterification, transesterification, and photodegradation reactions. Mohamed et al. (2020) and Mohamed and El-Faramawy. (2021) used a newly developed α-Fe_2O_3/AlOOH(γ-Al_2O_3) nanocatalyst to produce biodiesel from waste oil. The α-Fe_2O_3/AlOOH(γ-Al_2O_3) catalyst presented the highest FAME yield and recyclability due to its large surface area of 323.3 m^2/g, high acidity of 0.45 mmol/g, and exposed active site planes. Furthermore, thermal analyses showed that the catalytic reaction system was endothermic.

In a study conducted by Changmai et al. (2021a), a recoverable Fe_3O_4@SiO_2–SO_3H core@shell magnetic catalyst was successfully prepared by a stepwise co-precipitation, coating, and functionalization method. The obtained magnetic Fe_3O_4@SiO_2-SO_3H had a magnetic saturation of 30.94 emu/g, a relatively large surface area of 32.88 m^2/g, and a high acidity of 0.76 mmol/g. The Fe_3O_4@SiO_2–SO_3H catalyst achieved a high conversion of *Jatropha curcas* oil of 98 ± 1% under optimal reaction conditions. Mohammadpour and Safaei (2022) developed a novel sulfonated carbon-coated magnetic catalyst (Fe_3O_4@C@OSO_3H), which was used for the Pechmann condensation of phenol derivatives and β-ketoesters. The resulting yield values were as high as 98%, and the catalyst could be reused fifteen times with no significant loss in activity. Table 1 shows a summary of supported magnetic catalysts utilized for the synthesis of biodiesel.

2.3 Magnetic catalysts functionalized with ionic liquids (ILs)

Recently, due to their highly tunable nature, low volatility, and strong chemical and thermal stability, ionic liquids (ILs) have been widely reported for use in the catalysis field (Sharma

TABLE 1 Recent findings on green biodiesel production using supported magnetic catalysts.

Entry	Feedstock/oil	Catalyst	Conditions (time, temperature, catalyst amount, and molar ratio of acid or oil to alcohol	Yield (*Y*/%) or conversion(*C*/%)	Times catalyst reused; yield	*Ea* (KJ/mol)	Reference
1	Jatropha oil + methanol	$CaSO_4/Fe_2O_3–SiO_2$	4 h, 120°C, 12%, 1:9	Y = 94%	9 cycles; Y = 83%	\	Teo et al. (2019)
2	Rapeseed oil + methanol	Fe_3O_4-CeO_2-25K	2 h, 65°C, 4.5%, 1:7	Y = 96.13%	5 cycles; Y = 80.94%	\	Ambat et al. (2019)
3	*Amygdalus scoparia* oil + methanol	NaOH/clinoptilolite–Fe_3O_4	2.5 h, 65°C, 0.5%, 1:10.43	Y = 91%	4 cycles; Y = 82%	9.21	Joorasty et al. (2021)
4	Fat + methanol	Fe_3O_4/Cs_2O	5 h, 65°C, 7%, 1:21	Y = 97.1%	9 cycles; Y = 78%	43.8	Booramurthy et al. (2020)
5	*Pongamia pinnata* raw oil + methanol	CES-Fe_3O_4	2 h, 65°C, 2%, 1:12	Y = 98%	7 cycles; Y = 98%	\	Chingakham et al. (2023)
6	*Chlorella vulgaris* oil + ethanol	KF/KOH-Fe_3O_4	6 h, 25°C, 1.5%, 1:6	Y = 80%	Not reported	\	Farrokheh et al. (2021)
7	Used cooking oil + methanol	CaO-ZSM-5/Fe_3O_4	4 h, 65°C, 3%, 1:5	C = 83%	4 cycles; Y = 85%	\	Lani and Nagi, (2022)
8	Soybean oil + methanol	Co/Fe_2O_3-CaO	2.5 h, 70°C, 3%, 1:16	Y = 98.2%	5 cycles; Y = 78.8%	\	Xia et al. (2022)
9	Waste cooking oil + methanol	KOH/Fe_3O_4@MCM-41	3 h, 65°C, 8%, 1:40	Y = 93.95%	3 cycles; C>80%	115.79	Khakestarian et al. (2022)
10	Soybean oil + methanol	$Na_2CO_3·H_2O$@BFD	2 h, 65°C, 7%, 1:15	Y = 100.0%	12 cycles; Y = 92.56%	\	Wang et al. (2022b)
11	Sunflower oil + methanol	Fe_2O_3/MS	4 h, 70°C, 0.03 g, 1:10(volume)	Y = 84.5%	Not reported	\	Nizam et al. (2022)
12	Glyceryl trioleate + methanol	Sulfamic acid-functionalized Fe/Fe_3O_4	20 h, 100°C, —, —	C = 100%	5 cycles; C = 95%	\	Wang et al. (2015)
13	Adipic acid + *n*-butanol	Sulfonated magnetic SiO_2	4 h, 105°C, 2.95%, 1:3	C = 99%	6 cycles; C = 85.61%	\	Ke et al. (2019)
14	Acetic acid + methanol	Fe_2O_3–MCM-48–SO_4	4.5 h, 60°C, 15 g/L, 1:10	C = 90%	5 cycles; C = 44.4%	29.077	Sharma et al. (2019)
15	Waste cooking oil + methanol	CSPA@Fe_3O_4	3 h, 65°C, 6%, 1:6	Y = 98%	9 cycles; Y = 91%	34.41	Changmai et al. (2021b)
16	Oleic acid + methanol	EFB-MCC/γ-Fe_2O_3	2 h, 60°C, 9%, 1:12	Y = 92.1%	5 cycles; Y = 77.6%	\	Krishnan et al. (2022)
17	Yeast oil + methanol	Fe_3O_4@SiO_2-CHO	10 h, 55°C, 2.5 g, —	Y = 98.12%	10 cycles; Y = 90%	\	Cao et al. (2021)
18	Cottonseed oil + methanol	α-Fe_2O_3/AlOOH(γ-Al_2O_3)	3 h, 60°C, 3%, 1:6	Y = 100%	3 cycles; Y = 95%	57.4	Mohamed et al. (2020)
19	Waste cooking oil + methanol	α-Fe_2O_3/AlOOH	3 h, 60°C, 3%, 1:6	Y = 95%	4 cycles; Y = 91.3%	51.54	Mohamed and El-Faramawy, (2021)
20	Soybean oil + methanol	Fe_3O_4-poly(GMA-co-MAA)@ lipase	60 h, 40°C, 20%, 1:4	Y = 92.8%	5 cycles; Y = 79.4%	\	Xie and Huang, (2020)
21	Soybean oil + methanol	Fe_3O_4-poly(AGE-DVB-GMA)	8 h, 65°C, 7%, 1:20	Y = 92.6%	4 cycles; no significant decrease	\	Xie et al. (2021a)

(Continued on following page)

TABLE 1 (*Continued*) **Recent findings on green biodiesel production using supported magnetic catalysts.**

Entry	Feedstock/oil	Catalyst	Conditions (time, temperature, catalyst amount, and molar ratio of acid or oil to alcohol	Yield (*Y*/%) or conversion(*C*/%)	Times catalyst reused; yield	*Ea* (KJ/mol)	Reference
22	Jatropha oil + methanol	Fe_3O_4@SiO_2–SO_3H	3.5 h, 80°C, 8%, 1:9	C = 98%	9 cycles; C = 81%	37.0	Changmai, et al. (2021a)
23	Oleic acid + methanol	SC-F-Plg-3	4 h, 65°C, 0.02 g, 1:55	C = 88.69%	5 cycles; C = 70.31%	\	Wu et al. (2022)
24	Cooking oil + methanol	Fe_3O_4@SiO_2-APTES-L^{AE}-$Mo^{VI}O_2$	0.75 h, RT, 0.04 g, 1:3	C = 99%	12 cycles; C = 92%	\	Mohammadpour and Safaei, (2022)

et al., 2022). Among these, many IL-functionalized magnetic catalysts have been tested for the production of biodiesel because of their unique properties and commercial availability. Fauzi et al. (2014) used oleic acid as raw material and 1-butyl-3-methylimidazolium tetrachloroferrate ([BMIM][$FeCl_4$]) as a magnetic catalyst to prepare biodiesel by esterification, with a yield of methyl oleate of 83.4% under optimum conditions. In addition, the [BMIM][$FeCl_4$] catalyst was reused for six runs with little loss; the activation energy of the esterification system was 17.97 kJ/mol.

A novel IL-functionalized magnetic catalyst was fabricated by covalent bonding of [SO_3H-PIM-TMSP]HSO_4 ILs onto mesoporous silica-modified Fe_3O_4 nanoparticles (FSS–IL) (Wu et al., 2014; Wan et al., 2015). The characterization results revealed that the FSS–IL catalyst possessed a uniform core–shell structure and high specific surface area. In the process of preparing biodiesel, the conversion was 93.5% after 4 h using oleic acid as a raw material. More importantly, this FSS–IL catalytic system remained active for six cycles. In another study, magnetically hydrophobic acidic polymeric ionic liquids (FnmS-PILs) were prepared and exhibited good activity and reusability (Zhang et al., 2018). Xie and Wang. (2020a) prepared a magnetic Fe_3O_4/SiO_2-supported polymeric sulfonated ionic liquid (Fe_3O_4/SiO_2-PIL) for simultaneous transesterification and esterification of low-cost oils, and the highest conversion obtained under optimal conditions was 93.3%. Additionally, the reusability study showed that the Fe_3O_4/SiO_2-PIL could be recycled and reused five times. The higher activity and excellent reusability were attributed to the polymeric acidic ILs and porous magnetic nanoparticles. An immobilized dual acidic-ionic liquid on core–shell-structured magnetic silica was also prepared, and the as-prepared magnetic acid catalyst exhibited a large surface acidity of 3.93 meq H^+/g, a strong magnetism of 27.5 emu/g, and achieved the highest conversion of biodiesel at 94.2%. The catalyst was reused for five runs, and the conversion still reached 86% (Xie et al., 2021).

Similar catalysts [$NiFe_2O_4$@BMSI]Br, Fe_3O_4@GO@PBIL, Fe_3O_4@SiO_2@[C4mim]HSO_4, Fe_3O_4@SiO_2@PIL, and [BSO_3HMIm][HSO_4]@IRMOF-3 were also studied (Ding et al., 2021; Naushad et al., 2021; Yu et al., 2021; Zhao et al., 2021; Cheng et al., 2022). Among them, the magnetic [$NiFe_2O_4$@BMSI]Br catalyst was synthesized by an ion-exchange process, and the resulting catalyst had a BET surface area of 89.21 m^2/g. Moreover, the [$NiFe_2O_4$@BMSI]Br catalyst attained a maximum yield of 86.4% for the transesterification of palm oil, and the catalytic activity was retained up to six cycles without obvious loss of yield (Naushad et al., 2021). Based on recent literature projections, ILs are expected to develop as potential acid materials for the synthesis of functionalized composite magnetic catalysts in the future.

2.4 Magnetic catalysts based on heteropolyacids

Heteropolyacids are inorganic compounds with a Keggin structure that acts as a strong Brønsted acid. Heteropolyacids have a low surface area and easily dissolve in polar solvents, so researchers bonded them to magnetic supports to overcome these problems. Wu et al. (2016a) investigated the application of magnetic material grafted onto a poly(phosphotungstate)-based acidic ionic liquid as a heterogeneous catalyst for the esterification of oleic acid. Under optimal conditions, the conversion of oleic acid reached 93.4%. More specifically, the catalyst exhibited good reusability after six runs using an external magnetic field.

As reported by Helmi et al. (2021), phosphomolybdic acid was supported on clinoptilolite–Fe_3O_4, and the prepared catalyst showed excellent activity (80% yield in 8 h at 75°C) and reusability in the production of biodiesel from *Salvia mirzayanii* oil. The HPA/clinoptilolite–Fe_3O_4 catalyst was able to recycle up to four times with minimal loss in activity. A magnetic heteropolyanion-based ionic liquid (MNP@HPAIL) was synthesized by Dadhania et al. (2021), and was evaluated

for the esterification of oleic acid under ultrasonic irradiation. The maximum oleic acid conversion of 58% was reached, and the catalyst could be reused for six consecutive cycles.

On the same note, Zhang et al. (2021) immobilized a 12-tungstophosphoric acid (HPW)-based magnetic catalyst (Fe_3O_4@SBA-15@HPW and Fe_3O_4@SBA-15-NH_2-HPW) for the production of biodiesel from palm oil with methanol. The synthesized magnetic catalysts have a high content of Brønsted acid sites due to the induction of HPW. In particular, the Fe_3O_4@SBA-15-NH_2-HPW exhibited a high biodiesel yield of 91% under optimal reaction conditions, and also exhibited high reusability. Ghasemzadeh et al. (2022) adapted a cotton/Fe_3O_4@SiO_2@$H_3PW_{12}O_{40}$ magnetic nanocomposite to catalyze the transesterification of sunflower oil. The catalyst had an excellent magnetism of 45 emu/g and demonstrated a high FAME yield of 95.3% under optimum conditions. After four cycles of transesterification, the FAME yield was still relatively high at 85.5%. In addition, the physical properties of the synthetic biodiesel meet the ASTM and EU standards. According to the reported literature, heteropolyacids grafted onto magnetic supports can be an effective solution to overcome the loss of heteropolyacids.

2.5 MOF-based magnetic catalysts

Recently, metal–organic frameworks (MOFs), as a newly emergent type of stable and tunable material, have become promising magnetic catalysts and supports, and MOF derivatives have been used for heterogeneous catalysis. Wu et al. (2016b) investigated the ability of the Fe_3O_4@NH_2-MIL-88B(Fe) catalyst to perform the esterification of oleic acid with ethanol. The Fe_3O_4@NH_2-MIL-88B(Fe) catalyst had an acidity of 1.76 mmol/g and achieved a high yield of 93.2% at 90°C. Moreover, the Fe_3O_4@NH_2-MIL-88B(Fe) catalyst could be recycled six times without significant loss of activity.

Xie's group (Xie and Wan, 2018; Xie and Huang, 2019; Xie and Wang, 2020; Xie et al., 2021b) has studied biodiesel production from soybean oil and low-quality oils using magnetic Fe_3O_4@HKUST-1-ABILs, Fe_3O_4@MIL-100(Fe)/*Candida rugosa* lipase, $CoFe_2O_4$/MIL-88B(Fe)-NH_2/(Py-Ps)PMo, and $H_6PV_3MoW_8O_{40}$/Fe_3O_4/ZIF-8 catalysts. Their results revealed that all magnetic catalysts exhibited good catalytic performance and excellent reusability. Thus, these MOF-based magnetic catalysts comprise an excellent potential alternative for processing low-quality oils into biofuels. In another study by Zhou's group (Zhou et al., 2019; Zhou et al., 2023), a MIL-100(Fe) was embedded in magnetic Fe_3O_4 nanoparticles (Fe_3O_4/MIL-100(Fe), and the Fe_3O_4/MIL-100(Fe) composite exhibited unexpectedly high catalytic activity with a rosin conversion of 94.8% at 240°C. Furthermore, the Fe_3O_4/MIL-100(Fe) composite showed good stability and recyclability over six cycles. An annealed Fe_3O_4/MOF-5 was also synthesized and used to catalyze rosin esterification with glycerol. The highest conversion of 94.1% was attained in 2.5 h at 240°C, and the annealed catalyst showed excellent reusability.

A novel TiO_2-decorated magnetic ZIF-8 nanocomposite (Fe_3O_4@ZIF-8/TiO_2) was synthesized by Sabzevar et al. (2021). The as-prepared nanocomposite demonstrated excellent performance in the esterification of oleic acid (92.25% yield), which was mainly attributed to its acidic properties and large surface area. After five cycles, the yield of biodiesel was still 77.22%. Abdelmigeed et al. (2021a), Abdelmigeed et al. (2021b) prepared NaOH/magnetized ZIF-8 catalysts for the production of high-quality biodiesel from a blend of sunflower and soybean oil with ethanol. The transesterification reaction with the blended oil produced 70% biodiesel in 1.5 h at 75°C. The ethanolysis reaction followed a pseudo-second-order kinetic model, and the activation energy was calculated as 77.27 kJ/mol.

In another important area of catalyst research, MOFs were pyrolized at various temperatures to act as self-sacrificial templates for the synthesis of structured nanoporous metal oxides (Reddy et al., 2020). Li et al. (2019), Li et al. (2020), Li et al. (2021) reported on a series of magnetic catalysts based on MOF derivatives (MM–SrO, magnetic CaO-based catalyst, carbonized MIL-100(Fe) supporting ammonium sulfate), and the physical, chemical, and thermal properties of the MOF-derived magnetic catalysts were evaluated. The researchers discovered that these catalysts exhibited strong magnetism and excellent catalytic activity and could be easily separated by an external magnetic field after each cycle. In another study, a bifunctional magnetic catalyst with various coordination states of Co and non-coordinated N sites was developed by Guo et al. (2022). The prepared bifunctional magnetic catalyst (550–30) was evaluated for biodiesel production from microalgal lipids. It had a high conversion efficiency of 96.0%, owing to the generated structural defects that formed a mesopore-dominated structure in the bifunctional magnetic catalyst. Also, the catalyst could be magnetically separated and reused for six cycles with a conversion efficiency of 89.7%.

3 Summary and outlook

In the field of catalysis, magnetic catalysts promote catalytic reactions efficiently and their strong magnetic properties allow them to be easily reused, which make magnetic catalysts more cost-effective and efficient when used in industrial catalysis. The current mini-review highlights recent applications of magnetic catalysts and their functionalized magnetic materials utilized for biodiesel production. Although remarkable progress has been achieved in the area of magnetic catalyst research, there are still some limitations that need to be overcome by continuing design improvements. The catalytic mechanisms and deactivation processes are not well understood, supported magnetic

catalysts show weak interactions between active ingredients and magnetic supports, and the complex synthesis processes for some magnetic catalysts need to be simplified. Thus, future investigation into the preparation methods, performance, mechanisms, and economics of the magnetic catalyst is essential to correct the present issues. In light of the current evidence, however, we strongly believe that the integrated development of novel magnetic catalysts will play a key role in further developing a cost-effective biorefinery industry.

Author contributions

YTZ conceived the article, discussed the outline, and wrote the manuscript; WL, JW, JJ, YXZ, and JC made preliminary revisions to the manuscript; YTZ and QZ coordinated the entire content of the manuscript and made detailed revisions; QZ was in charge of project administration.

Funding

This work was financially supported by the Anshun Science and Technology Planning Project ((2021)1), National Natural Science Foundation of China (22262001), Creative Research Groups Support Program of Guizhou Education Department (KY (2017)049), Youth Growth Science and Technology Personnel Foundation of Guizhou Education Department (KY (2019)147), Guizhou Province Key Laboratory of Ecological Protection and Restoration of Typical Plateau Wetlands ((2020) 2002), and Project of Anshun University supporting Doctors Research ((2021)asxybsjj01).

Conflict of interest

The authors declare that the research was conducted in the absence of any commercial or financial relationships that could be construed as a potential conflict of interest.

Publisher's note

All claims expressed in this article are solely those of the authors and do not necessarily represent those of their affiliated organizations, or those of the publisher, the editors, and the reviewers. Any product that may be evaluated in this article, or claim that may be made by its manufacturer, is not guaranteed or endorsed by the publisher.

References

Abdelmigeed, M. O., Al-Sakkari, E. G., Hefney, M. S., Ismail, F. M., Abdelghany, A., Ahmed, T. S., et al. (2021b). Magnetized ZIF-8 impregnated with sodium hydroxide as a heterogeneous catalyst for high-quality biodiesel production. *Renew. Energy* 165, 405–419. doi:10.1016/j.renene.2020.11.018

Abdelmigeed, M. O., Al-Sakkari, E. G., Hefney, M. S., Ismail, F. M., Ahmed, T. S., and Ismail, I. M. (2021a). Biodiesel production catalyzed by NaOH/Magnetized ZIF-8: Yield improvement using methanolysis and catalyst reusability enhancement. *Renew. Energy* 174, 253–261. doi:10.1016/j.renene.2021.04.057

Ali, R. M., Elkatory, M. R., and Hamad, H. A. (2020). Highly active and stable magnetically recyclable $CuFe_2O_4$ as a heterogenous catalyst for efficient conversion of waste frying oil to biodiesel. *Fuel* 268, 117297. doi:10.1016/j.fuel.2020.117297

AlKahlaway, A. A., Betiha, M. A., Aman, D., and Rabie, A. M. (2021). Facial synthesis of ferric molybdate ($Fe_2(MoO_4)_3$) nanoparticle and its efficiency for biodiesel synthesis via oleic acid esterification. *Environ. Technol. Innov.* 22, 101386. doi:10.1016/j.eti.2021.101386

Ambat, I., Srivastava, V., Haapaniemi, E., and Sillanpää, M. (2019). Nano-magnetic potassium impregnated ceria as catalyst for the biodiesel production. *Renew. Energy* 139, 1428–1436. doi:10.1016/j.renene.2019.03.042

Ashok, A., Ratnaji, T., John Kennedy, L., Vijaya, J. J., and Pragash, R. G. (2021). Magnetically recoverable Mg substituted zinc ferrite nanocatalyst for biodiesel production: Process optimization, kinetic and thermodynamic analysis. *Renew. Energy* 163, 480–494. doi:10.1016/j.renene.2020.08.081

Bai, L. Q., Tajikfar, A., Tamjidi, S., Foroutan, R., and Esmaeili, H. (2021). Synthesis of $MnFe_2O_4$@graphene oxide catalyst for biodiesel production from waste edible oil. *Renew. Energy* 170, 426–437. doi:10.1016/j.renene.2021.01.139

Booramurthy, V. K., Kasimani, R., Subramanian, D., and Pandian, S. (2020). Production of biodiesel from tannery waste using a stable and recyclable nano-catalyst: An optimization and kinetic study. *Fuel* 260, 116373. doi:10.1016/j.fuel.2019.116373

Cao, X. Y., Xu, H., Li, F. S., Zou, Y. J., Ran, Y. L., Ma, X. R., et al. (2021). One-step direct transesterification of wet yeast for biodiesel production catalyzed by magnetic nanoparticle-immobilized lipase. *Renew. Energy* 171, 11–21. doi:10.1016/j.renene.2021.02.065

Changmai, B., Rano, R., Vanlalveni, C., and Rokhum, L. (2021a). A novel *Citrus sinensis* peel ash coated magnetic nanoparticles as an easily recoverable solid catalyst for biodiesel production. *Fuel* 286, 119447. doi:10.1016/j.fuel.2020.119447

Changmai, B., Wheatley, A. E. H., Rano, R., Halder, G., Selvaraj, M., Rashid, U., et al. (2021b). A magnetically separable acid-functionalized nanocatalyst for biodiesel production. *Fuel* 305, 121576. doi:10.1016/j.fuel.2021.121576

Chen, R., Qiao, X. Q., and Liu, F. M. (2022). Ionic liquid-based magnetic nanoparticles for magnetic dispersive solid-phase extraction: A review. *Anal. Chim. Acta X.* 1201, 339632. doi:10.1016/j.aca.2022.339632

Cheng, J., Mao, Y. X., Guo, H., Qian, S., Shao, Y., Yang, W. J., et al. (2022). Synergistic and efficient catalysis over Brønsted acidic ionic liquid [BSO_3HMIm][HSO_4]-modified metal-organic framework (IRMOF-3) for microalgal biodiesel production. *Fuel* 322, 124217. doi:10.1016/j.fuel.2022.124217

Chingakham, C., David, A., and Sajith, V. (2023). Fe_3O_4 nanoparticles impregnated eggshell as a novel catalyst for enhanced biodiesel production. *Chin. J. Chem. Eng.* 27, 2835–2843. doi:10.1016/j.cjche.2019.02.022

Dadhania, H., Raval, D., and Dadhania, A. (2021). Magnetically separable heteropolyanion based ionic liquid as a heterogeneous catalyst for ultrasound mediated biodiesel production through esterification of fatty acids. *Fuel* 296, 120673. doi:10.1016/j.fuel.2021.120673

Ding, J., Zhou, C. W., Wu, Z. W., Chen, C., Feng, N. J., Wang, L., et al. (2021). Core-shell magnetic nanomaterial grafted spongy-structured poly (ionic liquid): A recyclable brönsted acid catalyst for biodiesel production. *Appl. Catal. A General* 616, 118080. doi:10.1016/j.apcata.2021.118080

Farrokheh, A., Tahvildari, K., and Nozari, M. (2021). Comparison of biodiesel production using the oil of Chlorella Vulgaris micro-algae by electrolysis and reflux methods using CaO/KOH-Fe_3O_4 and KF/KOH-Fe_3O_4 as magnetic nano catalysts. *Waste Biomass Valorization* 12, 3315–3329. doi:10.1007/s12649-020-01229-5

Fauzi, A. H. M., Amin, N. A. S., and Mat, R. (2014). Esterification of oleic acid to biodiesel using magnetic ionic liquid: Multi-objective optimization and kinetic study. *Appl. Energy* 114, 809–818. doi:10.1016/j.apenergy.2013.10.011

Foroutan, R., Peighambardoust, S. J., Mohammadi, R., Peighambardoust, S. H., and Ramavandi, B. (2022). Application of waste chalk/$CoFe_2O_4$/K_2CO_3 composite

as a reclaimable catalyst for biodiesel generation from sunflower oil. *Chemosphere* 289, 133226. doi:10.1016/j.chemosphere.2021.133226

Ghasemzadeh, B., Matin, A. A., Habibi, B., and Ebadi, M. (2022). Cotton/Fe_3O_4@SiO_2@$H_3PW_{12}O_{40}$ a magnetic heterogeneous catalyst for biodiesel production: Process optimization through response surface methodology. *Ind. Crops Prod.* 181, 114806. doi:10.1016/j.indcrop.2022.114806

Gonçalves, M. A., Lourenço Mares, E. K., Zamian, J. R., da Rocha Filho, G. N., and da Conceição, L. R. V. (2021). Statistical optimization of biodiesel production from waste cooking oil using magnetic acid heterogeneous catalyst MoO_3/$SrFe_2O_4$. *Fuel* 304, 121463. doi:10.1016/j.fuel.2021.121463

Guo, H., Cheng, J., Mao, Y. X., Qian, L., Shao, Y., and Yang, W. J. (2022). Fabricating different coordination states of cobalt as magnetic acid-base bifunctional catalyst for biodiesel production from microalgal lipid. *Fuel* 322, 124172. doi:10.1016/j.fuel.2022.124172

Gutierrez-Lopez, A. N., Mena-Cervantes, V. Y., García-Solares, S. M., Vazquez-Arenas, J., and Hernandez-Altamirano, R. (2021). $NaFeTiO_4$/Fe_2O_3-$FeTiO_3$ as heterogeneous catalyst towards a cleaner and sustainable biodiesel production from *Jatropha curcas* L. *Oil. J. Clean. Prod.* 304, 127106. doi:10.1016/j.jclepro.2021.127106

Hanif, M., Bhatti, I. A., Zahid, M., and Shahid, M. (2022). Production of biodiesel from non-edible feedstocks using environment friendly nano-magnetic Fe/SnO catalyst. *Sci. Rep.* 12, 16705. doi:10.1038/s41598-022-20856-7

Helmi, M., Ghadiri, M., Tahvildari, K., and Hemmati, A. (2021). Biodiesel synthesis using clinoptilolite-Fe_3O_4-based phosphomolybdic acid as a novel magnetic green catalyst from salvia mirzayanii oil via electrolysis method: Optimization study by Taguchi method. *J. Environ. Chem. Eng.* 9, 105988. doi:10.1016/j.jece.2021.105988

Hoang, A. T., Tabatabaei, M., Aghbashlo, M., Carlucci, A. P., Ölçer, A. I., Le, A. T., et al. (2021). Rice bran oil-based biodiesel as a promising renewable fuel alternative to petrodiesel: A review. *Renew. Sustain. Energy Rev.* 135, 110204. doi:10.1016/j.rser.2020.110204

Iuliano, M., Sarno, M., Pasquale, S. D., and Ponticorvo, E. (2020). *Candida rugosa* lipase for the biodiesel production from renewable sources. *Renew. Energy* 162, 124–133. doi:10.1016/j.renene.2020.08.019

Joorasty, M., Hemmati, A., and Rahbar-Kelishami, A. (2021). NaOH/clinoptilolite-Fe_3O_4 as a novel magnetic catalyst for producing biodiesel from Amygdalus scoparia oil: Optimization and kinetic study. *Fuel* 303, 121305. doi:10.1016/j.fuel.2021.121305

Ke, P., Zeng, D. L., Wu, J., Cui, J. W., Li, X., and Wang, G. H. (2019). Preparation and characterization of sulfonated magnetic SiO_2 microspheres as the solid acid catalysts for esterification. *ACS Omega* 4, 22119–22125. doi:10.1021/acsomega.9b03262

Khakestarian, M., Taghizadeh, M., and Fallah, N. (2022). Magnetic mesoporous KOH/Fe_3O_4@MCM-41 nanocatalyst for biodiesel production from waste cooking oil: Optimization of process variables and kinetics study. *Environ. Prog. Sustain. Energy* 2022, e13863. doi:10.1016/j.enconman.2022.116292

Krishnan, S. G., Pua, F. L., and Zhang, F. (2022). Oil palm empty fruit bunch derived microcrystalline cellulose supported magnetic acid catalyst for esterification reaction: An optimization study. *Energy Convers. Manag. X* 13, 100159. doi:10.1016/j.ecmx.2021.100159

Lani, N. S., and Ngadi, N. (2022). Highly efficient CaO-ZSM-5 zeolite/Fe_3O_4 as a magnetic acid-base catalyst upon biodiesel production from used cooking oil. *Appl. Nanosci.* 12, 3755–3769. doi:10.1007/s13204-021-02121-x10.1007/s13204-021-02121-x

Li, H., Liu, F. S., Ma, X. L., Wu, Z. J., Li, Y., Zhang, L. H., et al. (2019). Catalytic performance of strontium oxide supported by MIL-100(Fe) derivate as transesterification catalyst for biodiesel production. *Energy Convers. Manag.* 180, 401–410. doi:10.1016/j.enconman.2018.11.012

Li, H., Wang, J. C., Ma, X. L., Wang, Y. Y., Li, G. N., Guo, M., et al. (2021). Carbonized MIL-100(Fe) used as support for recyclable solid acid synthesis for biodiesel production. *Renew. Energy* 179, 1191–1203. doi:10.1016/j.renene.2021.07.122

Li, H., Wang, Y. B., Ma, X. L., Wu, Z. J., Cui, P., Lu, W. P., et al. (2020). A novel magnetic CaO-based catalyst synthesis and characterization: Enhancing the catalytic activity and stability of CaO for biodiesel production. *Chem. Eng. J.* 391, 123549. doi:10.1016/j.cej.2019.123549

Li, Y. C., Zhu, K. X., Jiang, Y. Y., Chen, L., Zhang, H., Li, H., et al. (2023). Biomass-derived hydrophobic metal-organic frameworks solid acid for green efficient catalytic esterification of oleic acid at low temperatures. *Fuel Process. Technol.* 239, 107558. doi:10.1016/j.fuproc.2022.107558

Liu, K., Zhang, L. Y., Wei, G. T., Yuan, Y. H., and Huang, Z. Y. (2022). Synthesis, characterization and application of a novel carbon-doped mix metal oxide catalyst for production of castor oil biodiesel. *J. Clean. Prod.* 373, 133768. doi:10.1016/j.jclepro.2022.133768

Luadthong, C., Khemthong, P., Nualpaeng, W., and Faungnawakij, K. (2016). Copper ferrite spinel oxide catalysts for palm oil methanolysis. *Appl. Catal. A General* 525, 68–75. doi:10.1016/j.apcata.2016.07.002

Mohamed, M. M., Bayoumy, W. A., El-Faramawy, H., El-Dogdog, W., and Mohamed, A. A. (2020). A novel *a*-Fe_2O_3/AlOOH(γ-Al_2O_3) nanocatalyst for efficient biodiesel production from waste oil: Kinetic and thermal studies. *Renew. Energy* 160, 450–464. doi:10.1016/j.renene.2020.07.006

Mohamed, M. M., and El-Faramawy, H. (2021). An innovative nanocatalyst α-Fe_2O_3/AlOOH processed from gibbsite rubbish ore for efficient biodiesel production via utilizing cottonseed waste oil. *Fuel* 297, 120741. doi:10.1016/j.fuel.2021.120741

Mohammadpour, P., and Safaei, E. (2022). Biodiesel and adipic acid production using molybdenum(VI) complex of a bis(phenol) diamine ligand supported on Fe_3O_4 magnetic nanoparticles. *Fuel* 327, 124831. doi:10.1016/j.fuel.2022.124831

Naushad, M., Ahamad, T., and Khan, M. R. (2021). Fabrication of magnetic nanoparticles supported ionic liquid catalyst for transesterification of vegetable oil to produce biodiesel. *J. Mol. Liq.* 330, 115648. doi:10.1016/j.molliq.2021.115648

Nizam, A., Warrier, V. G., Devasia, J., and Ganganagappa, N. (2022). Magnetic iron oxide nanoparticles immobilized on microporous molecular sieves as efficient porous catalyst for photodegradation, transesterification and esterification reactions. *J. Porous Mat.* 29, 119–129. doi:10.1007/s10934-021-01150-9

Paiva, M. F., de Freitas, E. F., de França, J. O. C., da Silva Valadares, D., Dias, S. C. L., and Dias, J. A. (2022). Structural and acidity analysis of heteropolyacids supported on faujasite zeolite and its effect in the esterification of oleic acid and *n*-butanol. *Mol. Catal.* 532, 112737. doi:10.1016/j.mcat.2022.112737

Pan, H., Xia, Q. N., Li, H., Wang, Y. G., Shen, Z. F., Wang, Y. Q., et al. (2022a). Direct production of biodiesel from crude Euphorbia lathyris L. Oil catalyzed by multifunctional mesoporous composite materials. *Fuel* 309, 122172. doi:10.1016/j.fuel.2021.122172

Pan, H., Xia, Q. N., Wang, Y., Shen, Z. F., Huang, H., Ge, Z. G., et al. (2022b). Recent advances in biodiesel production using functional carbon materials as acid/base catalysts. *Fuel Process. Technol.* 237, 107421. doi:10.1016/j.fuproc.2022.107421

Reddy, R. C. K., Lin, J., Chen, Y. Y., Zeng, C. H., Lin, X. M., Cai, Y. P., et al. (2020). Progress of nanostructured metal oxides derived from metal-organic frameworks as anode materials for lithium-ion batteries. *Coord. Chem. Rev.* 420, 213434. doi:10.1016/j.ccr.2020.213434

Rezania, S., Kamboh, M. A., Arian, S. S., Al-Dhabi, N. A., Arasu, M. V., Esmail, G. A., et al. (2021). Conversion of waste frying oil into biodiesel using recoverable nanocatalyst based on magnetic graphene oxide supported ternary mixed metal oxide nanoparticles. *Bioresour. Technol.* 323, 124561. doi:10.1016/j.biortech.2020.124561

Sabzevar, A. M., Ghahramaninezhad, M., and Shahrak, M. N. (2021). Enhanced biodiesel production from oleic acid using TiO_2-decorated magnetic ZIF-8 nanocomposite catalyst and its utilization for used frying oil conversion to valuable product. *Fuel* 288, 119586. doi:10.1016/j.fuel.2020.119586

Sharma, J., Kumar, P., Sillanpaa, M., Kumar, D., and Nemiwal, M. (2022). Immobilized ionic liquids on Fe_3O_4 nanoparticles: A potential catalyst for organic synthesis. *Inorg. Chem. Commun.* 145, 110055. doi:10.1016/j.inoche.2022.110055

Sharma, N., Guliani, D., Kaur, K., Verma, A., Sobti, A., and Toor, A. P. (2019). Enhanced catalytic activity of nano-Fe_2O_3–MCM-48–SO_4 as a green catalyst for the esterification of acetic acid with methanol. *Iran. J. Sci. Technol. Trans. Sci.* 43, 2831–2842. doi:10.1007/s40995-019-00779-1

Shylesh, S., Schuenemann, V., and Thiel, W. R. (2010). Magnetically separable nanocatalysts: Bridges between homogeneous and heterogeneous catalysis. *Angew. Chem. Int. Ed.* 49, 3428–3459. doi:10.1002/anie.200905684

Teo, S. H., Islam, A., Chan, E. S., Choong T, S. Y., Alharthi, N. H., Taufiq-Yap, Y. H., et al. (2019). Efficient biodiesel production from Jatropha curcus using $CaSO_4$/Fe_2O_3-SiO_2 core-shell magnetic nanoparticles. *J. Clean. Prod.* 208, 816–826. doi:10.1016/j.jclepro.2018.10.107

Ul Islam, M. G., Jan, M. T., Farooq, M., Naeem, A., Khan, I. W., and Khattak, H. U. (2022). Biodiesel production from wild olive oil using TPA decorated Cr-Al acid heterogeneous catalyst. *Chem. Eng. Res. Des.* 329, 540–549. doi:10.1016/j.cherd.2021.12.040

Wan, H., Wu, Z. W., Chen, W., Guan, G. F., Cai, Y., Chen, C., et al. (2015). Heterogenization of ionic liquid based on mesoporous material as magnetically recyclable catalyst for biodiesel production. *J. Mol. Catal. A Chem.* 398, 127–132. doi:10.1016/j.molcata.2014.12.002

Wang, H., Covarrubias, J., Prock, H., Wu, X., Wang, D., and Bossmann, S. H. (2015). Acid-functionalized magnetic nanoparticle as heterogeneous catalysts for biodiesel synthesis. *J. Phys. Chem. C* 119, 26020–26028. doi:10.1021/acs.jpcc.5b08743

Wang, X. M., Zeng, Y. N., Jiang, L. Q., Wang, Y. T., Li, J. G., Kang, L. L., et al. (2022a). Highly stable $NaFeO_2$-Fe_3O_4 composite catalyst from blast furnace dust for efficient production of biodiesel at low temperature. *Ind. Crops Prod.* 182, 114937. doi:10.1016/j.indcrop.2022.114937

Wang, Y. T., Wang, X. M., Gao, D., Wang, F. P., Zeng, Y. N., Li, J. G., et al. (2022b). Efficient production of biodiesel at low temperature using highly active bifunctional Na-Fe-Ca nanocatalyst from blast furnace waste. *Fuel* 322, 124168. doi:10.1016/j.fuel.2022.124168

Woo, J., Joshi, R., Park, Y. K., and Jeon, J. K. (2021). Biodiesel production from jatropha seeds with bead-type heterogeneous catalyst. *Korean J. Chem. Eng.* 38, 763–770. doi:10.1007/s11814-021-0759-7

Wu, M., Yao, X. J., Jiang, J. L., Ji, Y. N., Gu, Y. X., Deng, Q. L., et al. (2022). Synthesis of magnetic sulfonated carbon/Fe_3O_4/palygorskite composites and application as a solid acid catalyst. *Clays Clay Min.* 70, 514–526. doi:10.1007/s42860-022-00199-0

Wu, Z. W., Chen, C., Wan, H., Wang, L., Li, Z., Li, B. X., et al. (2016b). Fabrication of magnetic NH2-MIL-88B (Fe) confined Brønsted ionic liquid as an efficient catalyst in biodiesel synthesis. *Energy fuels.* 30, 10739–10746. doi:10.1021/acs.energyfuels.6b01212

Wu, Z. W., Chen, C., Wang, L., Wan, H., and Guan, G. F. (2016a). Magnetic Material Grafted Poly(phosphotungstate-based acidic ionic liquid) as efficient and recyclable catalyst for esterification of oleic acid. *Ind. Eng. Chem. Res.* 55, 1833–1842. doi:10.1021/acs.iecr.5b02906

Wu, Z. W., Li, Z., Wu, G. M., Wang, L. L., Lu, S. Q., Wang, L., et al. (2014). Brønsted acidic ionic liquid modified magnetic nanoparticle: An efficient and green catalyst for biodiesel production. *Ind. Eng. Chem. Res.* 53, 3040–3046. doi:10.1021/ie4040016

Xia, S. G., Li, J., Chen, G. Y., Tao, J. Y., Li, W. Q., and Zhu, G. B. (2022). Magnetic reusable acid-base bifunctional Co doped Fe_2O_3-CaO nanocatalysts for biodiesel production from soybean oil and waste frying oil. *Renew. Energy* 189, 421–434. doi:10.1016/j.renene.2022.02.122

Xie, W. L., Gao, C. L., and Li, J. B. (2021b). Sustainable biodiesel production from low-quantity oils utilizing $H_6PV_3MoW_8O_{40}$ supported on magnetic Fe_3O_4/ZIF-8 composites. *Renew. Energy* 168, 927–937. doi:10.1016/j.renene.2020.12.129

Xie, W. L., and Huang, M. Y. (2019). Enzymatic production of biodiesel using immobilized lipase on core-shell structured Fe_3O_4@MIL-100(Fe) composites. *Catalysts* 9, 850. doi:10.3390/catal9100850

Xie, W. L., and Huang, M. Y. (2020). Fabrication of immobilized *Candida rugosa* lipase on magnetic Fe_3O_4-poly(glycidyl methacrylate-co-methacrylic acid) composite as an efficient and recyclable biocatalyst for enzymatic production of biodiesel. *Renew. Energy* 158, 474–486. doi:10.1016/j.renene.2020.05.172

Xie, W. L., and Wan, F. (2018). Basic ionic liquid functionalized magnetically responsive Fe_3O_4@HKUST-1 composites used for biodiesel production. *Fuel* 220, 248–256. doi:10.1016/j.fuel.2018.02.014

Xie, W. L., and Wang, H. (2021). Grafting copolymerization of dual acidic ionic liquid on core-shell structured magnetic silica: A magnetically recyclable brönsted acid catalyst for biodiesel production by one-pot transformation of low-quality oils. *Fuel* 283, 118893. doi:10.1016/j.fuel.2020.118893

Xie, W. L., and Wang, H. (2020a). Immobilized polymeric sulfonated ionic liquid on core-shell structured Fe_3O_4/SiO_2 composites: A magnetically recyclable catalyst for simultaneous transesterification and esterifications of low-cost oils to biodiesel. *Renew. Energy* 145, 1709–1719. doi:10.1016/j.renene.2019.07.092

Xie, W. L., and Wang, Q. (2020b). Synthesis of heterogenized polyoxometalate-based ionic liquids with brönsted-lewis acid sites: A magnetically recyclable catalyst for biodiesel production from low-quality oils. *J. Ind. Eng. Chem.* 87, 162–172. doi:10.1016/j.jiec.2020.03.033

Xie, W. L., Xiong, Y. F., and Wang, H. Y. (2021a). Fe_3O_4-poly(AGE-DVB-GMA) composites immobilized with guanidine as a magnetically recyclable catalyst for enhanced biodiesel production. *Renew. Energy* 174, 758–768. doi:10.1016/j.renene.2021.04.086

Yu, J. T., Wang, Y. H., Sun, L. Q., Xu, Z., Du, Y. D., Sun, H. L., et al. (2021). Catalysis preparation of biodiesel from waste schisandra chinensis seed oil with the ionic liquid immobilized in a magnetic catalyst: Fe_3O_4@SiO_2@[C4mim]HSO_4. *ACS Omega* 6, 7896–7909. doi:10.1021/acsomega.1c00504

Zhang, H., Li, H., Pan, H., Wang, A. P., Souzanchi, S., Xu, C., et al. (2018). Magnetically recyclable acidic polymeric ionic liquids decorated with hydrophobic regulators as highly efficient and stable catalysts for biodiesel production. *Appl. Energy* 223, 416–429. doi:10.1016/j.apenergy.2018.04.061

Zhang, P. B., Liu, P., Fan, M. M., Jiang, P. P., and Haryono, A. (2021b). High-performance magnetite nanoparticles catalyst for biodiesel production: Immobilization of 12-tungstophosphoric acid on SBA-15 works effectively. *Renew. Energy* 175, 244–252. doi:10.1016/j.renene.2021.05.033

Zhang, P., Han, Q., Fan, M., and Jiang, P. (2014). Magnetic solid base catalyst CaO/$CoFe_2O_4$ for biodiesel production: Influence of basicity and wettability of the catalyst in catalytic performance. *Appl. Surf. Sci.* 317, 1125–1130. doi:10.1016/j.apsusc.2014.09.043

Zhang, Q. Y., Ling, D., Lei, D. D., Wan, J. L., Liu, X. F., Zhang, Y. T., et al. (2020). Green and facile synthesis of metal-organic framework Cu-BTC supported Sn (II)-substituted Keggin heteropoly composites as an esterification nanocatalyst for biodiesel production. *Front. Chem.* 8, 129. doi:10.3389/fchem.2020.00129

Zhang, Q. Y., Luo, Q. Z., Wu, Y. P., Yu, R. F., Cheng, J. S., and Zhang, Y. T. (2021a). Construction of a Keggin heteropolyacid/Ni-MOF catalyst for esterification of fatty acids. *RSC Adv.* 11, 33416–33424. doi:10.1039/D1RA06023F

Zhang, Q. Y., Wang, J. L., Zhang, S. Y., Ma, J., Cheng, J. S., and Zhang, Y. T. (2022a). Zr-Based metal-organic frameworks for green biodiesel synthesis: A minireview. *Bioengineering* 9, 700. doi:10.3390/bioengineering9110700

Zhang, Q. Y., Yang, B. B., Tian, Y. Y., Yang, X. J., Yu, R. F., Wang, J. L., et al. (2022b). Fabrication of silicotungstic acid immobilized on Ce-based MOF and embedded in Zr-based MOF matrix for green fatty acid esterification. *Green process. Synth.* 11, 184–194. doi:10.1515/gps-2022-0021

Zhang, W. L., Wang, C. R., Luo, B. N., He, P. H., Li, L., and Wu, G. Q. (2023). Biodiesel production by transesterification of waste cooking oil in the presence of graphitic carbon nitride supported molybdenum catalyst. *Fuel* 332, 126309. doi:10.1016/j.fuel.2022.126309

Zhao, R., Yang, X. Y., Li, M. Z., Peng, X. J., Wei, M. X., Zhang, X. C., et al. (2021). Biodiesel preparation from *Thlaspi arvense* L. seed oil utilizing a novel ionic liquid core-shell magnetic catalyst. *Ind. Crops Prod.* 162, 113316. doi:10.1016/j.indcrop.2021.113316

Zhou, D., Chen, X. P., Liang, B. F., Fan, X. X., Wei, X. J., Liang, J. Z., et al. (2019). Embedding MIL-100(Fe) with magnetically recyclable Fe_3O_4 nanoparticles for highly efficient esterification of diterpene resin acids and the associated kinetics. *Microporous Mesoporous Mat.* 289, 109615. doi:10.1016/j.micromeso.2019.109615

Zhou, D., Wang, L. L., Chen, X. P., Wei, X. J., Liang, J. Z., Tang, R., et al. (2023). Reaction mechanism investigation on the esterification of rosin with glycerol over annealed Fe_3O_4/MOF-5 via kinetics and TGA-FTIR analysis. *Chem. Eng. J.* 401, 126024. doi:10.1016/j.cej.2020.126024

Frontiers in Chemistry

Explores all fields of chemical science across the periodic table

Advances our understanding of how atoms, ions, and molecules come together and come apart. It explores the role of chemistry in our everyday lives - from electronic devices to health and wellbeing.

Discover the latest Research Topics

See more →

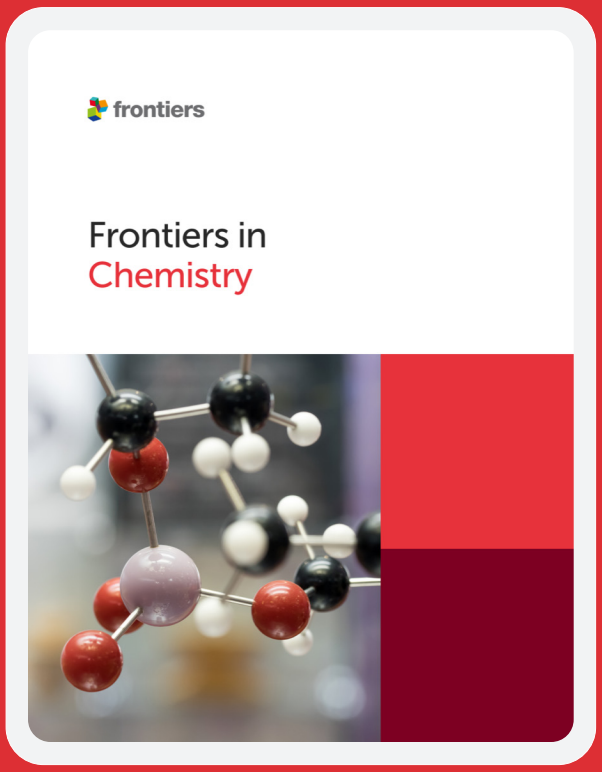

Frontiers

Avenue du Tribunal-Fédéral 34
1005 Lausanne, Switzerland
frontiersin.org

Contact us

+41 (0)21 510 17 00
frontiersin.org/about/contact